# DEVELOPMENT OF BECLIN 1-TARGETING STAPLED PEPTIDES AS NOVEL ANTI-PROLIFERATION STRATEGY FOR HEPATOCELLULAR CARCINOMA

**GAO SHAN**

**PhD**

**The Hong Kong Polytechnic University**

**2023**

The Hong Kong Polytechnic University

Department of Applied Biology and Chemical Technology

# DEVELOPMENT OF BECLIN 1-TARGETING STAPLED PEPTIDES AS NOVEL ANTI-PROLIFERATION STRATEGY FOR HEPATOCELLULAR CARCINOMA

**GAO SHAN**

A thesis submitted in partial fulfilment of the requirements for

the degree of Doctor of Philosophy

March 2023

CERTIFICATE OF ORIGINALITY

I hereby declare that this thesis is my own work and that, to the best of my knowledge and belief, it reproduces no material previously published or written, nor material that has been accepted for the award of any other degree or diploma, except where due acknowledgement has been made in the text.

Signature:

Name of student: GAO SHAN

## Abstract

Hepatocellular carcinoma (HCC) is the most common form of primary liver cancer, accounting for around 90% of cases. HCC is a growing health problem globally and is now the third leading cause of cancer-related deaths. Unfortunately, the majority of HCC cases are detected at later stages when therapeutic options are limited. Due to liver dysfunction, many chemotherapy treatments cannot be used for HCC patients. Drugs like sorafenib or Lenvatinib, which are used as first-line treatments, only offer limited survival benefits of 2-3 months. The effectiveness of sorafenib is further reduced by the development of primary and acquired resistance after a period of treatment. Although a combination of monoclonal antibody drugs has shown little improvement in survival compared to targeted drugs, HCC patients exhibit a low response rate of around 20-30%. The overall 5-year survival rate for HCC patients is only about 18%. There is a pressing need for effective HCC therapies.

Autophagy is an essential process of cellular metabolism that involves the degradation and recycling of intracellular macromolecular components in eukaryotic cells. It is a conserved process that is important for maintaining cellular homeostasis, eliminating damaged organelles, and protecting cell survival under stress. The liver is a major metabolic

organ that is closely linked to autophagy. Autophagy also plays multiple roles in HCC tumorigenesis, promotion and drug resistance and autophagy-related proteins regulate various processes of HCC as suppressors or promoters can serve as prognostic biomarkers and therapeutic value.

Beclin1 is an essential autophagy protein and is part of the Class III PI3K complex. It interacts with Atg14L and UVRAG in a mutually exclusive manner and forms Atg14L/UVRAG-containing Beclin1-Vps34 subcomplexes to promote autophagy and endolysosomal trafficking. In our previous work, the structure of the Beclin1-UVRAG coiled-coil complex was revealed to be strengthened by hydrophobic pairings and electrostatically complementary interactions. Using structure-based rational design, we developed hydrocarbon stapled peptides that bind specifically to Beclin1 to enhance the interaction between Beclin1 and UVRAG, further promoting Vps34-dependent autophagy and endolysosomal trafficking. Tat-SP4 is one of the leading Beclin1-targeting stapled peptides developed in our lab.

In our project, Tat-SP4 was found to enhanced autophagy in several HCC cell lines. Interestingly, Tat-SP4 shows no further effect on EGFR endolysosomal degradation, while it was able to induce significant and rapid c-MET turnover. Additionally, Tat-SP4 had an anti-proliferative

effect in several HCC cell lines and was able to override the adaptive sorafenib resistance effect in HCC cells. Mechanistic studies showed that Tat-SP4 induced cell death could be blocked by an inhibitor of autosis called digoxin. Tat-SP4 was also found to induce mitochondrial dysfunction. Tat-SP4 can disrupt intracellular calcium homeostasis, including the release of calcium ions from the endoplasmic reticulum (ER) and an increase in the levels of cytosolic and mitochondrial calcium ions. The presence of extracellular calcium ions protects against Tat-SP4-induced cell death and mitochondrial dysfunction by stabilizing intracellular ion homeostasis. In HCC patient-derived tumor xenograft (PDTX) mouse models, Tat-SP4 significantly reduced tumor volume at a dose of 40 mg/kg/day for approximately 30 days with no observable toxicity. As there is currently no effective targeted therapy for HCC, our results provide a promising new strategy for inhibiting HCC proliferation.

## Publications arising from the thesis

**Shan Gao**, Na Li, Xiaozhe Zhang, Jingyi Chen, Ben C.B. Ko, Yanxiang Zhao. (2022). An autophagy-inducing stapled peptide promotes c-MET degradation and overrides adaptive resistance to sorafenib in c-MET$^{+}$ hepatocellular carcinoma. Biochemistry and Biophysics Reports, 33, p.101412.

Jingyi Chen, Xiaozhe Zhang, **Shan Gao**, Na Li, Vincent Keng, Yanxiang Zhao. (2022). A Beclin 1-targeting stapled peptide synergizes with erlotinib to potently inhibit proliferation of non-small-cell lung cancer cells. Biochemistry and Biophysics Research Community, 636 (Pt 1):125-131.

Na Li, Xiaozhe Zhang, Jingyi Chen, **Shan Gao**, Lei Wang, and Yanxiang Zhao. (2023). Perturbation of autophagy by a Beclin 1-targeting stapled peptide induces mitochondria stress and inhibits proliferation of pancreatic cancer cells. Cancers, 15, no. 3: 953.

## Acknowledgments

During my Ph.D. studies and the preparation of my dissertation, I have received a lot of invaluable help from many people. At the final stage of this journey, I am glad to have the opportunity to show my appreciation to those who have provided me with numerous encouragement and support.

First of all, I would like to express my sincere gratitude to my supervisor, Prof. Zhao Yanxiang, for her professional guidance, invaluable suggestions, and constant encouragement throughout my studies. I am grateful to her for giving me the opportunity to study in her group. I am honored to benefit from her passion and respect for science, enthusiasm for research work, and creative and critical thinking, which I will cherish throughout my life.

I am grateful to Prof. Terence Lee for kindly providing me with some HCC cell lines and animal models. Special thanks to Dr. Carmen for helping me to set up animal models and providing useful suggestions for data analysis of my in vivo experiments. I would like to thank Dr. Vincent Keng and Dr. Ben Ko for generously providing HCC cell lines for my study and providing valuable suggestions for my data analysis. I would also like to thank Dr. Yue Jianbo for allowing me to use the

equipment in his laboratory. I would like to thank colleagues from the general office for their kind help in the routine work of my study.

I would also like to thank all my teammates in Prof. Zhao's group for their kind help and guidance. Many thanks to Dr. Qiu Xianxiu and Dr. Wu Shuai for giving me useful and valuable guidance at the beginning of my study. Special thanks to Dr. Zhang Xiaozhe, who not only shared many experimental experiences and techniques with me, but also gave me so much help in my daily life. Many thanks to Dr. Li Na and Dr. Yang Xian for giving me a lot of encouragement and sharing their life experiences in my study and life. Thanks to Ms. Chen Jingyi, Miss. Wang Lei, Miss. Feng Yu, Miss. Yu Yingting, and Ms. Xia Yuhui for their help with the in vivo experiments and in routine laboratory work. I am really happy to have met many good friends in the lab. Our shared experiences and fun are the most precious memories that I will never forget.

Finally, I would like to thank my family members and friends for their generous support and endless love.

# Content

# 1.Introduction

## 1.1 HCC has poor prognosis and limited therapeutic options

### 1.1.1 HCC remains a global health challenges

Liver cancer is ranked as the sixth most common cancer and the fourth leading cause of cancer death in the whole world (Wang, Naghavi et al. 2016). It is known for its high fatality rate, largely due to the late-stage diagnosis and high recurrence rate. Currently, liver cancer continues to be a major health issue in the world, with over 830,000 deaths annually due to liver cancer-related diseases (Singal, Lampertico et al. 2020). The National Cancer Institute estimates that the incidence of liver cancer is still increasing (Sung, Ferlay et al. 2021). By 2050, it is projected that over 1 million people will be affected by liver cancer globally (Villanueva 2019). Liver cancer has become a critical health and economic burden in many developing countries, especially in East Asia and Africa (Kulik and El-Serag 2019). The International Agency for Research on Cancer reports global liver cancer incidence rates for 2020, with East Asia and West Africa having the highest incidence rates (Figure 1.1). In Asia, liver cancer ranks as the sixth most common cancer and the third leading cause of cancer-related death (Singal, Lampertico et al. 2020). In 2020, over 600,000 cases of liver cancer were diagnosed in Asia, accounting for about 72.5% of all cases globally (Singal, Lampertico et al. 2020). The

incidence of male patients is more than twice of females worldwide (Ferlay, Shin et al. 2010). The World health organization (WHO) notes that liver cancer incidence rates are higher in China than in other countries, with liver cancer being the fourth most commonly diagnosed malignant and the second leading cause of cancer-related death in China. According to WHO's Globocan 2020 China fact sheet, nearly 400,000 Chinese people are diagnosed with liver cancer each year, and around 368,000 dies from it. This means that almost half of all new liver cancer cases worldwide are in China, posing a serious threat to the health and well-being of the Chinese people (Petrick, Florio et al. 2020).

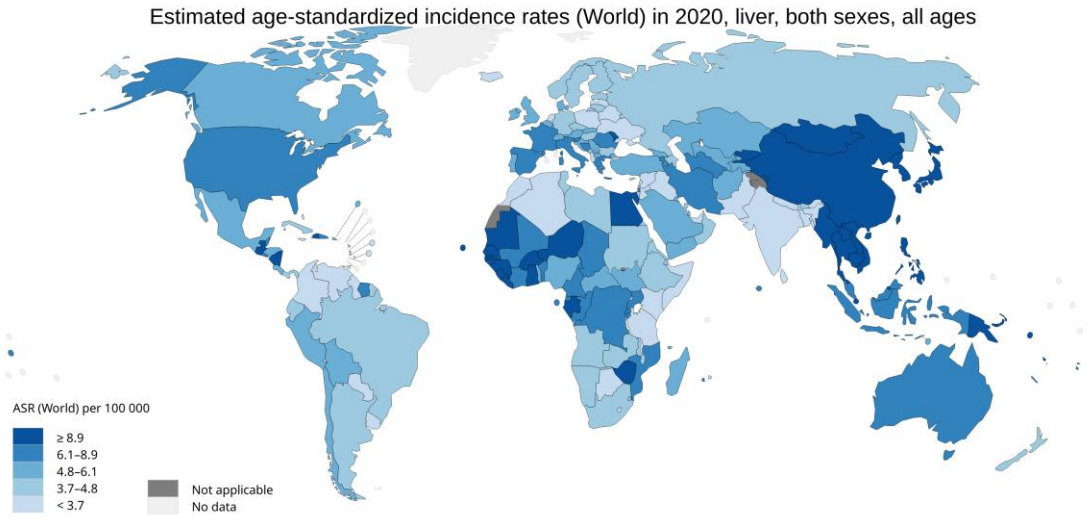


**Figure 1.1 HCC remains a global health challenge.** Estimated global age-standardized incidence rates (ASR) of liver cancer in 2020 (Map reference from http://gco.iarc.fr/today).

Hepatocellular carcinoma (HCC) is a type of liver cancer that originates from hepatocytes almost in every parts of the whole liver. HCC is one of the most common types of primary liver cancer, accounting for approximately 90% of all cases. It is an aggressive tumor that often develops in the presence of chronic liver disease or cirrhosis. Many HCC patients are accompanied by varying degrees of cirrhosis, making treatment challenging. Surgical resection is the mainstay of therapy, but most patients are not eligible due to the extent of their tumors or underlying liver dysfunction. The median survival time following a HCC diagnosis is approximately 6 to 20 months. HCC is one of the leading causes of liver cancer death.

Various environmental and lifestyle risk factors contribute to the high incidence of HCC in these developing countries. Specifically, Mongolia has the highest incidence of liver cancer in the world, the average incidence rate is 8 times than the global data. These HCCs can be attributed to high hepatitis B virus (HBV) and hepatitis C virus (HCV) infection and excessive alcohol consumption. Chain is another country with a high incidence of HCC and approximately 54% of HCC patients are infected by hepatitis B virus (HBV). Dietary exposure to aflatoxin B1 is also a major risk factor for developing HCC, particularly in sub-Saharan Africa and Southeast Asia. For example, approximately 60% of

HCCs in Sudan have aflatoxin B1 as a cofactor. In the United States, where there is a high prevalence of obesity, non-alcoholic steatohepatitis (NASH) associated with obesity or diabetes is a cofactor for HCC development.

### 1.1.2 The mechanism of hepatocarcinogenesis

Risk factors vary by geographic region because of the close relationship between an environmental agent and the incidence of viral infection (Waly Raphael, Yangde et al. 2012). Chronic HBV and HCV infection, excessive alcohol consumption, aflatoxin B1 (AFB1), metabolic syndrome, and NASH are important risk factors associated with the development of HCC (Figure 1.2) (Aravalli, Steer et al. 2008) (Farazi and DePinho 2006).

The mechanism of HBV and HCV infection-induced hepatocarcinogenesis is complex, involving both viral and host factors. HBV is a double-stranded, noncytopathic hepatotropic DNA virus. This double-stranded DNA can encode several viral proteins, HBx, which is required for its cell cycle. Following HBV infection, normal liver cells suffer cell injury, inflammation and abnormal proliferation, followed by the formation of fibrosis and eventually cirrhosis. Long-term cirrhosis is usually associated with genetic alterations, chromosomal aberrations, inhibition of tumor suppressor genes, activation of oncogenes, and

ultimately the development of HCC. The molecular mechanism of HBV infection involves three different ways. First, double-stranded DNA can insert directly into the host genome, resulting in chromosomal rearrangement and genomic instability (Sanyal, Yoon et al. 2010). Second, HBV encodes several proteins, HBx functions as a regulator of cell proliferation pathways such as PI3K/AKT/mTOR and RAS/RAF/MEK/ERK. In addition, HBx can bind and inhibit the activation of tumor suppressor genes such as p53 in vitro (Farazi and DePinho 2006, Sanyal, Yoon et al. 2010).

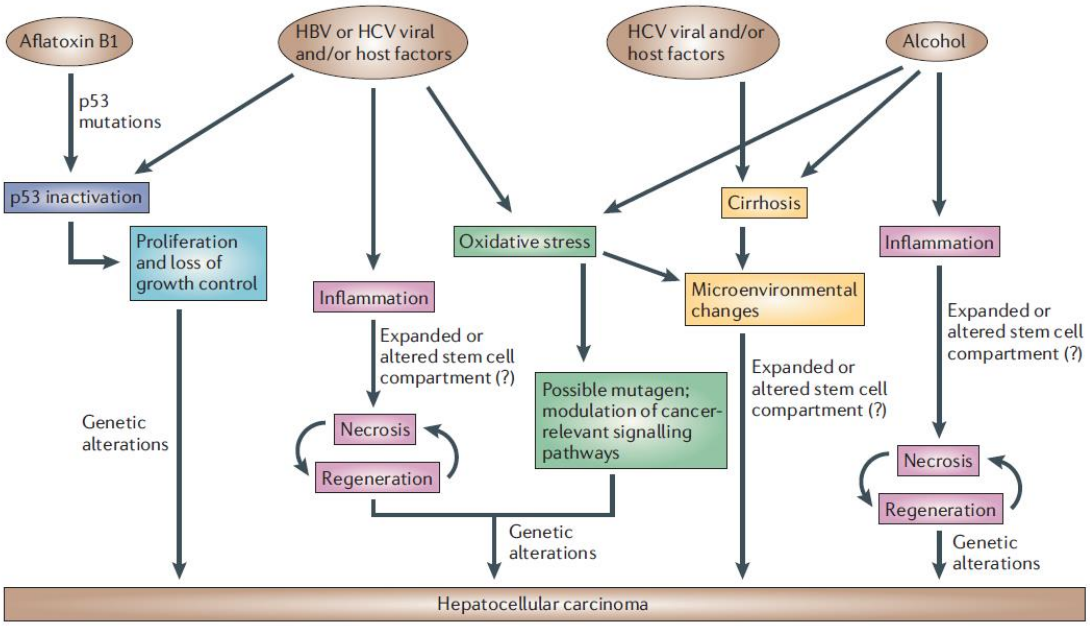


**Figure 1.2 The mechanism of HCC development (Farazi and DePinho 2006).** The main risk factors cause HCC hepatocarcinogenesis in several ways. Different colors indicate different ways to induce HCC development.

In addition, host-virus interactions contribute to hepatocarcinogenesis in several ways. Viral infection triggers activation of the host immune system to produce inflammation. Chronic active infection leads to a continuous replication of hepatocyte death-inflammation-regeneration (Rehermann and Nascimbeni 2005). Such sustained cycles of hepatocytes could promote lesion development and genomic environmental instability (Figure 1.2). Another mechanism of HBV infection-induced hepatocarcinogenesis may be the oxidative stress generated by viral-host interactions (Shimoda, Nagashima et al. 1994). Oxidative stress can activate cell proliferation and survival pathways, stimulate stellate cells, and induce mutations (Galli, Svegliati-Baroni et al. 2005). HBV infection may trigger many different molecular mechanisms to promote HCC development.

HCV is an RNA virus that can't directly affect genomic stability by integrating into the host genome. The mechanism of HCV infection-induced hepatocarcinogenesis is similar to that of HBV infection, particularly in the host-virus interaction (Figure 1.2). HCV-encoded proteins also induce hepatocyte death-inflammation-regeneration, oxidative stress, and inactive tumor suppressors such as p53 (Majumder, Ghosh et al. 2001, Moriya, Nakagawa et al. 2001, Macdonald, Crowder et al. 2003). HCV core proteins associated with cell proliferation signaling

pathways such as MAPK regulate cell growth. In addition, HCV nonstructural proteins can also increase reactive oxygen species (ROS) levels, which promote the development of HCC (Moriya, Nakagawa et al. 2001). Unlike HBV, HCV infection carries a higher potential to promote liver cirrhosis. Studies have shown that excessive alcohol consumption associated with HCV infection causes a higher incidence of cirrhosis and ultimately HCC (Sanyal, Yoon et al. 2010).

Alcohol consumption is a risk factor for the development of HCC. Chronic alcohol intake triggers persistent inflammation of hepatocytes, leading to elevated levels of pro-inflammatory cytokines. Alcohol consumption increases endotoxin levels and activates specific macrophages in the liver, resulting in the release of cytokines such as TNFα and interleukin-1β (IL-1β), which eventually cause liver cell damage and cell death (Hoek and Pastorino 2002, McClain, Hill et al. 2002). Furthermore, chronic alcohol exposure causes oxidative stress, contributing to HCC development in several ways, including the accumulation of oncogenic mutations, repression of signaling pathways, and promotion of fibrotic response of stellate cells (Marrogi, Khan et al. 2001, Osna, Clemens et al. 2005, Farazi and DePinho 2006).

Aflatoxin B1 function as an inducer of hepatocarcinogenesis. The main mechanism of aflatoxin B1 facilitates as a mutagen of tumor

suppressors such as p53 mutation and activation oncogenes such as Ras (Aguilar, Harris et al. 1994, Riley, Mandel et al. 1997). Aflatoxin B1 is also as a cofactor associated with HBV infection the incidence of HCC hepatocarcinogenesis is higher than only aflatoxin B1 exposure (Kew 2003).

As mentioned above, the development of HCC often stems from the setting of chronic hepatocyte damage and death and then lead to fibrosis or cirrhosis formation eventually resulting in liver dysfunction (Venook, Papandreou et al. 2010). HCC development like other cancers is a multi-step process that transforms normal cells into invasion and migration. The basic features of cancer cells involve genomic instability, losing control of cell proliferation, invasion, and migration. Pathogenesis of different stages of HCC is usually regulated through different mechanisms. Genetic instability is one of the most obvious consequences in the development of HCC which mainly includes chromosomal rearrangement, mutations of tumor suppressor p53, aberrant activation of oncogenic pathways signaling, and epigenetic alterations. For instant, p53 mutations and p16 gene silencing are more frequently detected in the end-stage of HCC. In addition, the molecular analysis of human HCC has shown the pathogenesis of HCC associated with multiple receptor tyrosine kinase pathways. The activation of several different abnormal cellular signaling

pathways linked to HCC including epidermal growth factor receptor (EGFR), fibroblast growth factor receptor (FGFR), insulin-like growth factor/IGF-1 receptor (IGF/IGF-1R), hepatocyte growth factor (HGF/MET), the vascular endothelial growth factor receptor (VEGFR), wingless (Wnt/β-catenin) pathways (Figure 1.3).

The Wnt/β-catenin signaling pathway participates in the regulation of cellular growth, differentiation, and cell death to maintain cellular homeostasis (Figure 1.3) (Nelson and Nusse 2004). Cysteine-rich glycoprotein ligands, such as Wnts, are the main members of this pathway and bind to transmembrane-fizzled receptors, leading to the phosphorylation of downstream proteins and activation of the pathway. In an inactive Wnt pathway condition, β-catenin localizes in the cytosol interacts with axis inhibition proteins (Axin) and adenomatous polyposis coli (APC) to form a complex. Glycogen synthase kinase 3β (GSK-3β) and casein kinase 1 as a regulator mediates cytosolic β-catenin phosphorylation and degradation (Dimri and Satyanarayana 2020) (Dhanasekaran, Bandoh et al. 2016).

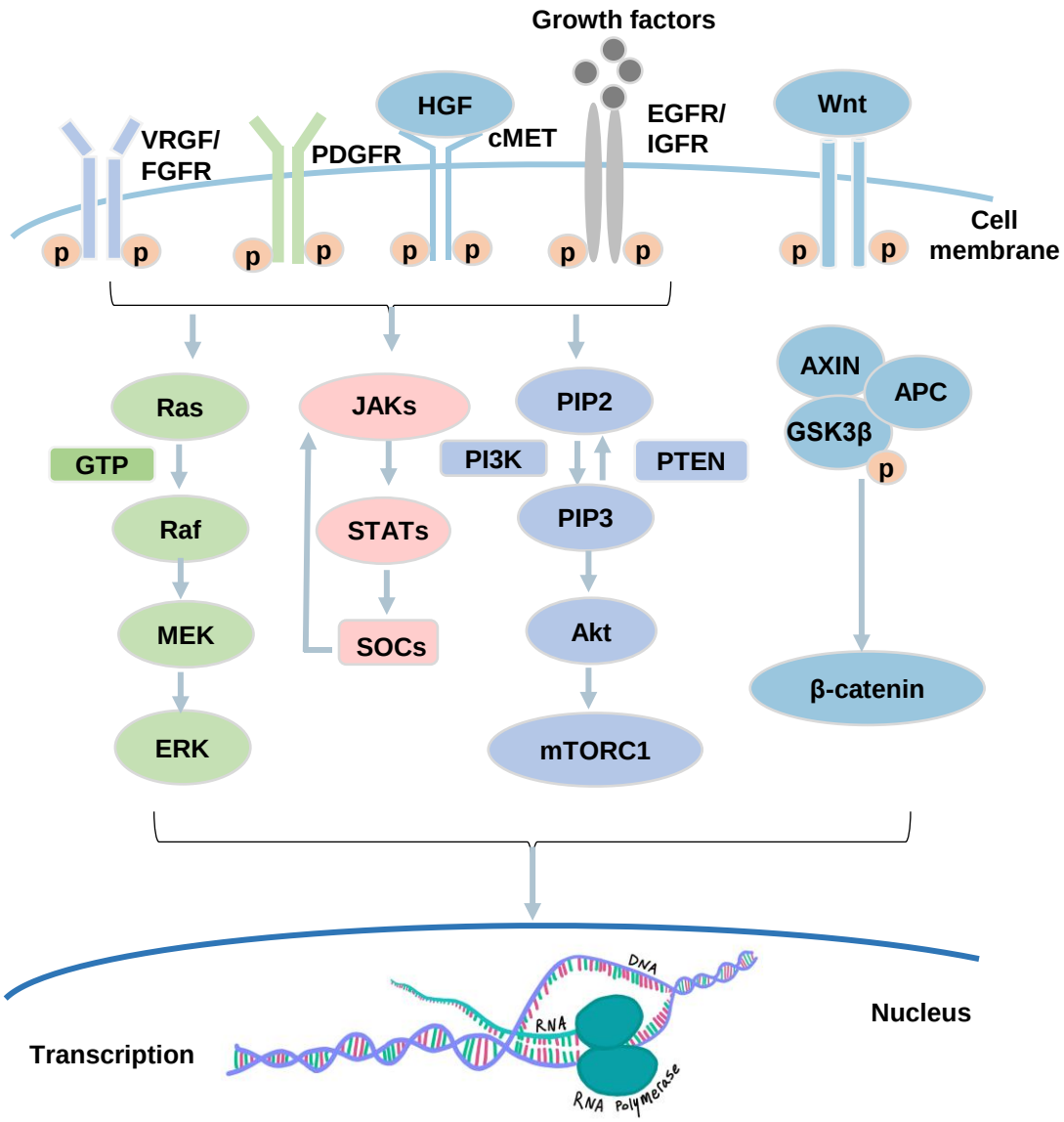


**Figure 1.3 The major cell surface receptors and their downstream signaling pathways in HCC** (Dimri and Satyanarayana 2020). The transcription image source is from Sylvia Freeman.

Upon activation of the Wnt pathway by the interaction between Wnt ligands and Frizzled receptor, GSK-3β is phosphorylated and suppressed, allowing for the accumulation of cytosolic β-catenin. This accumulated β-

catenin then transfers to the nucleus, where it interacts with the transcription factor LEF/TCF, activating transcription genes involved in cell growth, cell death, and angiogenesis (Apte, Thompson et al. 2008, Dimri and Satyanarayana 2020). In HCC, HCV infection and aflatoxin B1 exposure can cause aberrant expression in some components of the Wnt signaling pathway, resulting in its overactivation (Wang, Smits et al. 2019). Approximately 20-40% of HCC cases have mutations in this pathway, including 12-26% with β-catenin gene mutations and 8-13% with Axin mutations (Giles, Van Es et al. 2003, Apte, Thompson et al. 2008).

The Ras/Raf/MAPK pathway is one of the core signal transduction pathways involved in HCC development (Figure 1.3). This pathway is crucial for regulating cell growth and survival. Multiple cell surface growth receptors, including VEGFR, FGFR, PDGFR, and c-Met receptor, which are involved in cell proliferation and angiogenesis, can regulate various cellular activities through this pathway. These receptors bind to their respective ligands, triggering activation and phosphorylation of the receptors. This activation is then transferred to the downstream Ras/Raf/MAPK pathway via Grb2/Shc/SOS proteins. Finally, transcription factor genes are activated in the nucleus, driving cell proliferation (Alqahtani, Khan et al. 2019). The Ras family, a type of

oncogene, can be activated by some point mutations, but this type of mutation is not common in HCC cases (Merle and Trepo 2009, Alqahtani, Khan et al. 2019). The main cause of dysfunction in the Ras/Raf/MAPK pathway is abnormal upstream signals. HBV and HCV infections can lead to excessive activation of Raf kinase, causing aberrant cell proliferation and eventually promoting HCC development.

The PI3K/AKT/mTOR pathway plays a crucial role in regulating cell proliferation, apoptosis, and survival (Figure 1.3). It is the most important pathway that is overactivated in approximately 50% of HCC cases (Whittaker, Marais et al. 2010). Multiple cell surface receptors, such as IGFR and EGFR, can activate this pathway by activating PI3K. PI3K then phosphorylates PIP2, a membrane lipid phosphatidylinositol 4,5-biphosphate, to activate the serine-threonine kinase Akt (Alqahtani, Khan et al. 2019). Activated Akt can then regulate the critical protein mTOR (mammalian target of rapamycin), which is responsible for cell proliferation, cell survival, cell metabolism, and autophagy. The phosphatase and tensin homolog (PTEN) is a critical tumor suppressor in this pathway. PTEN functions as a negative regulator by inhibiting PI3K phosphorylation (Alqahtani, Khan et al. 2019). In HCC, mutations in PTEN usually cause hyperactivation of the PI3K/AKT/mTOR pathway,

and studies have shown that PTEN deficiency significantly increases the incidence of HCC in mouse models (Horie, Suzuki et al. 2004).

The JAK/STAT pathway can also be activated by multiple cytokines and growth factors, like the above-mentioned pathways (Figure 1.3). This pathway facilitates cell growth, survival, differentiation, and apoptosis. The pathway includes four JAK family members and six STAT family members. Upstream growth factors activate this pathway by phosphorylating the JAK family, which then stimulates the activation of the STAT family members (Rawlings, Rosler et al. 2004, Aittomäki, Pesu et al. 2014, Dimri and Satyanarayana 2020). The protein inhibitors of activated Stats (PIAS) control this pathway by inhibiting STAT-DNA interaction. SH2-containing phosphatases (SHP) and suppressors of cytokine signaling (SOCS) are also inhibitors of this pathway. Activated JAKs trigger the transcription of SOCS genes, which then inhibit the binding between ligands and their receptors as part of a negative feedback loop(Seif, Khoshmirsafa et al. 2017). In HCC, increasing number of studies have detected JAK mutations leading to activation of the JAK/STAT pathway. Abnormal changes such as the inactivation of SOCS, the degradation of JAK-binding proteins, and JAK1 mutations all contribute to enhanced JAK/STAT pathway activation in HCC (Dimri and Satyanarayana 2020).

The HGF/c-MET signaling pathway plays a key role in maintaining cellular homeostasis, including liver regeneration, tissue remodeling, and repairing cardiac tissue injuries (Figure 1.3) (Nakamura, Mizuno et al. 2000, Huh, Factor et al. 2004). HGF binding to c-MET induces receptor homodimerization and phosphorylation. Activated c-MET then recruits a series of signaling effectors, with Gab1 and Gab2 being the most important adaptors in this pathway. These adaptors directly interact with c-MET to trigger their phosphorylation and regulate downstream signaling pathways. Similarly, to other tyrosine kinase receptors, activated c-MET can regulate several canonical downstream signaling pathways, including the Ras/Raf/MAPK, JAK/STAT, and PI3K/Akt/mTOR. The HGF-c-MET axis has been implicated in the development of HCC through multiple pathogenic mechanisms. HGF and c-MET overexpression can cause overactivation of this pathway, which is observed in approximately 33% of HCC patients with HGF overexpression and 20–48% of HCC patients with c-MET overexpression (Boix, Rosa et al. 1994, Kiss, Wang et al. 1997, Garcia-Vilas and Medina 2018). In addition, c-MET gene amplification or mutations can induce abnormal function of HGF/c-MET pathway to activate several signaling cascades in HCC (Birchmeier, Birchmeier et al. 2003, Lengyel, Prechtel et al. 2005).

### 1.1.3 The prognosis for HCC is poor with limited therapeutic options

HCC is often diagnosed at an advanced stage, making palliative therapies the main course of treatment. The median survival after diagnosis is typically 6-12 months and only 10% of patients survive 5 years past diagnosis (Cha and Dematteo 2005, Golabi, Fazel et al. 2017). While surgical resection, radiofrequency/microwave ablation, trans-arterial chemoembolization, liver transplantation, and systemic chemotherapy are traditional treatments for early-stage HCC, each has its own limitations. Curative treatments such as surgical resection are hindered by the high rate of HCC recurrence, which affects over 70% of patients within 5 years (Liu, Chen et al. 2015, Golabi, Fazel et al. 2017). Additionally, many patients with liver dysfunction are unable to undergo chemotherapy.

The Barcelona Clinic Liver Cancer (BCLC) staging system provides a framework for determining appropriate therapeutic options based on the patient's liver function, performance status, and tumor burden. Patients in the early stages (BCLC 0 and A) with a single small tumor and good liver function are candidates for surgical treatments like ablation, resection, and transplantation. About 60% of these patients have a survival time of over 5 years with low mortality, but a high recurrence rate of 70% (Ishizawa, Hasegawa et al. 2008, Roayaie, Jibara et al. 2015). However,

only a small percentage of patients (less than 5%) are diagnosed at this stage. The majority of HCC patients (more than 95%) are diagnosed at later stages (BCLC B-D), where treatment options are limited. Trans-arterial chemoembolization (TACE) is the main option for intermediate-stage tumors (BCLC B) with a median survival time of 26-40 months (Burrel, Reig et al. 2012).

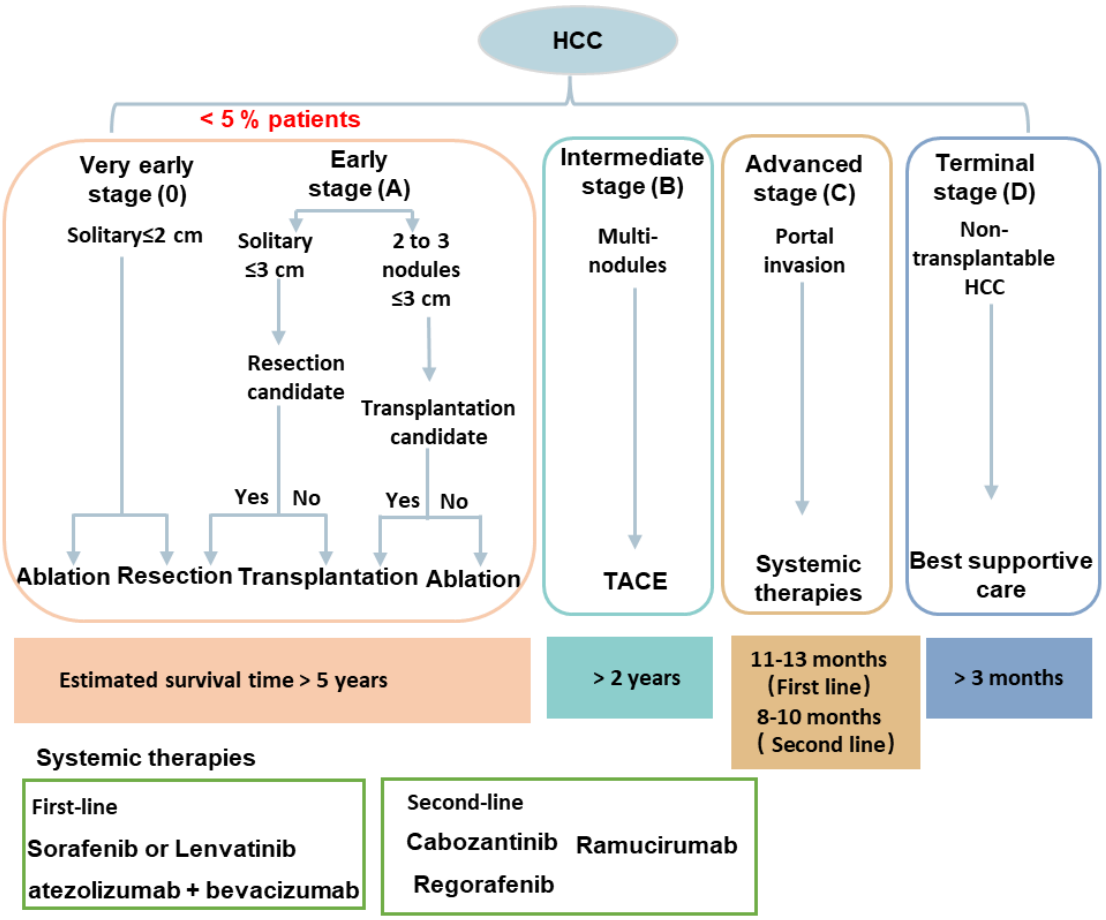


**Figure 1.4 The prognosis for HCC is poor with limited therapeutic options.** The Barcelona Clinic Liver Cancer (BCLC) staging system classifies five different stages of HCC patients based on their liver function, performance status, and tumor burden. Different stages are

indicated by different colors, and their primary therapeutic options and estimated survival times are also shown. Systemic therapies are the options for patients with advanced-stage HCC.

In recent years, molecularly targeted therapies have been used for systemic treatment. Although many research groups are exploring effective treatments for HCC, only five targeted therapies have been approved so far. Sorafenib (approved in 2005) and Lenvatinib (approved in 2018) belong to the family of tyrosine kinase inhibitors (TKIs) and exert their anti-proliferative effect by blocking multiple kinases and tyrosine kinase receptors such as VEGFR, PDGFR, FGFR, MET, and the Ras/Raf/MAPK signaling pathways (Capozzi, De Divitiis et al. 2019). Sorafenib and Lenvatinib are used as first-line treatments for advanced-stage HCC. Unfortunately, these drugs only provide modest survival benefits of 2 to 3 months compared to placebo. The estimated survival time of BCLC stage C ranges from 11 to 13 months after first-line treatment (Balogh, Victor III et al. 2016). A combination of two monoclonal antibody drugs, atezolizumab (anti-PDL1) and bevacizumab (anti-VEGF), has also been approved as a first-line therapy. Compared to sorafenib, this combination improves median survival time from 13.4 months to 19.2 months (Llovet, Villanueva et al. 2021). Regorafenib, Cabozantinib, and Ramucirumab are used as second-line therapies and

are inhibitors of tyrosine receptor kinases involving VEGFR and MET. These drugs can decrease the risk of death by about 30% (Zhu, Park et al. 2015, Bruix, Qin et al. 2017, Abou-Alfa, Meyer et al. 2018). The overall survival time after second-line therapy ranges from 8 to 10 months. Nivolumab (approved in 2017) and pembrolizumab (approved in 2018) are anti-PD-1 monoclonal antibodies (mAbs) that are approved for second-line therapy. While the survival benefit can last 6 months or longer, the overall response rate is limited to only ~14%.

Compared to other cancer therapies, the treatment options for HCC are still limited. Only five targeted drugs have been approved for HCC treatment, all of which are TKIs with limited survival benefits for patients. Although a few monoclonal antibody drug combinations show improved efficacy compared to targeted drugs, their side effects, lower response rate, and contraindications limit their application. Given the significant unmet medical need, there is intense interest in searching for more novel and effective HCC therapies.

### 1.2 Autophagy and its functions in HCC

Autophagy, also known as self-eating, is a lysosome-dependent process for the degradation and recycling of intracellular macromolecular components in eukaryotic cells (Mizushima and Komatsu 2011). It is regulated by approximately 40 identified autophagy-related genes (ATGs)

(Mizushima and Levine 2020). This process is crucial for the elimination of damaged organelles and protecting cells' survival in adverse conditions, such as nutritional deficiency and toxicity stimulation. Under normal physiological conditions, autophagy acts as a self-protective mechanism, promoting cell growth control and protecting cells from metabolic stress and oxidative damage (Levine, Mizushima et al. 2011). This process plays an important role in maintaining cellular homeostasis and helps to recycle and degrade intracellular materials. However, excessive autophagy can result in metabolic stress, degradation of excessive cellular components, and even cell death. Autophagy plays a significant role in human health and diseases, including tumorigenesis, cell homeostasis, aging, immunity, and neurodegenerative diseases (Levine and Kroemer 2019).

Autophagy can be classified into three types based on the mode of cargo delivery to the lysosome: macroautophagy, chaperone-mediated autophagy (CAM), and microautophagy. Macroautophagy, the most common type of autophagy, is responsible for engulfing most of the cytosolic content through a double-membraned autophagosome and delivering it to the lysosome for degradation and recycling. Chaperone-mediated autophagy is assisted by chaperone molecules in the

degradation process. Microautophagy involves direct engulfment and invagination by lysosomes.

### 1.2.1 The process of autophagy

The process of autophagy, specifically macroautophagy, involves rearrangement of intracellular membranes. It can be roughly divided into four stages: initiation, nucleation-elongation-maturation, fusion, and degradation (Figure 1.5) (Yim and Mizushima 2020). The central step is the formation of autophagosomes, which are double-membraned vesicles that can engulf long-lived proteins, intact or damaged organelles, and other cytoplasmic components. The autophagosome then matures by fusing and docking with an endosome or lysosome to form an autolysosome. Finally, the degradation and recycling of the autophagosome inner membrane and its cargo occur (Figure 1.5) (Yang and Klionsky 2010).

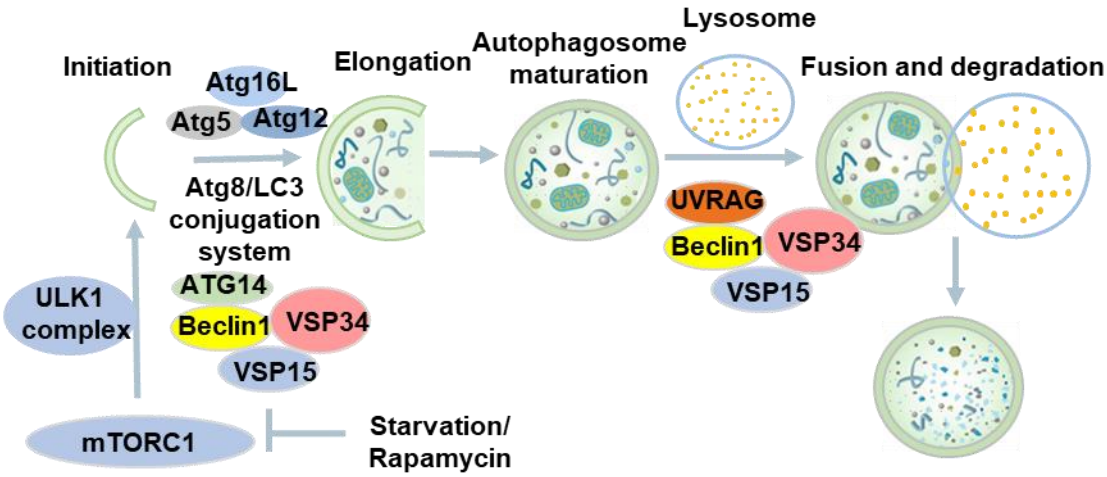

**Figure 1.5 The molecular mechanism of autophagic process in mammalian cells.**

The molecular mechanisms behind the process of autophagy in mammalian cells are orchestrated and controlled by four systems. Autophagy-related genes (ATG) proteins, which encode multiple complexes, have been evolutionarily conserved and identified in yeast. Of the more than 40 ATG proteins, about 18 are essential for the formation of a double-membraned vesicle and are referred to as the core ATG proteins (Mizushima and Levine 2020). Additionally, two ubiquitin-like conjugation systems regulate the formation and size of the final autophagosome.

The first system is the Atg1/unc-51-like kinase (ULK) 1/2 complex, which regulates the initiation of autophagy along with other membrane traffic factors (Matsuura, Tsukada et al. 1997, Kuroyanagi, Yan et al. 1998). In response to stimuli such as amino acid starvation or other stress, the mammalian target of rapamycin kinase complex (mTOR) is inactivated in mammalian cells, leading to the dephosphorylation of Atg13 and ULK1/2. This dephosphorylation increases the formation of the ULK1/2-mAtg13-FIP200 complex (Egan, Shackelford et al. 2011). he activated ULK1/2 can also phosphorylate Beclin1 and AMBRA1 to activate the VPS34 complex and localize the initiation site of autophagy.

Under glucose starvation, ULK1 can be phosphorylated, acting downstream of the AMPK pathway.

The second system is comprised of two ubiquitin-like protein conjugation systems: the Atg12 conjugation system and the Atg8/LC3 conjugation system. These systems are necessary for the expansion and elongation of the phagophore membrane (Mizushima, Sugita et al. 1998). The formation of the Atg12-Atg5 conjugate depends on Atg7 (E1-like enzyme) and Atg10 (E2-like enzyme). Atg16L then interacts with the Atg12-Atg5 conjugate to form an Atg16L complex localized to the phagophore. Unlike Atg12, Atg8/LC3 is a precursor that is catalyzed by Atg4 to generate cytosolic LC31-I with a carboxyl-terminal, which is conjugated to phosphatidylethanolamine (PE) to form Atg8-PE and LC3 II (Lane and Nakatogawa 2013). This process is activated by the E1-like enzyme Atg7 and E2-like enzyme Atg3. The lipidated form of LC3 (LC3 II) can localize on both sides of the phagophore membrane. Autophagosomes with LC3-II localized on the outer membrane are removed to form LC3I for recycling, while LC3 II in the inner membrane is degraded, leading to the fusion of the autophagosome and endosome. The LC3 II form is a common marker for autophagy detection due to the accompanying transition of LC3 I and LC3 II (Mizushima, Yoshimori et al. 2010). The level of LC3 II protein can be monitored to assess

autophagy flux through Western blot or by monitoring changes in GFP-LC3 using a fluorescent microscope.

The third complex is the phosphatidylinositol 3-kinase (PI3KC3) / Vps34 complex, which is centered on Beclin1 (a homolog of Atg6) as a scaffold protein that interacts with Vps34, p150 (a homolog of Vps15), Atg14-like protein (Atg14L), and ultraviolet irradiation resistant-associated gene (UVRAG) (He and Levine 2010). The mammalian PI3K complex, also known as the Beclin1-Vps34 complex, plays a role in various steps of autophagy regulation. It promotes the formation of autophagosomes at the early stage and contributes to their maturation at the late stage.

The fourth system involves two transmembrane proteins, Atg9/mammalian Atg9 (mAtg9) and Vacuole Membrane Protein 1 (VMP1) (Tooze 2010, Yang and Klionsky 2010). mAtg9 undergoes multiple transmembrane cycles and is located on the endosomes and Golgi membrane in the late stage (Hamasaki and Yoshimori 2010). In conditions of starvation or rapamycin treatment, the cycling of Atg9 is dependent on ULK1 and facilitated by Vps34. This protein is involved in delivering membranes to form autophagosomes. Unlike Atg9, VMP1 does not have a known yeast ortholog. This spanning membrane protein

interacts with Beclin1 and other components of the PI3K complex to enhance autophagy (Zachari and Ganley 2017).

### 1.2.2 The role of autophagy in cancer

The relationship between autophagy and cancer is complex. Autophagy has a dual role in both cancer development and therapy, depending on the stage, type, or genetic background of the cancer in question (Lorin, Hamaï et al. 2013).

Autophagy as a Suppressor of Cancer:

Autophagy is critical in the degradation of damaged proteins and organelles and helps to maintain genomic stability, which is beneficial in the elimination of impaired tissues, injured cells, and inflammation. It also inhibits the accumulation of oncogenic p62 protein aggregates, making it a suppressor of tumor induction and cancer development, invasion, and metastasis (Mathew, Karp et al. 2009, Yue, Yang et al. 2017).

Some core autophagy genes act as tumor suppressors. For example, Beclin1, which is encoded by the BECN1 gene, is involved in the autophagy of human cancers. Monoallelic deletion of BECN1 has been observed in various human cancers such as hepatocellular carcinoma (HCC), ovarian, and breast cancers (Aita, Liang et al. 1999, Liang, Jackson et al. 1999, Jin and White 2007, Ding, Shi et al. 2008).

Decreased expression levels of Beclin1 have also been observed in 44 HCC patients, indicating that Beclin1 functions as a tumor suppressor (Ding, Shi et al. 2008). Similarly, complete deletion or ectopic expression of the UVRAG-binding protein and Bax interacting factor-1 (Bif-1) has been linked to cell proliferation in breast, colon, gastric, and prostate cancers (Takahashi, Coppola et al. 2007, Kim, Jeong et al. 2008, He, Zhao et al. 2015).

Other autophagy-related genes are also associated with oncogenesis. The deletion of ATG5 and ATG7 promotes the generation of multiple cancers in mouse models (Kuma, Hatano et al. 2004, Komatsu, Waguri et al. 2005, Saitoh, Fujita et al. 2008). Frameshift mutations of autophagy-related genes ATG5, ATG2B, ATG12, and ATG9B with mononucleotide repeats have been observed in gastric and colorectal cancers (Kang, Kim et al. 2009). These studies suggest that autophagy can suppress cancer generation.

Autophagy suppresses cancer by inhibiting necrosis and inflammation. Autophagy with bulk protein degradation is essential for regulating the inflammatory immune response (Saitoh, Fujita et al. 2008, Harris, Hartman et al. 2011). In the early stages of cancer, chronic inflammation is a common feature and trigger. Inflammatory environments are a major risk factor for various cancers, and the

occurrence of cancer can also lead to inflammation. Some studies have shown that tumors with defective autophagy increase necrosis levels and chronic inflammation in tumor cells (White, Karp et al. 2010). Intact autophagy can eliminate damaged proteins and organelles, preventing cellular dysfunction, inflammation, cell death, and ultimately decreasing the occurrence of cancer.

The accumulation of SQSTM1/p62 acts as a suppressor of tumorigenesis. p62 is a selective substrate of autophagy and can be specifically degraded by autophagy. When autophagy is blocked, especially at the end stage, p62 will be upregulated. The level of p62 can be used as a marker to monitor the effects of autophagy inhibition or defective autophagy (Pankiv, Clausen et al. 2007). Abnormally increased levels of p62 have been observed in multiple cancers such as HCC, breast cancer, lung cancer, prostate cancer, and gastrointestinal cancer (Kitamura, Torigoe et al. 2006, Inoue, Suzuki et al. 2012, Saito, Ichimura et al. 2016, Umemura, He et al. 2016, Li, Xu et al. 2017). Studies have shown that the elimination of p62 can be used to suppress tumorigenesis (Mathew, Karp et al. 2009).

The role of autophagy as a promoter in cancer

Autophagy as a Promoter of Cancer:

On the other hand, when tumors reach the late stage, the poor vascularization surrounding the tumor causes nutrient depletion, DNA damage, and hypoxia conditions (Degenhardt, Mathew et al. 2006). The functions of autophagy can be activated under certain conditions as a protective mechanism to safeguard cancer cells from environmental or intracellular stresses. Autophagy can be utilized by cancer cells to prevent damage, promote metastasis, and increase resistance against therapy.

However, autophagy can also facilitate the development of cancer by promoting metastasis. For example, starvation-induced autophagy has been shown to enhance the migration and epithelial-mesenchymal-transition (EMT) of HCC (hepatocellular carcinoma) cells (Li, Yang et al. 2013). In contrast, inhibition of autophagy has been found to significantly reduce HCC migration to the lung (Peng, Shi et al. 2013). In a hypoxic tumor environment, autophagy can be induced to protect HCC cells from apoptosis through a Beclin1-dependent mechanism (Song, Guo et al. 2011). Additionally, autophagy can promote metastasis in pancreatic cancer under hypoxic conditions through the activation of Hypoxia-inducible factor-1α (HIF-1α) and MET (Zhu, Wang et al. 2014). Moreover, autophagy also acts as a promoter of invasion and migration in HCC and bladder cancer cells through TGF-β1 signaling-mediated MET activation (Li, Yang et al. 2013, Tong, Yin et al. 2019). Furthermore, in

oncogenic RAS-driven cell migration, autophagy plays a protective role through secreted cytokines (Lock, Kenific et al. 2014).

Autophagy also plays a significant role in cancer stem cells and regulates their differentiation and pluripotency in ovarian, gastric, and breast cancer (Maycotte, Jones et al. 2015, Peng, Qin et al. 2017, Li, Pan et al. 2018). For instance, a higher expression of Beclin1 and autophagy is required for the tumorigenesis of breast cancer stem cells (Gong, Bauvy et al. 2013). Other autophagy-related factors such as p62 and DRAM1 have also been shown to regulate glioblastoma stem cell metastasis (Galavotti, Bartesaghi et al. 2013). Inhibiting autophagy has been found to enhance the efficacy of chemotherapy drugs in non-small cell lung cancer stem cells (Hao, Liu et al. 2019). Moreover, combining an autophagy inhibitor with photodynamic therapy has been found to contribute to the treatment of colorectal cancer stem-like cells (Macintosh, Timpson et al. 2012).

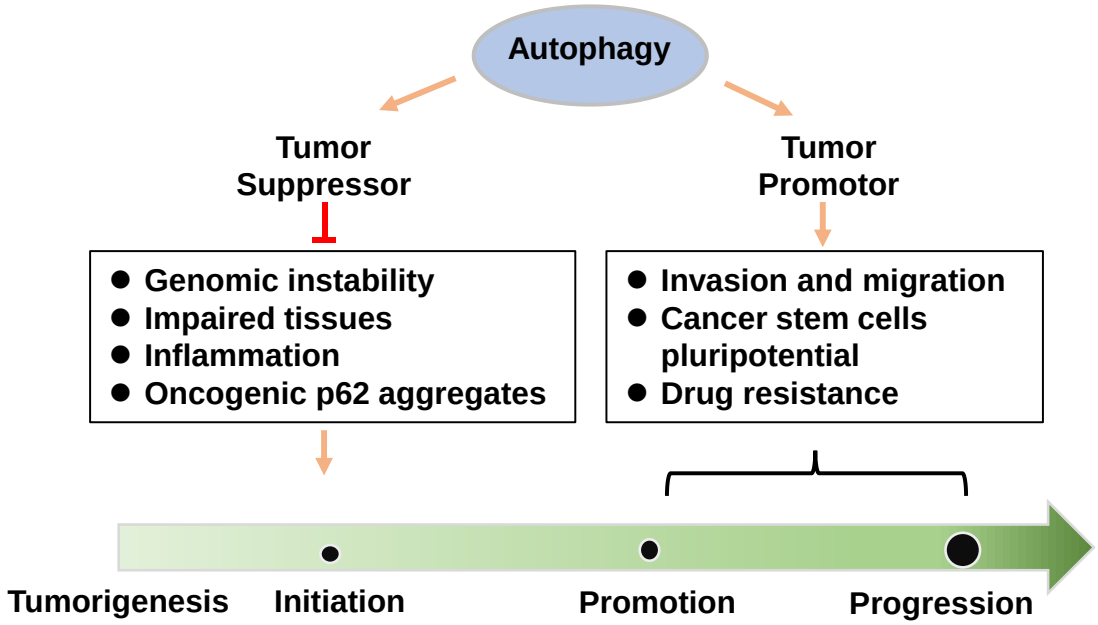


**Figure 1.6 The dual role of autophagy in tumor development.**

In short, autophagy plays dual roles in tumor suppression and promotion (Figure 1.6). At the early stages of tumor development, autophagy-related proteins function as tumor suppressors by inhibiting necrosis, inflammation, and the accumulation of oncogenic p62 protein aggregates. However, at later stages of tumor development, autophagy can act as a promoter of tumor metastasis, the pluripotency of cancer stem-like cells, and drug resistance. Therefore, further research is needed to fully understand the therapeutic potential of autophagy inducers or inhibitors as cancer treatments.

### 1.2.3 The role of autophagy in HCC

The role of autophagy in HCC is controversial (Figure 1.7). In the early stage of HCC, abnormal mitochondria and lipid droplets accumulate

in liver cells. The autophagy regulation mechanism is essential to maintain the homeostasis of liver cells to suppress the growth of early-stage neoplasm. However, late-stage HCC needs to maintain a higher metabolic status than normal liver tissue and under the stress of genotoxicity or chemotherapeutic drugs. Under this condition, active autophagy becomes a cancer promoter to relieve metabolic stress and promote cancer cell survival and proliferation of liver cancer cells. Autophagy is a dynamic change in the occurrence and development of HCC. In this dynamic process, ATG and the autophagy pathway play an important role, which also provides potential prognostic biomarkers and therapeutic value in HCC.

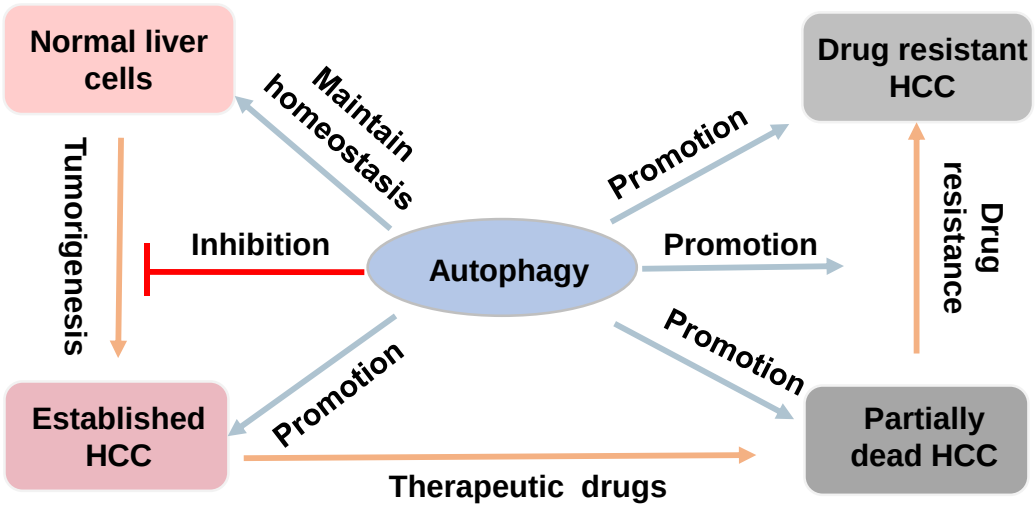


**Figure 1.7 Multiple roles of autophagy in HCC development and therapy.**

**ATG and HCC development.** Some core ATG genes have a significant impact on HCC (Table 1.1). Beclin1 is a key member of the Beclin1-

Vps34 complex, which participates in the initiation of autophagy and the maturation of autophagosomes. Studies showed Beclin1 is a haploinsufficient tumor suppressor in HCC (Yue, Jin et al. 2003). The deletion of *the BECN* gene (encoded Beclin1) in mice leads to autophagy damage, which can promote the establishment of HCC in aged mice (Qu, Yu et al. 2003). Meanwhile, the expression level of Beclin1 has a negative relationship with HCC grading. HCC tissues with a higher expression level of Beclin1 show lower recurrence and higher survival rates (Qiu, Wang et al. 2014). Beclin1-dependent apoptotic activity can be used as a prognostic indicator based on the negative correlation between Beclin1 expression level and HCC markers such as alpha-fetoprotein, cirrhosis, and vascular invasion (Shi, Ding et al. 2009, Liang, Li et al. 2018). Another key autophagy related complex UKL1 also is associated with the HCC. The high expression level of ULK1 and LC3B combination showed a poorer survival rate of HCC patients (Wu, Wang et al. 2018).

**Table 1.1** The relationship between ATG mutation or abnormal expression and HCC

| ATG | Autophagy | HCC | Ref |
|---|---|---|---|
| Beclin1$^{-/+}$ | Damaged autophagy | Promote HCC | (Qu, Yu et al. 2003) |
| High expression Beclin1 | Inhibit autophagy | Lower recurrence/ higher survival rates | (Qiu, Wang et al. 2014) |
| High expression ULK1 | Upregulate autophagy | Poor survival rate | (Wu, Wang et al. 2018) |
| p62 accumulation | Inhibit autophagy | Promote HCC formation | (Umemura, He et al. 2016) |
| ATG5 and ATG7 | Damaged autophagy | Promote HCC formation | (Komatsu, Waguri et al. 2005) |

Furthermore, autophagy-disordered induced p62 accumulation contributes to the HCC tumor formation. p62 as another autophagy marker protein also functions as a scaffold protein participating in cell proliferation, cell survival, signal transduction, and tumorigenesis. p62 accumulation is needed for HCC-related liver disease and the most HCC.

High-level expression of p62 actives NRF2 and mTORC1 and then induces c-Myc to protect HCC from oxidation stress-induced death (Umemura, He et al. 2016). Besides, the absence of *the ATG5* and *ATG7* gene with damaged autophagy in mice model, cause liver cells disordered and promote the occurrence of premalignant liver diseases (Komatsu, Waguri et al. 2005).

LC3 becomes an accomplice of cancer cell survival under stress. Meta-analysis results showed that LC3 expression level increase has a relationship with the HCC tumor size and overall survival (Meng, Lou et al. 2020). LC3 expression level in HCC tumors relates to clinical prognosis after surgical treatment (Hsu, Hsieh et al. 2019).

All those studies demonstrated ATGs participate in the formation of HCC and the role of those ATGs is intricate. Some of them have anti-tumorigenesis effects and some of them show verse effects. The application of regulation autophagic proteins as a potential therapeutic opinion for HCC still need a large of amount studies to support.

**Signaling pathway of autophagy in HCC.** PI3K/AKT/mTOR pathway is critical in promoting autophagy, apoptosis, and regulation the cell proliferation, cell death, and metabolism under physiological conditions (Figure 1.8 A). At the same time, this pathway also plays an important role in the process of various solid tumor development

including HCC (Zhou, Lui et al. 2011). Akt is a key mediator in this pathway and regulates autophagy in different manners. Using phosphatase PTEN (a key tumor suppressor) induced Akt activates the mTORC1, which can decrease the level of PI3K and induce the initiation of autophagosome formation. PI3K/Akt/mTOR pathway is positively related to HCC development (Sahin, Kannangai et al. 2004, Villanueva, Chiang et al. 2008). Activation of this pathway shows an inhibition effect on autophagy and then promotes HCC cell growth. For example, overexpression alpha-fetoprotein (AFP) interacts with PTEN to inhibit autophagy and then promotes HCC cell proliferation, migration, and invasion via activation PI3K/AKT/mTOR pathway (Wang, Zhu et al. 2018). Vice versa, inhibition of the PI3K/AKT pathway can induce autophagy and contribute to HCC therapy. For example, IL-37 activates autophagy via inhibition of this pathway and suppresses HCC. Therefore, inducing autophagic cancer cell death via targeting this pathway may be a potential therapeutic method for HCC.

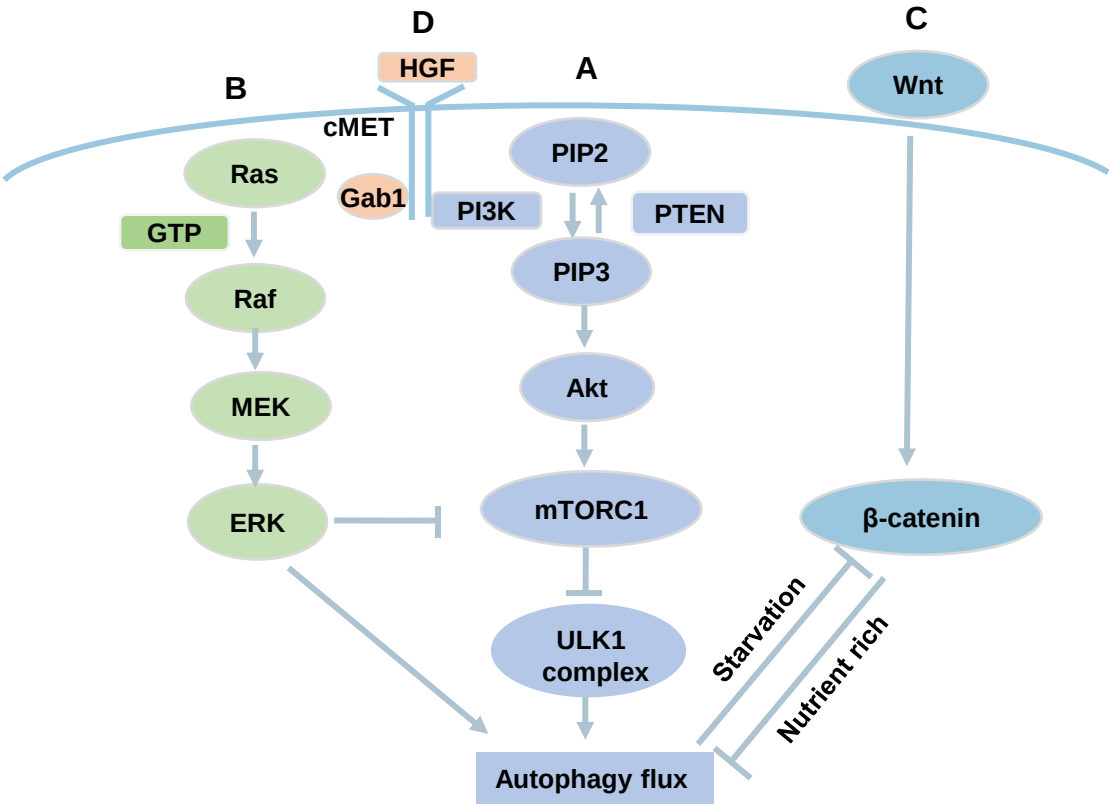


**Figure 1.8 Main pathways of autophagy in HCC.** A. The role of PI3K/AKT/mTOR pathway of autophagy. B. RAS/RAF/MEK/ERK signaling promote autophagy. C. Wnt/β-catenin pathway D. HGF/cMET pathway

The RAS/RAF/MEK/ERK pathway responds to cell surface receptors to regulate the cell cycle, apoptosis, differentiation, and the induction of autophagy in different cancer cell lines(Steelman, Pohnert et al. 2004, Balmanno and Cook 2009) (Figure 1.8 B). Firstly, this pathway plays a complex role in multiple steps of autophagy. Studies showed that ERK can promote autophagy by inhibiting mTORC1. At the same time, activation of this pathway can increase the expression level of autophagy

markers LC3 and p62 in a non-canonical way (Kim, Hong et al. 2014). By contrast, inhibition of ERK can lead to lysosomal-associated membrane protein 1 and 2 (LAMP1 and LAMP2) downregulation, thereby inhibiting autophagic degradation (Sivaprasad and Basu 2008). In addition, studies showed the abnormal mutation members of the RAS/RAF/MEK/ERK pathway contribute to HCC tumorigenesis, development, and metastasis (Samatar and Poulikakos 2014, Peng, Li et al. 2015). Clinical studies showed RAF paralogue mutation is positively related to a higher recurrence rate and survival rate in HCC (Schirripa, Bergamo et al. 2015). To eliminate the effects of mutation of the RAS gene, association domain family 1 isoform A can be used as a suppressor of HCC via activating the autophagy process (Li, Yue et al. 2019). Novel 2-phenyloxypyrimidine derivative (E5) induces autophagic cell death and apoptosis by activating MAPK/ERK pathway in HCC cells (Wang, Sun et al. 2018). Accordingly, targeting this pathway can induce autophagy and contributes to the HCC therapeutic methods development.

The wnt/β-catenin signaling pathway is an important pathway in the regulation of cell proliferation, cell death, and cell differentiation to maintain the homeostasis of tissues (MacDonald, Tamai et al. 2009) (Figure 1.8 C). The wnt/β-catenin signaling pathway especially plays a critical role in HCC tumorigenesis and determines various tumor cell

processes such as initiation, proliferation, differentiation, and migration (Whittaker, Marais et al. 2010, Shanbhogue, Prasad et al. 2011). When this pathway is in a state in the presence of the Wnt ligand, β-catenin is activated and then upregulates the target genes in the nucleus functions the process of HCC. Abnormal mutations of members in this pathway may lead to some diseases such as cancer, and birth defects. The poor prognosis of HCC is positively related to the upregulation Wnt/ β-catenin pathway (Inagawa, Itabashi et al. 2002). Besides, this pathway can also negatively regulate autophagy. β-catenin acts as a transcriptional co-repressor of p62 to inhibit the process of autophagy under nutrient-rich conditions. In addition, inhibition of this pathway causes autophagic protein accumulation such as LC3-II, Beclin1, and ATG7 (Su, Wang et al. 2016). β-catenin can also directly interact with LC3 and then induce autophagic degradation under nutrient deficiency (Petherick, Williams et al. 2013). However, the relationship among autophagy, Wnt pathway, and HCC is still unclear. Some studies showed the Wnt/β-catenin pathway inhibition by FH535 and its derivative (FH535-N) perform anti-tumor effects on HCC via regulation of autophagy flux (Turcios, Chacon et al. 2019). Tetrandrine suppresses HCC metastasis and invasion via inhibition of liver cells' autophagy, which regulates the Wnt/β-catenin pathway and decreases metastatic tumor antigen 1 (Zhang, Liu et al. 2018). In

summary, the Wnt/β-catenin pathway, autophagy, and HCC have a complex relationship. Inhibition autophagy in HCC via targeting the Wnt/β-catenin pathway may be a new target for HCC therapeutic opinions.

HGF/c-Met signaling is the hepatocyte growth factor (HGF) and its receptor tyrosine kinase, MET, which is a high expression in many HCC patients (Xie, Su et al. 2013) (Figure 1.8 D). HGF/c-MET signaling plays a key role in the development of HCC by promoting hepatocyte proliferation, epithelial-to-mesenchymal transition, invasion, and regeneration. It is observed that HGF and c-MET overexpress in almost 33% and 20–48% of human HCC samples, respectively. Compared with normal tissue, the expression of c-MET at the protein level increases obviously from 25% to 100% of liver cells, which all suggest HGF/c-MET has potential in HCC carcinogenesis (Kaposi-Novak, Lee et al. 2006). HGF/c-MET tyrosine kinases interact with phosphorylation Gab1 and regulate the downstream signaling PI3K pathway. HGF/c-MET signaling inhibits autophagy flux through interaction with PI3K. A MET inhibitor combination with an autophagy suppressor can target tyrosine1234/1235-dephosphorylated MET and autophagy to inhibit HCC tumors in vivo (Huang, Gan et al. 2019).

Many different pathways are involved in the interaction between HCC and autophagy, such as EGFR crosstalk, AMPK pathway, and Hippo pathway (Berasain, Latasa et al. 2011, Huang, Li et al. 2016, Huang, Li et al. 2016). The functions of those signaling in autophagy and HCC still need to be further investigated.

**Autophagy and sorafenib resistant in HCC**

Sorafenib is considered the first FDA-approved systemic drug for the treatment of advanced HCC patients. Clinical representative phase III trials claimed sorafenib significantly expand the median survival time of patients by about 3 months (Llovet, Ricci et al. 2008). Sorafenib as a multitargeted kinase inhibitor can block the RAS/RAF/MEK/ERK signaling pathway to suppress cancer cell growth. Sorafenib also inhibits other multiple tyrosine kinase receptors such as platelet-derived growth factor receptor-β (PDGFR-β) vascular endothelial growth factor receptor 2 (VEGFR2), and VEGFR 3 to inhibit angiogenesis (Cervello, Bachvarov et al. 2012). Nevertheless, only approximately 30% of HCC patients benefit from sorafenib treatment and acquired resistance (Cheng, Kang et al. 2009). Moreover, the treatment effectiveness of sorafenib is limited due to the primary and acquired resistance often after 6 months of treatment (Llovet, Ricci et al. 2008).

Currently, the mechanisms of HCC sorafenib resistance are still unclear and complex. Multiple factors promote the development of sorafenib resistance such as tumor microenvironment, hypoxia, and sorafenib-induced overexpression of cytokines (Shimizu, Takehara et al. 2012, Mazzoccoli, Miele et al. 2016). One of the most possible reasons is the promotion of multiple survival pathways' activity that may neutralize sorafenib-induced death signals. Autophagy as one of the most common survival pathways plays intricate roles in sorafenib resistance. Sorafenib can induce autophagy and thus protect HCC cells from drug treatment stress and excessive autophagy leads to apoptosis (Shimizu, Takehara et al. 2012). At the same time, sorafenib as a multi-kinase inhibitor can impact AMPK and Akt/mTOR pathways and some autophagy-related proteins to inhibit autophagy.

Beclin1 as a core autophagic protein can be impacted by sorafenib in different manners. Sorafenib induces Beclin1 overexpression and Beclin1 acetylation to promote autophagic response, which makes HCC cells sensitive to sorafenib treatment (Yuan, Li et al. 2014). Besides acetylation of Beclin1, sorafenib also reduces the Mcl-1 gene expression via the downregulation of STAT3 phosphorylation. Subsequently, the interaction between Beclin1 and Mcl-1 is affected resulting in the release of Beclin1 promoting autophagy in HCC cells (Tai, Shiau et al. 2013). In addition to

autophagy induction, sorafenib also inhibits autophagic response by promoting Beclin1 ubiquitination. Specifically, sorafenib induces larger tumor suppressor kinase1 (LATAS1) and subsequently promotes Beclin1 ubiquitination at its amino acid residues K32 AND K263. Beclin1 ubiquitination leads to the formation of a stable inactive dimer to inhibit autophagy and that has a relationship with sorafenib sensitivity (Tang, Gao et al. 2019).

Multiple pathways participate in sorafenib-induced autophagic response via regulating Beclin1 or modification of Beclin1 (Figure 1.9). AMPK and AKT/mTOR signaling pathway as the upstream of autophagy has a close relationship with multiple kinase activities related to sorafenib resistance. Specifically, AMPK can be induced by sorafenib via increasing the AMP/ATP ratio, which can inhibit mTORC1-induced phosphorylation of ULK1 to repress autophagy (Dai, Huang et al. 2018). In addition to the AMPK signaling pathway, sorafenib inhibits the mTOR pathway via the ERK pathway to recruit ULK1 to suppress autophagy (Li, Zhang et al. 2019). Literature demonstrated that sorafenib combined with ULK1 inhibitor or ULK1 silencing significantly suppresses the HCC malignant proliferation compared with sorafenib treatment alone (Xue, Li et al. 2020). Besides the interaction of multiple kinase pathways, sorafenib can stimulate endoplasmic reticulum (ER) stress to promote the

formation of autophagosomes via the accumulation of LC3II via the IRE1 signaling pathway (Shi, Ding et al. 2011). Sorafenib also induces ER stress-related autophagy through PKR-like ER stress kinase (PERK)-activating transcription factor (ATF)-Beclin1 pathway to produce sorafenib resistance (Zhou, Lu et al. 2019).

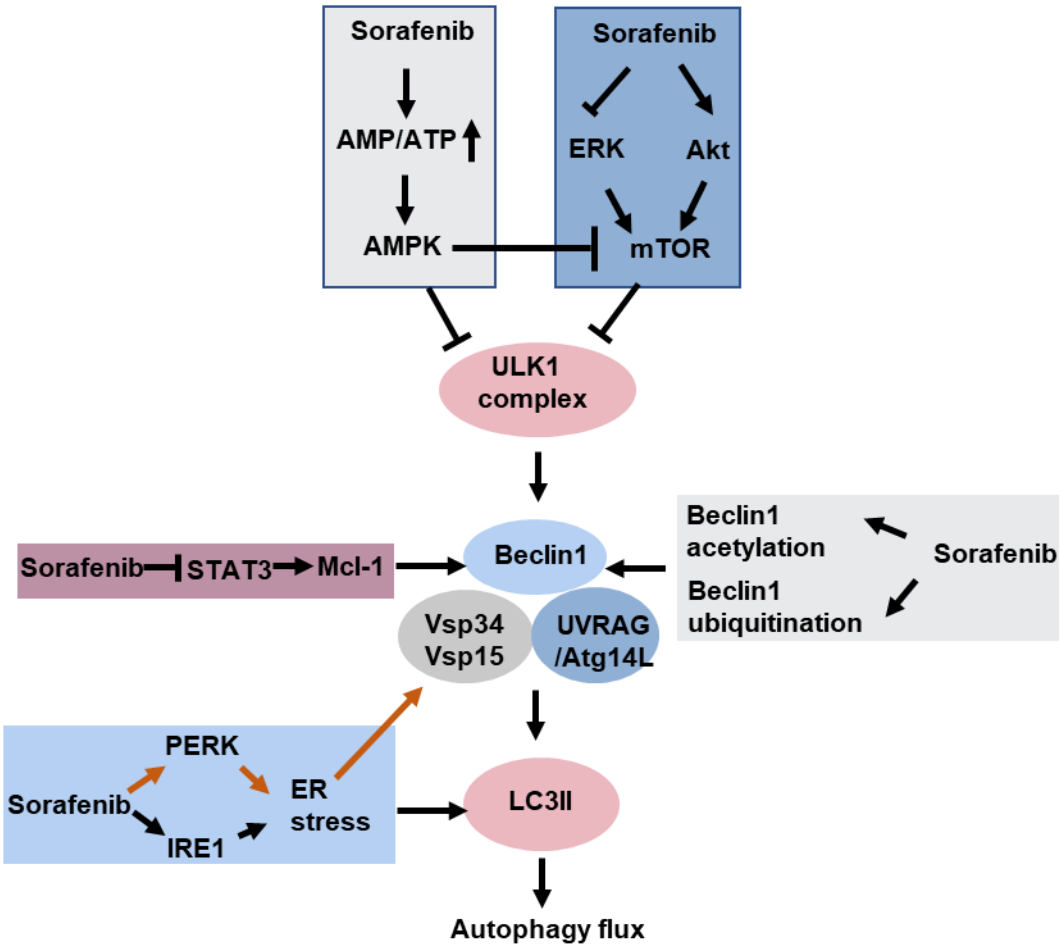


**Figure 1.9 Multiple pathways participate sorafenib induced autophagic response via regulating Beclin1 or modification Beclin1.** → refers to positive regulation or activation; ⊣ refers to negative regulation or blockade.

## 1.3 Beclin1-targeting stapled peptides as developed by our lab

### 1.3.1 The structure and function of Beclin1 in autophagy and cancer

Beclin1 is a member of the B cell lymphoma-2 (Bcl-2) family proteins. In 1998, Beth Levine's group identified a 60 kDa protein with a coiled-coil domain that interacts with Bcl-2 in a yeast two-hybrid screen. It was termed Beclin (Liang, Kleeman et al. 1998). Beclin1 is the first mammalian autophagy gene homolog of yeast Atg6/vps30 (Aita, Liang et al. 1999).

Beclin1 is the first gene that makes autophagy associated with human cancers (Liang, Jackson et al. 1999). As mentioned before, Beclin1 is a tumor suppressor gene. Mono-allelically deleted Beclin1 was detected in 40-75% of human breast cancer, prostate cancer, ovarian cancer (Liang, Jackson et al. 1999). Monoallelic deletion of Beclin1 in mice models may play a critical role in tumorigenesis. Direct knockout or mutation at a mono-allelic Beclin1 causes higher rate of the development of spontaneous sporadic cancers such as HCC, ovarian, breast, lymphoma, lung cancer, and ovarian cancers (Aita, Liang et al. 1999, Liang, Jackson et al. 1999, Jin and White 2007, Ding, Shi et al. 2008). Heterozygous knockout of Beclin1 also accelerates the development of hepatitis B virus induced HCC (Qu, Yu et al. 2003). Beclin1-dependent apoptotic activity can be used as a prognostic indicator based on the negative correlation

between Beclin1 expression level and HCC markers such as alpha-fetoprotein, cirrhosis, and vascular invasion (Shi, Ding et al. 2009, Liang, Li et al. 2018). In addition, Beclin1 modifications such as phosphorylation, ubiquitination, and acetylation have been functionally implicated autophagy to suppress tumor growth. For an instant, some oncogenic receptor tyrosine kinases such as EGFR in NSCLC, HER2 in breast cancer, and Akt in a Rat2 fibroblasts xenograft model involve the phosphorylation of Beclin1 at different tyrosine residues that eventually regulate the activity of the PI3KC3 to inhibit autophagy and affect tumor growth (Wang, Wei et al. 2012, Vega-Rubín-de-Celis, Kinch et al. 2020). Furthermore, the expression level of Beclin1 links to tumorigenesis and prognosis of HCC via inhibition autophagy. Higher Beclin1 expression in HCC patients is positively correlated with 5-year survival rates (Qiu, Wang et al. 2014).

Human Beclin1 is a protein with 450 amino acids and is usually divided into three main functional domains: an intrinsically disordered N-terminal region (1-150 residues) contains multiple phosphorylation sites, and a Bcl-2 homology-3 (BH3) domain responsible for interaction with Bcl-2 proteins (Lee, Perugini et al. 2016, Yao, Lee et al. 2016). A coiled coil (CC) domain (residues 174–266) is responsible for interactions with UVRAG or Atg14L. And the β-α autophagy-specific

(BARA) domain (residues 266–450) is a class of membrane-binding domain (Figure 1.10 A).

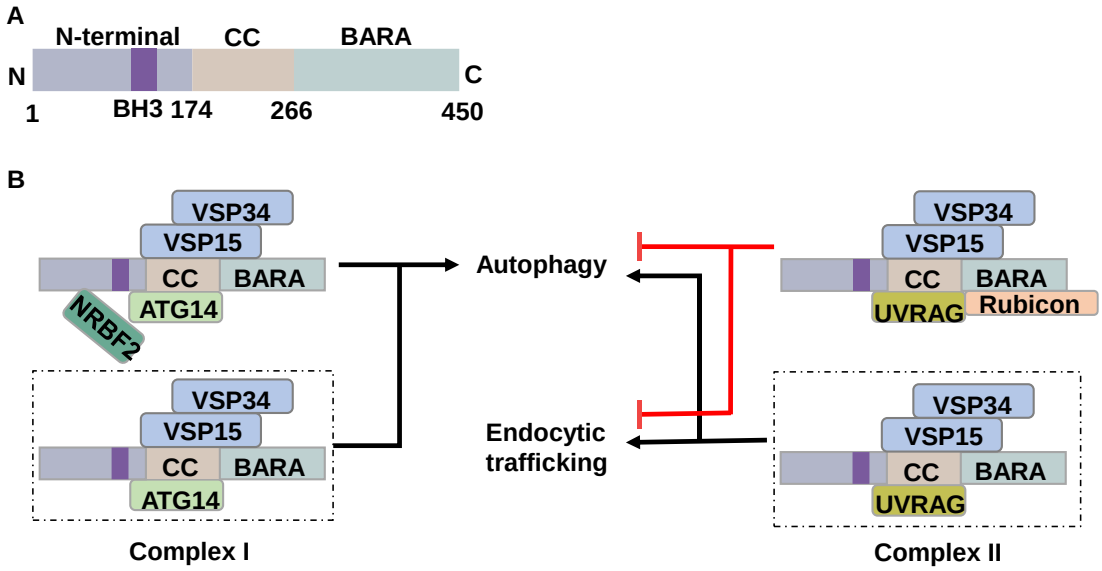


**Figure 1.10 The structure and function of Beclin1 in autophagy** (Tran, Fairlie et al. 2021). **A**. the diagram model of the structure of Beclin1. CC refers to coiled coil domain, BARA refers to β-α autophagy-specific domain. **B.** The function of Beclin1 in autophagy and the main compounds of Class III PI3K complex.

Beclin1 forms complexes with different proteins to regulate autophagy (Figure 1.10 B). Beclin1 is a core scaffold protein in mammalian Class III phosphatidylinositol 3-kinase (PI3KC3) complex. Class III PI3K complex phosphorylates phosphoinositides (PIs) at the 3'-hydroxyl group on the inositol ring (Kihara, Kabeya et al. 2001). Class III PI3K is indispensable in membrane trafficking and assessment of different proteins to mediate intracellular membrane transportation

processes involved in autophagy, phagocytosis, endocytosis, and cytokinesis. Beclin1 interacts with PI3KC3 catalytic unit Vacuolar Protein Sorting 34 (Vps34), therefore, PI3KC3 complex is also called Beclin1-Vps34 complex. Mammalian beclin1-Vps34 forms multiple complexes including the core proteins beclin1, Vps34, and Vps15 that interacts with Vps34 as a stable binding partner that associates with some other assistant proteins involved in UVRAG, Atg14L, Rubicon, Bif-1 and Ambra1(McKnight, Zhong et al. 2014). Beclin1 as an indispensable regulator in the PI3KC3 complex, facilities multiple physiological processes involving innate immunity, embryonic development, and glucose metabolism. Beclin1 is associates with various human pathologies such as cancers, infectious diseases, and neurodegenerative diseases (Levine, Liu et al. 2015, Levine and Kroemer 2019).

As a scaffolding protein, Beclin1 interacts with Vps34, and Vps15 and directly recruits Atg14L/UVRAG or other accessory proteins to form three classes of PI3KC3. All complexes are composed of the three core proteins Beclin1, Vps15, and Vps34, but differ in their fourth or fifth core subunit. In PI3KC3-C1, Atg14L is the fourth core subunit and sometimes includes nuclear receptor binding factor 2 (NRBF2). The C1 complex primarily participates the autophagy specifically in the nucleation of autophagosomes (Itakura, Kishi et al. 2008, Sun, Fan et al. 2008). The

subunit of NRBF2 promotes the interaction of Atg14L with Vps34 (Cao, Wang et al. 2014). The C2 complex including UVRAG as the fourth core subunit regulates autophagosome nucleation and endocytic trafficking (Itakura, Kishi et al. 2008, McKnight, Zhong et al. 2014). Based on the structure of the C2 complex, sometimes UVRAG and Rubicon as the fourth and fifth core subunits to form a C3 complex that inhibits the autophagic process (Matsunaga, Saitoh et al. 2009, Zhong, Wang et al. 2009, Sun, Zhang et al. 2011). The presence of Rubicon in C3 regulates both autophagy and endocytic trafficking negatively (Matsunaga, Saitoh et al. 2009, Zhong, Wang et al. 2009). Taken together, Beclin1 is critical for the formation of PI3KC3 to regulate autophagy and endocytic trafficking.

Structural studies from our lab and others delineate the molecular mechanism of how Beclin1 regulates PI3KC3 complex activities. Our previous crystal structure of the homodimerized Beclin1 CC domain indicates that a homodimer is a metastable form due to the presence of several imperfect and destabilizing residue pairings in the hydrophobic interface (Li, He et al. 2012). However, mutually exclusive binding between Beclin1 and Atg14L or UVRAG depending critically on their respective coiled-coil domains is more stable than that of homodimer (Wu, He et al. 2018). The molecular mechanism of stable heterodimers is

that hydrophobic pairings and electrostatically complementary interactions significantly strengthen the coiled-coil interface (Wu, He et al. 2018). Interestingly, Beclin1-UVRAG dimers have a higher binding affinity than that of Beclin1-ATG14 dimers resulting in Beclin1 being prone to form C2 complexes, which may associate with the different activities of C1 and C2.

### 1.3.2 Structure-based rational design of Beclin1-targeting stapled peptides

Using the above-mentioned structure information as guidance, we designed a series of peptides that specifically bind to the Beclin1 coiled-coil domain. Those peptides facilitate disruption of the metastable CC domain interface in the Beclin1 homodimer and promote the formation of Beclin1-UVRAG/Atg14L heterodimer to induce autophagy and endocytic trafficking(Wu, He et al. 2018). These novel peptides have been issued a US patent in 2020 (Patent No. US 10,618,939 B2).

The design principle of stapled peptides. Protein-protein interaction is fundamental for the design of stapled peptides. Proteins are the workhorses that facilitate most biological processes in cells. Many proteins interact with others for proper biological activity. Protein-protein interaction (PPI) is a hot point in current clinical research. PPIs are potential drugs targeted by blocking specific interaction sites. While

small molecule inhibitors have had some success and reached clinical trials, they remain no substitute for the natural properties of proteins and their peptide subunits in most PPIs. Some larger biologics were developed for PPI surfaces, and they have successfully targeted PPIs in vitro. However, larger biologics have low bioavailability and cannot reach intracellular targets.

A novel class hydrocarbon stapled α-helical structure through the site-specific introduction of a chemical linker has shown promise to avoid the above issues. The building blocks for hydrocarbon stapling are α, α-disubstituted non-natural amino acids bearing terminal olefin tethers of varying lengths. Hydrocarbon stapled α-helical structure has many excellent properties such as soluble, protease-resistant, cellular penetrant, and biological activity upon successful incorporation of a series of design and application principles (Walensky and Bird 2014). Stapled peptides have wide applications in various diseases such as cancer, infectious diseases, metabolism, and neuroscience (Walensky and Bird 2014).

A s above mentioned, Hydrocarbon stapled α-helical structure has many excellent properties. Our lab designed a series of Beclin1-specific targeting stapled peptides. Structure studies from our lab show the N-terminal CC domain (residues 174-223) of Beclin1 is essential for interacted with UVRAG and Atg14L and disruption of C-terminal

(residue 241 and 245) of CC domain weak Beclin1 homodimer interaction. To avoid designed stapled peptides interference with the Beclin1-UVRAG interaction of the CC domain, stapled peptides specific binding to the C-terminal region of the Beclin1 CC domain. In addition, residues Y231 and S232 are phosphorylation sites targeted by EGFR and Akt, which is related to tumorigenesis. Inhibition of these phosphorylation sites potentially suppresses cancer cell proliferation. Therefore, the C-terminal region (residues 231-245) of the CC domain becomes an effective target (Figure 1.11AB).

We have computationally generated a series of Beclin1-targeting stapled peptides by simply taking the α-helical segment that ensures specific binding to the target region. A two-turn hydrocarbon staple is introduced *in silico* that links residues (i) and (i+7) to maintain the helical structure of this short segment (Figure 1.11 C). Un-natural amino acids R8 and S5 with olefin terminal were applied at residues (i) and (i+7) to stabilize the alpha helices, protect small peptides from proteolytic degradation, and increase cell penetration ability (Figure1.11 D).

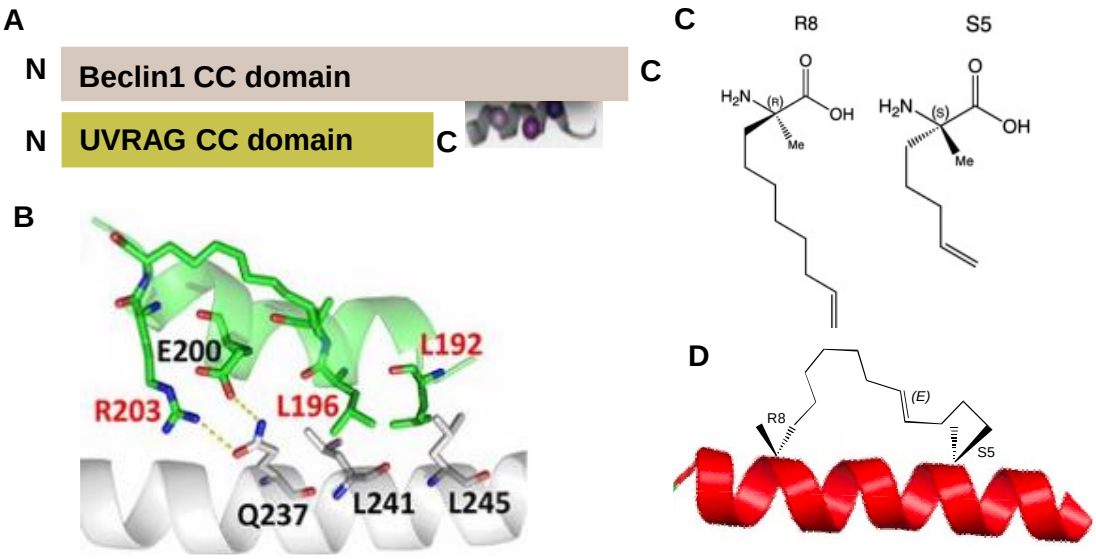


**Figure 1.11 Structure-based rational design of Beclin1-targeting stapled peptides A.** The design principle of stapled peptides. UVRAG interacts with the N-terminal of Beclin1 CC domain. The α-helix structure refers to the stapled peptide binding to the C-terminal of Beclin1 CC domain. **B.** A model of Beclin1-targeting stapled peptides binding to C-terminal region of Beclin1 CC domain. **C.** The structure of two un-natural amino acids. **D.** The structure and position model of hydrocarbon staple. The hydrocarbon staple is added at residues (i) and (i+7) to stabilize the alpha helices.

A library of stapled peptides (SPs) was generated after computational optimization to increase the binding affinity between peptides and the target region. Amino acid residues at essential targeting sites were maintained and amino acid residues at other sites were computationally varied (Table 1.2). Based on the binding ability to the

target region, 12 stapled peptides were designed as the top candidates. Peptides SP4, SP9, and SP12 with high binding affinities were synthesized.

**Table 1.2** Computationally designed 12 stapled peptides and their binding affinity.

| Number | Sequence | Interaction energy (kcal/mol) |
|---|---|---|
| SP1 | Ac-RLIQEL(R8)DREAQR(S5)V-$NH_2$ | -29.75±6.62 |
| SP2 | Ac-TLIQEL(R8)DREAQR(S5)S-$NH_2$ | -43.69±5.21 |
| SP3 | Ac-RLISEL(R8)DREKQR(S5)V-$NH_2$ | -47.51±3.96 |
| SP4 | Ac-RLISEL(R8)DREKQR(S5)A-$NH_2$ | -56.05±6.87 |
| SP5 | Ac-RLIQEL(R8)DREKQR(S5)S-$NH_2$ | -40.75±5.59 |
| SP6 | Ac-RLISEL(R8)DREKQR(S5)S-$NH_2$ | -47.40±6.90 |
| SP7 | Ac-RLIQEL(R8)DREKQR(S5)R-$NH_2$ | -45.77±5.13 |
| SP8 | Ac-RLIQEL(R8)DREKER(S5)A-$NH_2$ | -49.78±6.34 |
| SP9 | Ac-LLISEL(R8)DREKQR(S5)A-$NH_2$ | -74.52 ±4.31 |
| SP10 | Ac-RLLSEL(R8)DREKQR(S5)A-$NH_2$ | -55.69 ±5.15 |
| SP11 | Ac-LLLSRL(R8)DREKQR(S5)A-$NH_2$ | -50.47 ±5.23 |
| SP12 | Ac-LLISQL (R8)DREKQR(S5)A-$NH_2$ | -56.05±4.35 |

### 1.3.3 Strategies to generate cell-penetrating stapled peptides for drug discovery

The presence of cell membranes protects cells from outside environments and is also a natural barrier to the entrance of drugs. To achieve the intended effect of a drug, it must transport across the plasma membrane and reach its target region. It is difficult because the

cytoplasmic membrane consists of two layers of phospholipids, proteins, cholesterols, and glycolipids and it also has membrane potential. It is selectively permeable to ions and some small molecules. Only some highly lipophilic or very small drugs can transport across the plasma membrane. It is very restrictive for practical applications of a broad range of bioactive agents such as peptides and oligonucleotides due to their cell-impermeable features. An even more difficult specific case is the delivery of drugs into the blood-brain barrier which is very critical for neurodegenerative diseases treatments. Current strategies for the delivery of macromolecules such as viral-based vectors, electroporation, microinjection, and other membrane perturbation approaches may lead to high cytotoxicity, low delivery efficiency, poor specificity, as well as immunogenicity (Kang, Sun et al. 2016, Shi, Ma et al. 2018, Hao, Li et al. 2019, Yang, Shi et al. 2020). Recently, the advent of cell-penetrating peptides (CPPs) has received more attentions because CPPs can carry a wide range of biologically active cargoes to transport into the cell with a high transduction efficiency.

CPPs also termed protein transduction domains (PTDs). They are positively charged short peptides with no more than 30 amino acids. Different from other delivery approaches mentioned above, CPPs can transport across the plasma membrane in a noninvasive way, as they

usually do not damage the structure of biological membranes and are considered low toxicity and high delivery efficient. CPPs can transport across the cell membrane with different types of drugs not only including small macromolecular drugs such as nucleic acids, peptides, imaging agents, and viruses but also involving some cargo complexes (Tobin, Laban et al. 1991, Bechara and Sagan 2013, Tripathi, Arami et al. 2018). Recently the number of CPP-based preclinical trials has increased which makes CCPs become a promising strategy to be predominantly applied in basic and preclinical studies for therapeutic and diagnostic diseases such as cancer, central nervous system disorders, inflammation, ocular disorders, and diabetes. Table 1.3 shows a list of the majority of characterized CPPs that are common used in drug delivery and scientific studies (Guidotti, Brambilla et al. 2017).

The strategies for linking delivery cargos to CPPs include covalent bonds or non-covalent complexes. Agents such as peptides, proteins, and small drug molecules can be covalently coupled to CPPs by chemical linkages or expression CPPs fusion proteins. However, the main drawbacks of this strategy are covalent linkage may interfere with the bioactivity of cargo and can be digested by proteases. Non-covalent complex formation mainly relies on electrostatic and hydrophobic

interactions between cargos with negative charges such as oligonucleotides and CPPs with positive charges.

**Table 1.3** Samples of some common CPPs in different classes.

| Name | Sequence | Origin | Class | Ref |
|---|---|---|---|---|
| $Tat_{47-57}$ | YGRKKRRQRRR | HIV-1 Tat protein | Cationic | (Park, Ryu et al. 2002) |
| $Tat_{48-60}$ | GRKKRRQRRRPPQ | HIV-1 Tat protein | Cationic | (Vives, Brodin et al. 1997) |
| Penetratin | RQIKIWFQNRRMKWKK | Drosophila | Cationic | (Joliot, Pernelle et al. 1991) |
| Poly-arginines | Rn (n>8) | Synthetic | Cationic | (Futaki, Suzuki et al. 2001) |
| DPV1047 | VKRGLKLRHVRPRVTRMDV | Synthetic | Cationic | (De Coupade, Fittipaldi et al. 2005) |
| MPG | GALFLGFLGAAGSTMGAWSQPKKKRKV | HIV glycoprotein 41/SV40 T antigen NLS | Amphipathic | (Morris, Deshayes et al. 2008) |
| Pep-1 | KETWWETW | Tryptophan- | Amphipathic | (Morris, |

| | | | | |
|---|---|---|---|---|
| | WTEWSQPKKKRKV | rich cluster/SV40 T antigen NLS | | Deshayes et al. 2008) |
| pVEC | LLIILRRRIRKQAHAHSK | Vascular endothelial cadherin | Amphipathic | (Elmquist, Hansen et al. 2006) |
| BPrPr | MVKSKIGSWILVLFVAMWSDVGLCKKRP | N terminus of unprocessed bovine prion protein | Amphipathic | (Magzoub, Sandgren et al. 2006) |
| MAP | KLALKLALKALKAALKLA | Synthetic | Amphipathic | (Oehlke, Scheller et al. 1998) |
| VT5 | DPKGDPKGVTVTVTVTVTGKGDPKPD | Synthetic | Amphipathic | (Oehlke, Krause et al. 1997) |
| Bac7 | RRIRPRPPRLPRPRPRPLPFPRPG | Bactenecin family of antimicrobial peptides | Amphipathic | (Sadler, Eom et al. 2002) |
| C105Y | CSIPPEVKFNKPFVYLI | α1-Antitrypsin | Hydrophobic | (Rhee and Davis 2006) |
| Pep-7 | SDLWEMMMVSLACQY | CHL8 peptide phage clone | Hydrophobic | (Gao, Mao et al. 2002) |

Based on the physicochemical properties, CPPs could be simply classified into three groups: cationic, amphipathic, and hydrophobic peptides. the cationic class CPPs is a short peptide rich in arginine (R) and lysine (K) with highly positive charges at physiological pH conditions. This class peptide includes Tat-derived peptides, penetration, polyarginine, and Diatos peptide vector 1047 (DPV1047) (Derossi, Joliot et al. 1994, Vives, Brodin et al. 1997, Wender, Mitchell et al. 2000, Park, Ryu et al. 2002, De Coupade, Fittipaldi et al. 2005) (Table 1). The transduction properties of cationic CPPs mainly rely on the number of arginines and the order of the amino acids within the peptide sequence. The ability to penetrate the membrane gradually increases with the increase of the number of arginines. To achieve a good membrane-penetrating effect, the structural requirements of cationic CPPs contain at least 8 positively charged amino acids (Wender, Mitchell et al. 2000, Tünnemann, Ter-Avetisyan et al. 2008). Although lysine has a cation like an arginine, arginine residues contribute more to transmembrane efficiency than lysines (Wender, Mitchell et al. 2000, Tünnemann, Ter-Avetisyan et al. 2008). Arginine contains a guanidinium group that is capable of connecting with the negatively charged cell membrane by hydrogen bonds. At variance, lysine does not contain a guanidinium group.

Amphiphilic CPPs contain both hydrophilic and hydrophobic domains. Amphiphilic CPPs are generally divided into four subgroups: primary, secondary α-helical, β-sheet, and proline-rich amphiphilic (Milletti 2012). One of the primary amphipathic CPPs is covalently linked with a hydrophobic domain to NLSs (nuclear localization signal) of the simian virus 40 (SV40) such as MPG, and Pep-1 (Table 1) (Morris, Deshayes et al. 2008). Other primary amphipathic CPPs are isolated from natural proteins, such as vascular endothelial cadherin (pVEC), the p14 alternative reading frame (ARF) protein-based (1-22), and the N-terminus of the unprocessed bovine prion protein BPrPr (1-28) (Elmquist, Hansen et al. 2006, Magzoub, Sandgren et al. 2006, Johansson, El-Andaloussi et al. 2008). Secondary α-helical amphipathic CPPs with both hydrophilic and hydrophilic residues localized on different surfaces of the helical structure that binds to the membrane through α-helix such as model amphipathic peptide (MAP) (Oehlke, Scheller et al. 1998). For β-sheet amphiphilic CPPs, the ability to form β-sheets is crucial to their membrane penetration ability such as VT5. In proline-rich CPPs, polyproline is very easy to form and stabilize the standard an α-helix or a β-sheet such as bovine antimicrobial peptide 7 (Bac7)(Sadler, Eom et al. 2002). Hydrophobic CPPs mainly contain non-polar amino acid residues that cause a net charge is less than 20%. Those hydrophobic motifs or

chemical groups are critical for membrane penetration. This class CPPs has a limited number such as C105Y, Pep-7 (Rhee and Davis 2006).

The mechanisms for cellular uptake of CPPs are still unclear and not fully understood. The route of CPPs entry cells is broadly divided into direct penetration and endocytosis. The process of direct penetration is energy-independent and mainly depends on initial electrostatic interactions or hydrogen bonding between the positively charged CPP and phospholipid bilayer (Pescina, Ostacolo et al. 2018).

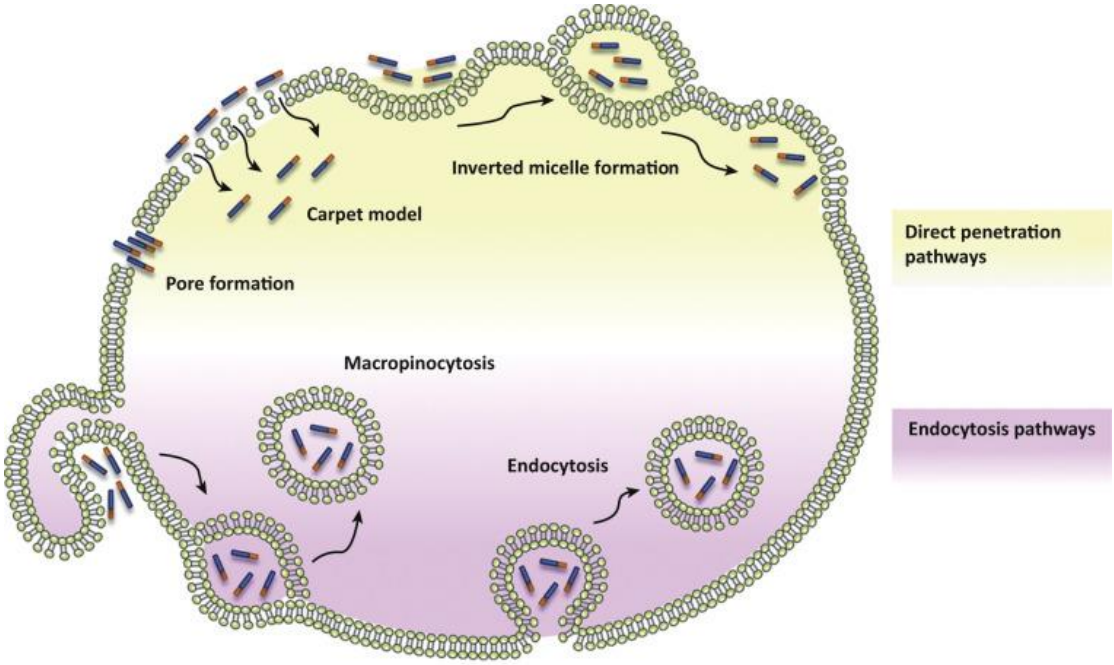


**Figure 1.12. The mechanisms of CPPs transport across the cell membrane.** This figure shows the mechanism of CPPs internalization are classified into two pathways: direct penetration and endocytosis (Guidotti, Brambilla et al. 2017).

Based on the different mechanisms of CPP internalization, direct penetration is mainly grouped into three models: pore formation models, “carpet-like” model, and inverted-micelle model (Figure 1.12). In pore formation models, two different kinds of pores “toroidal” pores and “barrel-stave pores” are shaped by CPPs. In the “toroidal” pore model, CPPs accumulate on the outer membrane and interact with different components of the membrane leading to the distortion of the membrane and then causing the formation of transient pores (Herce and Garcia 2007). Interaction with glycosaminoglycans, fatty acids, and cell membrane potential plays a critical role in the cellular uptake of CPPs. Specifically, CPPs with guanidinium groups that binds to fatty acids mediate the formation of a transient toroidal pore at high pH conditions. In the “barrel-stave pore” model, amphipathic CPPs transient the plasma membrane. Their hydrophobic domains interact with the phospholipid of the membrane, while hydrophilic domains interact with the hydrophilic head of the phospholipid to form an α-helical structure based barrel-stave pore in the membrane (Järver, Mäger et al. 2010, Kauffman, Fuselier et al. 2015). This model is capable of the uptake of hydrophilic parts of CPPs. In addition, membrane destabilization triggers other direct translocation models: the “carpet-like model” and the “inverted-micelle” model. In the former case, positively charged residues of CPPs combine

with the membrane surface resulting in a transient increment in membrane fluidity (Pouny, Rapaport et al. 1992, Thennarasu, Tan et al. 2010). The “inverted-micelle” model mainly relies on the invagination of a phospholipid bilayer and the formation of the inverted micelle (Alves, Goasdoué et al. 2008). Recently, a study showed a new mechanism of CPP's direct translocation is membrane potential dependent. Cationic CPPs such as Tat or Tat-linked with cargos directly penetrate cells by decreasing the membrane potential (Trofimenko, Grasso et al. 2021). Direct penetration routes are most suitable for CPPs binding with small cargoes passing through the cell, while large molecules weight CPPs and their cargos mainly rely on endocytosis.

Endocytosis is an energy-dependent process for CPPs penetration. Compared with a direct translocation manner, endocytosis is the prevailing mechanism for large molecules weight CPPs or CPPs cargoes. According to the district pathways, endocytosis is divided into micropinocytosis, clathrin-mediated endocytosis, caveolin-mediated endocytosis, and clathrin/caveolin-independent endocytosis (Figure 1.12). The main process of micropinocytosis is in a lipid raft-dependent and receptor-independent manner. CPPs active rac-protein to trigger F-actin organizations that is responsible for endocytic vesicle formation to complete CPP/cargoes internalization (Xu, Khan et al. 2019). Clathrin-

mediated endocytosis is receptor-mediated endocytosis. clathrin and hetero-tetrameric protein accumulation lead to a pit formation that further develop to form a clathrin-coated vesicle encasing CPPs (Yang, Luo et al. 2019). Similar to clathrin, caveolin participates in endocytosis which is also a receptor-dependent manner. CPPs interact with lipid rafts at a hydrophobic region rich in cholesterol and sphingomyelin (Zhao, Chen et al. 2015). The feature of CPPs and cargoes such as size, and physicochemical nature decides which pathway is predominant. Although endocytosis can translocate most of the CPPs and cargoes, peptides remain trapped in endosomes in cellular. Therefore, escape from endocytic vesicles is essential for the application of delivery cargoes. Unfortunately, the precise mechanism of endosomal escape is still unclear. Various agents have been explored to increase escape efficiencies such as endosmotic peptides and modified polymers (Lundberg, El-Andaloussi et al. 2007, Sugita, Yoshikawa et al. 2007, Sirsi, Schray et al. 2008). For example, a transduction of Tat-HA peptides introduction of a sequence of pH-sensitive domains destabilizes lipid membranes at acidic pH endosomes (Wadia, Stan et al. 2004). In addition, a Tat peptide insertion into histidine moieties enhances the escape ability from endosomes for DNA delivery (Lo and Wang 2008).

Tat (trans-activator of transcription) also named protein transduction domain (PTD) protein comes from human immunodeficiency virus 1 (HIV-1). $Tat_{48-60}$ is one of the primary truncated versions with 13 amino acids functionally cellular uptake (Vives, Brodin et al. 1997). Park and collaborators further investigated Tat sequence could be reduced to 8 residues Tat $_{49-57}$. Those Tat sequences belong to cationic CPPs which are one of the most common tools to deliver drugs into cells. Based on district features of cargoes, Tat-cargoes enter cells even the blood-brain barrier by either direct penetration or endocytosis. Tat-derived CPPs are widely applied in various drug delivery such as proteins, peptides, DNAs, siRNAs, and small drugs. Even some Tat-derived drugs have been investigated in preclinical or clinical trials and became promising therapeutic methods in various diseases including neurological disorders, cancers, and myocardial IR injury.

Cerebral ischemia is one of the common neurological disorders, which cause oxygen deprivation in brain tissue resulting in neuronal cell death. A PTD (Tat $_{47-57}$) hemagglutinin (HA)-Bcl-XL fusion protein significantly reduces the onset of ischemia in a dosage-dependent manner in mice models (Cao, Pei et al. 2002). In addition, Tat $_{47-57}$ conjugates with a mutant form of the Bcl- $X_L$ also shows neuroprotective effect in ischemia model (Asoh, Ohsawa et al. 2002). Furthermore, Tat $_{48–57}$

conjugates with the BH4 domain of Bcl- XL and reduces focal degeneration of astrocytes in amyotrophic lateral sclerosis via the regulation of intracellular calcium signals (Martorana, Brambilla et al. 2012). The same cargo BH4 domain conjugates to anther Tat-derives (Tat $_{48–60}$) prevents myocardial ischemia-reperfusion (IR) injury in mice model (Boisguerin, Redt-Clouet et al. 2011). Tat-JBD$_{20}$ is Tat conjugated with c-Jun N-terminal kinase (JNK) interaction protein-1 that protects against cerebral ischemia and prevents synaptic dysfunction in AD mice model (Borsello, Clarke et al. 2003, Sclip, Tozzi et al. 2014). Tat-derived drugs also shows protective effects in ischemia-reperfusion (IR) damage in animal model. For example, Tat $_{47-57}$ linked with an activation of delta protein kinase C (δ-PKC) -selective inhibitor peptide δV1-1 reduced cellular injury in IR damage model (Bright, Raval et al. 2004).

Some traditional chemotherapies lack specificity and cause high toxicity. Tat-derived sequence conjugated with drugs has been investigated for providing novel therapeutic approaches in cancers. p53 plays an important role in the cell cycle and apoptosis during the development of cancers. The loss or mutation of p53 is present in various human cancers (Vousden and Lu 2002). Thus, rescuing the endogenous proapoptotic activity of p53 in cancer cells becomes a strategy to inhibit

the abnormal proliferation of tumor cells. $Tat_{47-57}$ linked to a modified version of the C-terminal functional region of p53 form stable peptides named RI-TAT-p53C' that can induce apoptosis and significant extent lifespan in peritoneal carcinomatosis and peritoneal lymphoma models (Snyder, Meade et al. 2004).

As mentioned above, Tat-derived CPPs are widely used in various drug delivery. To ensure our stapled peptides enter cells to target Beclin1 in vivo, Tat $_{47-57}$ (YGRKKRRQRRRP) was introduced in front of SPs. In addition, to stabilize SPs, an acetyl group (Ac-) and an amine group (-$NH_2$) was used to modify the N- and C- terminals of peptides. Tat-SPs contain two features, including the N-terminal Tat sequence with positive charges to assist cell penetration and the C-terminal α-helix that specifically binds to the coiled coil domain of Beclin1 (Figure 1.13). A two-turn hydrocarbon staple is added to the C-terminal region *in silico* that un-natural amino acids R8 and S5 with olefin terminal were applied at residues (i) and (i+7) to stabilize the alpha helices, ensuring small peptides specifically targeting Beclin1 CC domain, protect them from proteolytic degradation, and enhance cell penetration ability. These peptides readily promoted Beclin1-mediated processes including autophagy and endolysosomal degradation of EGFR in multiple cell lines including HEK293T, non-small-cell lung cancer cell lines (NSCLC)

A549 and H1975, and the $HER^{2+}$ breast cancer cell line SKBR3 (Wu, He et al. 2018, Yang, Qiu et al. 2021). Tat-SP4 as one of the top candidates was synthesized by chemical methods. Tat-SP4 also showed an anti-proliferative effect in SKBR3 by enhancing EGFR/HER2 degradation and inducing necrotic cell death (Yang, Qiu et al. 2021). Encouraged by this finding, we set out to explore if Tat-SP4 would show similar effect in HCC cells and investigate the mechanism of Tat-SP4 induced cell death.

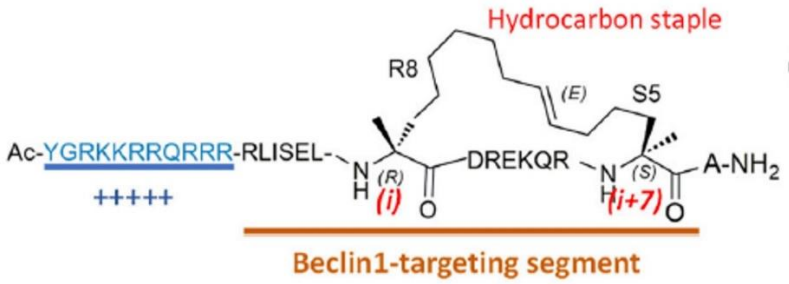


**Figure 1.13 The structure of our Beclin1-targeting stapled peptides Tat-SP4.** Beclin1-targeting stapled peptide consists of two segments, including the N-terminal $Tat_{47-57}$ with positively charged segment and the C-terminal α-helix that is stabilized by a hydrocarbon staple for specific binding to Beclin1.

In this project, we first investigate whether Tat-SP4 can induce a diverse autophagic response in HCC cell lines with different genetic backgrounds. In contrast to our previous observation in other cancer cell lines, Tat-SP4 shows a limited effect on endolysosomal EGFR degradation in HCC cell lines. Interestingly, Tat-SP4 significantly induces

the degradation of the cell surface receptor c-MET. Furthermore, Tat-SP4 induces significant cell death in HCC cell lines with different genetic backgrounds in vitro. Interestingly, Tat-SP4 can override the sorafenib resistance effect in various sorafenib-resistant HCC cells. In addition, we also explored the molecular mechanism of Tat-SP4-induced HCC cell death. Finally, the anti-proliferation effect of Tat-SP4 was further investigated in the HCC patient-derived xenograft tumor mouse model. These data suggest that our Beclin1-targeting stapled peptides may become one of the potential and novel therapeutic candidates for HCC treatment.

## 2 Objective

HCC is the most common primary liver cancer accounting for about 90%. Currently, it is the fourth leading cause of cancer-related death in the world. And China counting for nearly half of all new cases, which brings a huge health burden for China and HK. Unfortunately, only a few patients are diagnosed at an early stage. Most HCC cases are diagnosed at the mid-to-late stage with a very low survival rate. At this stage, the treatment options are limited. Due to liver dysfunction, most patients can't stand for chemotherapy agents. Poor response to treatment with higher recurrence. Currently, targeted therapies and immune checkpoint therapies can be used as the first-line drugs for advanced HCC patients. However, they usually offer limited survival benefits and low response rates. Hence, there is an urgent need for effective treatment strategies in HCC.

In my project, we plan to investigate the possibility of our lab-designed Beclin1-targeting stapled peptide (Tat-SP4) as a novel therapeutic option for HCC. We first confirm whether Beclin1-targeting stapled peptides can promote autophagic response and endolysosomal degradation of cell surface receptors in HCC cell lines with various genetic backgrounds. Next, we investigate the anti-proliferation effect of our peptide in HCC cell lines and drug-resistant cell lines. Furthermore,

we also explored the molecular mechanism of our peptides-induced HCC cell death. Finally, the anti-proliferation effect of Tat-SP4 was further investigated in the HCC patient-derived xenograft tumor mice model.

**Objective 1 Cell-based characterization of designed peptides in promoting Beclin 1-mediated autophagy and endolysosomal trafficking in HCC cells.**

In our previous work, Beclin-1 targeting stapled peptide (Tat-SP4) could induce autophagy and endolysosomal trafficking in NSCLC and $HER^{2+}$ TNBC. However, the impact of Beclin1-targeting stapled peptides in HCC's autophagy and endolysosomal trafficking is unclear. Thus, we firstly plan to investigate whether the designed peptides can promote Beclin1-dependent autophagy and endolysosomal trafficking. We plan to use the western blot assay to detect the levels of autophagy markers such as LC3II and p62 in different HCC cell lines. Next, we will apply the western blot and immunofluorescence assay to investigate the endolysosomal degradation levels of different cell surface receptors such as EGFR and c-MET in HCC cell lines.

**Objective 2 Assessment of the anti-proliferative efficacy of Tat-SP4 in HCC cell lines with diverse genetic backgrounds**

Based on our purpose, we will investigate the anti-proliferation efficacy of Tat-SP4 in different HCC cell lines. We plan to measure the half-maximal inhibitory concentration (IC50) value and detect a 5-day cell proliferation assay in different HCC cell lines.

Sorafenib is a first-line drug for HCC treatment. However, its application is limited by drug resistant. To overcome this problem, we also plan to assess the efficacy of Tat-SP4 in adaptive sorafenib resistant HCC cell lines.

**Objective 3 Mechanistic study to delineate the cellular pathways implicated in cell death induced by designed peptides**

After confirmed the anti-proliferation effect of Tat-SP4 in multiple HCC cell lines, we will investigate the mechanisms of Tat-SP4 induced cell death. We plan to detect which cell death manner is induced by Tat-SP4. We will first investigate the possibility of different programmed cell death manners such as apoptosis, ferroptosis, necroptosis, and autosis using different cell death inhibitors. Tat-sequence as a kind of CPP can interact with the plasma membrane and membrane of cellular organelles. To explore the molecular mechanisms of Tat-SP4 induced cell death, we plan to investigate the impact of Tat-SP4 on mitochondrial a double

membrane organelle. Papers also reported that Tat-sequence showed an impact on plasma membrane potential. Thus, we also wonder to detect whether our peptide-induced cell death is related to the membrane potential.

**Objective 4 Assessing the anti-proliferative efficacy of Tat-SP4 in HCC patient- derived xenograft tumor (PDTX) mouse models**

After we confirm the anti-proliferation efficacy and investigate the mechanism of Tat-SP4 induced cell death, we will further assess the anti-proliferative efficacy of Tat-SP4 in vivo. We will use a patient-derived xenograft tumor (PDTX) mouse model to detect the anti-tumor efficacy of Tat-SP4.

Overall, we hope our Beclin1-targeting stapled peptide (Tat-SP4) can serve as a potential and novel candidate for HCC treatment. Or our peptide can be an ideal co-combination option with some first-line drugs to improve the survival benefits of advanced HCC patients.

# 3 Materials and Methodology

## 3.1 Cell lines and cell culture

The hepatocellular carcinoma (HCC) cell lines HepG2, Hep3B, MHCC97H, were purchased from Stem Cell Bank, Chinese Academy of Sciences, Shang Hai, China. PLC5, Huh7 were kindly gifted by Dr. Ben Ko's lab (The Hong Kong polytechnic university). MHCC97L and MHCC97L-luciferase was kindly provided by Prof. Terence Lee's lab (The Hong Kong polytechnic university). SK-Hep1, SNU449 was kindly provided by Dr. Vincent's lab (The Hong Kong polytechnic university). All cells cultured in Dulbecco's Modified Eagle's Medium (DMEM) (ThermoFisher, 11965118) or RPMI1640 medium (ThermoFisher, A1049101) supplemented with 10% (v/v) fetal bovine serum (FBS) (ThermoFisher, 10270106) and 1% (v/v) penicillin/streptomycin (Thermofisher, 15140122). Cells were grown in a humidified incubator with 5% $CO_2$ at 37℃. For a long term experiments those cell lines with a lower passage were frozen in the lipid nitrogen tanks. To protect cells from frozen environment, cells were preserved in freezing medium containing 20% FBS and 10% dimethylsulfoxide (DMSO) (sigma, D2650). For recovery cells from 1ml frozen stock, cells need to be thawed immediately in a 37 ℃ water bath. 1ml stock cells were transferred into 5ml complete medium rapidly. To avoid the impairment

of cryoprotectant, cells were centrifuge (800rpm,3min) and removed from the freezing medium. Using 10 ml complete medium resuspend cells and cultured cells in a 10cm petri dish (SPL life science, 10035).

When cells confluence reached 90%, cells passed to a new dish. The process of cells passaging is as follows. Completed medium, phosphate buffer saline (PBS), 0.5% Trypsin-EDTA (Thermo fisher, 15400054) were prewarmed at 37℃ in water bath. Removing cultured medium, using 2ml PBS washing twice removed remained medium. 1ml trypsin was added into petri dish and incubated cells in 37℃ incubator for 1-2 minutes to dissociated adherent cells from the dish. Trypsinization of cells was terminated by the addition of 2-3ml complete medium. Cells were collected by centrifuge (800rpm,3min) and supernatant was removed. Cell pellet was resuspended by fresh complete medium and added into a new dish with an ideal cell density. Shake the petri dish manually to ensure even distribution of cells. Cells were incubated in an incubator at 37℃ with 5% $CO_2$.

All cell lines should be passed two passages followed the routine process before the formal experiments. And cells more than 30 passages will be discarded. Cell lines regularly tested and verified to be mycoplasma negative by DAPI staining before and during experiments. The procedure of DAPI staining is as listed. Cells were seeded in a 24

well plate. After cells attached, using 4% formaldehyde (FDA) fixed cell for 10 minutes and then using DAPI stained cells for 10 minutes. Using fluorescence microscope detected the mycoplasma.

### 3.2 Synthesis of Tat-SP4

The top-ranked Tat-SP4 are synthesized following standard solid-phase protocol with olefin-containing amino acids incorporated at the designated positions. The Tat-SP4 stapled peptide was purchased from *GL Biochem (Shanghai) Ltd.* The hydrocarbon staple was added using the established protocol of Ru-mediated metathesis (Walensky and Bird 2014). The chemical structure and purity of the final synthesized product were characterized by high-resolution MS and HPLC. Purity of each synthesized peptides is > 95%All samples are readily water-soluble. Peptide stock (20 mM) was made by dissolving samples in $H_2O$.

### 3.3 Immunoblot analysis

Using immunoblot analysis the proteins level of LC3 and p62 is one of the most common methods to detect the autophagic response. HCC cells were plated into a 6-well plate with a final confluence at 60%. After starvation by serum-free medium overnight, different concentrations Tat-SP4 were used to treat cells for indicated times and cultured at 37 ℃, 5% incubator. To remove the medium in cells, PBS was be used to wash cells twice. Laemmli sample buffer (62.5 mM Tris-HCl, pH 6.8, 2% SDS, 25%

glycerol, 5% β-mercaptoethanol) supplemented with phosphorylation inhibitor (Sigma, B15001) and EDTA-free protease inhibitor cocktail (Sigma, B14001) was be used to obtain the whole cell lysates that is further denatured by heating at 100 ℃ for 10 min. Protein concentration was measured using a Nano Drop (Themor fisher). Protein samples were mixed with 5×loading buffer and separated by 12% SDS-PAGE gel by 80 V and 120 V constant voltage. Protein samples were transferred to a 0.45μm PVDF membrane (Millipore, USA) by 250 mA constant Ampere for 150 minutes. The membrane was blocked using 5% (w/v) skim milk soluble in TBST buffer 137mM NaCl, 20mM Tris, 0.1% Tween 20 incubated 1 h at room temperature. Primary antibody of LC3, p62 and β-Actin, a loading control, was used to bind targeted proteins and incubated at 4 ℃ overnight. Using HRP-conjugated secondary antibodies detected the targeted proteins. Protein bands were visualized using horseradish peroxidase substrate. ChemiDoc imaging system (Bio-Rad) was used to detect the images. Using ImageJ analyzed results.

**3.4 EGFR and c-MET degradation assay.**

HCC cells were seeded in a 6-well plate at a 60% confluence. After washed with PBS twice, cells were starved by serum-free medium overnight. Cells were treated by 200ng/mL of EGF or 100ng/mL of HGF, and different concentrations Tat-SP4 at 37 ℃ for indicated times,

respectively, which is responsible for inducing endocytosis of EGFR, c-MET. Cells were collected after EGF or HGF and Tat-SP4 stimulation and lysed as described in immunoblot analysis. Primary antibodies and final concentrations are anti-EGFR antibody 1:2000 (Santa Cruz), Rabbit anti-cMET antibody in WB 1:2000 (Cell Signaling Technology), anti-pMET antibody 1:2000 (Cell Signaling Technology), anti-Akt antibody 1:2000 (Cell Signaling Technology), anti-pAkt antibody 1:1000 (Cell Signaling Technology).

**3.5 Immunofluorescence analysis of c-MET degradation and EGFR degradation**

60% confluence cells were seeded on a 18mmx18mm glass slides in 6-well plate and cultured in a routine complete medium before immunofluorescence assay. Cells were washed twice by PBS and serum-starved for overnight. Then, cells were treated by Tat-SP4 (40μM) at indicated times before harvested. Using 4% paraformaldehyde to fix cells and permeabilized by 1% Triton X-100 in PBS. Cells were blocked with 1% BSA in PBS with 0.2% Triton X-100. Cells were washed three times with PBS and incubated with the primary antibodies and Alexa Fluor 555-conjugated secondary antibodies. Slides were examined under a Leica invert confocal microscope (TCS-SP8-MP system). Images were

taken with 63X oil immersion objective lens at room temperature and image acquisition was performed by LAS X software (Leica).

### 3.6 Cell viability assay

To assess the cancer cells viability after treatment with Tat-SP4, cell viability was examined by Trypan Blue cell counting method. HCC cells were seeded into 96-well plates based on optimal cell growth rates determined for each cell line with 80-90% final confluency and incubated overnight before adding Tat-SP4. Cells were treated with gradual concentrations of Tat-SP4. After treatment with Tat-SP4 for 24 h, the cells were digested by 100 µl trypsin and counting by the Z1 Particle Counter (Beckman Coulter).

To assess the cancer cells viability after treatment with Sorafenib, cell viability was examined by 3-(4,5-Dimthylthiazol-2-yl)-2,5-Diphenyltetrazolium Bromide (MTT) assay were used. HCC cells were seeded into 96-well plates based on optimal cell growth rates determined for each cell line with 80-90% final confluency and incubated overnight before adding sorafenib. Cells were treated with gradual concentrations of sorafenib. After treatment with sorafenib for 72 h, the medium was replaced by 100 µl /well MTT solution at a concentration of 0.5% mg/ml and incubated for 4 h at 37 ℃ in a 5% CO2 incubator. Then, MTT solution was removed and 100 µl DMSO was added into each well to

dissolve the purple crystal. Cell viability was reflected by absorbance value measured by Bio-Rad Microplate Reader (Model 680, Bio-Rad Laboratories, Hercules, CA, USA) at the wavelength of 570nm.

### 3.7 Cell proliferation assays

Trypan Blue exclusion is a common method to detect the number of live cells from dead cells in cells suspension. The principle is that only live cells with intact cell membranes can exclude trypan blue dye and live cells will have a clear cytoplasm whereas dead cells will have a blue cytoplasm. Cells were seeded into 24-well plates and the initial cell number was determined by optimal cell growth rates for each cell line. Cells were incubated overnight before adding Tat-SP4 or Tat-SC4. Cell growth will be monitored daily. Cells were trypsin and counted using the Z1 Particle Counter (Beckman Coulter) 24 hours after plating of cells, daily for 4 days.

### 3.8 Establishing Sorafenib-resistant cells using the Sleeping Beauty transposon insertional mutagenesis system

The *SB* transposon system is generally used as a gene delivery tool for long-term expression delivery and integration into the host chromosomal DNA. It is composed of two components: a transposon that contains the gene(s)-of-interest flanked by inverted repeat/direct repeats (IR/DR) sequences; and a transposase, the enzyme responsible for

binding the IR/DRs, excising and randomly integrating the transposon into the genome at TA-dinucleotide sites (Dupuy, Rogers et al. 2009). The *SB* transposon mutagenesis system is similar to the above but relies on the mutagenic transposon called T2/Onc3 to generate gain-of-function and loss-of-function mutations as the result of its integration into the host chromosome (Keng, Villanueva et al. 2009, Keng, Tschida et al. 2011, Keng, Sia et al. 2013). The T2/Onc3 consists of splicing acceptors (SA) with polyadenylation sequence to interrupt endogenous splicing mechanisms, resulting in loss-of-function (Dupuy, Rogers et al. 2009) . It also consists of a CMV enhancer/chicken β-actin promoter (CAG) with splice donor (SD), a strong promoter enhancer element that can cause misexpression or cause gene truncations when integrated into the host genome, causing a gain-of-function mutation (Dupuy, Rogers et al. 2009). The hyperactive SB100 transposase was used in this study (Mates, Chuah et al. 2009).

Transfection was performed using 3 μg of T2/Onc3 transposon plasmid, 1 μg of SB100 transposase plasmid and 8 μL of ViaFect™ Transfection Reagent (Promega) per 1 X $10^5$ cells. After 1 week of exposure to *SB* transposons mutagenesis, cells were selected with 8 μM Sorafenib (MedChem Express) for SUN449 cells, until all parental cells were nearly dead (~1 week). Cells that survive the selection process was

treated with 2 μM Sorafenib to allow for recovery and growth to 80% confluence, where they will be maintained by culturing in the presence of Sorafenib at their parental IC50 concentration.

### 3.9 Establishment of Sorafenib-Resistant MHCC97L Cells

Sorafenib-Resistant MHCC97L with luciferase cells were kindly provided by Prof. Terence Lee's lab. This sorafenib-resistant cell line was established by subjecting cells to continuous administration of gradually increasing sorafenib concentrations up to 10 μM. The same volume of dimethyl sulfoxide (DMSO) was added to the cells as mock controls during establishment of these resistant cells (Leung, Tong et al. 2020).

### 3.10 Tat-SP4 induce HCC cell death without involvement of apoptosis

**Cell survival number** after treated by Tat-SP4 and apoptosis inhibitor Z-VAD-FMK was measured by trypan blue exclusion assay following the standard protocol. Z-VAD-FMK (Sigma, V116) is a well-known inhibitor of caspases and apoptosis without cytotoxicity. After cells pretreatment with or without 50μM Z-VAD-FMK for 2 hours, we measured the viable cell number after treatment with different concentrations Tat-SP4 for 24 hours in MHCC97L, PLC/PRF/5, and Hep3B cells. Compared the survival cell number of with or without 50 μM Z-VAD-FMK pre-treatment detected whether apoptosis inhibitor affect Tat-SP4 induced cell death.

**PI/Annexin V staining assay** is one of the common methods to detect the degree of cellular apoptosis and necrosis by flow cytometry following the standard protocol provided by the manufacturer. Annexin V is a 35 kDa phospholipid-binding protein that has a high affinity for phospholipid phosphatidylserine (PS). In normal cells, PS is located on the cytoplasmic surface of the cell membrane. However, in apoptotic cells PS is translocated from the inner to the outer leaflet of the plasma membrane thus exposing PS to the external cellular environment. Annexin V marked by a green fluorophore that can identify apoptotic cells by binding to PS exposed on the outer leaflet. PI (propidium iodide) a red fluorescence is a nucleic acid binding dye. PI is impermeant to live cells and apoptotic cells, while staining dead cells binding tightly to nucleic acids in the cells.

MHCCC97L cells seeded into a 12 well plate and culture in a routine complete medium before treatment with indicated peptide and harvested by trypsin. Using Annexin V Alexa Fluor$^{TM}$ 488 and PI in binding buffer (Thermo fisher, V13241) to label Tat-SP4 treated cells, the cells were subjected to flow cytometer system (BD Accuri C6) and analyzed by BD Accuri C6 software. The apoptotic cells show green fluorescence on the lower right quadrant represents early apoptotic cells (Annexin $V^+$, $PI^-$). Necrotic cell population can be stained by both

Annexin V and PI on the upper left quadrant. Cellular population in the lower left quadrant is live cells without labeled by both dyes.

**Western blot.** The apoptosis can be further detected through analysis the level of classical marker Caspase 3, cleaved-caspase3, and cleaved PARP by Western blot. MHCC97L cells were seeded into a 6-well plate. After cells attachment, cells were treated by Tat-SP4 (30 μM) for 1, 3, 6 h and doxorubicin (1, 2 μM) for 48 h as a positive control. After treatment, cells were washed by PBS for twice and lysed as described in immunoblot analysis. The primary antibodies and final concentrations are anti-cleaved PARP 1:2000 (Cell Signaling Technology), anti-Caspase3 1:2000 (Cell Signaling Technology), anti-cleaved Caspase3 1:1000 (Cell Signaling Technology).

### 3.11 Tat-SP4 induce HCC cell death without involvement of ferroptosis and necroptosis

Cell survival number after treated by Tat-SP4 and ferroptosis and necroptosis inhibitor Ferrostatin-1 (Fer-1) and Nerrostatin-1 (Nec-1) was measured by trypan blue exclusion assay following the standard protocol. Ferrostatin-1 (Fer-1) (Sigma) is a well-known inhibitor of ferroptosis, a lipid ROS scavenger, was used to determine whether Tat-SP4 induced ferroptosis. After cells treatment with or without 10 μM Fer-1, we measured the viable cell number after treatment with different

concentrations Tat-SP4 for 24 hours in MHCC97L, PLC/PRF/5, and Hep3B cells. Erastin is a positive control for inducing ferroptosis. Necroptosis inhibitor Nerrostatin-1 (Nec-1) (Sigma, N9037) was applied to block cells necroptosis. MHCC97L, PLC/PRF/5, and Hep3B cells were seed into 96 well and treated with or without Nec-1 (25μM, 50μM) and followed with different concentrations Tat-SP4. Compared the survival cell number of with or without Fer-1 and Necro-1 detected whether those inhibitors affect Tat-SP4 induced cell death.

### 3.12 Tat-SP4 induce HCC cell death can be rescued by autosis inhibitor

Digoxin (sigma, D6003), a kind of cardiac glycosides, was employed to inhibit autosis that can inhibit autotic cell death in vitro. MHCC97L, PLC/PRF/5, and Hep3B cells were seed into 96 well and treated with or without pre-treatment with Digoxin (5 μM) for 5h and followed with different concentrations Tat-SP4. Compared the viable cell number of with or without Digoxin detected whether this inhibitor affect Tat-SP4 induced cell death. The survival cell number was measured by trypan blue exclusion assay following the standard protocol.

### 3.13 Measurement of mitochondria membrane potential (Δψ)

During cellular respiration, nutrients are oxidized to generate energy through a mechanism called oxidative phosphorylation, which occurs in

the mitochondria. During oxidative phosphorylation, the gradual degradation of molecules through the TCA cycle releases electrons from the covalent bonds that are broken. These electrons are captured by $NAD^+$ through its reduction into NADH. Finally, NADH transports the electrons to the complexes of the electron chain in the internal membrane of mitochondria. These complexes use the energy released by the electrons to pump protons into the intermembrane space, generating an electrochemical gradient across the internal membrane of mitochondria, which provides energy for the ATP-synthase complex, ultimately producing adenosine triphosphate (ATP).

The impact of Tat-SP4 on mitochondrial metabolism was also assessed by measuring the mitochondria membrane potential ($\Delta\psi$). We assessed the mitochondrial membrane potential **(**$\Delta\psi$**)** using tetramethylrhodamine methyl ester (TMRM) (Thermo Fisher), a cell-permeant, cationic, red fluorescent dye. HCC cells grown to sub-confluency at $10^6$ cells/well in complete medium and plated in 6-well plates incubated overnight. To measure specifically the mitochondrial membrane potential **(**$\Delta\psi$**)**) we quantified the fluorescence intensity before and after applying CCCP, a mitochondrial electron chain uncoupler as a positive control, and our Tat-SP4 as experiment groups. HCC cells were treated by different concentration Tat-SP4 for indicated time. At the same

times using 100 μM TMRM stained HCC cells for 30 min. Finally, HCC cell lines were harvested and analyzed using the Accuri C6 Flow Cytometer (BD Biosciences) and analyzed by BD Accuri C6 software.

**3.14 Oxygen consumption rate (OCR) analysis**

The impact of Tat-SP4 on mitochondrial metabolism was analyzed by measuring the oxygen consumption rate (OCR) of HCC cells upon treatment by Tat-SP4. OCR is a parameter for the mitochondrial OXPHOS process. OCR was measured using a Seahorse Bioscience Extracellular Flux analyzer (XF24). The procedure is provided by the machine manufacturer. The procedure is as listed. Cells were plated in a XF 24 cell culture microplates at a seeding density of 30,000-50,000 cells per well. The cells confluence is dependent on different cells with different growth rates. 250μl complete medium (DMEM or RPMI1640) was added in each well and incubated overnight at one day prior to the experiment. In the same day, 1ml Seahorse XF calibrant (Seahorse Bioscience, 100840-000) was added into each well of calibration plate. Sensor cartridge with lids was put on the calibration plate. The whole setting was placed in an incubator at 37℃ with non-$CO_2$.The next day, media was changed to mitochondrial assay buffer supplement with 180 mg/ml glucose and 100 μM L-Glutamine at pH 7.4. Cells were washed twice in mitochondrial assay buffer and added 500 μl the same buffer.

After 1 h of incubation at 37℃ without $CO_2$, cells were tested by XF Analyzer. Following the OCR measurements, the first injection contained corresponding concentration Tat-SP4 or vehicle, the second injection is 1μM oligomycin, followed by 1 μM FCCP, and 0.5 μM rotenone and antimycin A, and those chemicals are injected into wells at the indicated time points. At the end of this experiment, using cell numbers in each well normalized the different groups. Measurement data were showed by Wave software.

### 3.15 Measurement of cellular ROS level

The impact of Tat-SP4 on mitochondrial metabolism was assessed by measuring the cellular ROS level. The CellROX™ kit from Thermo Fisher Scientific (C10492) was used according to the manufacturer's instructions. The CellROX™ Green Detection Reagent is cell-permeable and non-fluorescent or very weakly fluorescent while in the reduced state. Upon oxidation, the reagent binds DNA and exhibits a strong fluorogenic signal that has absorption/emission maxima of 508/525 nm and remains localized to the nucleus and cytoplasm. HCC cells grown to sub-confluency at $10^6$ cells/well in complete medium and plated in 6-well plates incubated overnight. Prepared negative and positive control as protocol shown. Using different concentrations Tat-SP4 treated cells for indicated time as experiment groups induced ROS in HCC cells. Cells are

then digested and harvested into tubes for staining. Add the CellROX™ Detection Reagent at a final concentration of 1000 nM incubate for 1 h at 37°C, 5% $CO_2$, protected from light. During the final 15 minutes of staining, add 1 μl of the appropriate SYTOX® Dead Cell Stain solution per mL cell suspension. Finally, cells were harvested for flow cytometry analysis using the Accuri C6 Flow Cytometer (BD Biosciences). Results were analyzed by BD Accuri C6 software.

**3.16 Mitochondrial permeability transition pore (MPTP).**

To investigate whether Tat-SP4 induced MPTP, the MitoProbe™ Transition Pore Assay Kit (Thermo Fisher, MP34153 and MP 35103) was employed to detect the mitochondrial permeability transition pore opening. This kit provides a direct method to observe the MPTP. Firstly, cells are loaded with calcein AM, a colorless and non-fluorescent acetoxymethyl esterase substate, which passively diffuses into the cells without selectivity in cytosol and mitochondria. Upon calcein AM into cells can be cleaved into calcein and acetoxymethyl esters by intracellular esterases and liberate the fluorescent dye calcein. And then add $CoCl_2$, a quencher of calcein fluorescence and located in cytosol only, which can quench cytosolic calcein fluorescence and maintain mitochondrial fluorescence. As a positive control, cells were treated with ionomycin, an ionophore, to carry excess $Ca^{2+}$ from cytosol into mitochondria leading to

mitochondrial membrane permeability changes and MPTP opening. Subsequently, $CoCl_2$ can entry mitochondria and quench mitochondrial fluorescence. This process can be directly detected by flow cytometer and confocal imaging.

For flow cytometer detection assay, cells were plated into 12 well plates firstly. MHCC97L cells were treated with Tat-SP4 (20, 40 μM) for 1 h and then staining with calcein AM (final concentration 2 μM) followed by calcein quencher $CoCl_2$ (final concentration 0.4 mM) for 30 min. For positive control group, cells were treated with Ionomycin (250 nM) for 15 min in HBSS with calcium buffer. Finally, collection cells in different groups for analysis by the Accuri C6 Flow Cytometer (BD Biosciences).

For confocal imaging detection assay, cells were plated into confocal dishes and staining cells by MitoTracker Red solution (final concentration 200 nM) for label mitochondria, Hoechst 33342 dye (final concentration 1Mm) staining for nuclear firstly, and then staining with calcein AM (final concentration 1μM) and 1.0 M $CoCl_2$ (1mM), respectively and warm to 37˚C protected from light. Cells were examined under a Leica invert confocal microscope (TCS-SP8-MP system). Images were taken with 63X oil immersion objective lens at room temperature and image acquisition was performed by LAS X software (Leica).

### 3.17 Detection the morphology of mitochondria in HCC cells.

Confocal imaging was used to assess morphology of mitochondria in Hep3B cells. Live Hep3B cell lines were seeded into a confocal dish (SPL life company, 200350) after the glass coverslip coated by Cell-Tak$^{TM}$ (Corning, 354240). 50% confluence cells seeded into the coated confocal dish and cultured in a routine complete medium overnight before transfection. GFP-Tom20 plasmids were transfected into Hep3B cells for labeled the mitochondria. 1ng GFP-Tom20 plasmids were transfected into cells by Lipofectamine 3000 (Thermo Fisher, L3000075) following the standard protocol. After 24h, the image study was conducted by confocal. Cells were examined under a Leica invert confocal microscope (TCS-SP8-MP system). Images were taken with 63X oil immersion objective lens at room temperature and image acquisition was performed by LAS X software (Leica).

### 3.18 Detection the impact of Tat-SP4 on intracellular $Ca^{2+}$ homeostasis

Chemically synthesized calcium indicators and genetically encoded calcium indicators were used to detect intracellular calcium concentration changes.

Fura-2 AM (Thermo Fisher, F1221) as a representative chemically synthesized calcium indicators were used to monitor cytosolic calcium

concentration changes. Fura-2 AM is a membrane permeant fluorophore dye. This acetoxymethyl (AM) ester form can bring Fura-2 group through cell membrane without significant damage. Fura-2 can be released by intracellular esterase. Fura-2 is classical dual $Ca^{2+}$ indicator. This dye shows an excitation spectrum at 380 nm and an emission spectrum at 510 nm in a $Ca^{2+}$ free condition. When this dye binds to $Ca^{2+}$, this dye possesses an excitation spectrum at 340 nm with the same emission at 510 nm. When $Ca^{2+}$concentration increase, the fluorescence intensity at 340 nm increase alone with a fluorescence intensity decrease at 380 nm. The $Ca^{2+}$ concentration can be calculated by Fura-2 fluorescence intensity ratio of 340 nm/380 nm.

In this experiment, MHCC97L cells were seeded into a 24-well plate at a 60%-70% confluence for overnight attachment. Preparation and cell loading of Fura-2 AM is processed followed the manufacturer's instructions. Briefly, dilute the Fura-2 AM stock solution (1mM) to a final concentration of 1μM firstly. Addition of 20% (w/v) Pluronic F-127 （Thermo Fisher, P6866）assists in the nonpolar AM dispersion in medium making the final concentration about 0.02%. Fura-2 AM stain cells in serum-free medium at room temperature for 1h. After staining, remove medium and wash cells 3 times by HBSS with 1.2 mM $Ca^{2+}$ (Thermo Fisher, 14025092) or HBSS without $Ca^{2+}$ (Thermo Fisher,

14025092). Before imaging, 250 μl HBSS (with or without $Ca^{2+}$) was added into wells for 30 min at room temperature.

Three genetically encoded $Ca^{2+}$ indicators pCAG cyto-RCaMP1h (Addgene, 105014), pCAG mito-GCaMP5G (Addgene, 105009) and pCAG G-CEPIA1er (Addgene, 105012) were used to detect the calcium concentration changes of cytosol, mitochondrion and endoplasmic reticulum (ER). HCC cells (MHCC97L) and Hela cells were seeded into 24-well plates at a desired confluence 60%-70% and cultured overnight. Cells were transfected using Lipofectamine 3000 (Thermo Fisher, L3000015) 48h (MHCC97L) before imaging. Briefly, cells were seeded to be 60-70% confluent at transfection firstly. Lipofectamine™ 3000 reagent was diluted using Opti-MEM™ (Thermo Fisher, 31985070). Using Opti-MEM™ medium dilute plasmids and P3000 reagent mixture (DNAμg: P3000μl =1:2). Different cells have different transfection efficiency. Transfected cells were culture 48h in MHCC97L. The transfection efficiency was detected by fluorescence microscope, and the experiment could be carried out when the efficiency reached more than 60%. Before imaging, cultured medium was replaced with HBSS buffer (with or without $Ca^{2+}$).

The images were captured using an Olympus inverted epifluorescence microscope (Telefon, Germany) equipped with a 20×

objective, an electron-multiplying cooled-coupled device (CCD) camera. Images were obtained at a rate of one frame per 3 second with the following excitation filter settings: 340 nm and 380 nm for fura-2; 472 nm for GCaMP5G and CEPIA1er; 562nm for RCaMP1h. for analysis of the Fura-2 (a ratio-metric indicator) we calculate the fluorescence ratio $F_{340}/F_{380}$. All images were analyzed with Cell R imaging software. For $Ca^{2+}$ time course of cytosol, mitochondria, and ER, we treated cells with different concentrations peptides at 60 seconds.

### 3.19 Animal experiments

The *in vivo* suppression effect of Mito-SP4 was performed on HCC patient derived tumour xenograft (PDTX) mouse model. The tumor samples in this PDTX model are derived from the xenograft model PDTX#1(Ma, Lau et al. 2017), which has been successfully constructed by the laboratory of Dr. Terence Lee from the Hong Kong Polytechnic University. The clinical samples were obtained from HCC patients who undergone liver resection at the Surgery Department of Queen Mary Hospital, Hong Kong. The experiment was approved by the Institutional Review Board of the University of Hong Kong and Hong Kong Hospital Authority. Samples were collected with the informed consent of the patients. The PDTX#1 model was successfully constructed by using the clinical samples for xenotransplantation experiments. This PDTX mouse

model was kindly provided by Dr. Terence Lee group (The Hong Kong polytechnic university).

**Isolation of single tumor cells from tumor tissue**. Tumors from the PDTX#1 model with a length of 10 × 10 mm (length × width) were harvested. Tumors were placed in a petri dish immediately filling 10 ml pre-cooled DMEM/F12 medium (Thermo Fisher, 2276810) and washing twice. Tumors were first cut into small pieces by a scalpel blade and transferred to a 50ml low-speed centrifuge tube filling 10 ml of pre-cooled DMEM/F12 medium. To obtain single cells, 4μg/ml liberase (Roche, 5401119001) and 20μg/ml DNase I (Roche, 10104159001) was added into tubes. Incubated tubes at a 37°C water bath for 15min and vortexed every 5min for 30s to provide a suitable enzymes reaction environment. To obtain a single-cell mixture, mixture need to be filtered using a 100μm filter and a 70μm filter, respectively. In this process 20ml of DMEM/F-12 medium could be added.

Differential centrifugation is used to remove other cells such as blood cells and obtain purer tumor cells. First, cells mixture was centrifuged at 12000 rpm for 2 min at room temperature. Removing the supernatant and addition 50 ml of DMEM/F-12 medium resuspend the cells. Centrifuged the above resuspend cells at 800 rpm for 3 min at room temperature and discard the supernatant. Resuspend the pellet by 50 ml of

DMEM/F-12 medium. The above step was repeated 3 times. Eventually white tumor cells were obtained. Use trypan blue (Thermo Fisher, 15250061) to determine cell viability and count the number of viable cells.

**Tumorigenicity assay.** Resuspend cells in PBS and diluted cells to $1x10^8$ cells/ml and added 1:1 (v/v) with Matrigel (Corning, 356237). The final concentration of cells is $5x10^7$ cells/ml. Using a 21G syringe with a needle, 100 μl ($5 \times 10^6$) cells were subcutaneously injected into the right back of 4-to 6-week-old male nude mice. The injected mice were placed in a clean cage and kept under observation for 10 minutes to make sure no abnormal behaviors.

Treatment was started once the size of tumors reached approximately 5× 5mm (length× width). The mice were randomly grouped into three groups, each consisting of 6 mice. Make sure that the mean values of body weight and tumor size of mice in the experimental and control groups are similar. To investigate the effect of Tat-SP4, daily administration was started by intraperitoneal injection (experimental group: Tat-SP4 40 mg/ml and control group: PBS). The tumor size was recorded and calculated the tumor volume (length × width × width)/2 $mm^3$ every day for 33 days. At the same time, body weight of the mice was measured every day. After 33 days of administration, the experiment

was terminated. The vital organs and tumors were harvested for further analysis.

### 3.20 Statistical analysis

Statistical analysis was performed using Graphpad Prism 7.0 (GraphPad). Results are expressed as mean ± SEM. unless otherwise indicated. For each box-and-whisker plot, centre line is the median and whiskers represent the minimum and maximum values. For confocal imaging studies, the image acquisition and analysis will be performed by LAS X software. For OCR measurement, the data acquisition and analysis will be performed by the Seahorse Wave Desktop Software (Agilent). For flow cytometry analysis of cellular ROS and mitochondria membrane potential, the data acquisition and analysis will be performed by BD Accuri C6 software. All these software are standard packages provided by the manufacturer. All assays will be executed with at least 3 independent experiments expressed as mean ± SEM. Statistical significance was considered with a P value less than 0.01.

# 4 Results

## 4.1 Cell-based characterization of designed peptides in promoting Beclin 1-mediated autophagy and endolysosomal trafficking in HCC cells

Our previous work showed we had designed a series of stapled peptides that could significantly induce Beclin1-mediated autophagy (Wu, He et al. 2018, Yang, Qiu et al. 2021). As shown in Introduction, these stapled peptides consist of two parts, a cell-penetrated peptide Tat sequence at the N-terminal responsible for cell translocation and an autophagic essential protein Beclin1 targeting stapled peptides at the C-terminal. This Beclin1 targeting stapled peptide can specially target the coiled-coil domain of Beclin1 that promotes the formation of Beclin1 and UVRAG heterodimers through inhibition of Beclin1 homodimers formation (Wu, He et al. 2018, Yang, Qiu et al. 2021). The mechanism of our peptides-induced autophagy and endolysosomal trafficking is shown in Figure 4.1. In our previous studies, Tat-SP4, one of the leading candidates with a higher binding affinity and good solubility, was used to study the effect of inducing autophagy and endolysosomal degradation of EGFR in various cell lines such as HEK293T, A549, H1975, and SKBR3 (Wu, He et al. 2018, Yang, Qiu et al. 2021). Based on these previous findings, we investigated if Tat-SP4 would induce autophagic response

and endolysosomal trafficking in HCC cell lines with different genomic backgrounds.

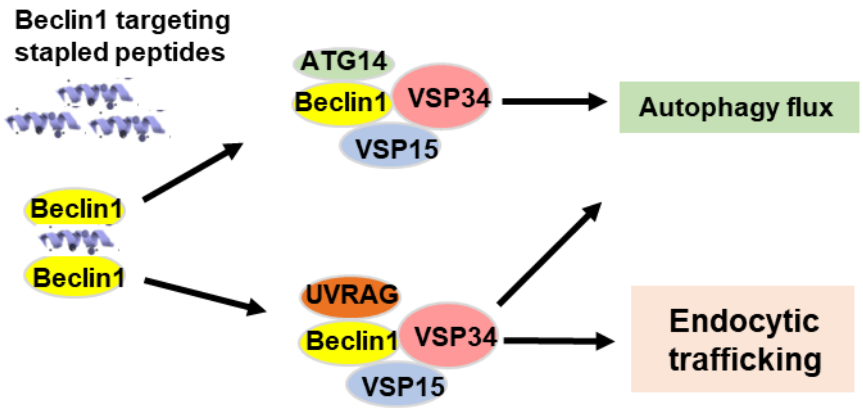


**Figure 4.1 The mechanism of Beclin1 targeting stapled peptides induce autophagy and endocytic trafficking.** Stabled peptides bind to Beclin1 the C-terminal of the coiled coil domain to inhibit the formation of homodimers and then enhance the interaction of Beclin1 and ATG14L and UVRAG to promote autophagic response and endocytic trafficking.

Hepatocellular carcinoma (HCC) is a kind of heterogeneous aggressive tumor with a low survival rate and poor response to treatment at the advanced stages. This could be related to the high degree of diversity and complexity of HCC tumors. Various HCC tumor-derived cell lines have been widely used as models to discover anticancer drugs and understand mechanisms of drug resistance. Firstly, we chose three HCC cell lines, MHCC97L, Hep3B, and PLC/PRF/5, to investigate the impact of Tat-SP4 on their autophagic response and lysosomal trafficking.

### 4.1.1 Tat-SP4 induces autophagy in HCC cell lines regardless of their genetic backgrounds

The impact of Tat-SP4 on inducing autophagy in HCC cells was studied using three different HCC cell lines PLC/PRF/5, Hep3B, and MHCC97L. These cell lines were selected based on different markers of HCC including hepatitis virus B (HBV), tumor suppressor p53, and proto-oncogene beta-catenin (β-cat). The autophagy process was monitored using two markers. LC3 and p62, through western blot analysis. A reliable indicator of cellular autophagy activity is an increase in lapidated LC3 (known as LC3-II) and the decrease of p62, a degraded autophagy receptor. To confirm the autophagy flux, cells were treated with an autolysosome neutralizer chloroquine (CQ) to inhibit autophagosome-lysosome fusion and lysosomal degradation. This treatment resulted in an increased level of lapidated LC3 II, suggesting an active autophagy process. HCC cells were exposed to two different concentrations of Tat-SP4 for 3 h and cell lysates were collected for WB detection.

Our results revealed that Tat-SP4 could induce a significant autophagic response in MHCC97L, PLC/PRF/5 and Hep3B cell lines. In MHCC97L cells, the LC3-II level increased by 2 folds after Tat-SP4 treatment at 20 μM for 3 h. After treatment with Tat-SP4 (30 μM) for 3 h

in MHCC97L cells, the increased level in LC3-II (about 2.5-fold) was higher than low concentration Tat-SP4 treatment, while the level of p62 shows no obvious change after two concentrations of Tat-SP4 treatment (Figure 4.2A). The autophagy inhibitor chloroquine (CQ) was further added to block non-specific autophagy induced LC3II levels. The results showed that even after the addition of CQ (25 μM for 3 h), Tat-SP4 could still induce an increase in LC3-II level, confirming that Tat-SP4 induces rather than blocks autophagy (Figure 4.2A). The changes in the LC3-II and p62 levels from Figure 4.2A was analyzed using Image J software and the results were shown in Figure 4.2 B&C. Similarly, in Hep3B and PLC/PRF/5 cells, different concentrations of Tat-SP4 could also induce the increase of LC3-II level and the p62 level remained unchanged (Figures 4.2 D & E). In summary, Tat-SP4 could significantly induce autophagic response in HCC cell lines with different genetic backgrounds.

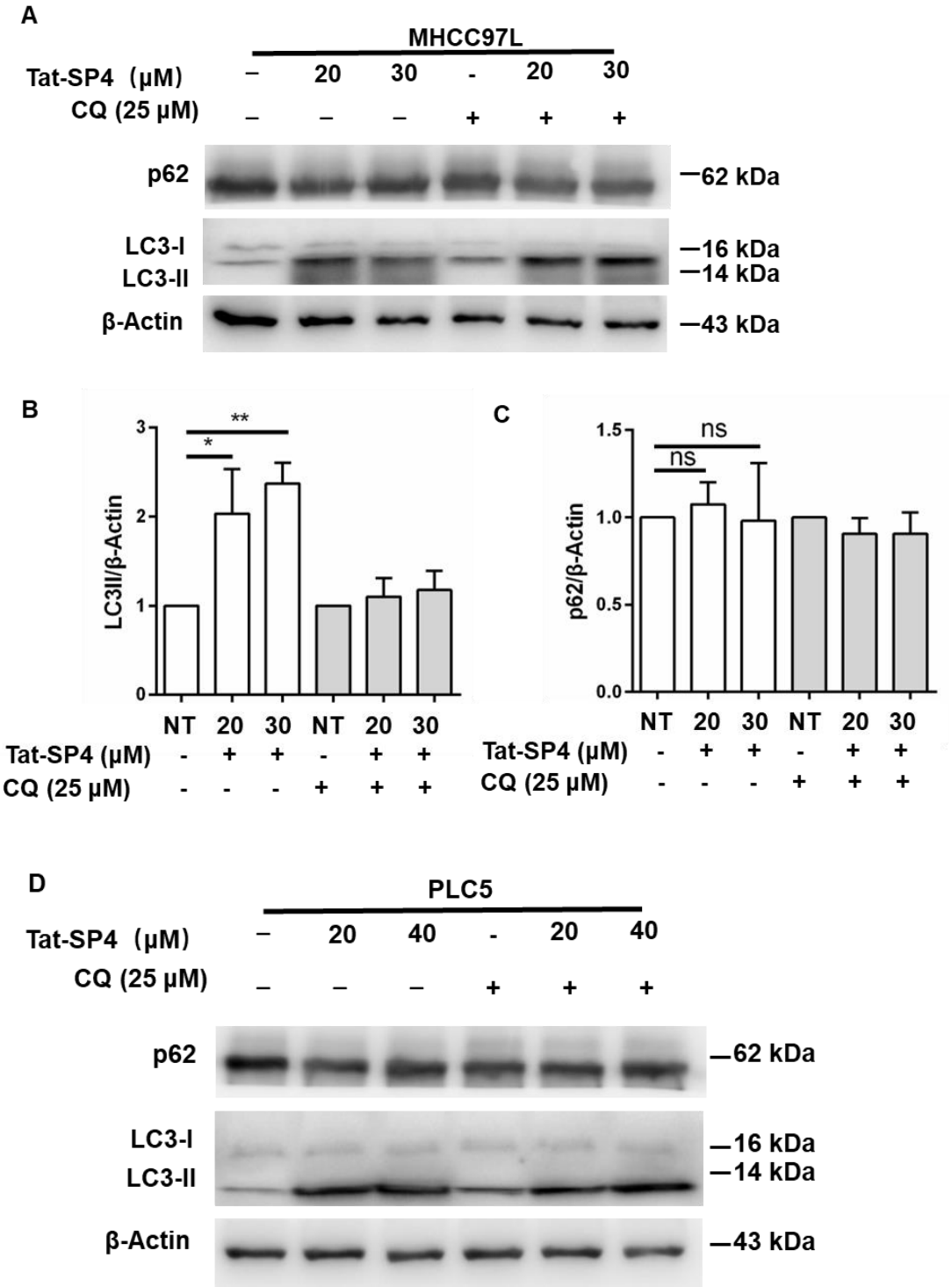
A
MHCC97L
Tat-SP4 (μM)
CQ (25 μM)
p62
LC3-I
LC3-II
β-Actin
62 kDa
16 kDa
14 kDa
43 kDa
B
LC3II/β-Actin
C
p62/β-Actin
ns
NT
Tat-SP4 (μM)
CQ (25 μM)
D
PLC5

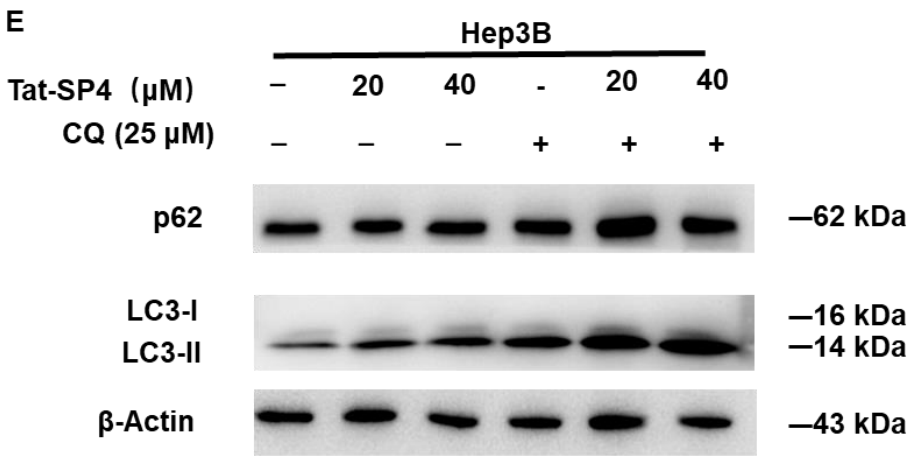


**Figure 4.2 Tat-SP4 induces autophagy in HCC cell lines regardless of their genetic backgrounds**. **A**. MHCC97L cells were treated with 20 μM and 30 μM of Tat-SP4 for 3 hours in the with or without 25 μM CQ. Two Classical autophagy markers LC3-II and p62 were detected by western blot. **B**. Statistic analysis of LC3-II level changes after normalization to the level of β-Actin. Bar represents mean ± SEM of three replicates, *P<0.5, **P<0.05, two-way ANOVA test. **C**. Statistic analysis of p62 level changes after normalization to the level of β-Actin. **D**. Similar western blots as (**A**), but cells are PLC/PRF/5. **E**. Similar western blots as (**A**), but cells are Hep3B after treatment with 20μM and 40μM of Tat-SP4 for 3 hours with or without 25μM CQ.

### 4.1.2 Tat-SP4 shows no further effect on the fast endocytic degradation of EGFR in HCC cell lines

In our previous work, Tat-SP4 could enhance endocytic degradation of the growth factor receptor EGFR in several cancer cells such as A549,

H1975 and SKBR3. We set out to investigate whether Tat-SP4 had a similar effect on HCC cell lines. Three HCC cell lines MHCC97L, Hep3B, PLC/PRF/5, were treated with either the agonist EGF or Tat-SP4. EGFR levels were then measured by Western blot. The results showed a rapid endolysosomal degradation of EGFR after treatment with 200 ng EGF only for 0, 1, 3, and 6 hours in MHCC97L. The level of EGFR decreased by more than 50% at 2 hours and further decreased by more than 80% at 4 hours (Figure 4.3A). However, after treatment of cells with Tat-SP4 20 μM of 0, 1, 3, and 6 hours, the level of EGFR remained largely unchanged even at 4 hours (Figure 4.3A). Similar to the EGF-triggered rapid endocytic degradation of EGFR, co-treatment with Tat-SP4 and EGF could also induce rapid EGFR degradation. However, this significant degradation efficiency was attributed to agonist-induced EGFR degradation (Figure 4.3A). In the other two HCC cell lines, PLC/PRF/5 and Hep3B, we observed similar results that agonist EGF induced fast EGFR degradation, while Tat-SP4 showed little effect on inducing endocytic EGFR degradation (Figures 4.3B&C). Overall, all three HCC cell lines exhibited rapid endolysosomal EGFR degradation, which was not further promoted by Tat-SP4 treatment.

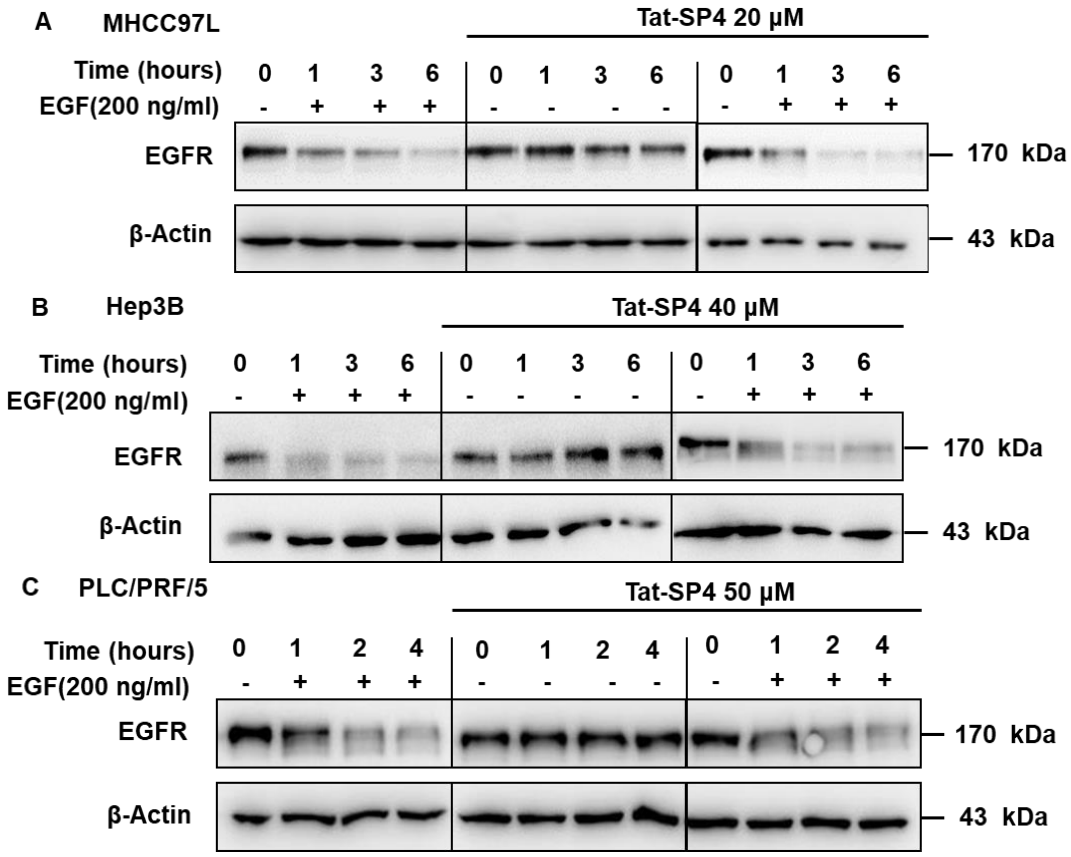


**Figure 4.3 Tat-SP4 showed no further effect on endolysosomal degradation of EGFR in HCC cells. A.** The EGFR level in MHCC97L cell lysate was measured by Western blot after overnight serum-free starvation (-) and treatment with either 200ng/ml EGF (+) or 20 μM Tat-SP4 for 0, 1, 3, 6 h. **B.** A similar set up was performed in Hep3B cells after treatment with 40 μM Tat-SP4 for 0, 1, 3, and 6 h. **C.** A similar set up was performed in PLC5/PRF/5 cells after treatment with 50 μM Tat-SP4 for 0, 1, 2, and 4 h.

To further validated the effect of Tat-SP4 on rapid endocytic EGFR degradation in HCC cell lines, immunofluorescence imaging studies were performed on MHCC97L cells. The results showed that the EGFR (green

fluorescence signal) was distributed throughout the cytosol without any treatment after overnight serum-free starvation. After treatment with 25 μM Tat-SP4, the level of EGFR in the whole cell remained largely unchanged regardless of the time of treatment (Figure 4.3E).

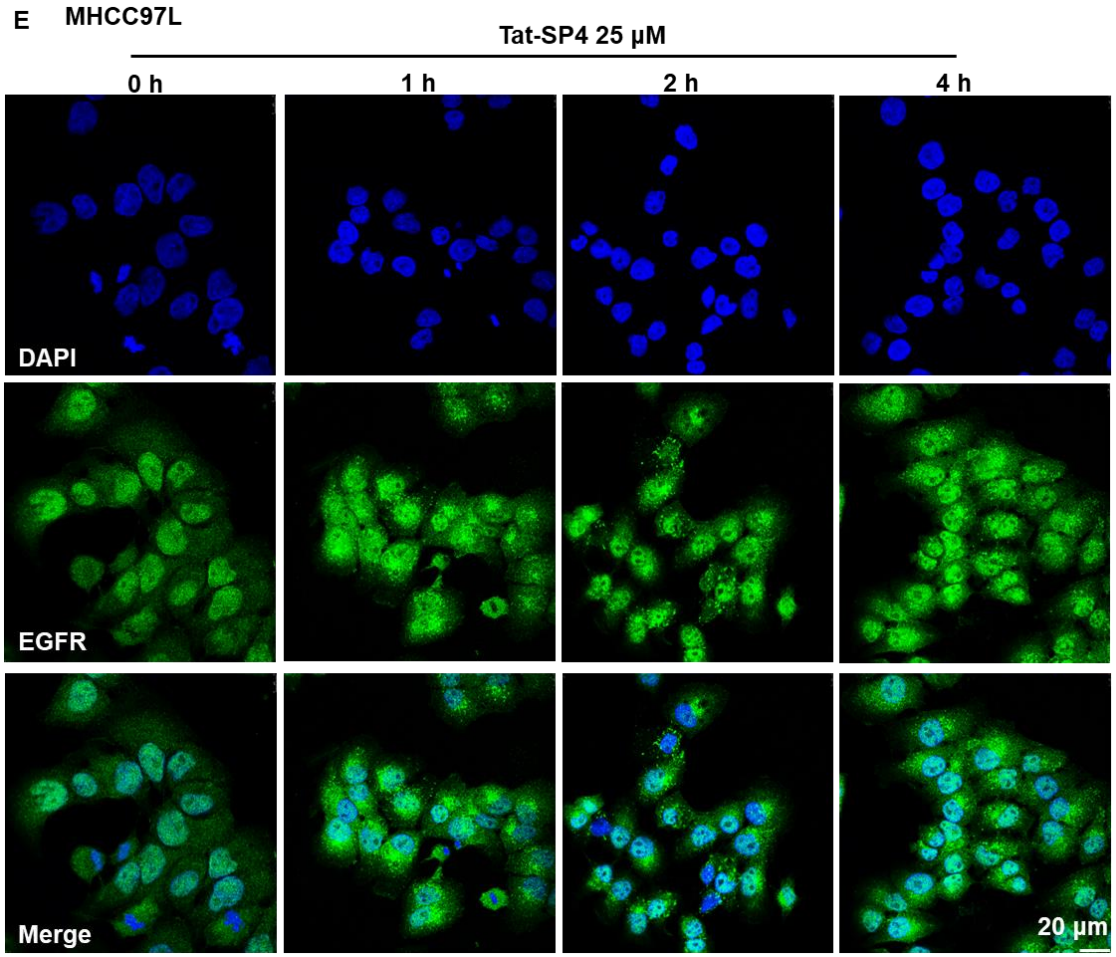


**Figure 4.3E Immunofluorescence imaging of EGFR in MHCC97L cells.**

After overnight serum-free cultured, MHCC97L cells were treated with 25 μM Tat-SP4 for different durations (0, 1, 2, 4 h). Then, cells were blocked and incubated with anti-mouse Alexa Fluor secondary antibodies

to label EGFR (green) and DAPI (blue) was used to label the nucleus. Scale bar:20 μm.

### 4.1.3 Tat-SP4 significantly enhances endolysosomal degradation of c-MET in HCC cells with c-MET over-expression

Interestingly, unlike our previous studies in other cancer cell lines, Tat-SP4 treatment only could not further promote rapid EGFR endolysosomal trafficking in HCC cell lines. We were curious whether Tat-SP4 had a similar effect on other growth factor receptors that also undergo agonist-induced endocytic degradation.

MHCC97L is a unique HCC cell line in this project that it overexpresses a hepatocyte growth factor (HGF) receptor, c-MET. This receptor is an important tyrosine kinase receptor in HCC. Similar to EGFR, c-MET can be activated by an agonist HGF instead of EGF (Giordano and Columbano 2014). As explained in the introduction, the HGF/c-MET signaling pathway plays multiple roles in hepatocarcinogenesis, autophagy, and drug resistance in HCC cells. c-MET is an important proto-oncogene in various tumors. It is one of the most potential drug-targets for exploring new anticancer drugs (Giordano and Columbano 2014).

Therefore, we investigated the effect of Tat-SP4 on endolysosomal degradation of c-MET in MHCC97L cells. MHCC97L cells were cultured

in a serum-free medium overnight and treated with 20 μM Tat-SP4 at the indicated time points. The level of c-MET in the cell lysate was measured by Western blot. As shown in other publications, we detected two bands of c-MET in MHCC97L cells. The molecular weight of the full-length precursor protein was approximately 170 kDa. The other 140 kDa band represented the mature receptor (Figure 4.4A). We first followed the level of c-MET after treatment with HGF alone. Our data show that HGF did not induce significant endolysosomal degradation of c-MET in MHCC97L cells (Figure 4.4A). However, after HGF stimulation, the total amount of 140-kDa mature c-MET increased significantly, and at the same time, the level of activated phosphorylated c-MET also increased significantly (Figure 4.4A). This result was different from the rapid degradation of EGFR after induction by EGF. Interestingly, the performance of these two tyrosine kinase receptors after stimulation by their respective agonist was a significant difference in the same cell line. Tat-SP4 alone at 20 μM induced a rapid and marked decrease in the level of 140-kDa mature c-MET, which decreased by >30% at 30 minutes after treatment (Figure 4.4B). However, treatment with HGF alone showed no such effect, with ~50% of total mature c-MET remaining stable even after 4 hours (Figure 4.4A). In addition, Tat-SP4 treatment alone also significantly decreased the phosphorylation level of mature c-MET and

its downstream target Akt (Figure 4.4B). Tat-SP4 and HGF co-treatment as well as Tat-SP4 treatment alone induced a rapid c-MET degradation (Figure 4.4C). Statistical analysis of the total amount of c-MET after treatment of either HGF or Tat-SP4 showed that Tat-SP4 induced rapid endolysosomal degradation of c-MET in MHCC97L. These data provided an interesting possibility that Tat-SP4 might downregulate the HGF/c-MET pathway by inducing rapid degradation of c-MET.

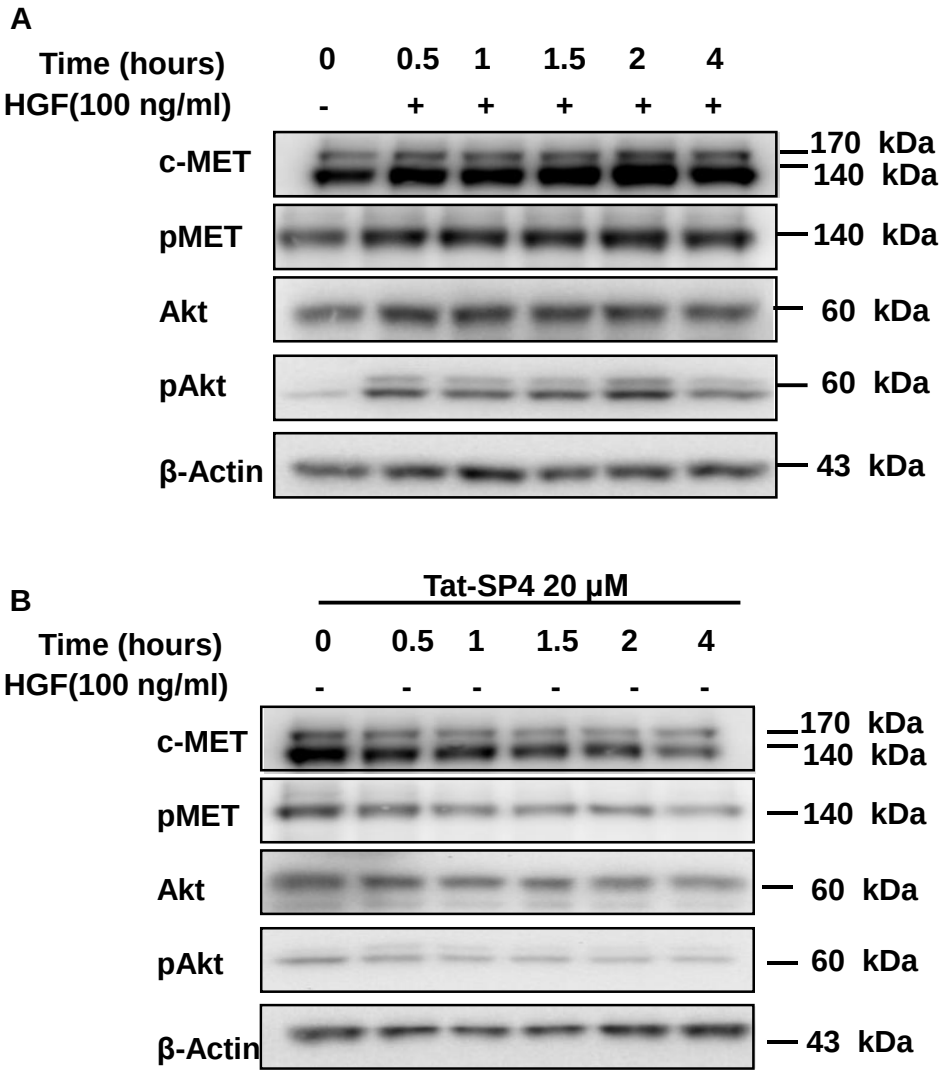

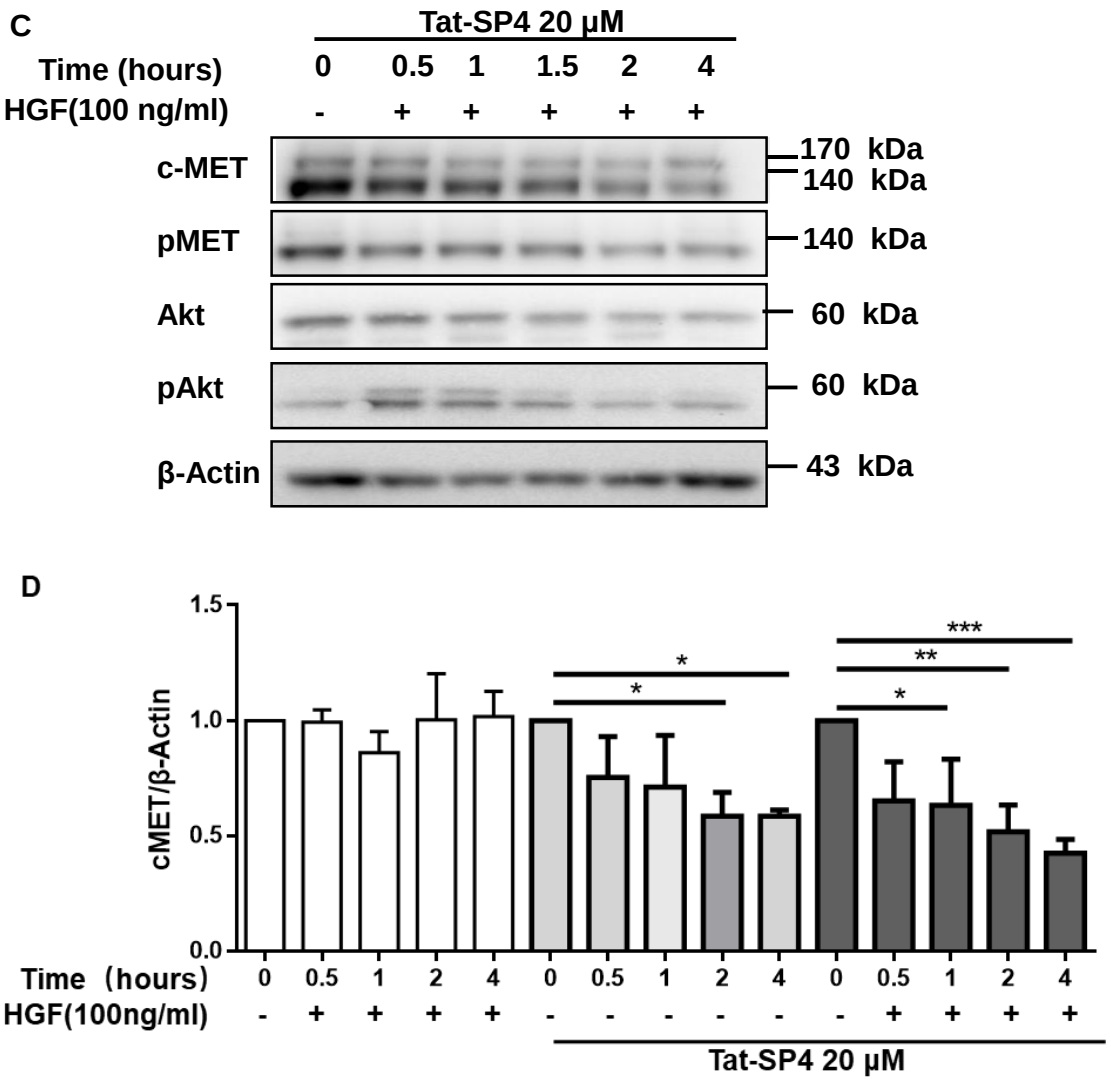


**Figure 4.4 Tat-SP4 significantly enhances endolysosomal degradation of c-MET in MHCC97L A**. After serum-free starvation overnight (-), MHCC97L cells were treated with 100 ng/ml HGF (+) for 0, 0.5, 1, 2, 4 h , respectively. The c-MET level in cell lysate was detected by western blot. **B**. After serum-free starvation overnight (-), MHCC97L cells were treated with 20 μM Tat-SP4 (+) for the same time of (A). The c-MET level in cell lysate was measured by western blot. **C**. After serum-free starvation overnight (-), MHCC97L cells co-treatment by 100 ng/ml HGF

(+) and 20μM Tat-SP4 (+) for the indicated durations. The c-MET level in cell lysate was measured by western blot. **D**. Statistical analysis of the levels of c-Met (A&B&C) after normalization to the β-Actin level. Data are presented as mean ± SEM (n = 3). *P<0.5, **P<0.05, One-way ANOVA test.

Immunofluorescence imaging studies were carried out to further investigate the effect of Tat-SP4 on the endogenous degradation of c-MET in MHCC97L cells. The results indicate that after serum-free starvation for 12 h, c-MET was mainly localized to two subcellular locations. The full-length precursor population of c-Met was mainly distributed at the Golgi as shown in the previous work (Frazier, Brand et al. 2019). The mature c-Met population spread as a well-defined thin layer on the plasma membrane (Figure 4.4E). At 2 hours after Tat-SP4 treatment, the population of mature c-MET on the plasma membrane was significantly reduced, as indicated by its weaker fluorescence intensity, whereas the population of c-MET precursor protein in the Golgi was less affected (Figure 4.4E). This difference between the two populations of c-MET was consistent with the Western blot results above. These data were also supported by previous studies because the mature c-MET on the plasma membrane was responsible for phosphorylation by ligands to

regulate its downstream and undergo endolysosomal degradation than the immature c-MET in Golgi.

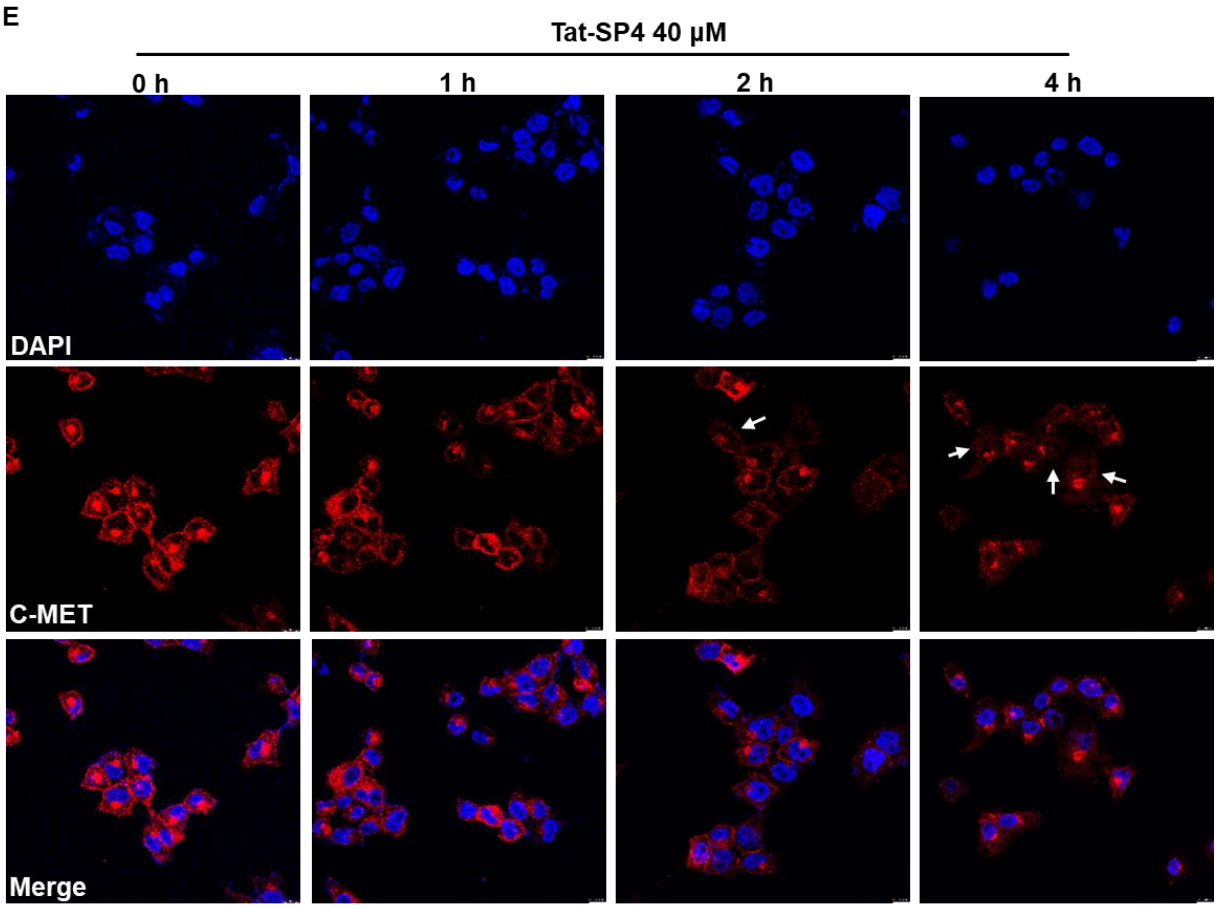


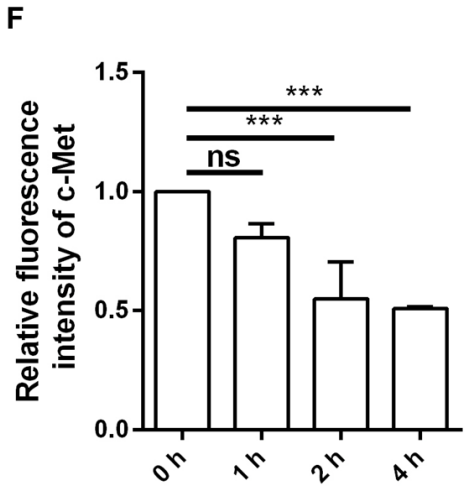

**Figure 4.4 E. Immunofluorescence imaging of c-MET in MHCC97L cells.** After overnight serum-free culture, MHCC97L cells were treated with 40 μM Tat-SP4 for different time points (0, 1, 2, 4 h). Subsequently, cells were blocked and incubated with anti-mouse Alexa Fluor secondary antibodies to label c-MET (red) and DAPI (blue) was used to label the nucleus. (Scale bar: 20 μm). **F**. Statistical analysis of c-Met levels (**E**) after normalization to the control group (0h). Data are expressed as mean ± SEM (n = 3). *P<0.5, **P<0.05, one-way ANOVA test.

**Discussion**

In our previous work, Beclin1 targeting stapled peptide (Tat-SP4) could induce autophagy and rapid EGFR turnover in lung and breast cancer cells. Here, the above results suggest that Tat-SP4 could also induce autophagy in several HCC cell lines with different genetic backgrounds. Interestingly, Tat-SP4 showed no further effect in promoting the endolysosomal degradation of EGFR in HCC cells, although such rapid degradation of EGFR could be observed in other cancer cell lines. We found that HCC cell lines usually showed rapid EGFR turnover after being induced by its agonist. This might leave little room for Tat-SP4 to further promote EGFR degradation. The rapid EGFR turnover might inhibit the efficacy of EGFR-targeted tyrosine kinase

inhibitors, thus limiting the application of EGFR-targeting drugs in HCC. Further studies are needed to investigate this interesting possibility.

c-MET mutations and overexpression are common in HCC patients and they are associated with poor prognosis. However, c-MET-targeting drugs have not shown any survival benefit to HCC patients. The multiple cross-talks of c-MET and other oncogenic growth factors may affect the efficacy of inhibiting cancer cell proliferation. Our results showed that Tat-SP4 could promote endolysosomal degradation of c-MET, which might attenuate the HGF/c-MET signaling pathway through decreased phosphorylation of c-MET and its downstream proteins Akt.

Tat-SP4 could promote autophagy-dependent c-MET degradation. To further investigate the possibility of Tat-SP4 as an anticancer drug for HCC, we demonstrated the anti-proliferation effect of Tat-SP4 in several HCC cell lines and adaptive sorafenib-resistant HCC cell lines.

**4.2 Assessment of the anti-proliferative efficacy of Tat-SP4 in HCC cell lines with diverse genetic backgrounds**

As mentioned above, HCC is a kind of heterogeneous disease caused by different risk factors, and the mechanism of hepatocarcinogenesis involveed multiple pathways. To overcome such heterogeneity, various HCC tumor-derived cell lines have been widely used as a model to discover anticancer drugs and understand various mechanisms of drug

resistance. In this project, 8 HCC cell lines from three different subgroups (driven by the differentiation state) of HCC cell lines were used to evaluate the antiproliferative efficacy of Tat-SP4 (Table 4.1).

**Table 4.1 Summary of HCC cell lines in this study.** HCC molecular classes and associated features were extracted from previous studies (Llovet, Montal et al. 2018, Caruso, Calatayud et al. 2019).

| | | | |
|---|---|---|---|
| Clinical features | HBV-related aetiology, poor differentiation-vascular invasion and worse clinical outcome | | |
| Cell lines | HepG2, Hep3B, Huh7, PLC/PRF5 | MHCC97L MHCC97H SK-Hep1 | SNU-449 |
| Differentiation | Hepatoblast-like | Mixed epithelial-mescenchymal like | Mesenchymal-like |
| Molecular features | *TERT* promoter, *TP53*, *AXIN1*, *and TSC1/TSC2* mutations; chromosome 11q13 amplification RAS-MAPK, AKT-mTOR, MET, and/or E2F1signalling | | |
| | progenitor markers: $IGF^{2+}$ $AFP^{+}$ $EPCAM^{+}$ $CK19^{+}$ | TGFβ and noncanonical β-catenin signaling pathways | |

α-fetoprotein (AFP), overexpression of epithelial cell adhesion molecule (EPCAM), cytokeratin 19 (CK19), and/or IGF2, HBV, hepatitis B virus

HepG2, Hep3B, Huh7, and PLC/PRF5 from the first subgroup are hepatoblast-like cell lines. MHCC97L, MHCC97H, and SK-Hep1 are mixed epithelial-mescenchymal-like cell lines from the second subgroups. Mesenchymal-like cell lines SNU-449 belong to the third subgroup. All these cell lines belong to the proliferation class driven by HVB with poor differentiation-vascular invasion and worse clinical outcomes.These HCC cell lines are characterized by activation of cell proliferation and survival signaling pathways, such as the PI3K–AKT–mTOR, RAS–MAPK, and MET cascades. They are TERT promoter, TP53, AXIN1, and TSC1/TSC2 mutations, and chromosome 11q13 amplification. Differently, the hepatoblast-like subgroup of cell lines has progenitor markers and expresses hepato-specific genes such as $IGF^{2+}$, $AFP^{+}$, $EPCAM^{+}$, and $CK19^{+}$, while the other two subgroups have an aberrant activation of the TGFβ and noncanonical β-catenin signaling pathways.

### 4.2.1 Determination of IC50 in HCC cell lines with the treatment of Tat-SP4

The sensitivity of HCC cell lines to Tat-SP4 was first assessed by the half-maximal inhibitory concentration (IC50). HCC cells were seeded in a 96-well plate and cultured with Tat-SP4 at different concentrations for 24 hours. The IC50 value was determined by measuring cell viability using the trypan blue exclusion assay. The results showed that Tat-SP4

can induce HCC cell death in a dose-dependent manner (Figure 4.5 A-H).

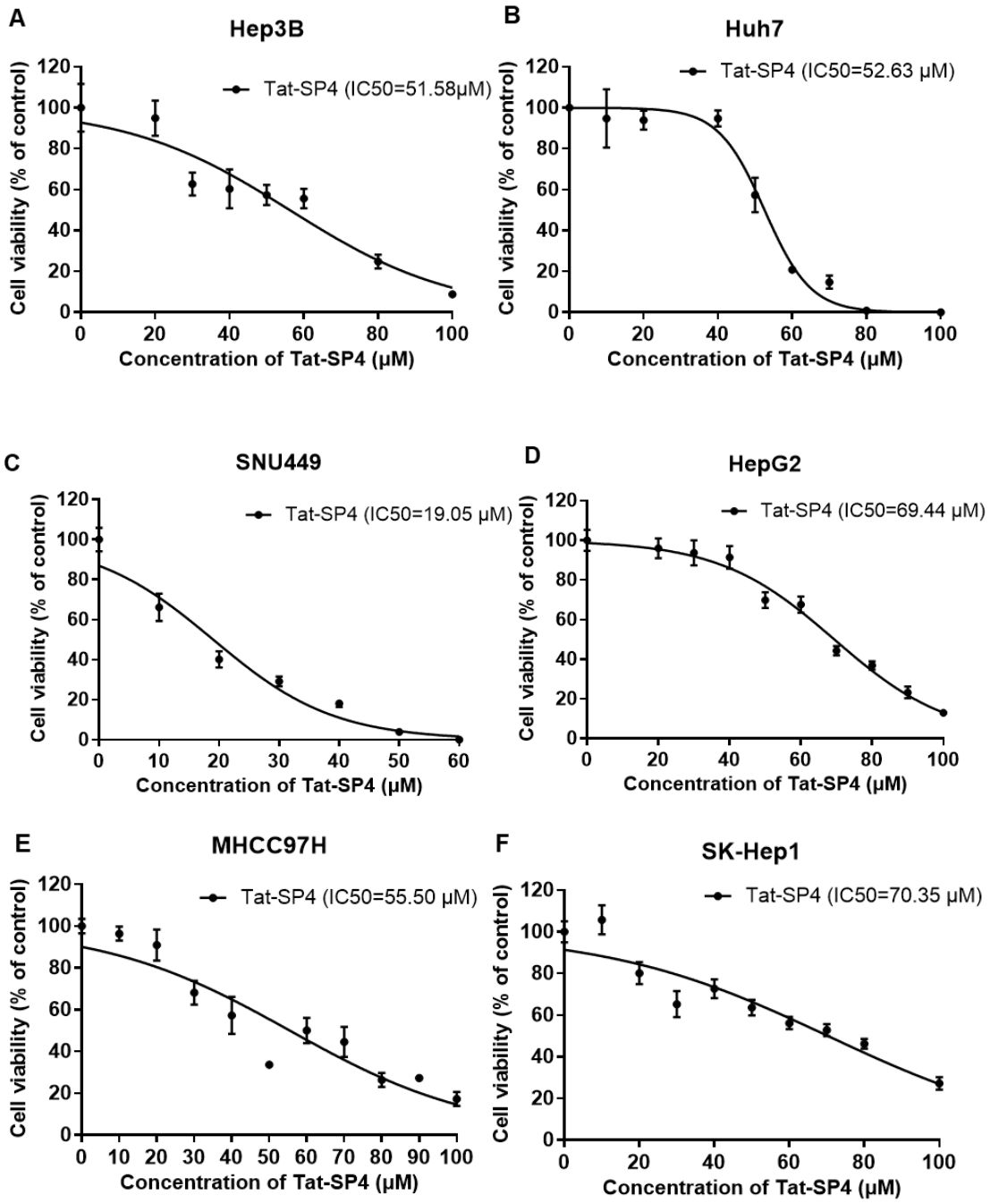

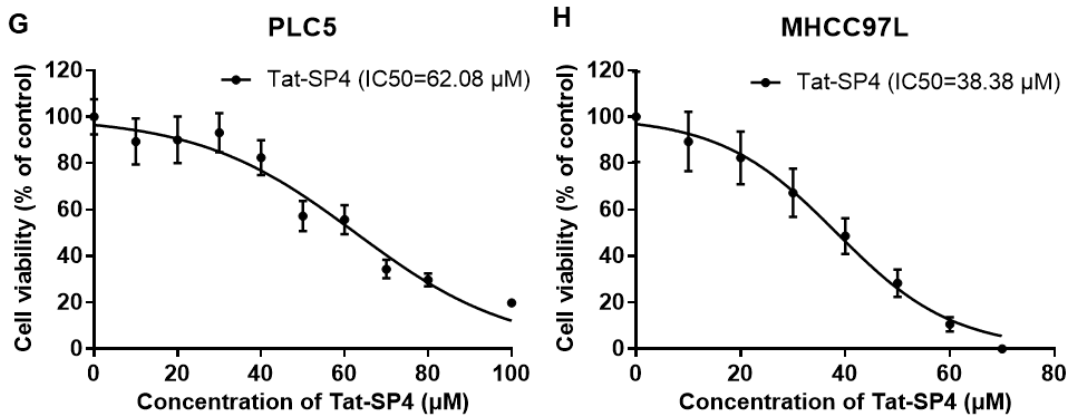


**Figure 4.5 Assessment of IC50 in HCC cell lines with the treatment of Tat-SP4.** **A**. Cell viability of Hep3B after treatment with different concentrations of Tat-SP4. The estimated IC50 value is 51.58 μM. **B**. Cell viability of Huh7 after treatment with different concentrations of Tat-SP4. The estimated IC50 value was 52.63 μM. **C**. Cell viability of SNU449 after treatment with different concentrations of Tat-SP4. The estimated IC50 value was 19.05 μM. **D**. Cell viability of HepG2 after treatment with different concentrations of Tat-SP4. The estimated IC50 value was 69.44 μM. **E**. Cell viability of MHCC97H after treatment with different concentrations of Tat-SP4. The estimated IC50 value was 55.50 μM. **F**. Cell viability of SK-Hep1 after treatment with different concentrations of Tat-SP4. The estimated IC50 value was 70.35 μM. **G**. Cell viability of PLC5 after treatment with different concentrations of Tat-SP4. The estimated IC50 value was 62.08 μM. **H**. Cell viability of MHCC97L after

treatment with different concentrations of Tat-SP4. The estimated IC50 was 38.38 μM. Data were mean ± SEM of three replicates.

The IC50 value of the control peptide Tat-SC4 in MHCC97L also be determined. However, the exact IC50 value of Tat-SC4 could not be determined due to out of the concentration range of designed (Figure 4.6). These results suggested that Tat-SP4 inhibits HCC cell viability specially. The inhibition efficiency came from Tat-SP4 itself other than peptides with random sequences.

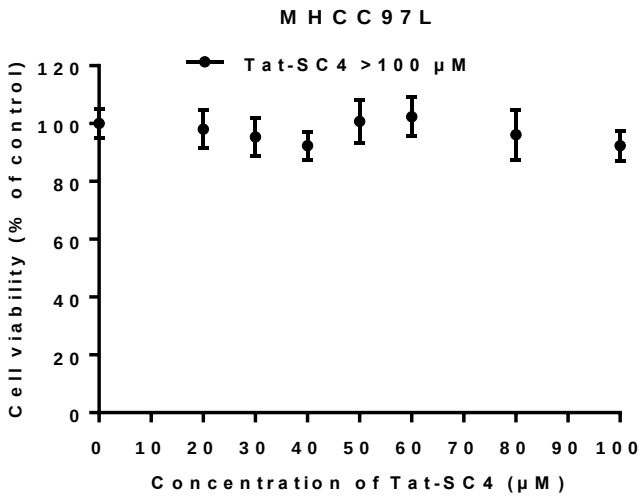


**Figure 4.6 Assessment of IC50 in HCC cell lines with the treatment of control peptides.** cell viability of MHCC97L after treatment by different concentrations of Tat-SC4. The estimated IC50 value was over 100μM.

### 4.2.2 Determination of the long-term anti-proliferation efficiency of Tat-SP4 in HCC cell lines

The IC50 value showed that Tat-SP4 could induce cell death in a

short period of time. To further determine whether Tat-SP4 had a long-term anti-proliferation effect on HCC cancer cells, a trypan blue exclusion assay was used to monitor cell proliferation. Hep3B, HepG2 and MHCC97L were seeded into 24 well plates. Cells were treated with a certain concentration (40μM or 60μM) of Tat-SP4 or the same concentration of Tat-SC4 on day 0, and the viable cell number was counted every 24 hours. According to the viable cell number from day 1 to day 5, a 5-day anti-proliferation curve was plotted. The results showed that Tat-SP4 could inhibit cell proliferation within 1 day, but from the second day, viable Hep3B, HepG2 and MHCC97L cells resumed proliferation at a normal rate. In contrast, Tat-SC4 had no effect on the 5-day proliferation assay (Figures 4.7A-C).

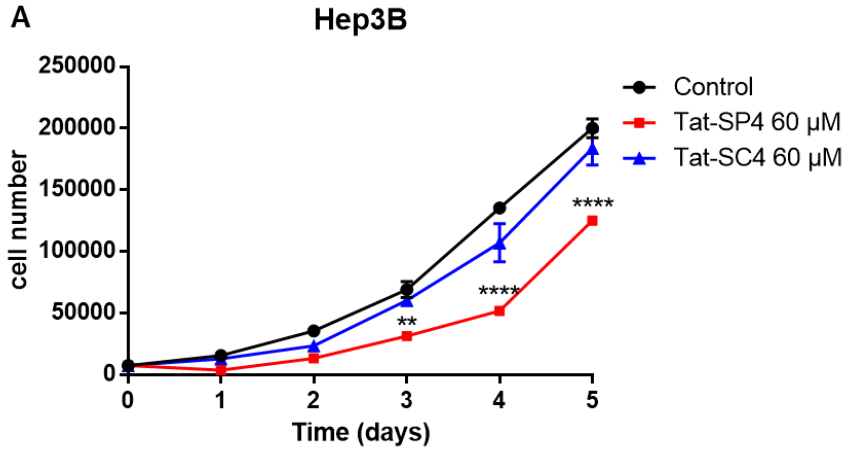

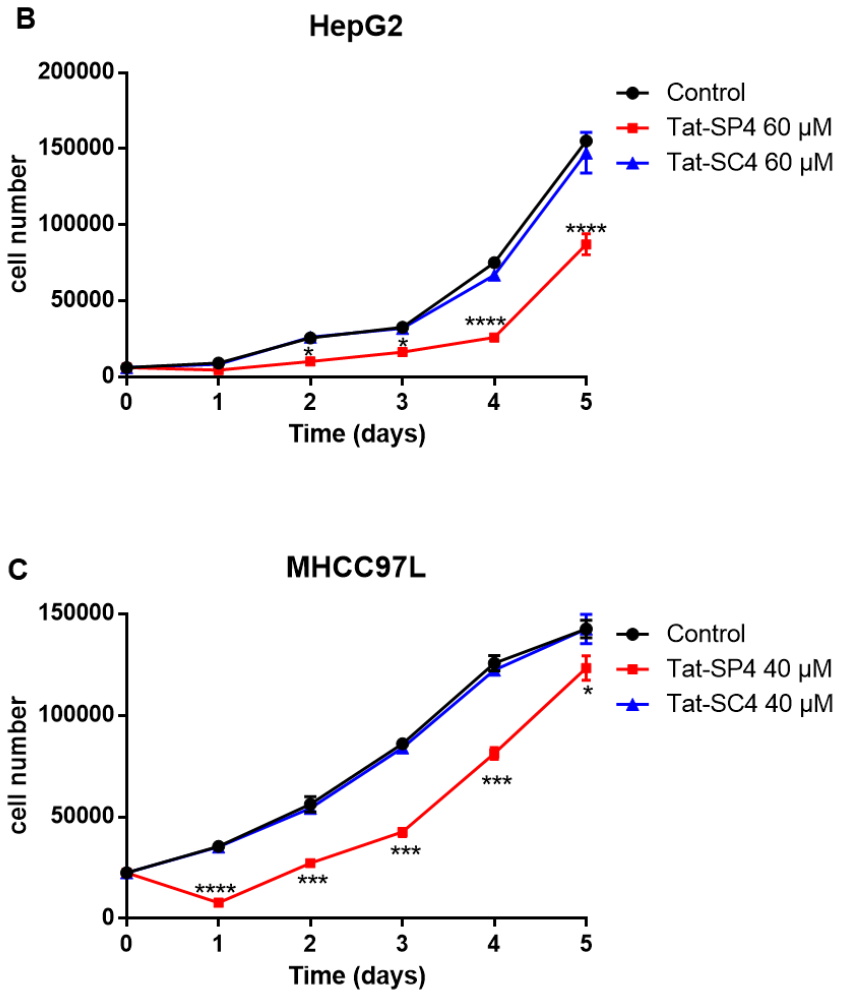


**Figure. 4.7 Long-term anti-proliferation efficacy of Tat-SP4 in HCC cell lines. A.** Cell viability results of Hep3B after treatment with 60μM Tat-SP4 or 60μM Tat-SC4 for five days. The number of viable cells was counted every 24 hours. **B**. Cell viability results of HepG2 after treatment with 60μM Tat-SP4 or 60μM Tat-SC4 for five days. The number of viable cells was counted every 24 hours. **C**. Cell viability results of MHCC97L after treatment with 40μM Tat-SP4 or 40μM Tat-SC4 for five days. The number of viable cells was counted every 24 hours. Bars

represent mean ± SEM (n=3). **P<0.01, ****P<0.0001; two-way ANOVA.

### 4.2.3 Tat-SP4 could override adaptive sorafenib resistance in different types of HCC cells.

Sorafenib, a multi-kinase inhibitor, exhibits anti-proliferative and anti-angiogenic effects by specifically inhibiting multiple growth factor pathways and tumor angiogenesis-related proteins (Wilhelm, Carter et al. 2004). Sorafenib is currently an effective first-line therapy for prolonging overall median survival in patients with advanced HCC. Clinical trials and the Sorafenib Assessment Randomized Protocol (SHARP) trials have shown that sorafenib is an effective drug to improve the outcome of advanced HCC patients. However, only a few patients can benefit from sorafenib, with a survival benefit of only 2 to 3 months. Usually, this unsatisfactory partial response may be because this population develops resistance to sorafenib within 6 months (Sui, Xue et al. 2001). To prolong the survival benefit of HCC patients, combination therapy is a better treatment option to overcome drug resistance. To further identify the possibility of Tat-SP4 as a potential option for combination therapy, the inhibitory effect of Tat-SP4 in sorafenib-resistant HCC cells was detected.

Thanks to our collaborator, Dr. Vincent W. Keng, who provided us with two HCC sorafenib resistance cell pools (SNU449 cell pool, SK-

Hep1 cell pool), we were able to assess the effect of Tat-SP4 on sorafenib resistance HCC cell lines. They used the Sleeping Beauty transposon system to first mutate the genome of HCC cell lines. And then resistance selection was performed by exposing mutant cell pools to different concentrations of sorafenib after isolating sorafenib resistance colonies or pools. Finally, they obtained two sorafenib resistance cell pools (SNU449 pool and SK-Hep1 pool).

The sensitivity of the sorafenib-resistant HCC cell pools and wild-type cells to sorafenib was first measured by the half-maximal inhibitory concentration (IC50) value. Cells were seeded in a 96-well plate and cultured with sorafenib at various concentrations for 72 hours. The IC50 was determined by measuring cell viability using an MTT assay. The results showed that the resistance cell pools indeed had a higher IC50 value than the wild-type cell lines (Figures 4.8 A&B).

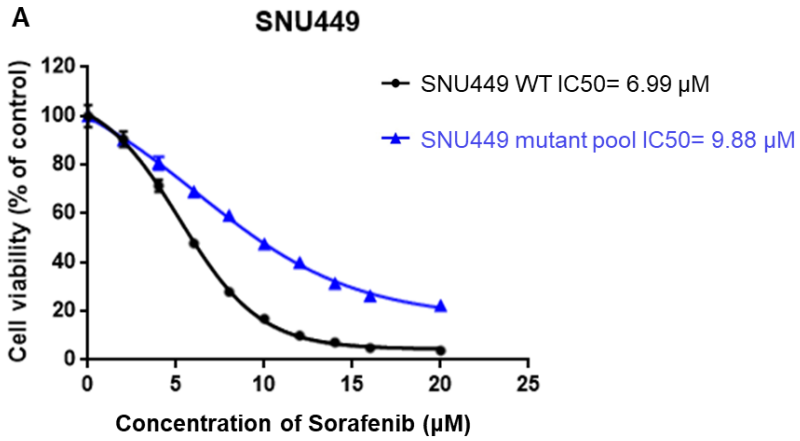

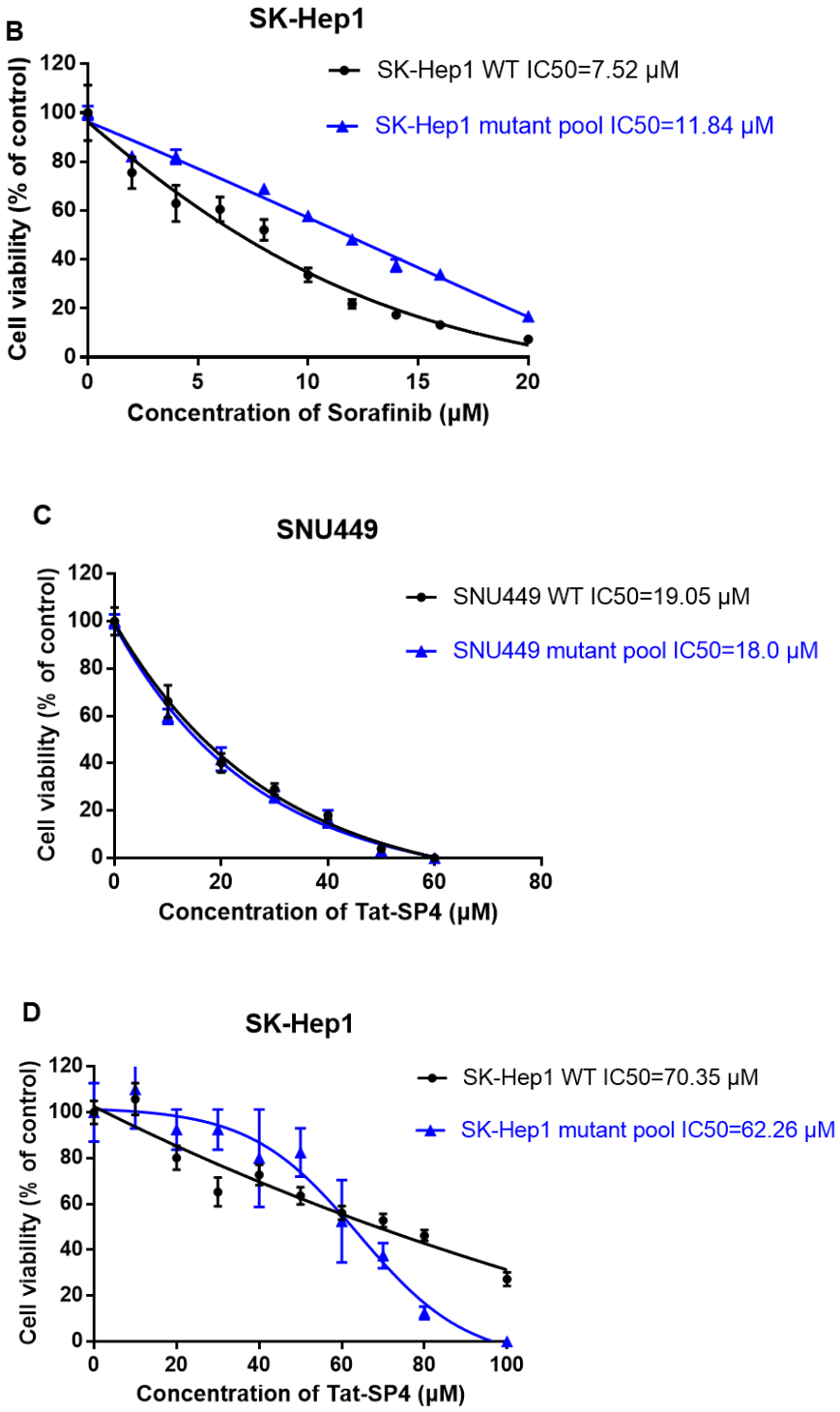


**Figure 4.8 Assessment of IC50 in sorafenib resistance HCC cell pools with the treatment of sorafenib and Tat-SP4. A**. cell viability of SNU449 WT and SNU449 mutant pool after treatment by different

concentrations of sorafenib. The estimated IC50 values were 6.99 μM and 9.88 μM, respectively. **B.** SK-Hep1 WT and SK-Hep1 mutant pool after treatment by different concentrations of sorafenib. The estimated IC50 values were 7.52 μM and 11.84 μM, respectively. **C.** cell viability of SNU449 WT and SNU449 mutant pool after treatment by different concentrations of Tat-SP4. The estimated IC50 values were 19.05 μM and 18.0 μM, respectively. **D.** SK-Hep1 WT and SK-Hep1 mutant pool after treatment by different concentrations of Tat-SP4. The estimated IC50 values were 70.35 μM and 62.26 μM, respectively. Data represent mean ± SEM of three replicates.

Subsequently, the sensitivity of the sorafenib-resistant HCC cell pools to Tat-SP4 was also assessed using the half-maximal inhibitory concentration (IC50) value. Cells were seeded in a 96-well plate and cultured with Tat-SP4 at various concentrations for 24 hours. The IC50 value was determined by measuring cell viability using the trypan blue exclusion assay. The results showed that there were no significant differences in IC50 value between the resistance cell pools and wild type cell lines. Tat-SP4 inhibition was independent of sorafenib resistance. Sorafenib-resistant cell pools showed no resistance effect to Tat-SP4 (Figures 4.8 C&D).

In addition, a sorafenib-resistant HCC cell line MHCC97L-lue

(luciferin) was kindly provided by our collaborator Prof. Terence Lee. A similar assay as above was performed to determine the sensitivity to Tat-SP4 of the sorafenib-resistant HCC cell line MHCC97L-lue and wild-type. The results showed that the sorafenib-resistant cell line was indeed resistant to sorafenib (Figure 4.9 A). And the sorafenib-resistant cell line showed no resistance effect to Tat-SP4. The anti-proliferation effect of Tat-SP4 was not affected by sorafenib resistance (Figure 4.9 B). In summary, Tat-SP4 could override adaptive sorafenib resistance in different types of HCC cells.

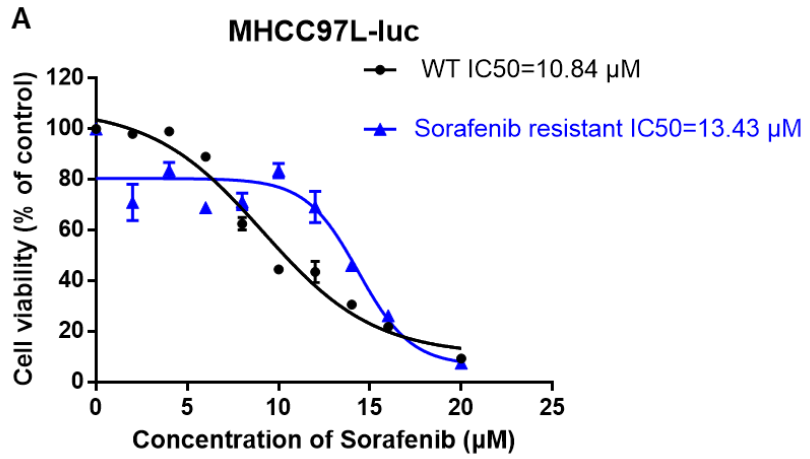


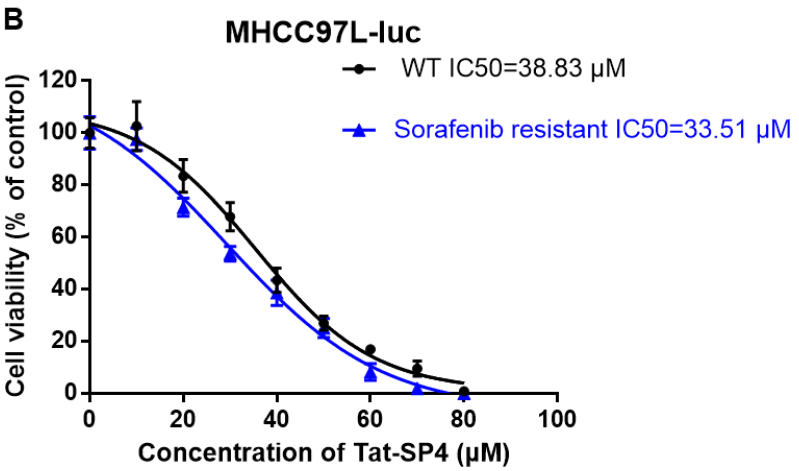

**Figure 4.9 Assessment of IC50 in sorafenib resistance HCC cell line MHCC97L-lue with the treatment of sorafenib and Tat-SP4. A.** cell viability of MHCC97L-lue WT cells and sorafenib resistant MHCC97L-lue cells after treatment by different concentrations of sorafenib. The estimated IC50 values were 10.84 μM and 13.43 μM, respectively. **B.** MHCC97L-lue WT cells and sorafenib resistant MHCC97L-lue cells after treatment by different concentrations of Tat-SP4. The estimated IC50 values were 38.83 μM and 33.51 μM, respectively. Data represents mean ± SEM of three replicates.

**Discussion**

Tat-SP4 could induce cell death in several HCC cell lines with different genetic backgrounds. Among them, the IC50 value of Tat-SP4 in SNU449 was the lowest, less than 20 μM. The IC50 value of Tat-SP4 in MHCC97L, Hep3B, MHCC97H and huh7 were in the middle range from 30 μM to 60 μM. PLC5, HepG2, and SK-Hep1 cells had higher IC50 values than of Tat-SP4 at more than 60μM. The mechanism behind the different IC50 values of Tat-SP4 in different HCC cell lines was unclear. We will discuss this issue in the next parts of this work.

Sorafenib is the primary option for the treatment of advanced HCC patients as a first-line drug. Sorafenib is a type of multi-targeted kinase inhibitor that can inhibit several important growth factor receptors such as

VEGFR and PDGFR. Treatment with sorafenib is limited by primary and acquired resistance. One possibility for the development of sorafenib resistance is that sorafenib-induced cell death is neutralized by sorafenib-induced activation of multiple survival pathways.

Interestingly, we found that Tat-SP4 could override adaptive sorafenib resistance in different types of HCC cells. Tat-SP4 could induce cell death in both wild-type and sorafenib-resistant HCC cells with similar IC50 values. This indicated that the mechanism of Tat-SP4-induced cell death was different from that of sorafenib-induced cell death. Our peptides might become a potential therapeutic agent to be combined with sorafenib for the treatment of HCC.

### 4.3 Tat-SP4 induces necrotic cell death that is only rescued by an inhibitor of autosis

#### 4.3.1 Tat-SP4 induces HCC cell death without the involvement of apoptosis.

In our previous studies, Beclin1-targeting stapled peptides could induce $HER^{2+}$ breast cancer cell death with a necrotic cell death feature but not an apoptosis manner (Yang, Qiu et al. 2021). Apoptosis is a form of programmed cell death and is widespread in eukaryotes. Apoptosis typically involves chromatin condensation, nuclear fragmentation, cytoplasmic shrinkage, and plasma membrane blebbing, forming

apoptotic bodies with intact small vesicles. Finally, these apoptotic bodies are engulfed by cells with phagocytic activity and degraded by lysosomes. Z-VAD-FMK is a known inhibitor of caspases and apoptosis without cytotoxicity. After pretreatment of cells with or without 50 μM Z-VAD-FMK for 2 hours, we measured the number of viable cells after treatment with different concentrations of Tat-SP4 (20, 30, 40 μM) for 24 hours in MHCC97L (Figure 4.10 A). However, Z-VAD-FMK could not rescue the cell death induced by Tat-SP4 in different concentrations. Similar results were observed in the other two HCC cell lines. The results showed that Z-VAD-FMK could block the effect of cisplatin but not Tat-SP4. After pretreatment with or without 50 μM Z-VAD-FMK for 2 hours, Hep3B cells were treated with 30 μM Tat-SP4 or 10 μM cisplatin (an apoptosis inducer) for 24 hours (Figure 4.10 B). In PLC/PRF/5 cells, different concentrations of Tat-SP4 (40 μM, 60 μM) or cisplatin 5 μM were added to cells after pre-treatment in the presence or absence of 50 μM Z-VAD-FMK for 2 hours (Figure 4.10 C).

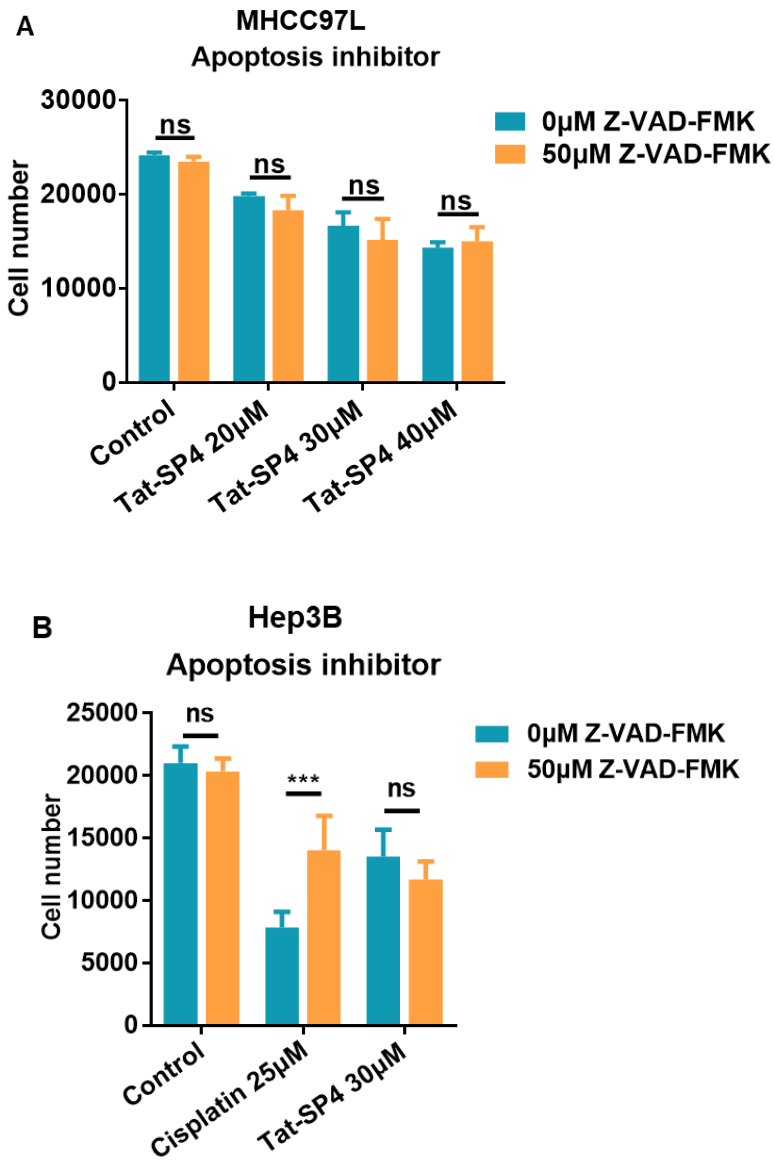
A
MHCC97L
Apoptosis inhibitor
Cell number
30000
20000
10000
0
ns
ns
ns
ns
0μM Z-VAD-FMK
50μM Z-VAD-FMK
Control
Tat-SP4 20μM
Tat-SP4 30μM
Tat-SP4 40μM
B
Hep3B
Apoptosis inhibitor
Cell number
25000
20000
15000
10000
5000
0
ns
***
ns
0μM Z-VAD-FMK
50μM Z-VAD-FMK
Control
Cisplatin 25μM
Tat-SP4 30μM

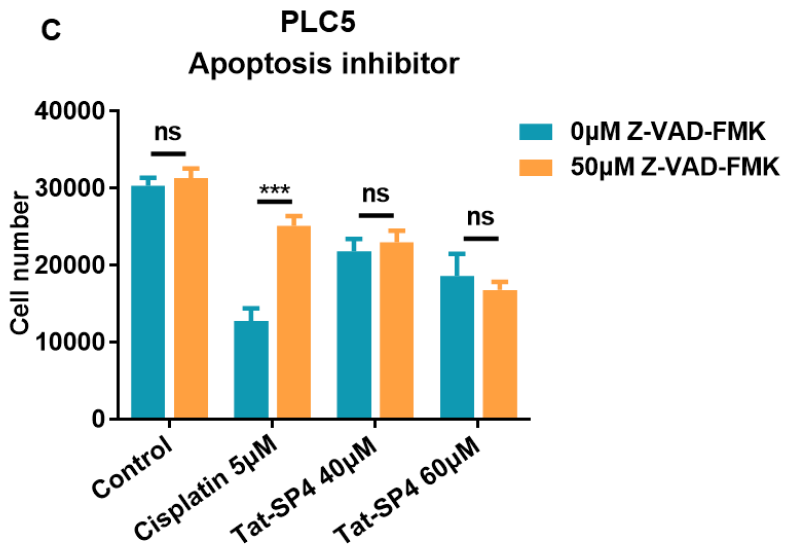


**Fig 4.10. Tat-SP4 induced HCC cells death couldn't be rescued by apoptosis inhibitor. A.** Survival of MHCC97L cells with or without pre-treatment of apoptosis inhibitor 50μM Z-VAD-FMK for 2 hours before treatment with Tat-SP4 (20, 30, 40 μM, 24h). **B.** the survival cell number of Hep3B treated by apoptosis activator cisplatin (10μM, 24h) or Tat-SP4 (30μM, 24h) in the presence or absence of apoptosis inhibitor. **C.** Survival of PLC/PRF/5 cells with or without pre- treatment of apoptosis inhibitor 50μM Z-VAD-FMK for 2 hours before treatment with apoptosis activator cisplatin (5μM, 24h), Tat-SP4 (40μM and 60μM, 24h). Error bars represent mean ± SEM. ns, not significant; ***P<0.001; t test.

Flow cytometry is a common and popular technology for differentiating between apoptotic and necrotic cell death. The Annexin V/PI double staining assay is used to analyze the early staged apoptotic cells (Annexin V positive and PI negative) and dead cells (positive for

both) according to the manufacturer's introduction. Our data showed that Tat-SP4 rapidly induced non-apoptotic cell death in a dose-dependent manner (Figure 4.11A). MHCC97L cells treated with Tat-SP4 20 μM for 3 h or 6 h didn't induce any significant cell death. The amount of apoptotic and dead cells in the control group was similar to that in the Tat-SP4 treatment group. After MHCC97L cells were treated with 40 μM, the amount of necrotic cell death increased immediately. Approximately 8.5% of MHCC97L cells underwent necrotic cell death at 3 hours, and this number was further increased by a factor of four at 6 hours. The rapid process was further evidence that Tat-SP4 induced non-apoptotic cell death, as apoptosis was known to proceed in a chronic and controlled manner, which requires more time to complete this process. In addition, the percentage of apoptotic cells after Tat-SP4 treatment was very low and did not increase in a dose-dependent manner.

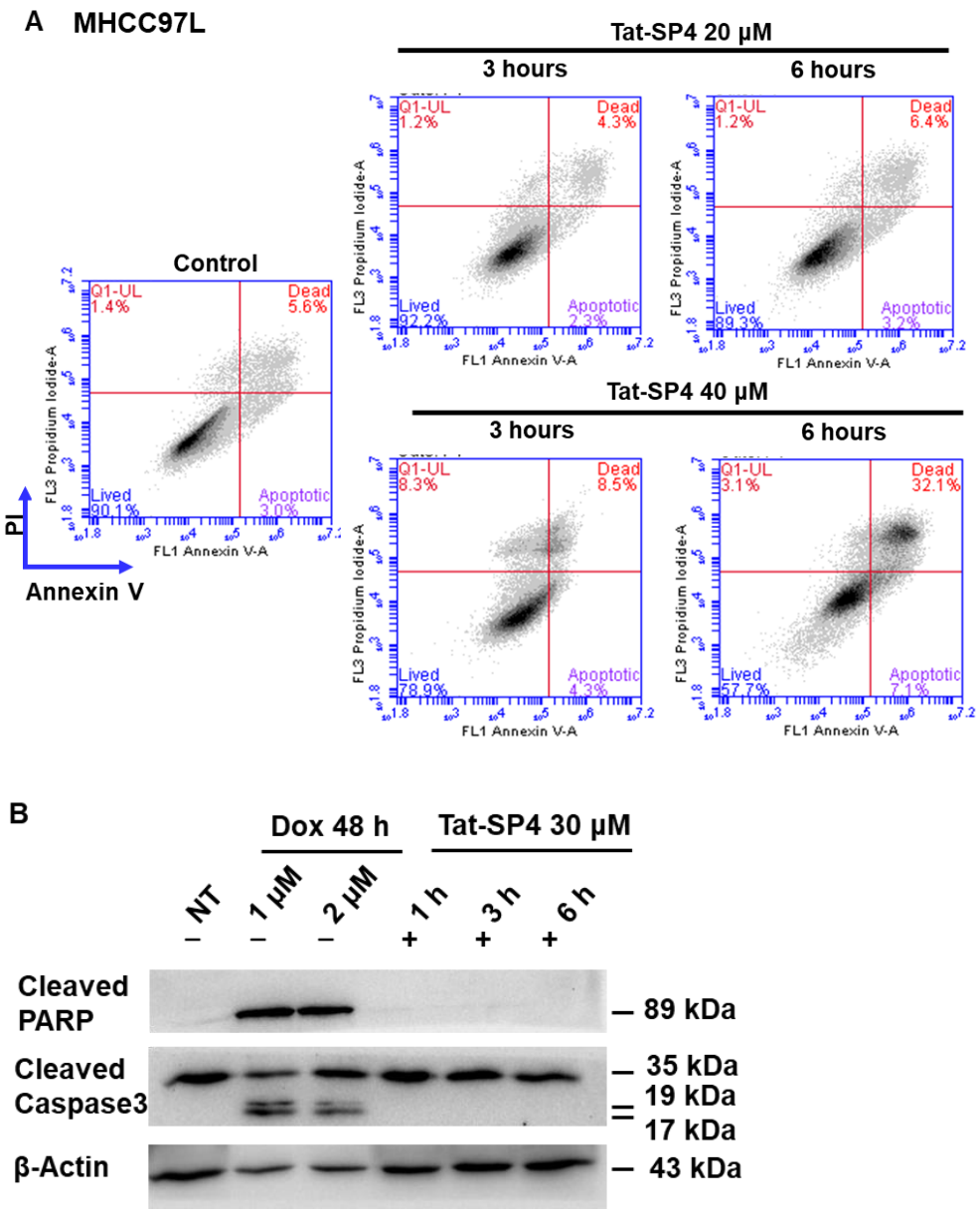


**4.11 Tat-SP4 induced non-apoptotic cell death in HCC cell lines. A.** Flow cytometry analysis with Annexin V and PI staining was performed in MHCC97L cells after treatment with Tat-SP4 (20 μM, 40 μM) for 3 or 6 hours. The percentage of dead cells positive for both annexin V and PI is shown in the upper right quadrant, and apoptotic cells for annexin V are shown in the lower right quadrant. Live cells are negative for both

stains. Data were collected on the BD FACSAria III Cell Sorter. **B**. Western blot of MHCC97L cells treated with doxorubicin (1, 2 μM for 48 hours) or Tat-SP4 (30 μM for 1, 3, 6 hours). Cell lysates were probed with cleaved caspase-3 antibody, cleaved PARP antibody, and β-actin antibody. Dox refers to doxorubicin.

Western blot was also used to detect the expression of key proteins of the apoptosis signaling pathway in MHCC97L cells treated with 30 μM Tat-SP4 at different time points. Caspase3 protein (35kd) plays an important role in the process of apoptosis. In normal cells, caspase3 protein is in an inactive state. After apoptosis, caspase3 is activated and then its conserved aspartic acid residue is hydrolyzed into two subunits, 17 kDa and 15 kDa. The caspase cascade reaction followed, and irreversible apoptosis occurs. Another apoptosis marker is cleaved PARP (89 kDa), which is a product of poly (ADP-ribose) polymerase (PARP), a 116 kDa nuclear protein that can be cleaved by apoptosis-induced caspases. The results showed that (as shown in Figure 4.11 B) MHCC97L cells treated with doxorubicin, a positive inducer of apoptosis, resulted in the cleavage of both caspase 3 and PARP. However, there was no significant production of cleaved caspase 3 and cleaved PARP after 30 μM Tat-SP4 treatment for 1, 3, or 6 hours. Taken together, these results showed that Tat-SP4 induced non-apoptotic cell death in HCC cell lines.

### 4.3.2 Tat-SP4 induces HCC cell death without involvement of ferroptosis and necroptosis

In addition to apoptosis, the manner of ferroptosis and necroptosis cell death also shows a necrotic cell death feature. Ferroptosis is a form of regulated cell death driven by ion-dependent intracellular oxidative perturbations. Ferroptosis-regulated cell death manifests a predominance of mitochondrial changes, including ultrastructural changes, reduced/disappearing mitochondrial cristae, mitochondrial membrane ruptures, and shrinkage. Since the morphological changes of ferroptosis were similar to Tat-SP4-induced cell death, we next asked whether the ferroptosis death machinery is involved in Tat-SP4-induced cell death.

The ferroptosis inhibitor, ferrostatin-1 (Fer-1), a lipid ROS scavenger, was used to determine whether Tat-SP4 induced ferroptosis. At the same time, the ferroptosis inducer, erastin, was used as a positive control. MHCC97L, PLC/PRF/5 and Hep3B cells were seeded in 96 wells and treated with Fer-1 (10 μM) followed by different concentrations of Tat-SP4 (30 μM, 40μM) or positive control group treated with erastin (6 μM, 8 μM or 10 μM). After incubation for 24 hours, cell viability was analyzed by the trypan blue staining method. The histograms show that Fer-1 could rescue erastin-induced cell death but failed to inhibit Tat-SP4-induced cell death in MHCC97L, PLC/PRF/5, or Hep3B cells (Figures

4.12 A&B&C).

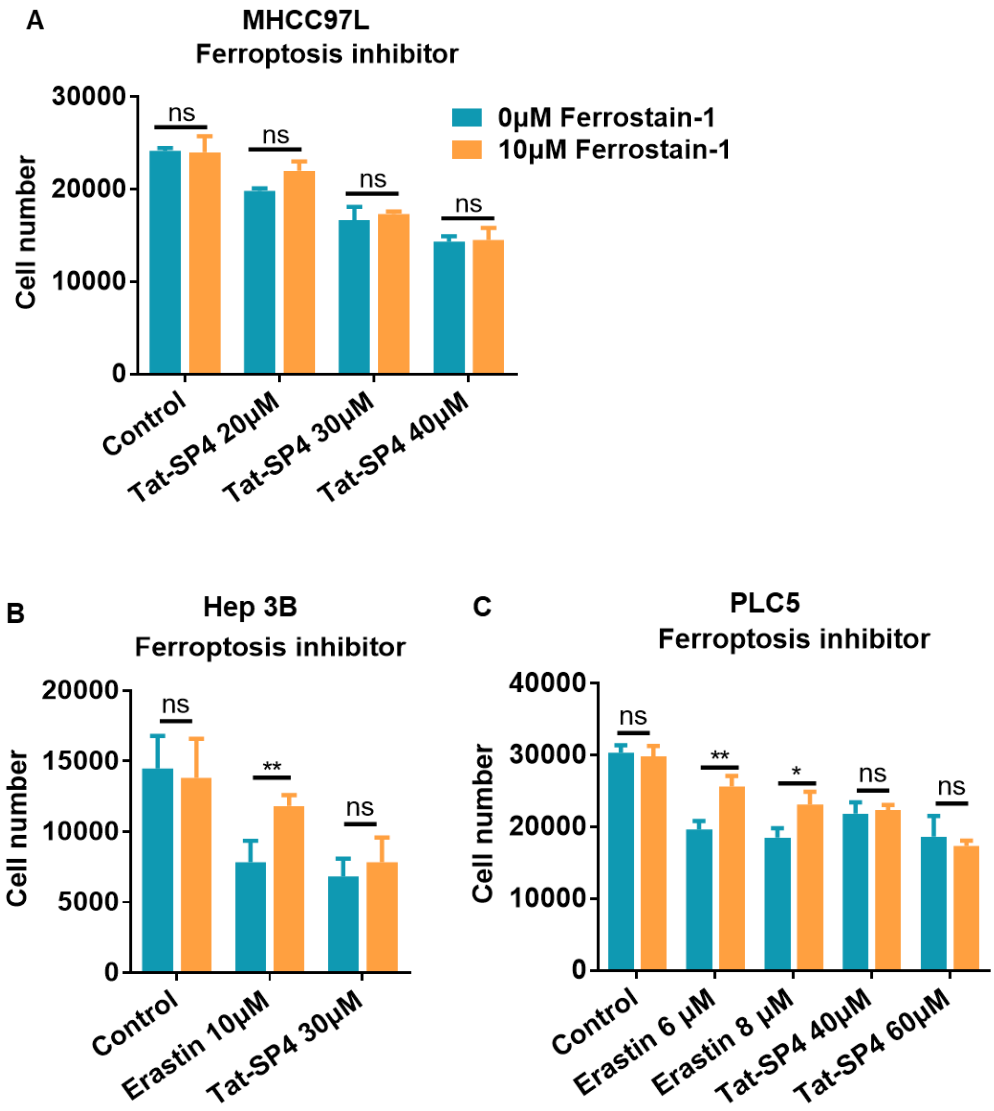


**Figure 4.12 Tat-SP4 induces HCC cell death without involvement of ferroptosis A.** Trypan blue staining method was used to measure the MHCC97L survival cell number after treatment with Tat-SP4 (20, 30,40 μM for 24 h) with or without the ferroptosis inhibitor (Ferrostain-1). **B.** Survival of Hep3B cells treated with or without ferroptosis inhibitor 10 μM Ferrostatin-1 for 24 hours and treatment with ferroptosis inducer

erastin (10μM, 24h), Tat-SP4 (30μM, 24h). **C.** Survival of PLC/PRF/5 cells treated with or without ferroptosis inhibitor 10μM Ferrostatin-1 for 24 hours and treatment with ferroptosis inducer erastin (6, 8 μM, 24h), Tat-SP4 (40μM and 60μM, 24h). Bars represent mean ± SEM (n = 3), ns, not significant *P <0.1, **P <0.01, t test.

Necroptosis is a form of regulated cell death driven by intracellular or extracellular microenvironmental perturbations. Necroptosis is generally manifested by a necrotic morphotype. Tumor necrosis factor (TNF) induces caspase-3-independent cell death and relies primarily on the sequential activation of receptor-interacting serine/threonine protein kinase 1 (RIPK1), mixed lineage kinase domain-like pseudokinase (MLKL), and RIPK3. Necrostatin-1 (Nec-1) is a chemical inhibitor of RIPK1 that can inhibit TNFR-driven necroptosis.

Necroptosis inhibitor Nerrostatin-1 (Nec-1) was used to block necroptosis of cells. MHCC97L, PLC/PRF/5, and Hep3B cells were seeded into 96 well plate and treated with or without Nec-1 (25μM, 50μM) followed treatment by different concentrations of Tat-SP4. After incubation 24 hours, cell viability was analyzed by the trypan blue staining method. The histograms showed that Nec-1 could not rescue Tat-SP4 induced cell death in MHCC97L, PLC/PRF/5 or Hep3B cells (Figures 4.13 A&B&C).

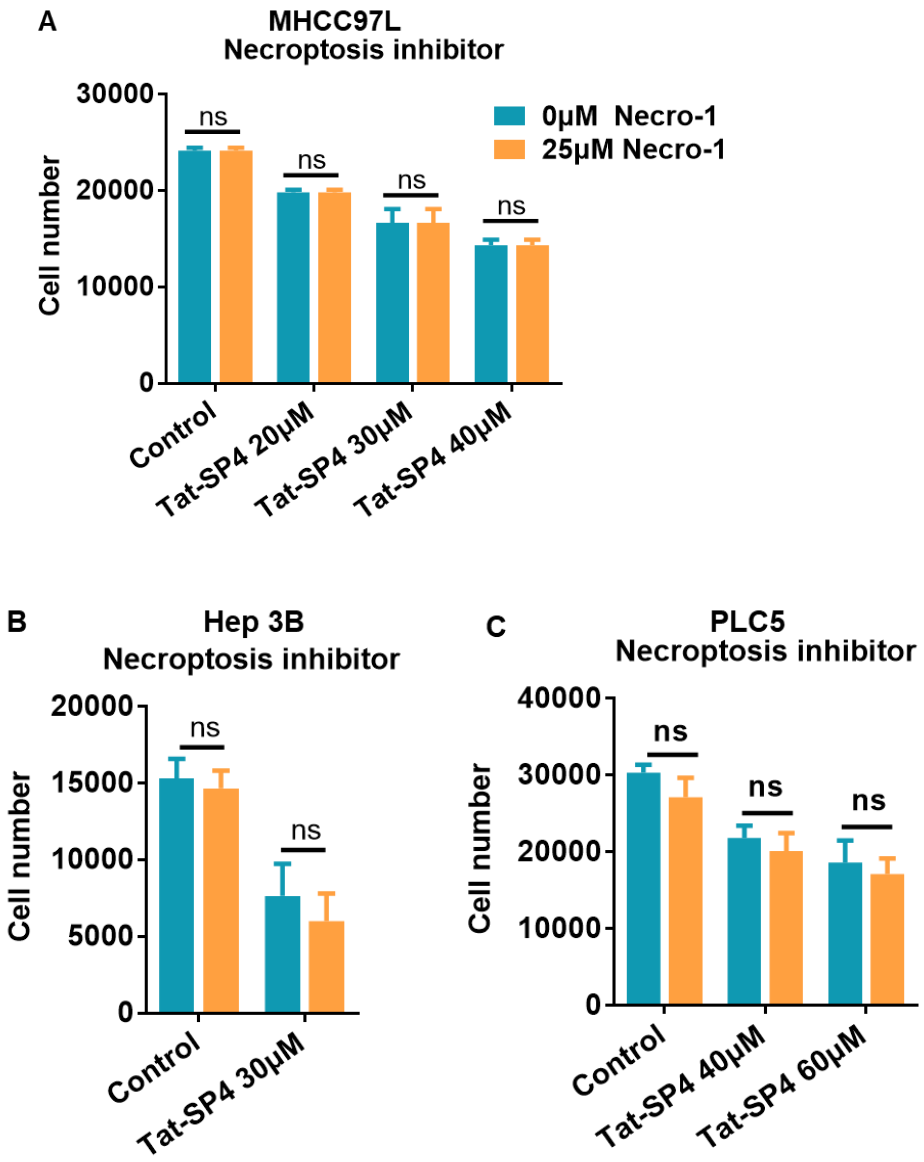


**Figure 4.13 Tat-SP4 induces HCC cell death without involvement of necroptosis A**. MHCC97L cell survival number was measured by Trypan blue staining method. Cells were treated by Tat-SP4 (20, 30,40 μM) for 24 h in with or without 25 μM necroptosis inhibitor (Necro-1). **B**. Survival of Hep3B cells treated with or without necroptosis inhibitor 50μM Nerrostatin-1 for 24 hours and treatment with Tat-SP4 (30μM, 24h). **C**. Survival of PLC/PRF/5 cells treated with or without necroptosis

inhibitor 25μM Nerrostatin-1 for 24 hours and treatment with Tat-SP4 (40μM and 60μM, 24h). Error bars represent mean ± SEM (n = 3), ns, not significant *P <0.1, **P <0.01, t test.

Overall, Tat-SP4 induced cell death is non-apoptotic cell death. Inhibitors of ferroptosis and necroptosis also show no significant protective effect on Tat-SP4 induced cell death in HCC cell lines.

### 4.3.3 Tat-SP4-induced cell death could be rescued by inhibitors of autosis

Autosis is a unique form of cell death caused by the selective overactivation of autophagy. Morphological features of autosis are different from apoptosis and necrosis. Unique morphological features occur in the abnormal nucleus, such as focal ballooning of the perinuclear space, mild chromatin condensation, and focal concavity of the nuclear surface (Liu, Shoji-Kawata et al. 2013). Autosis also shows swollen mitochondria. Some intracellular stresses can trigger the occurrence of autosis, such as nutrient starvation, hypoxia-ischemia, and excessive autophagy. Autosis can be induced by the stapled peptide Tat-Beclin1, which is also an autophagy-inducing peptide consisting of an N-terminal Tat sequence and a C-terminal region that binds to the Nef protein of HIV (Liu, Shoji-Kawata et al. 2013). Autosis can be regulated by $Na^+$, $K^+$-ATPase and inhibited by pharmacological and genetic inhibition of $Na^+$,

$K^+$-ATPase (Liu, Shoji-Kawata et al. 2013). Cardiac glycosides can inhibit autosis by targeting to $Na^+$, $K^+$-ATPase.

Digoxin, a type of cardiac glycoside, was used to inhibit autosis, which can inhibit autotic cell death in vitro and in vivo. To investigate whether such cell death is related to the mechanism of Tat-SP4-induced cell death, digoxin was used as an autosis inhibitor. After pre-treatment of cells with or without digoxin, we measured cell numbers after treatment with different concentrations of Tat-SP4 in MHCC97L and Hep3B (Figure 4.14 A&B). Our results indicated that digoxin could rescue Tat-SP4-induced cell death. Tat-SP4 induced cell death may be related to autosis.

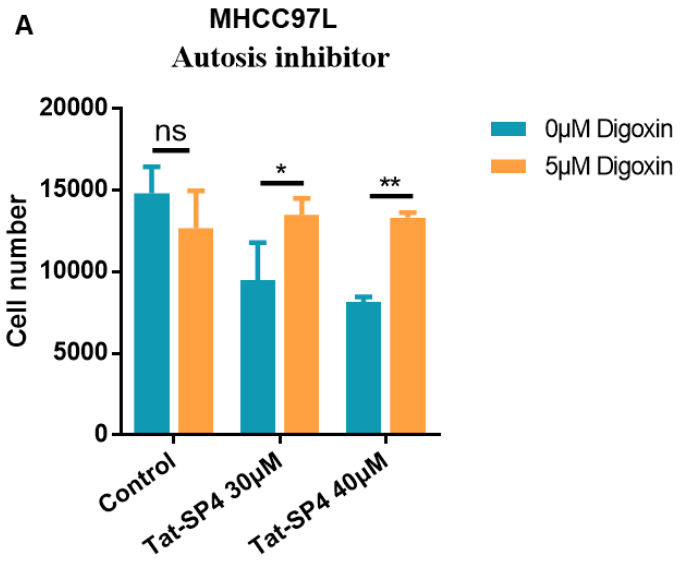

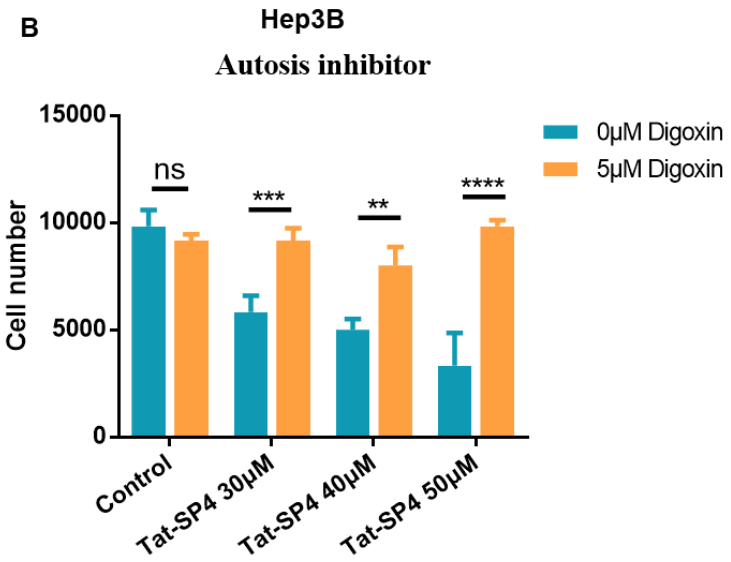


**Figure 4.14 Tat-SP4-induced HCC cell death could be rescued by autosis inhibitor. A.** Trypan blue assay was used to measure the viable cell number of MHCC97L cells after treatment with Tat-SP4 (30, 40 μM) for 2 hours in the presence or absence of pretreatment with digoxin (5μM, 5 hours). **B.** Hep3B cells treated with Tat-SP4 (30, 40, 50 μM, 2h) in with or without 5μM digoxin pre-treatment for 5 hours. The number of viable cells was counted by the trypan blue method. Error bars represent mean ± SEM (n = 3), ns, not significant *P <0.1, **P <0.01, ***P <0.001, ****P <0.0001, t-test.

### 4.3.4 Tat-SP4-induced cell death shows morphologic features of autosis

The morphological features of autosis are distinct from other common modes of cell death. Cells undergoing autosis show a number of

unique morphological features. In the early stage of autosis, cells show an existing membrane and nuclear membrane with an accumulation of vacuoles in the perinuclear region (Liu, Shoji-Kawata et al. 2013). In the late stage, cells undergo rapid nuclear shrinkage leading to rupture of the plasma membrane to release intracellular components and extracellular extrusion. After cell death, the cell is still attached to the dish (Liu, Shoji-Kawata et al. 2013). To characterize whether Tat-SP4-induced necrotic cell death is similar to autosis, we used confocal imaging studies to observe the morphological features of Tat-SP4-induced cell death. The results showed that Tat-SP4 could induce significant excessive vacuolization at 5 min, as indicated by the red arrow in Figure 4.14C. At 10 min, the rapid shrinkage of the nucleus and local separation of the inner and outer nuclear membranes are evident. This was followed by rupture of the plasma membrane and release of cytoplasmic components. In addition, similar to Tat-Beclin1-induced autosis, Tat-SP4-induced dead cells still attached to the dish (Figure 4.14 C).

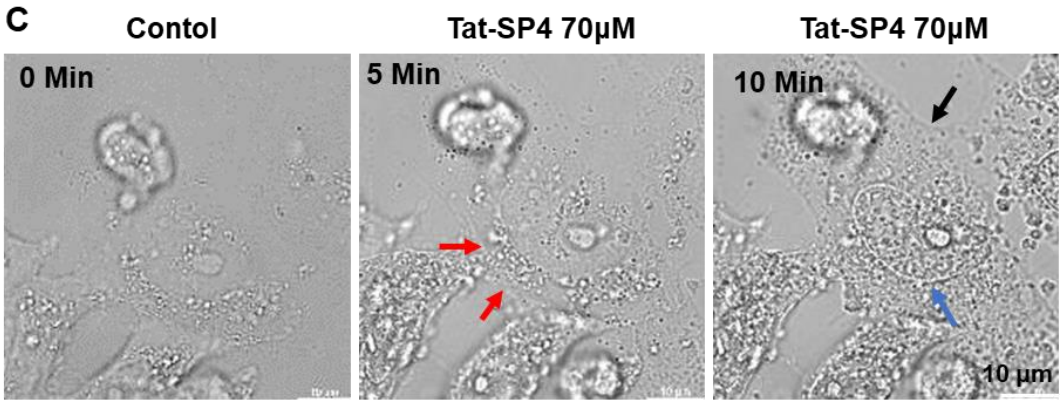

**Figure 4.14 Tat-SP4 induced cell death shows morphological features of autosis. C.** Hep3B cells were treated with 70μM Tat-SP4 and the changes in cell morphology were observed by confocal imaging at the indicated time points. The red arrow indicates the accumulation of vacuolization. The blue arrow indicates the site of nuclear membrane separation. The black arrow indicates the rupture of the plasma membrane. Scale bar: 10μm.

## Discussion

Tat-SP4-induced cell death did not involve programmed cell death such as apoptosis, ferroptosis and necroptosis. Interestingly, an inhibitor of autosis could rescue Tat-SP4-induced cell death and shows autosis-related morphological features. However, the molecular mechanism of autosis iss still not well defined. To investigate the molecular mechanism of Tat-SP4-induced cell death, we need more studies to explore other possibilities. Tat-labeled peptides are a kind of CCP rich in positive charges that help to cross the plasma membrane. The Tat sequence may be associated with other membrane-bound organelles through non-specific binding to lipids. A mitochondrion is a double membrane organelle that plays an important role in cell death. Therefore, we will investigate whether Tat-SP4 has an impact on mitochondria.

## 4.4 Tat-SP4 causes mitochondrial dysfunction and impairs oxidative phosphorylation activity

### 4.4.1 Tat-SP4 decreases mitochondrial membrane potential (Δψ)

The effect of Tat-SP4 on mitochondrial metabolism was first determined by measuring mitochondrial membrane potential. HCC cell lines HepG2 and MHCC97L were first treated with indicated concentrations of Tat-SP4 at different times. The cells were then stained with 100 nM TMRM for 30 minutes at 37°C. TMRM is a cell-permeable fluorescent dye that can accumulate at mitochondria with intact mitochondrial membrane potential. Healthy cells with active mitochondrial potential can be stained with detectable red fluorescence. Flow cytometry was used to quantify TMRM fluorescence intensity. The results showed that the TMRM fluorescence of three HCC cell lines, MHCC97L, HepG2, and Hep3B, significantly decreased upon treatment with different concentrations of Tat-SP4, which meant that the mitochondrial membrane potential has an obvious reduction (Figures 4.15 A&B&C). Tat-SP4 reduced mitochondrial membrane potential in HCC cell lines.

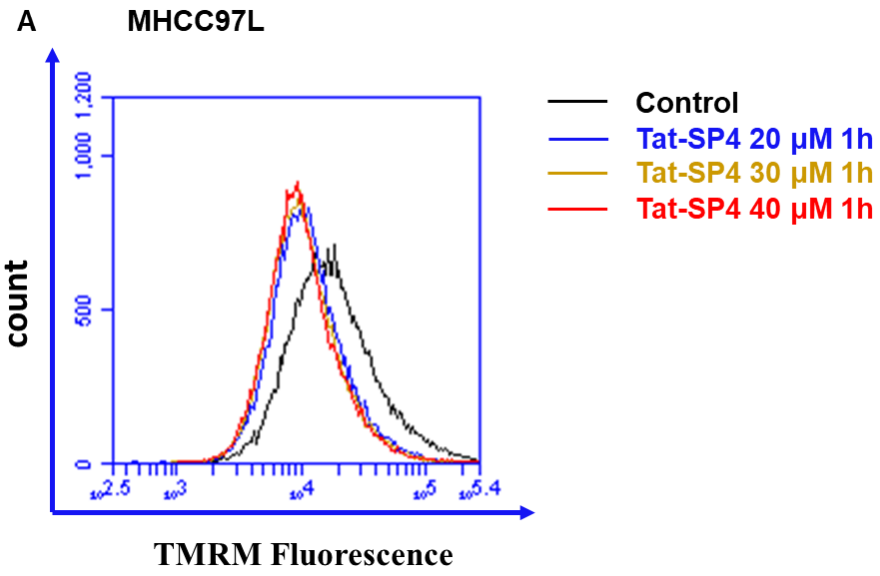
A
MHCC97L
count
1,200
1,000
500
0
$10^{2.5}$
$10^{3}$
$10^{4}$
$10^{5}$
$10^{5.4}$
TMRM Fluorescence
Control
Tat-SP4 20 μM 1h
Tat-SP4 30 μM 1h
Tat-SP4 40 μM 1h

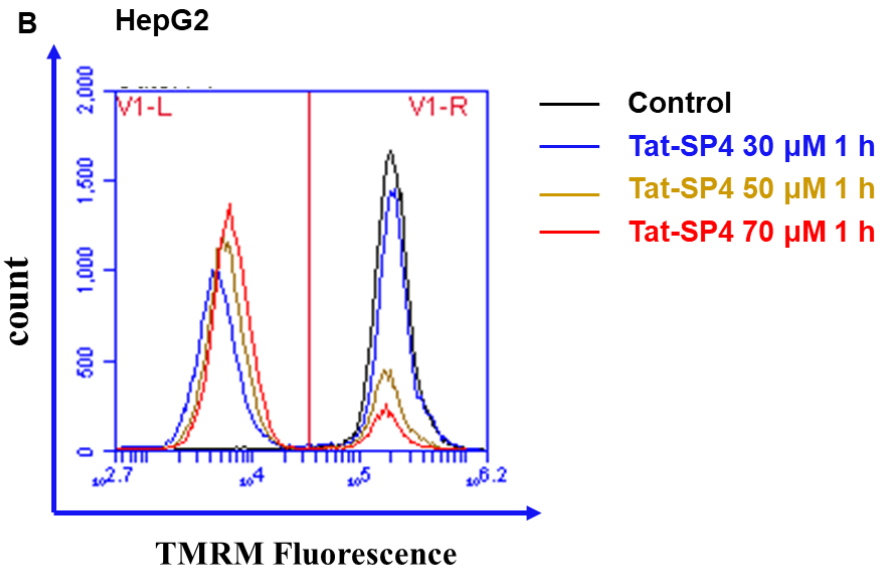
B
HepG2
count
2,000
1,500
1,000
500
0
V1-L
V1-R
$10^{2.7}$
$10^{4}$
$10^{5}$
$10^{6.2}$
TMRM Fluorescence
Control
Tat-SP4 30 μM 1 h
Tat-SP4 50 μM 1 h
Tat-SP4 70 μM 1 h

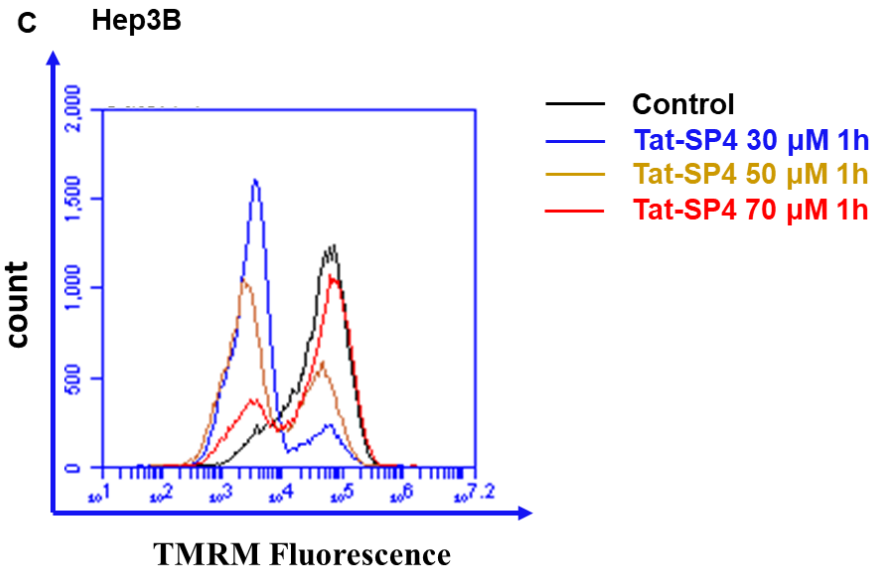


**Figure 4.15 Tat-SP4 decreases mitochondrial membrane potential (Δψ). A.** Representative flow cytometry plot of MHCC97L treated with Tat-SP4 (20, 30, 40 μM) for 1 h. **B**. Representative flow cytometry plot of HepG2 treated with Tat-SP4 (30, 50, 70 μM) for 1 h. **C**. Representative flow cytometry plot of Hep3B treated with Tat-SP4 (30, 50, 70 μM) for 1 h. TMRM was used to quantify mitochondrial membrane potential using a BD Accuri C6 flow cytometer.

### 4.4.2 Tat-SP4 reduces maximal oxygen consumption rate (OCR) in HCC cell lines

Damage to the mitochondrial membrane potential can directly affect mitochondrial oxidative phosphorylation (OXPHOS), a process that takes place at the inner mitochondrial membrane and is driven by mitochondria. Oxygen consumption rate (OCR) is an important parameter for the mitochondrial OXPHOS process. A Seahorse Bioscience Extracellular

Flux Analyzer (XF24) was used to monitor the change in intercellular OCR in the HCC cell lines MHCC97L and HepG2. After cells were treated with the indicated concentrations of Tat-SP4 or vehicle, 1 μM oligomycin, 1 μM FCCP, and 0.5 μM rotenone and antimycin A were added sequentially to inhibit complex V of the ETC process, dissipate mitochondrial membrane potential, and inhibit complex I/III of the ETC, respectively. The real-time change in OCR was detected by the Agilent Seahorse Analyzer. The results showed that the maximal oxygen consumption rate of MHCC97L cells was reduced after Tat-SP4 treatment. Statistical analysis showed that the maximal OCR was significantly decreased in a dose-dependent manner (Figures 4.16 A&B). Similar results were observed in HepG2 (Figures 4.16 C&D). Indeed, Tat-SP4 interferes with mitochondrial metabolism by reducing the maximal oxygen consumption rate.

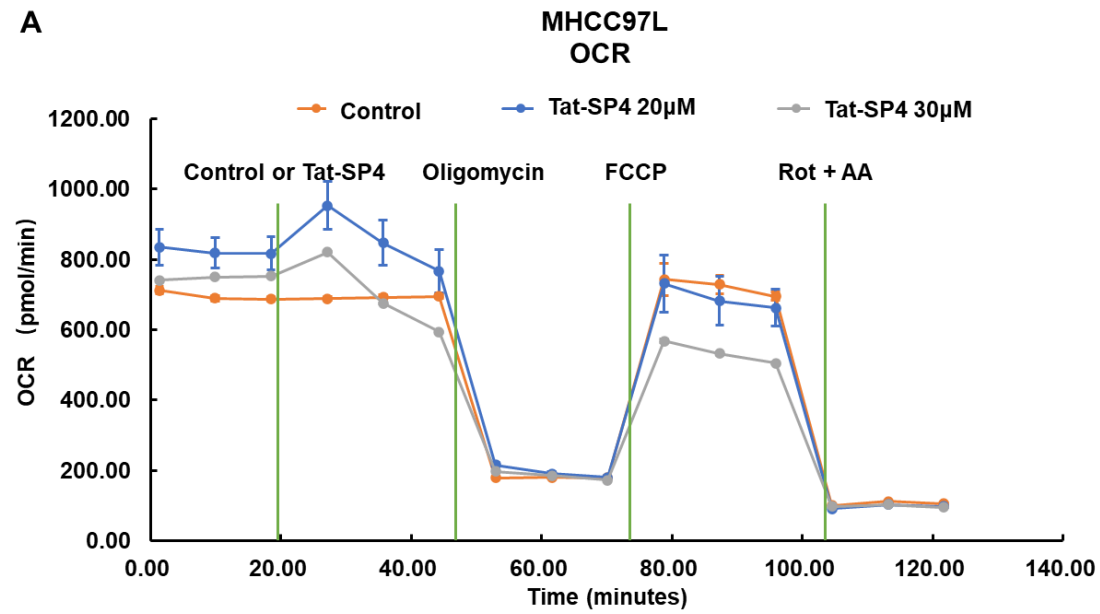
A
MHCC97L
OCR
Control
Tat-SP4 20μM
Tat-SP4 30μM
Control or Tat-SP4
Oligomycin
FCCP
Rot + AA
OCR (pmol/min)
1200.00
1000.00
800.00
600.00
400.00
200.00
0.00
0.00
20.00
40.00
60.00
80.00
100.00
120.00
140.00
Time (minutes)

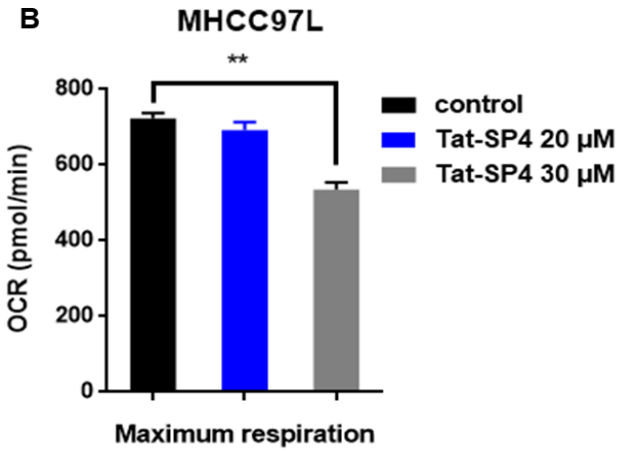
B
MHCC97L
**
800
600
400
200
0
OCR (pmol/min)
control
Tat-SP4 20 μM
Tat-SP4 30 μM
Maximum respiration

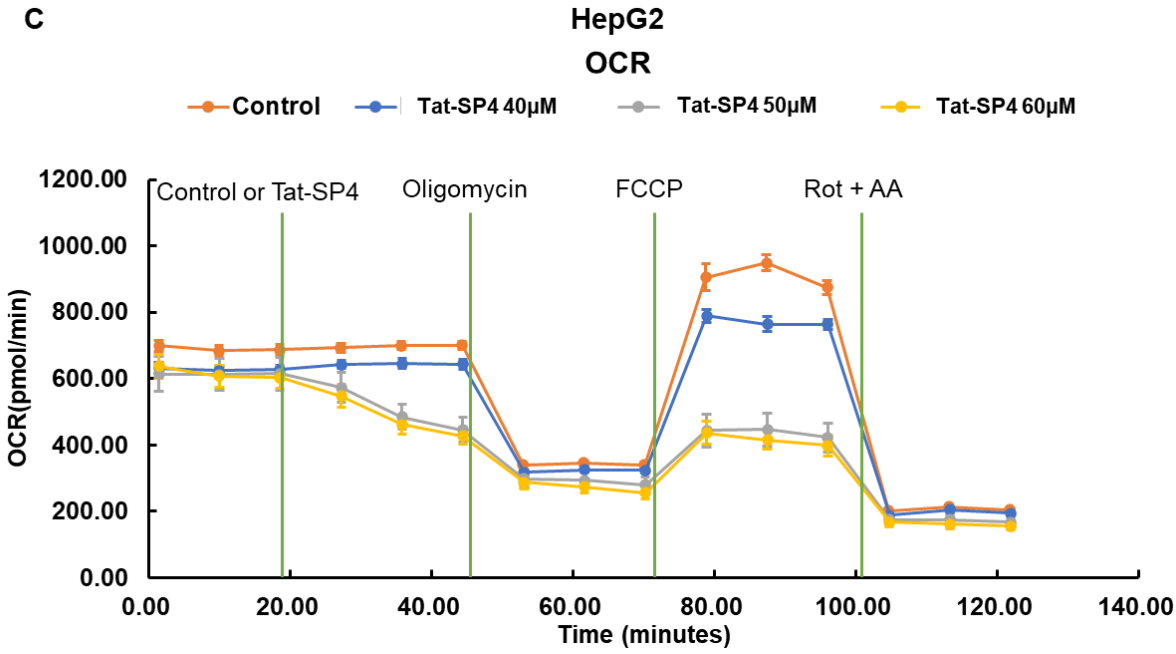
C
HepG2
OCR
Control
Tat-SP4 40μM
Tat-SP4 50μM
Tat-SP4 60μM
Control or Tat-SP4
Oligomycin
FCCP
Rot + AA
OCR(pmol/min)
1200.00
1000.00
800.00
600.00
400.00
200.00
0.00
0.00
20.00
40.00
60.00
80.00
100.00
120.00
140.00
Time (minutes)

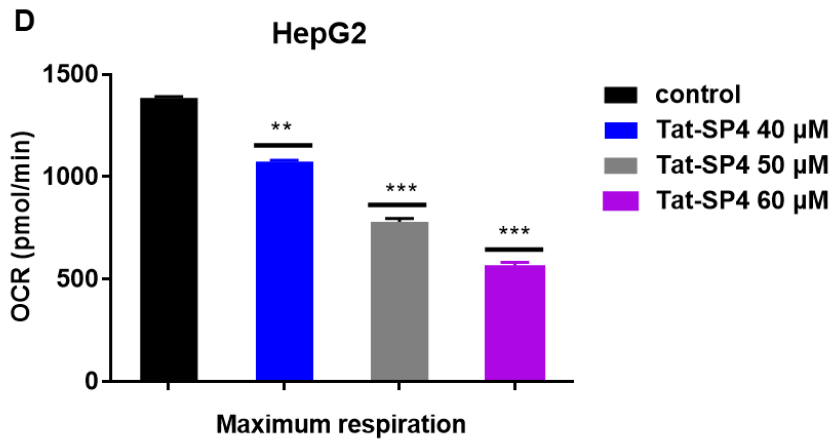


**Figure 4.16 Tat-SP4 reduces maximal oxygen consumption rate (OCR) in HCC cell lines. A.** Oxygen consumption rate (OCR) of MHCC97L cells was measured using the Agilent Seahorse Analyzer. Cells were either treated by PBS buffer (vehicle) or Tat-SP4 (20, 30 μM) followed by 1μM oligomycin, 1μM FCCP, and 0.5μM rotenone and antimycin A. Each point is the real-time OCR changes. **B.** Statistical analysis of maximal OCR as measured in (A). **C.** Oxygen consumption rate (OCR) of HepG2 cells was measured using the Agilent Seahorse Analyzer. Cells were either treated by PBS buffer (vehicle) or Tat-SP4 (40,50,60 μM) followed by 1μM oligomycin, 1μM FCCP, and 0.5μM rotenone and antimycin A. Each point means the real-time OCR changes. **D.** Statistical analysis of maximal OCR as measured in (C). Bars represent mean ± SEM ($n$ = 3). *$P$ < 0.05, **$P$ <0.01; $t$ test.

### 4.4.3 Tat-SP4 increases intracellular reactive oxygen species (ROS) levels in HCC cell lines

Furthermore, dysfunction in the OXPHOS process usually leads to mitochondrial damage in the form of increased cellular ROS levels. To evaluate the effect of Tat-SP4 on cellular ROS levels, we used the Cell ROXTM green probe to visualize the change in ROS. As the Tat-SP4 concentration increases, the ROX™ green fluorescence gradually increases. Tat-SP4 indeed induced the increase of ROS in MHCC97Land HepG2 cells (Figures 4.17 A&B).

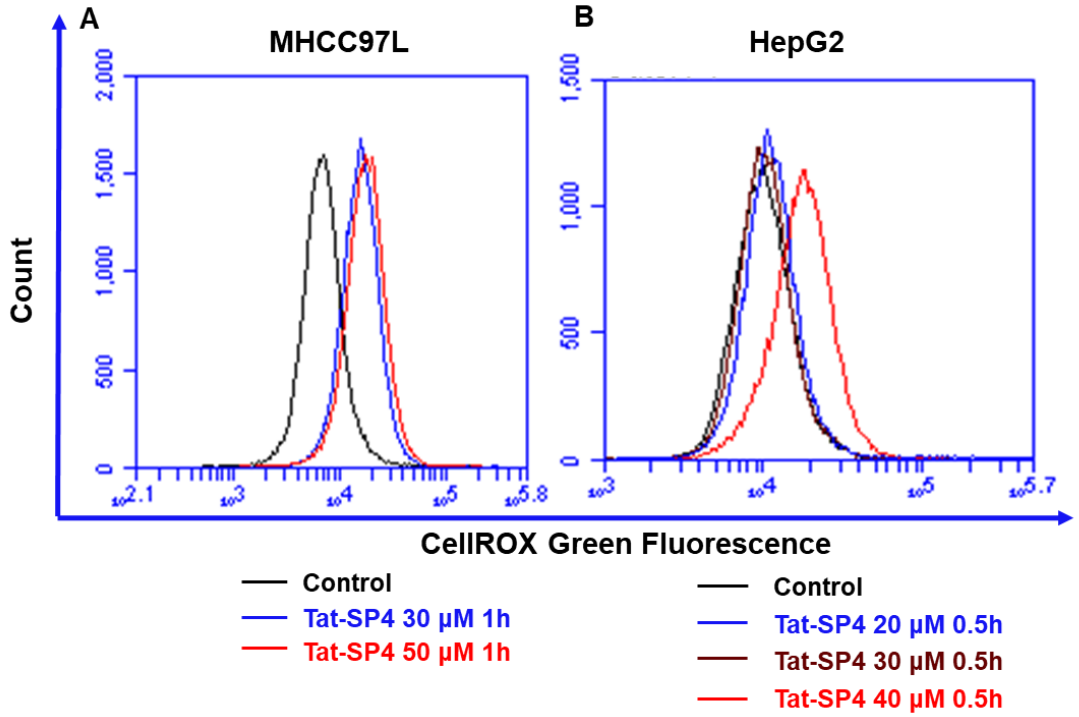


**Figure 4.17. Tat-SP4 increases intracellular ROS levels in HCC cell lines. A**. Representative flow cytometry plot of MHCC97L treated with Tat-SP4 (30, 50 μM) for 1 h. **B.** Representative flow cytometry plot of

HepG2 treated with Tat-SP4 (20, 30, 40 μM) for 3 h and 0.5 h. Cell ROX fluorescence was used to quantify intracellular ROS levels by a BD Accuri C6 flow cytometer.

By comparing the OXPHOS activity, cellular ROS level and mitochondrial membrane potential ($\Delta\psi$) of HCC cell lines after Tat-SP4 treatment. We confirmed that Tat-SP4 could indeed negatively affect mitochondrial metabolism.

### 4.4.4 Tat-SP4 induces mitochondrial permeability transition pore (MPTP) opening mediated necrotic cell death through a non-canonical pathway

As we found in our previous results, Tat-SP4 could affect mitochondrial metabolism at the same time, and this effect could be rescued by additional calcium. Dysfunctional mitochondria will induce cell death in various ways such as apoptosis and necrosis. Tat-SP4 induces HCC cell death without the involvement of apoptosis and Tat-SP4 can affect mitochondrial metabolism. Therefore, we hypothesized that Tat-SP4-induced cell death might be related to mitochondria mediating necrosis. The formation of mitochondrial permeability transition pore (MPTP) is the main trigger of mitochondrial-mediated necrosis, which is related to calcium overload. Although the composition, regulation, and precise mechanism of MPTP are still controversial, a

standard determination assay for the determination of MPTP has been applied. We used a commercial MPTP assay kit to measure whether Tat-SP4 induced MPTP. Based on the principle of this assay, cells that stain only with celcein AM have stronger fluorescence in the whole cell. After addition of calcein quencher $CoCl_2$ is located only in the cytosol, the cytosolic fluorescent calcein is quenched, and the fluorescence intensity of the cells comes only from the mitochondria. If the mitochondrial membrane permeability is destroyed by the treatment, the mitochondrial calcein will leak from the mitochondria into the cytosol and the fluorescence could be further quenched by $CoCl_2$. The change in fluorescence intensity could be observed in the flow cytometry plot. MHCC97L cells were treated with Tat-SP4 (20, 40 μM) for 1 hour. Ionomycin, a calcium ionophore, was used as a positive control and Tat-SC4 was used as a negative control peptide. The fluorescence intensity was first analyzed by flow cytometry. The result showed that Tat-SP4 treatment caused MPTP opening similar to the positive control ionomycin, whereas Tat-SC4 had no effect on MPTP (Figure 4.18A). Similar results were observed in HepG2 (Figure 4.18B).

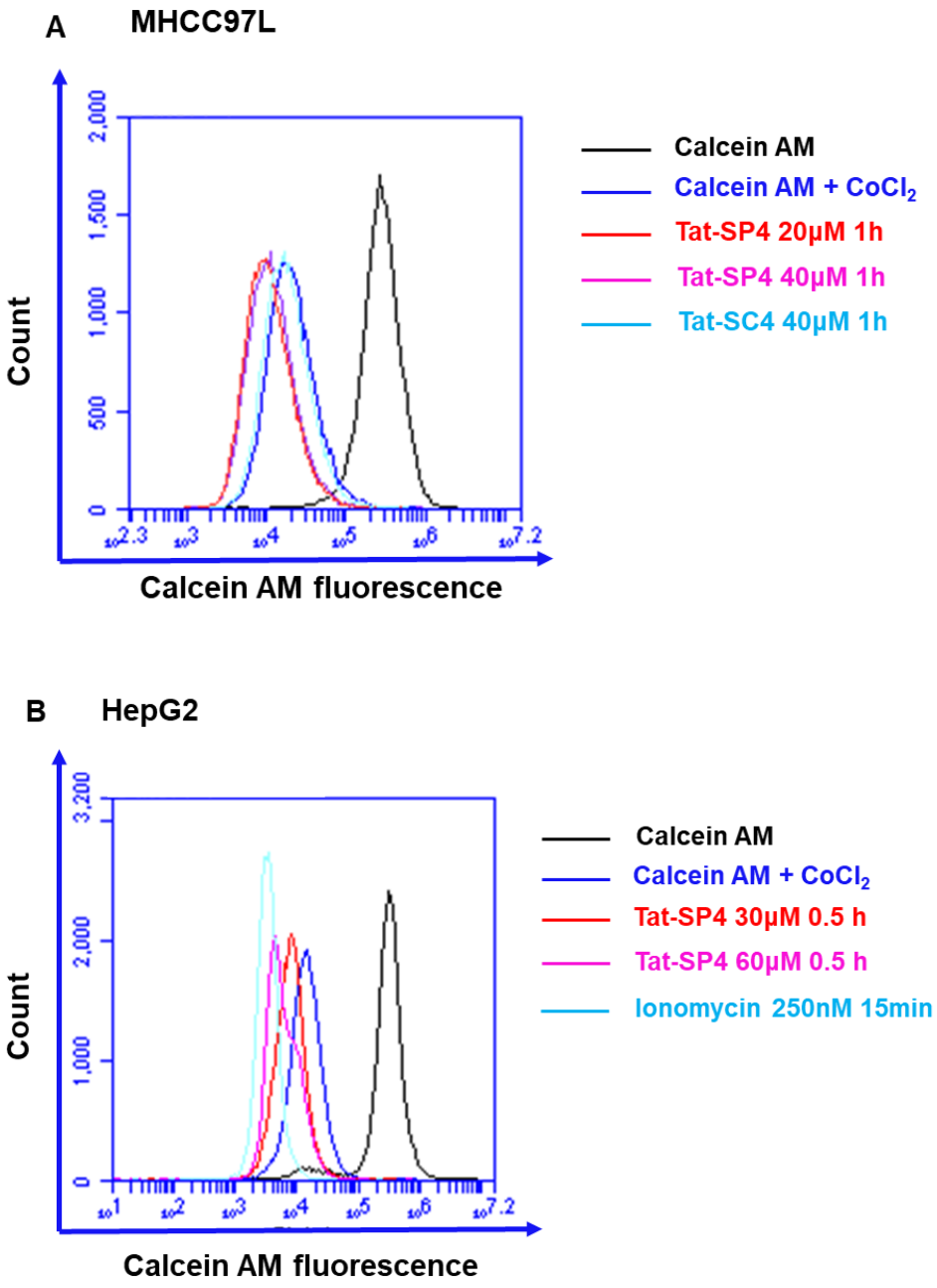


**Figure 4.18 Tat-SP4 induces mitochondrial permeability transition pore (MPTP) opening in HCC cell lines. A.** MHCC97L cells were pretreated with Tat-SP4 (20, 40 μM) or Tat-SC4 (40 μM) for 1 hour, then stained with calcein AM (final concentration 2 μM) followed by calcein quencher $CoCl_2$ (final concentration 0.4 mM). **B**. HepG2 cells were

stained by calcein AM fluorescence after treatment with Tat-SP4 (30, 60 μM) for 0.5 hours or 250 nM ionomycin for 15 minutes.

To further visualize Tat-SP4-induced MPTP opening, a confocal imaging study was o performed. Lived cells were labeled with MitoTracker (red, final concentration 200 nM) for mitochondrial staining, Hoechst 33342 dye (blue, final concentration 1Mm) for nuclear staining, and then stained with calcein AM (green, final concentration 1μM) and 1.0 M $CoCl_2$ (1mM), respectively. For the treatment groups, cells were treated with Tat-SP4 (20 μM) for 30 minutes before staining with calcein AM and $CoCl_2$. For the positive control group, cells were treated with ionomycin (250 nM) for 15 minutes before staining with Calcein AM and $CoCl_2$. Signals from MitoTracker (552 nm), Calcein AM (488 nm), and Hoechst 33342 (350 nm) were acquired sequentially. The confocal imaging results showed that only cells treated with calcein AM showed strong fluorescence. Treatment cells with calcein AM and $CoCl_2$ together, only mitochondria have fluorescence. In the positive control group, after treatment with ionomycin, the fluorescence of mitochondria was disappeared, which means the mitochondrial permeability transition pore opening. After treatment with control peptide Tat-SC4, calcein fluorescence was still present in the mitochondria and couldn't be released by Tat-SC4. In contrast to this negative control treatment, the

fluorescent mitochondria disappeared after the cells were treated with Tat-SP4 (40 μM), indicating that Tat-SP4 can induce MPTP in lived cells (Figure 4.18C).

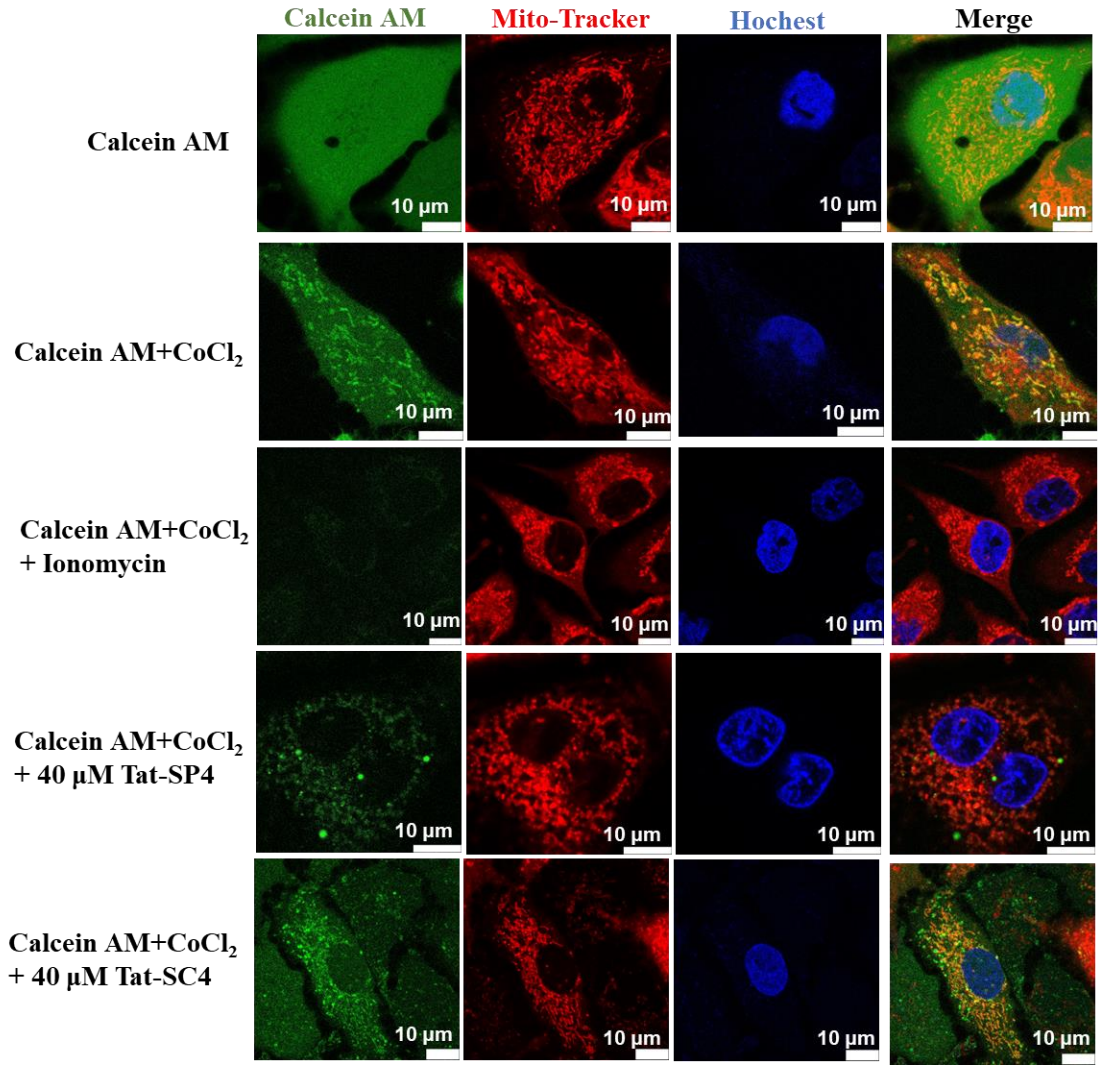


**Figure 4.18 C Confocal imaging study of MPTP in lived MHCC97L cells.** Cells were labeled with Hoechst 33342 (blue) for nuclear staining, MitoTracker (red) for mitochondrial staining, and Calcein AM (green) for intact mitochondrial staining. Cells were treated with 250 nM ionomycin

for 15 min, 40 μM Tat-SP4 and Tat-SC4. The merged figures show the colocalization of labeled organelles. Scale bar: 10 μm.

### 4.4.5 Tat-SP4 impairs mitochondrial morphology in HCC cells

MPTP opening usually leads to severe mitochondrial morphological changes, such as mitochondrial swelling. Previous studies by our group members found that transiently overexpressed GFP-tagged TOM20 (translocase of outer membrane 20, a peripheral subunit of the TOM40 complex on the mitochondrial outer membrane) could label the mitochondrial outer membrane without interference from the mitochondrial membrane potential. To investigate whether Tat-SP4 could induce a change in mitochondrial morphology, we transiently transfected 1ng GFP-tagged TOM20 plasmids into Hep3B cells using lipo3000 $^{TM}$ to label mitochondria. After overexpression of the transfected plasmids for 24 h, cells were treated with or without 40 μM Tat-SP4 for 0.5 h. In the control group, cells without Tat-SP4 treatment, active mitochondria showed intact mitochondrial morphology with dynamic shapes of fusion and fission (Figure 4.19A). In the treatment group, there was a significant change in the mitochondrial morphology. The shapes of the mitochondria became bubble-like but outer mitochondrial membrane integrity was maintained (Figure 4.18B), which was in agreement with the morphological feature of mitochondrial swelling.

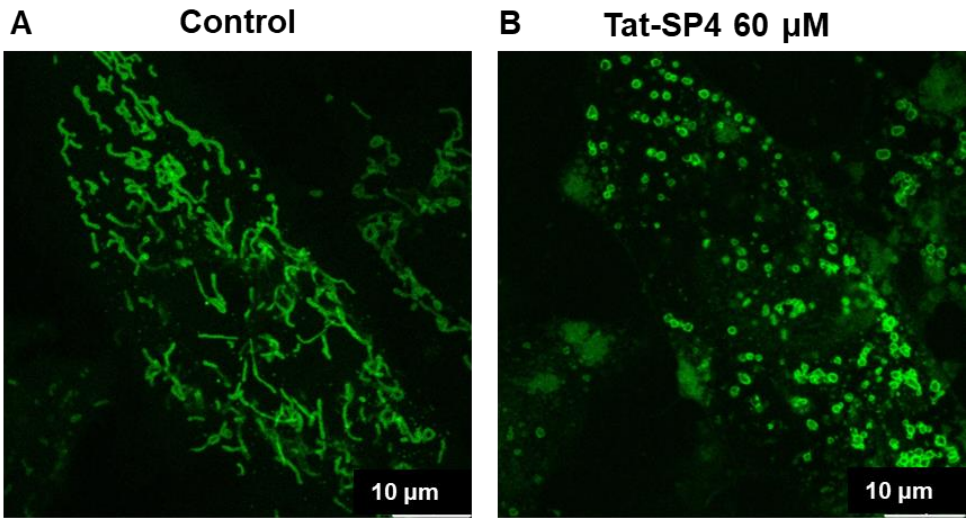


**Figure 4.19 Tat-SP4 impairs mitochondrial morphology in HCC cells.** Hep3B cells were transiently overexpressed with GFP-tagged TOM20, and the changes in the mitochondrial shapes of the live cells were labeled by the signal of GFP (488nm) and images were captured with a Leica inverted confocal microscope (TCS-SP8-MP system). A. Control group, cells not treated with Tat-SP4. B. Cells treated with Tat-SP4 (60 μM) for 0.5 h. Scale bar: 10μm.

## Discussion

The mitochondrial serves as the powerhouse in cells. A double membrane structure separates the mitochondrial into four parts. The mitochondrial membrane potential (Δψ) between the matrix and the intermembrane space, which is around 180 mV, is generated by the proton pumps of the electron transport chain complexes. The values of Δψ in cells are kept relatively stable under normal conditions. Δψ plays a

key role in mitochondrial homeostasis by selectively eliminating dysfunctional mitochondria. Mitochondria also provide sites and enzymes for the two main processes of ATP production: the tricarboxylic acid cycle (TCA cycle) and oxidative phosphorylation (OXPHOS). Based on these functions, we investigate the impact of Tat-SP4 on mitochondrial functions. As shown in the above results, Tat-SP4 could induce the loss of mitochondrial membrane potential. Tat-SP4 could also affect OXPHOS by decreasing the maximal respiratory rate and further inducing ROS increase.

Beyond their core metabolic functions, mitochondrial structure and dysfunction are closely linked to cell death. The mitochondrial permeability transition pore (MPTP) leads to loss of mitochondrial transmembrane potential, uncoupling of the respiratory chain, overproduction of ROS, failure of ATP synthesis, and ultimately cell death. However, the molecular mechanism of MPTP is not well characterized. A consensus on MPTP is that $Ca^{2+}$ overload is closely associated with MPTP. Flow cytometry and confocal imaging studies showed that Tat-SP4 could directly induce MPTP. To further investigate the molecular mechanism behind this phenomenon, we next determined the effect of Tat-SP4 on intracellular $Ca^{2+}$ concentration.

## 4.5 Tat-SP4 can disrupt intracellular $Ca^{2+}$ storage

### 4.5.1 Tat-SP4 can affect the intracellular calcium homeostasis via inducing ER calcium release, mitochondrial and cytosolic calcium increase.

The concentration of free calcium in the cytosol usually is maintained at a low concentration. Calcium can be transported into the cytosol from extracellular via different ion channels such as voltage-gated calcium channels (VGCC), P2X7, and transient receptor potential channels (TRPCs) that are located on the plasma membrane. The endoplasmic reticulum (ER) is a major membrane-bound intracellular organelle for $Ca^{2+}$ storage and transportation. At resting conditions, ER has a high calcium concentration of about 500 μM. The high $Ca^{2+}$ concentration is crucial to maintain ER proteins functions. To maintain calcium hemostasis, ER can also release calcium after stimulations by specific mediators. The ER calcium can be released via RyR and CICR channels to the cytosol and the IP3R to mitochondria. Mitochondria as another membrane-bound intracellular organelle can accumulate high levels of calcium via the connect sites between ER and mitochondria-associated membranes (MAMs) and mitochondrial calcium uniporter. We mainly detected the calcium concentrations of cytosol and mitochondria and ER after peptides treatment.

First, we used fura-2 AM, a fluorophore dye, to detect changes in cytosolic calcium concentration. MHCC97L cells were plated in a 24-well plate for overnight attachment, and then fura-2 AM was used to stain cells in serum-free medium at room temperature for 1 hour. Using HBSS buffer (with or without calcium), cells were washed three times and 250 μL HBSS was added to each well and incubated for 30 minutes at room temperature to ensure no extracellular fluorescence was excited. Using an Olympus inverted epifluorescence microscope, fluorescence changes were detected by alternating excitation waves at 340 nm and 380 nm, and images and fluorescence values were collected every 3 seconds. The calcium concentration has a positive relationship with the fura-2 AM fluorescence relative ratio of 340nm/380nm. The results showed that the fura-2 relative ratio in MHCC97L promptly and significantly increased by 50%, and then the fluorescence relative ratio rapidly decreased after treatment with 30 μM Tat-SP4 at 1min point in calcium-free HBSS buffer (Figure 4.20A). This meant that Tat-SP4 could cause cytosolic calcium levels to rise and fall rapidly. When cells were cultured in HBSS buffer containing 1.2 mM calcium, Tat-SP4 could also induce the cytosolic calcium concentration to increase by more than 70%, and then the increased level remained stable (Figure 4.20A). Compared with the Tat-SP4 treatment group, the control peptide Tat-SC4 showed little effect on

the cytosolic calcium concentration, it was increased by only about 30% rapidly and then it dropped back to the basal level in with or without extracellular calcium HBSS buffer (Figure 4.20B).

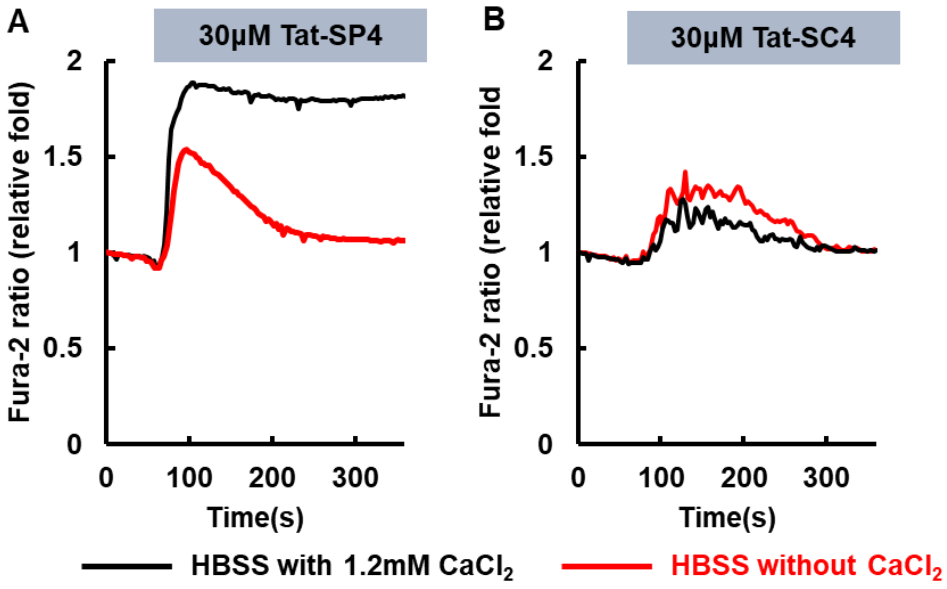


**Figure 4.20 Tat-SP4 can affect intracellular cytosolic $Ca^{2+}$ in MHCC97L stained by Fura-2 AM. A.** Representative traces of cytosolic $Ca^{2+}$ in stained MHCC97L cells treated with 30μM Tat-SP4 at 1 min point in with (black line) or without (red line) extracellular $Ca^{2+}$ HBSS as measured by Fura-2. The inset shows an average peak of 20 independent cells. **B.** Representative traces of cytosolic $Ca^{2+}$ in stained MHCC97L cells treated with 30μM Tat-SC4 at 1 min in with (black line) or without (red line) extracellular $Ca^{2+}$ HBSS as measured by Fura-2. The inset shows an average peak of 20 independent cells.

To further detect the effect of Tat-SP4 on intracellular $Ca^{2+}$ homeostasis, MHCC97L cells were transfected with cytosolic, mitochondrial and ER calcium sensor plasmids. After 48 h of transfection, the fluorescence of the calcium sensors could be observed. Changes in intracellular calcium concentrations were monitored by inverted epifluorescence microscopy. Cells were treated with Tat-SP4 20μM at 1 minute point and then the fluorescence value was collected every 3 seconds. The results showed that the fluorescence of calcium sensors had a significant change on cells treated with Tat-SP4 in extracellular $Ca^{2+}$-free HBSS buffer (Figures 4.21 A&B&C). The relative fluorescence ratio of plasmid G-CEPIA1er indicated the change in ER calcium. The results indicated that Tat-SP4 could induce ER $Ca^{2+}$ release, and the relative fluorescence ratio rapidly decreased by about 60%, and the addition of extracellular $Ca^{2+}$ could rescue the release of ER calcium (Figure 4.21 A). The relative fluorescence ratio of plasmid mito-GCaMP5G indicated the mitochondrial calcium change. Upon treatment of cells by Tat-SP4 at 1 min points, the relative fluorescence ratio of plasmid mito-GCaMP5G went up and down promptly, and additional extracellular $Ca^{2+}$ could rapidly increase the fluorescence and maintain this increased level steady (Figure 4.20 B). The cytosolic $Ca^{2+}$ level was indicated by the relative fluorescence ratio of plasmid cyto-RCaMP1h. After Tat-SP4 treatment,

the level of cytosolic $Ca^{2+}$ went up and down rapidly, and extracellular calcium could induce the level increase significantly (Figure 4.20 C). Similar results were also observed in cells cultured in HBSS buffer with extracellular $Ca^{2+}$ (Figures 4.20 D&E&F). And the mitochondrial and cytosolic $Ca^{2+}$ after treatment with Tat-SP4 increased promptly and maintain the increased level unchanged, which was different from that of cells in an extracellular $Ca^{2+}$-absent condition. This suggested that extracellular calcium might influence Tat-SP4-induced calcium homeostasis.

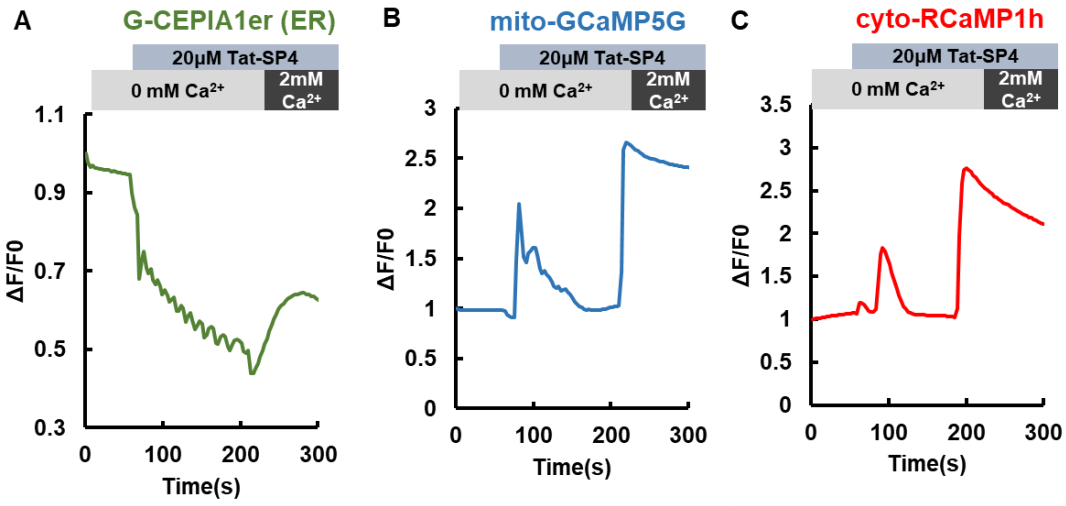

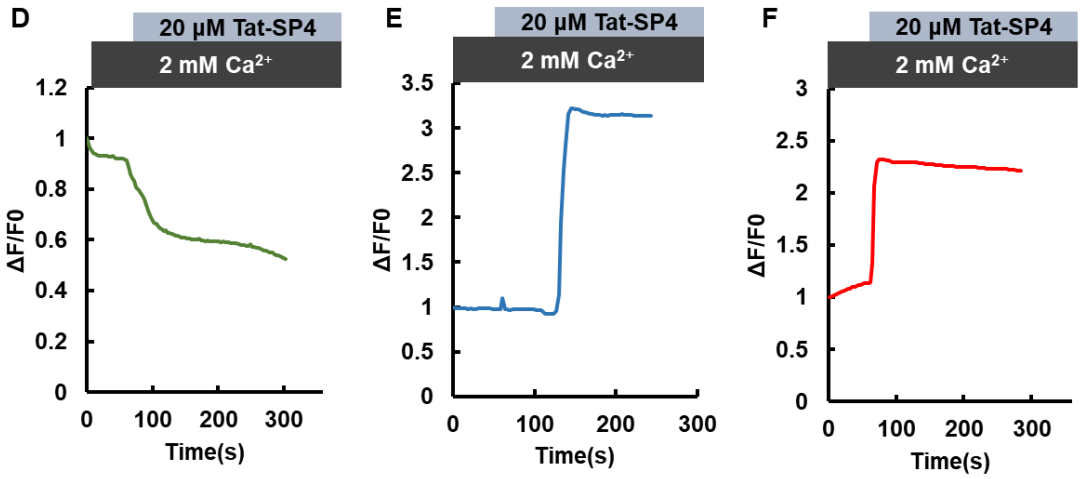


**Figure 4.21 Tat-SP4 can affect the intracellular calcium homeostasis via inducing ER calcium release, mitochondrial and cytosolic calcium increase. A.** The relative fluorescence ratio of plasmid G-CEPIA1er indicated the changes in ER calcium. **B.** The relative fluorescence ratio of plasmid mito-GCaMP5G indicated the changes in mitochondrial calcium. **C.** The relative fluorescence ratio of plasmid cyto-RCaMP1h indicated the changes of cytosolic calcium. MHCC97L cells were cultured in extracellular $Ca^{2+}$ free HBSS buffer and treated with 20 μM Tat-SP4 at the 1-min point. Additional 2mM $Ca^{2+}$ was added at the 3 min point. **D.** The relative fluorescence ratio of plasmid mito-GCaMP5G indicated the changes in mitochondrial calcium. **E.** The relative fluorescence ratio of plasmid mito-GCaMP5G indicated the changes in mitochondrial calcium. **F.** The relative fluorescence ratio of plasmid cyto-RCaMP1h indicated the changes in cytosolic calcium. MHCC97L cells were cultured in HBSS

buffer containing 2mM $Ca^{2+}$ and treated with 20 μM Tat-SP4 at the 1 min point.

### 4.5.2 Digoxin rescues Tat-SP4-induced intracellular calcium fluctuations

As mentioned in result 4.3, digoxin could rescue Tat-SP4-induced cell death. We hypothesized that digoxin might play a role in Tat-SP4-induced intracellular $Ca^{2+}$ homeostasis. To further investigate the effect of digoxin, we used intracellular organelle $Ca^{2+}$ sensor plasmids to detect the ER, mitochondrial and cytosolic $Ca^{2+}$ changes after treatment with digoxin and Tat-SP4. MHCC97L cells were pretreated with 5 μM digoxin for 3 hours, and then the effect of Tat-SP4 on intracellular calcium was detected. The results showed that Tat-SP4 had little effect on the relative fluorescence of the ER $Ca^{2+}$ sensor after pre-treatment with digoxin (the red line) compared with the group pre-treated without digoxin (the black line) in $Ca^{2+}$-free buffer (Figure 4.22A). The extracellular $Ca^{2+}$-induced ER $Ca^{2+}$ uptake couldn't be blocked by digoxin (Figure 4.22A). The protective effect of digoxin on mitochondrial and cytosolic $Ca^{2+}$ was even better than that of ER $Ca^{2+}$. After pretreatment with digoxin, Tat-SP4 couldn't induce ant significant mitochondrial and cytosolic $Ca^{2+}$ changes in the absence of extracellular $Ca^{2+}$ (Figures 4.22B&C). The extracellularly induced cytosolic and mitochondrial $Ca^{2+}$ uptake couldn't

be blocked by digoxin (Figures 4.22B&C). In short, digoxin could rescue Tat-SP4-induced intracellular $Ca^{2+}$ changes in the absence of extracellular $Ca^{2+}$ condition. However, the rescue effect of digoxin could be influenced by extracellular $Ca^{2+}$. On cells cultured in the presence of 2mM $Ca^{2+}$ condition, digoxin shows a little protective effect on Tat-SP4 induced intracellular $Ca^{2+}$ changes (Figures 4.22D&E&F). This could be related to the extracellular $Ca^{2+}$ that induced rapid $Ca^{2+}$ uptake after Tat-SP4 treatment.

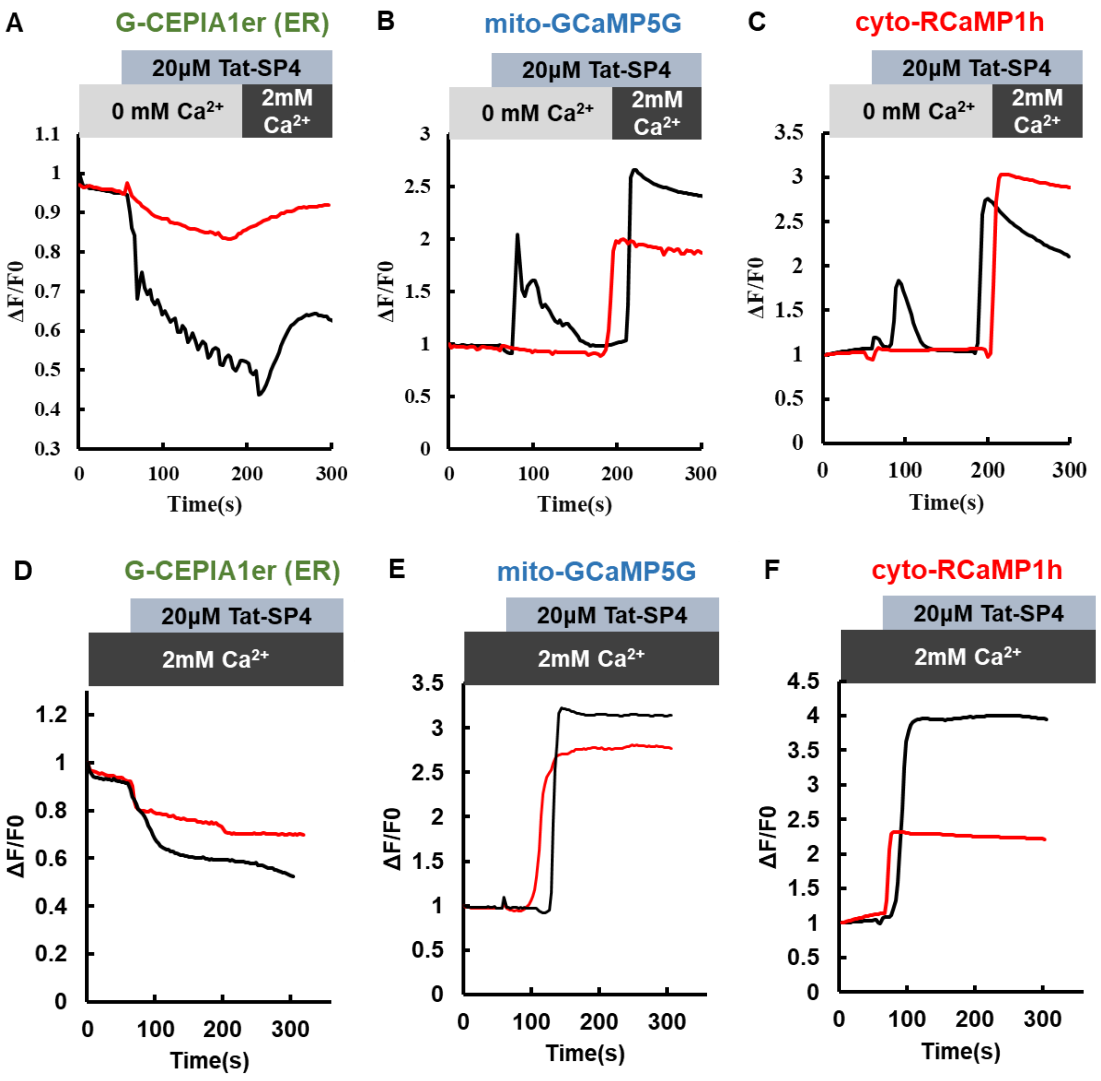

**Figure 4.22 Digoxin rescues intracellular calcium fluctuations induced by Tat-SP4. A.** The relative fluorescence ratio of plasmid G-CEPIA1er indicated the changes in ER calcium. **B.** The relative fluorescence ratio of plasmid mito-GCaMP5G indicated the changes in mitochondrial calcium. **C.** The relative fluorescence ratio of plasmid cyto-RCaMP1h indicated the changes in cytosolic calcium. MHCC97L cells were pretreated with 5 μM digoxin or without pre-treatment in extracellular $Ca^{2+}$-free HBSS buffer followed treatment by 20 μM Tat-SP4 at 1 min point. Additional 2mM $Ca^{2+}$ was added at the 3-min point. MHCC97L cells cultured in HBSS buffer with 2mM $Ca^{2+}$ and relative fluorescence of ER calcium sensor (D), mitochondrial calcium sensor (E), cytosolic calcium sensor (F), were detected after pre-treatment with 5 μM digoxin or without pre-treatment followed by treatment with 20 μM Tat-SP4 at 1 min point.

## Discussion

Overall, Tat-SP4 could reduce ER $Ca^{2+}$ release leading to cytosolic and mitochondrial $Ca^{2+}$ increase. Based on the results in 4.4, we concluded that the rapid increase in mitochondrial $Ca^{2+}$ concentration leads to $Ca^{2+}$ overload, resulting in MPTP and cell death.

A paper showed that Tat peptides can decrease the plasma membrane potential when they cross the membrane (Trofimenko, Grasso et al. 2021).

Digoxin is an inhibitor of $Na^+/K^+$ ATPase, which functionally maintains physiological chemical homeostasis to stabilize the plasma membrane potential. Digoxin can reverse Tat-SP4 induced abnormal disturbance on membrane potential. Thus, digoxin can rescue Tat-SP4-induced intracellular calcium fluctuations and further inhibit Tat-SP4-induced cell death (results in 4.3).

Interestingly, after Tat-SP4 treatment, extracellular $Ca^{2+}$ could induce significant mitochondrial and cytosolic $Ca^{2+}$ uptake in $Ca^{2+}$-free buffer. We hypothesized that this uptake may play a protective role for cell survival when Tat-SP4 disrupts intracellular $Ca^{2+}$ homeostasis. The mechanism of this $Ca^{2+}$ uptake could be related to the plasma membrane potential. We hypothesized that Tat-SP4 could affect the membrane potential when it translocated from the outer surface of the plasma membrane into the cytosol. Extracellular $Ca^{2+}$ uptake reserved the Tat-SP4-induced $Ca^{2+}$ flux to stabilize the membrane potential. Next, we determined whether extracellular $Ca^{2+}$ affected Tat-SP4-induced cell death and mitochondrial dysfunction.

## 4.6 Tat-SP4 induced cell death is sensitive to extracellular calcium concentration

### 4.6.1 Extracellular $Ca^{2+}$ concentration influences Tat-SP4 cytotoxicity in HCC

In addition to HCC cell lines, Tat-SP4 can also induce the death of many other types of cancer cells, such as triple negative breast cancer (TNBC), lung cancer cells, ovarian cancer cells, and acute myeloid leukemia (AML). Comparing the half maximal inhibitory concentration (IC50) of Tat-SP4 in different cell types, we found that the IC50 of cells cultured in RPMI1640 medium was lower than that of cells cultured in DMEM medium. When the culture medium of a cell line was changed from DMEM to RPMI1640, the IC50 of this cell line was decreased. Similarly, when cells originally cultured in RPMI1640 medium were cultured in DMEM medium, the IC50 of this cell line was increased. The IC50 valus for Tat-SP4 of HCC cells cultured in two types of medium were different (Figure 4.23). When cells are cultured in RPMI1640 medium, the IC50 for Tat-SP4 of HCC cells was lower than that of cells cultured in DMEM medium.

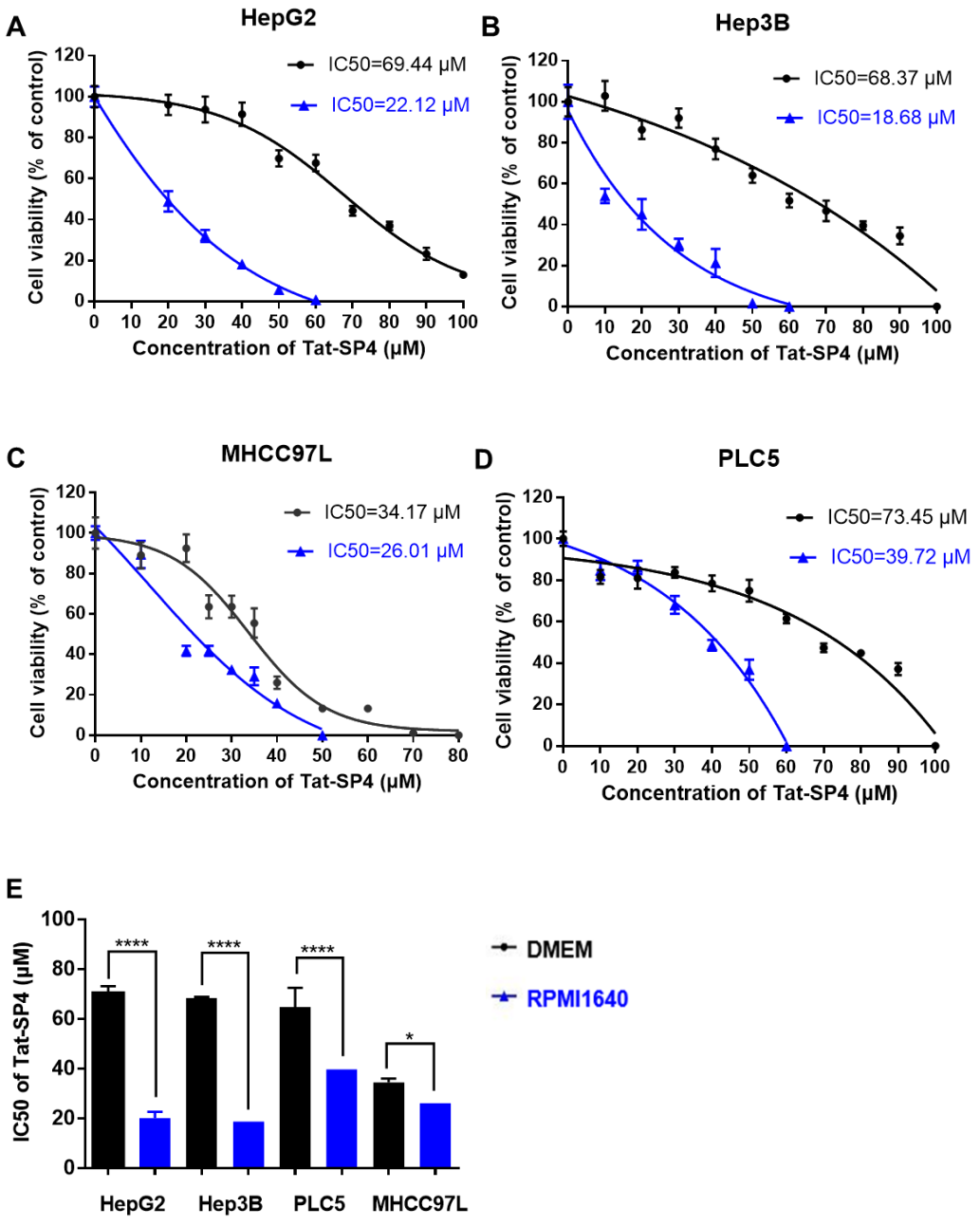


**Figure 4.23 Different culture media result in different sensitivities to Tat-SP4 in HCC cell lines. A.** Cell viability of HepG2 cultured in DMEM or PRMI1640 medium after treatment with different concentrations of Tat-SP4. The estimated IC50 values were 69.44 μM, 22.12 μM, respectively. **B.** Cell viability of Hep3B cultured in DMEM or

PRMI1640 medium after treatment with different concentrations of Tat-SP4. The estimated IC50 values were 68.37 μM, 18.68 μM, respectively. **C.** Cell viability of MHCC97L cultured in DMEM or PRMI1640 medium after treatment with different concentrations of Tat-SP4. The estimated IC50 values were 34.17 μM, 26.01 μM, respectively. **D.** Cell viability of PLC5 cultured in DMEM or PRMI1640 medium after treatment with different concentrations of Tat-SP4. The estimated IC50 values were 73.45 μM, 39.72 μM, respectively. Data represents mean ± SEM of three replicates. **E.** Statistical analysis of IC50 of HCC cell lines for Tat-SP4 as measured in (A-D). Bars represent mean ± SEM ($n$ = 3). *$P$ < 0.05, ****$P$ <0.0001; $t$ test.

We proposed that the different components of the two medium might influence the efficiency of Tat-SP4 to induce cell death. Based on the component table of the two media, we selected some components that have different concentrations in the two media, such as pyruvate, glutathione, L-glutamic acid, L-aspartic acid, and calcium. Corresponding components were added to a lower concentration medium to achieve the same concentration of a higher concentration medium. The cells were then cultured in the modified media. The IC50 values of cells in the original medium and modified medium were compared. The results showed that pyruvate, glutathione, L-glutamic acid, and L-aspartic acid

had no effect on the efficiency of Tat-SP4-induced cell death (Figure 4.24).

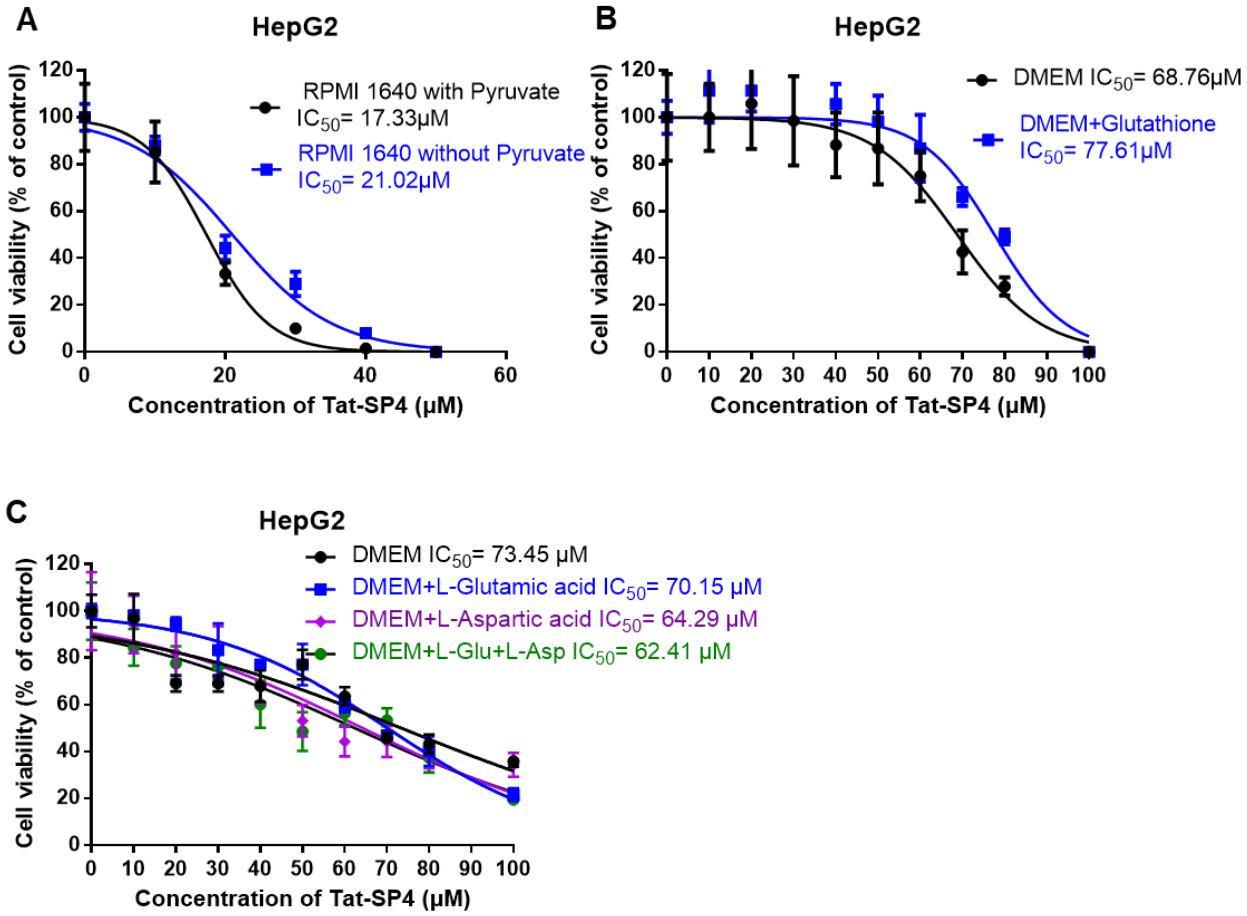


**Figure 4.24 Different medium conditions have no effect on the IC50 value of Tat-SP4 in HepG2.** A. Cell viability of HepG2 cultured in RPMI1640 with or without 1 mM pyruvate after treatment with different concentrations of Tat-SP4. The estimated IC50 values were 17.33 μM and 21.02 μM, respectively. B. Cell viability of HepG2 cultured in DMEM with or without 3.25 μM glutathione after treatment with different concentrations of Tat-SP4. The estimated IC50 values were 68.76 μM and 77.61 μM, respectively. C. Cell viability of HepG2 cultured in DMEM

with or without 20 mg/mL L-glutamic acid, L-aspartic acid, L-glutamic acid and L-aspartic acid after treatment with different concentrations of Tat-SP4. The estimated IC50 values were 73.45 μM, 70.15 μM, 64.29 μM, and 62.41 μM, respectively. Data are mean ± SEM of three replicates.

Extracellular $Ca^{2+}$ has an influence on the Tat-SP4 induced intracellular $Ca^{2+}$ fluctuations. By comparing the compounds of the two media, we found that the $Ca^{2+}$ concentration was different in DMEM (1.8 mM $Ca^{2+}$) and RPMI1640 (0.41mM $Ca^{2+}$). To further determine whether $Ca^{2+}$ was the main factor that causes the different IC50 value of Tat-SP4 for HCC in the two media, MHCC97L cells were seeded into a 96-well plate and cultured with Tat-SP4 at a range of concentrations for 24 hours. Cells were cultured in three different types of media: DMEM (containing 1.8 mM $Ca^{2+}$), RPMI1640 (containing 0.41 mM $Ca^{2+}$), and RPMI1640 with added calcium (containing 0.41 mM $Ca^{2+}$ plus 1.8 mM $Ca^{2+}$). After treatment with Tat-SP4 for 24 hours, cell viability was measured. The results showed that the IC50 value of cells cultured in DMEM was 33.51 μM higher than that of RPMI1640 (24.01 μM) and similar to the IC50 value of cells cultured in RPMI1640 with added calcium (37.02 μM) (Figure 4.25A). Additional indicated concentration of $Ca^{2+}$ could rescue Tat-SP4 induced cell death. To verify the range of $Ca^{2+}$ concentration with rescue efficiency, different concentrations of $Ca^{2+}$ (from 0.4 mM to

3.6 mM) was added to RPMI1640 medium and treatment with the same concentration of Tat-SP4 (30 μM) in MHCC97L and HepG2 (Figures 4.25B&C). The results showed that Tat-SP4 induces death that can be rescued by $Ca^{2+}$ in a dose-dependent manner when the $Ca^{2+}$ concentration was lower than 1.8 mM (Figures 4.25 B&C). The rescue efficiency was blocked by high dose $Ca^{2+}$ more than 1.8 mM due to a higher concentration of $Ca^{2+}$ with cytotoxicity (Figure 4.25 D).

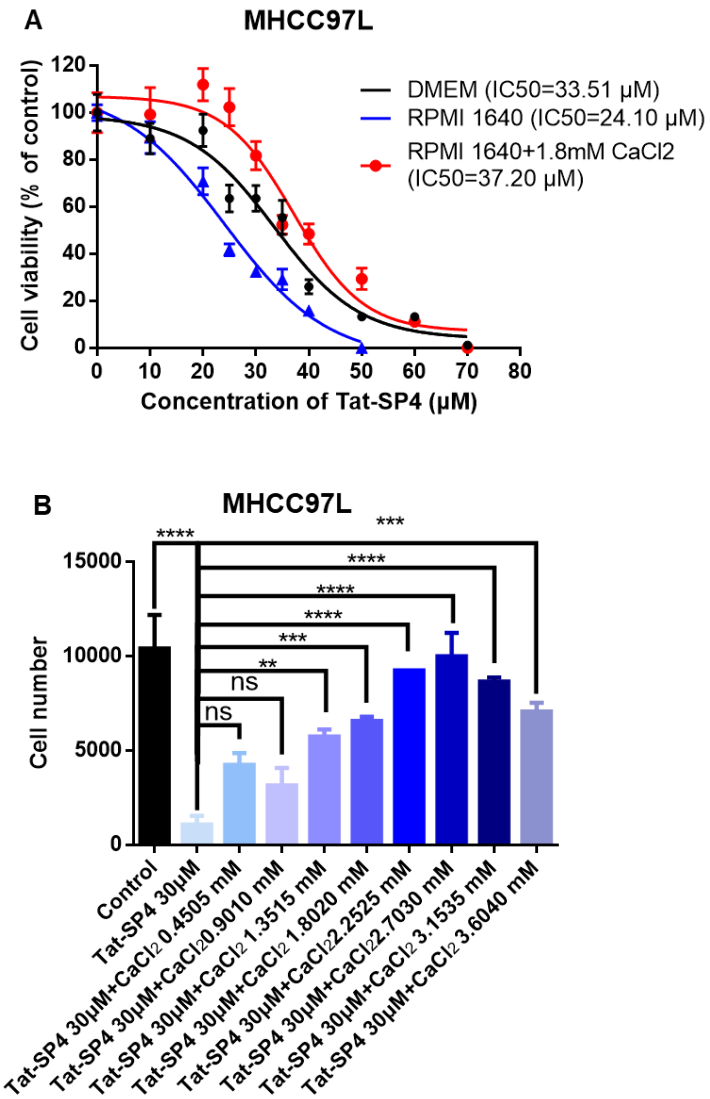

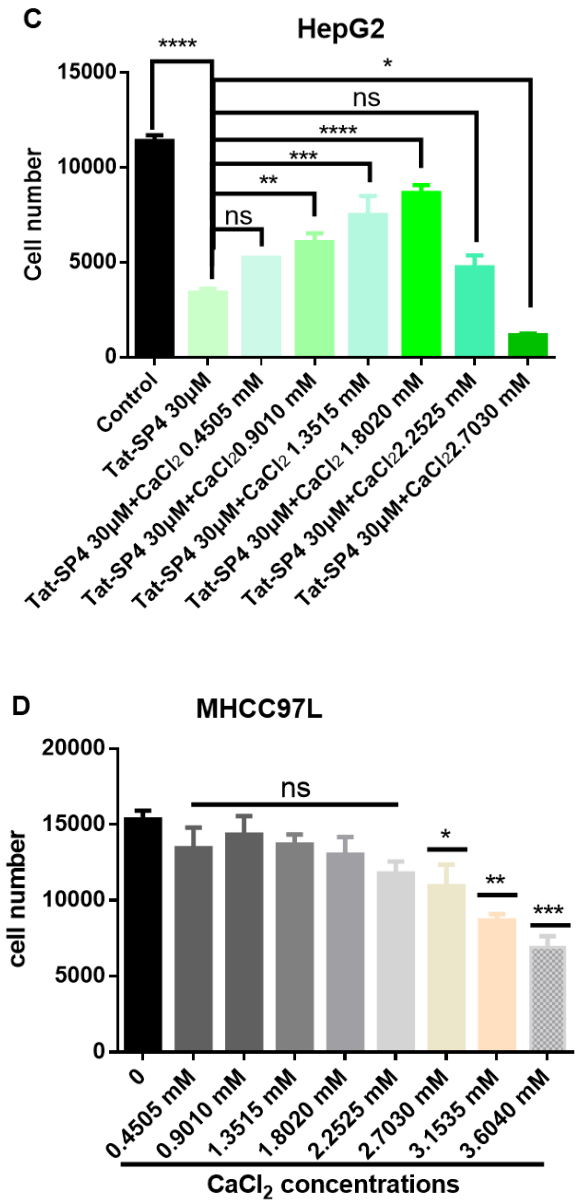


**Figure 4.25 IC50 for Tat-SP4 of MHCC97L cultured in different media DMEM, RPMI1640 and RPMI1640 containing 1.8mM $CaCl_2$.** **A.** Cell viability of MHCC97L cultured in DMEM, RPMI1640 and RPMI1640 containing 1.8mM $CaCl_2$ in after treatment with different concentrations of Tat-SP4. The estimated IC50 values were 33.51 μM, 24.01 μM, and 37.02 μM, respectively. Data are mean ± SEM of three

replicates. **B**. Cell viability of MHCC97L cultured in RPMI1640 supplemented with different concentrations of $CaCl_2$ after treatment with Tat-SP4 (30 μM). **C**. Cell viability of HepG2 cultured in RPMI1640 supplemented with different concentrations of $CaCl_2$ after treatment with Tat-SP4 (30 μM). **D**. Cell viability of MHCC97L cultured in RPMI1640 with different concentrations of $CaCl_2$ added. Bars represent mean ± SEM (n = 3). ****P <0.0001; ***P <0.001; **P <0.01; t-test.

### 4.6.3 Extracellular calcium attenuates Tat-SP4-induced mitochondrial depolarization and impairment of OXPHOS.

Addition of calcium can rescue Tat-SP4-induced cell death. Next, we investigated whether Tat-SP4 could also rescue Tat-SP4-induced mitochondrial damages. We first examined the effect of supplemental calcium on Tat-SP4-induced increases in mitochondrial membrane potential. Hep3B cells were cultured in RPMI1640 medium and treated with the indicated concentrations of Tat-SP4 (30 μM, 50 μM) with or without additional $CaCl_2$ (0.7 mM) for 1 h. Then the cells were stained with 100 nM TMRM for 30 min at 37 ℃. TMRM fluorescence intensity was quantified using a BD Accuri C6 flow cytometer. The results showed that the degree of cellular TMRM fluorescence reduction of cells treated with Tat-SP4 alone was greater than that of cells treated with the same concentration of Tat-SP4 with 0.7 mM $CaCl_2$ (Figure 4.26A). Additional

calcium could rescue the Tat-SP4-induced decrease in mitochondrial membrane potential. Similar results were observed in MHCC97L (Figure 4.26B).

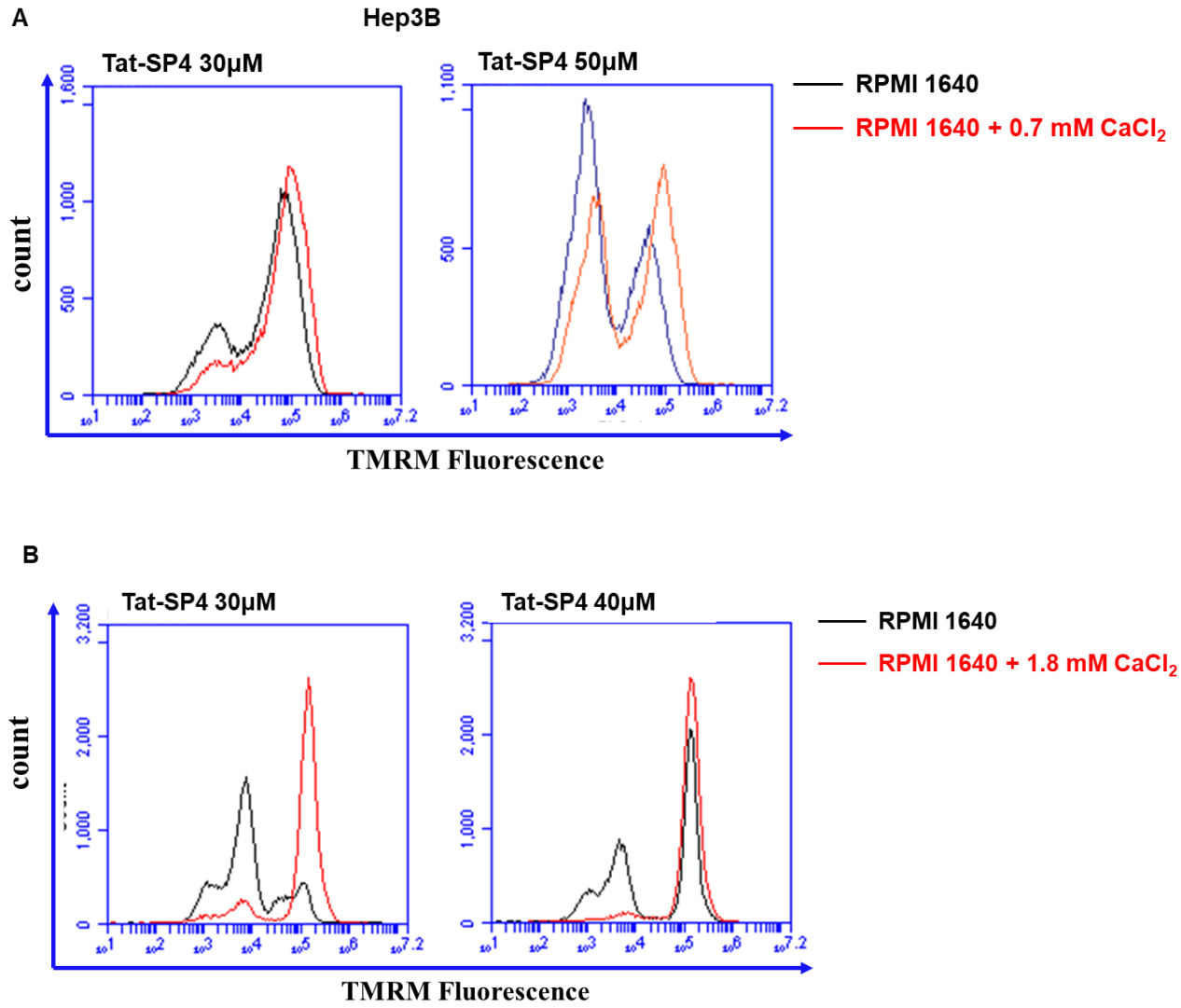


**Figure 4.26 Calcium can rescue Tat-SP4 induced mitochondrial membrane potential reduction in HCC cell lines. A.** Representative flow cytometry plot of Hep3B treated with Tat-SP4 (30, 50 μM) with or without 0.72 mM $CaCl_2$ for 1 h. **B.** Representative flow cytometry plot of

MHCC97L treated with Tat-SP4 (30, 40 μM) with or without 1.8 mM $CaCl_2$ for 1 h. TMRM was used to quantify mitochondria membrane potential by a BD Accuri C6 flow cytometer.

Next, we investigated whether additional calcium could rescue by Tat-SP4-induced the maximal oxygen consumption rate in HCC cells. MHCC97L cells were seeded in culture microplates with RPMI1640 medium or RPMI1640 medium with 1.8 mM $CaCl_2$. Then the cells were treated with Tat-SP4 (20, 30 μM) or vehicle, 1μM oligomycin, 1μM FCCP, and 0.5μM rotenone and antimycin A sequentially. Real-time changes in OCR were detected using the Agilent Seahorse Analyzer. The results showed additional calcium rescued Tat-SP4 induced reduction of maximal oxygen consumption rate of MHCC97L cells (Figure 4.27A). Statistical analysis showed maximal OCR reduction could be rescued by calcium even after treatment with different doses of Tat-SP4 (Figure 4.27B).

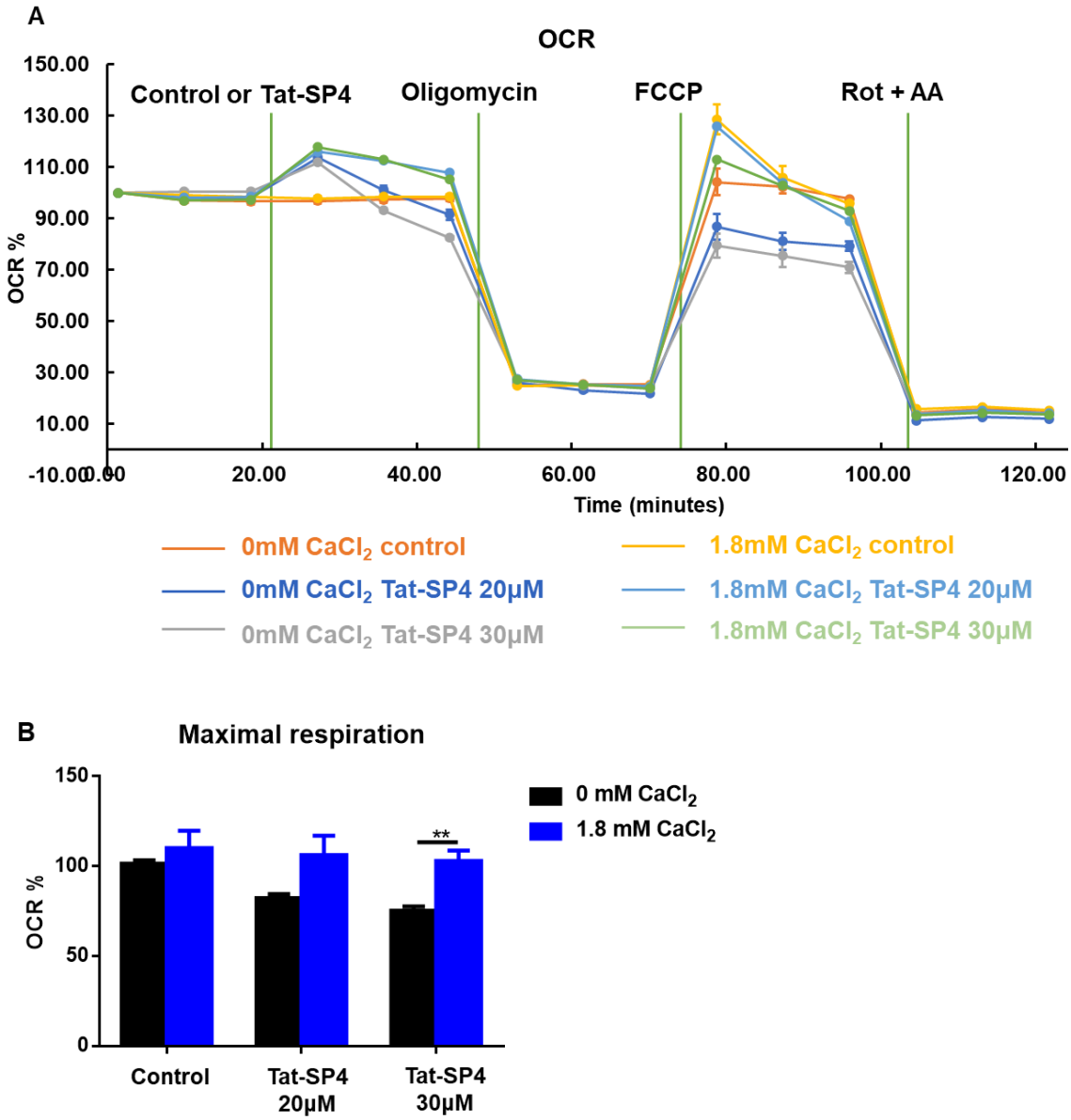


**Figure 4.27 Extracellular $Ca^{2+}$ rescues Tat-SP4 induced maximal oxygen consumption rate in MHCC97L cells. A.** Oxygen consumption rate (OCR) of MHCC97L cells cultured in RPMI1640 with or without 1.8 mM $CaCl_2$ was measured using the Agilent Seahorse Analyzer. Cells were either treated by PBS buffer (control) or Tat-SP4 (20, 30 μM) followed by 1 μM oligomycin, 1 μM FCCP, and 0.5 μM rotenone and

antimycin A. Each point means the real-time OCR changes. **B.** Statistical analysis of maximal OCR as measured in (A). Bars represent mean ± SEM ($n$ = 3). *$P$ < 0.05, **$P$ <0.01; $t$ test.

**Discussion**

Extracellular $Ca^{2+}$ plays a protective role in Tat-SP4-induced necrotic cell death and mitochondrial dysfunction. Extracellular $Ca^{2+}$ can regulate several ion channels in the plasma membrane, such as $Ca^{2+}$-related channels, $Na^{+}/K^{+}$-related channels, which is very important to stabilize the membrane potential. Membrane potential is very important for cell survival. Tat sequence that is reported can decrease the plasma membrane potential when it crosses the cell membrane (Trofimenko, Grasso et al. 2021). From the protective effects of extracellular $Ca^{2+}$, we assumed that our Tat-SP4 could also affect the membrane potential when it is transported into the cytosol. The molecular mechanism of Tat-SP4 across the cell membrane is still unclear and needs further investigation.

**4.7 Evaluation of anti-proliferative efficacy of Tat-SP4 in HCC patient-derived xenograft tumor (PDXT) mouse models**

The in vivo anti-proliferative efficacy of Tat-SP4 was assessed in HCC patient-derived xenograft tumor (PDXT) mouse models. This model can preserve the genetic and histologic heterogeneity of the primary tumors. The PDXT mouse model is an in vivo model that can accurately

reflect a broad spectrum of human HCC and overcome the limitations of cancer cell lines. The HCC PDXT model was a better tool to test the antitumor efficacy of potential drugs. Our PDXT mouse model was kindly provided by the group of Prof. Terence Lee. This mouse model was donated by an HCC patient from Queen Mary Hospital in Hong Kong. This tumor was derived from a 59-year-old male patient with HBV-positive recurrent tumor. The PDXT mouse model was derived from American Joint Committee on Cancer (AJCC) stage II HCC biopsies (Table 4.2). After the tumor was surgically removed from this patient, the tumor was implanted into a type of immunocompromised NOD/SCID mice for engraftment. To obtain a bank of liver tumors, the primary passaged tumors in NOD/SCID mice must be passaged to maintain their fidelity (Figure 4.28). This model was used to validate the antitumor activity of the co-combination of a novel SCD1 inhibitor and sorafenib in a previous work (Ma, Lau et al. 2017).

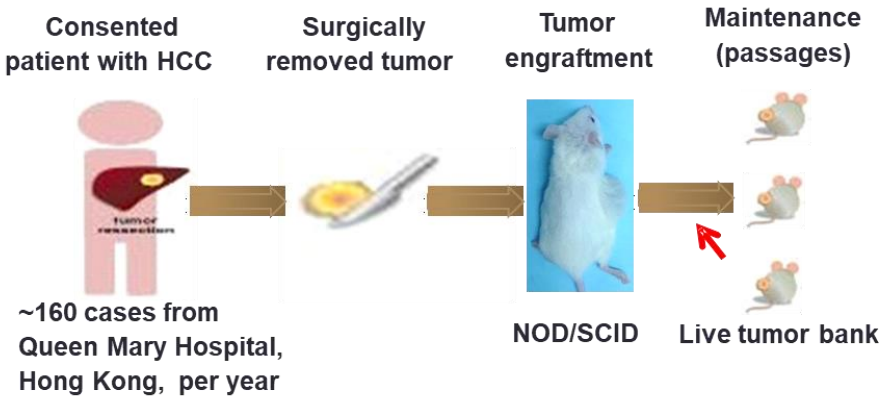

**Figure 4.28 The process of the establishing of patient-derived tumor xenograft model.**

**Table 4.2 The background information of the patient with donated tumors**

| Patient number | Gender | Age | HBV status | Tumor stage (AJCC) | Tumor recurrence |
|---|---|---|---|---|---|
| #1 | Male | 59 | HBV positive | II | Recurred |

We investigated the suppressive role of Tat-SP4 in vivo using the PDXT model. In this study, the patient-derived xenograft tumor cells kindly provided by the group of Prof. Terence Lee were subcutaneously injected into 6-week-old male nude mice ($5 \times 10^6$ cells/mouse). The administration of Tat-SP4 by daily intraperitoneal (i.p.) injection was initiated when the tumor volume reached approximately 5mm × 5mm (length × width). Tat-SP4 40 mg/kg was used. The same volume of PBS was injected as vehicle in a control group. The efficacy of Tat-SP4 treatment was evaluated by tumor size and compared with the control group. The tumor volumes of the treatment groups were significantly smaller than those of the control group (Figure 4.29A). The tumor size and its corresponding weight were shown in Figure 4.29 B&C after 33 days of treatment.

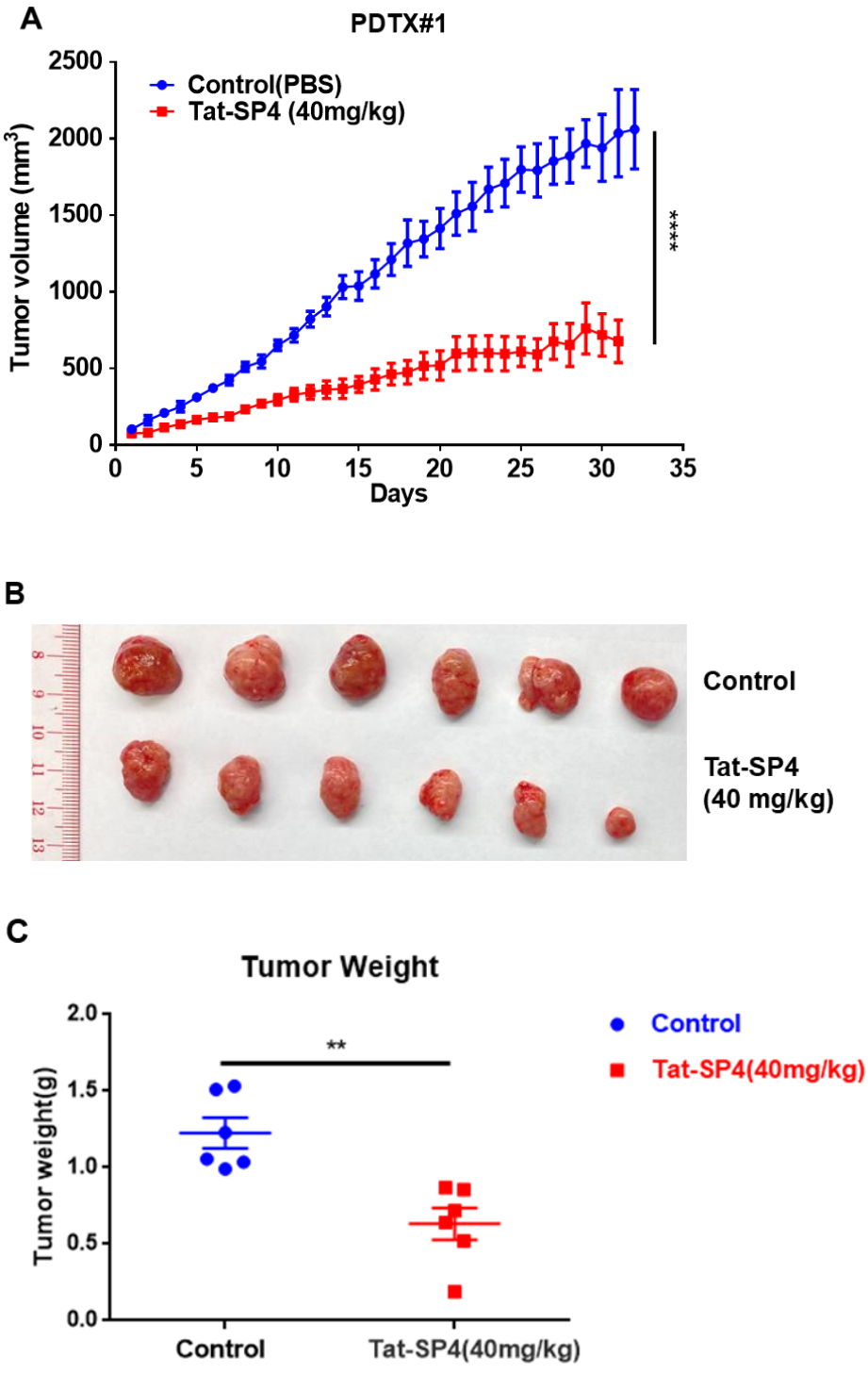


**Figure 4.29 The anti-proliferative efficacy of Tat-SP4 in HCC patient-derived xenograft tumor (PDXT) mouse models. A.** PDXT cells were injected subcutaneously into nude mice in a number of $5\times10^6$. The

administration of 40 mg/kg Tat-SP4 (treatment) or PBS (control) was started when the tumor length×width reached 5×5 mm. Tumor volume was recorded daily from the first treatment until tumor harvest (day 33). Tumor volume was defined as width2 × length/2. Data represent mean ± SEM, n=6; ****P<0.0001, unpaired t-test. B. Image of tumors after harvesting to confirm the anti-proliferative efficacy of Tat-SP4 in vivo. C. Tumor weight was measured after harvesting on day 33. Data represents mean ± SEM, n=6; *P<0.05, unpaired t-test.

During the experiment, no significant signs of toxicity such as diarrhea and infection were observed in the Tat-SP4-treated animals. In addition, the body weight of the mice was measured daily. The results showed no significant differences in the loss of body weight compared with the control group Figure 4.30 A. The vital organs of the treatment group mouse shown normal morphology and color in Figure 4.30B.

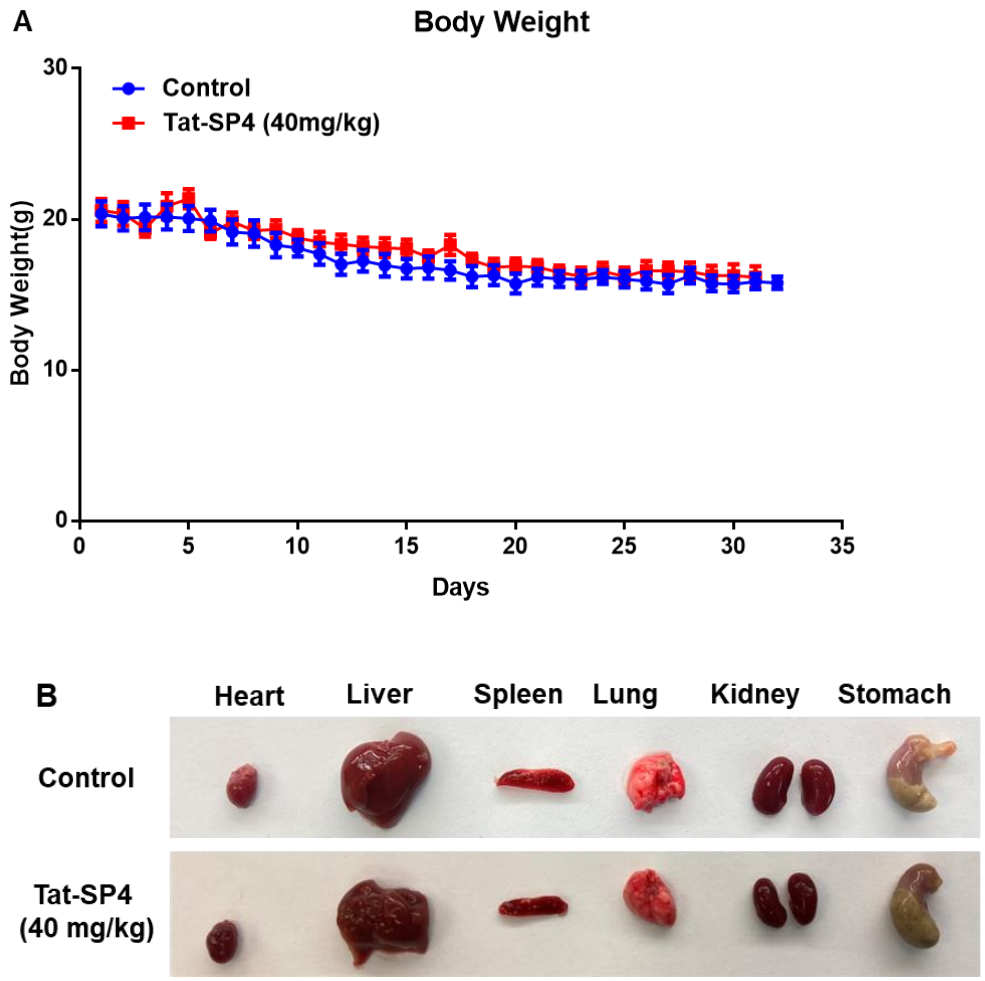


**Figure 4.30 Tat-SP4 showed no toxicity to mice in a dosage of 40mg/kg. A.** Body weight. Body weights of mice were recorded every three days after the initial treatment. Data are mean ± SEM, n=6. B. Vital organ samples.

## Discussion and future work

Our data suggests that the Beclin1-targeting stapled peptide (Tat-SP4) has the ability to induce autophagy in various HCC cell lines with distinct genetic backgrounds, which is in line with our previous findings on Tat-SP4's ability to induce autophagy in NSCLC and breast cancer cell lines. However, contrary to these findings, Tat-SP4 seems to have no additional impact on EGFR turnover in HCC cell lines, despite its ability to rapidly degrade EGFR in NSCLC and breast cancer cell lines (Yang, Qiu et al. 2021, Chen, Zhang et al. 2022). We observed that HCC cell lines frequently exhibit rapid EGFR turnover after stimulation with its agonist, which could limit the potential for further EGFR degradation by Tat-SP4. This high level of EGFR turnover may also hinder the effectiveness of EGFR-targeted tyrosine kinase inhibitors, thus reducing the utility of these drugs for HCC treatment. Further investigation is necessary to fully understand this intriguing possibility.

Interestingly, our results showed that Tat-SP4 could induce rapid c-MET turnover in a c-MET$^{+}$ HCC cell line. Although c-MET mutations and overexpression are common in HCC patients and associated with poor prognosis, c-MET-targeting drugs fail to show survival benefit in HCC patients (Yakes, Chen et al. 2011, Santoro, Rimassa et al. 2013). One possible reason is that the multiple crosstalk of c-MET with other

oncogenic growth factors such as VRGF, PDGFR, EGFR, and Wnt may affect the inhibited efficacy of c-MET-targeted tyrosine kinase inhibitors (TKIs) on cancer cell proliferation. Our results demonstrate that Tat-SP4 could promote endolysosomal degradation of c-MET, which may attenuate the HGF/c-MET signaling pathway through decreased phosphorylation of c-MET and its downstream proteins Akt. This may provide a novel method to inhibit c-MET by targeting the autophagy process. Compared to TKIs such as sorafenib, Tat-SP4 could inhibit c-MET signaling through autophagy-dependent degradation of the targeted protein rather than inhibiting the kinase domain alone. Such a unique mechanism may be advantageous as it could also eliminate the effects of crosstalk between c-MET signaling and other signals. Indeed, the results of IC50 measurement and a 5-day cell proliferation curve showed that Tat-SP4 had an inhibitory effect on the growth of several HCC cell lines.

Interestingly, Tat-SP4 could further override sorafenib resistance in adaptive and genetically mutated sorafenib-resistant HCC cell lines or cell pools. Sorafenib is the primary first-line treatment option for advanced HCC patients. Sorafenib is a type of multi-targeted kinase inhibitor that can inhibit several important growth factor receptors including VEGFR and PDGFR. Treatment with sorafenib is limited by primary and acquired resistance. One possibility for the development of

sorafenib resistance is that sorafenib-induced cell death may be neutralized by sorafenib-induced activation of multiple survival pathways. Tat-SP4 was able to induce cell death in both wild-type and sorafenib-resistant HCC cells with similar IC50 values. This suggests that the mechanism of Tat-SP4-induced cell death is different from that of sorafenib-induced cell death. Our peptides may become a potential therapeutic agent to be combined with sorafenib for the treatment of HCC.

Next, we investigated the molecular mechanism of Tat-SP4-induced HCC cell death. Our results show that Tat-SP4 can induce a unique form of cell death, which is different from the classical programmed cell death such as apoptosis, ferroptosis and necroptosis. Tat-SP4-induced necrotic cell death could be rescued by the autosis inhibitor digoxin, a cardioglycoside that inhibits $Na^+/K^+$-ATPase. In addition, Tat-SP4 induced necrotic cell death in HCC cell lines with prominent morphological features of autosis, including persistent adherence to culture dishes, accumulation of perinuclear vacuoles, and plasma membrane rupture.

Although autophagy is an essential process for cell survival, excessive autophagy has been reported to cause autosis (Liu, Shoji-Kawata et al. 2013). Autosis has been observed in various tissues and cell lines such as liver of patients with severe anorexia nervosa, neurons,

cardiomyocytes, and immune cells induced by Tat-Beclin1 and Tat-vFLIP-α2 nanopeptides (Liu, Shoji-Kawata et al. 2013, Kheloufi, Boulanger et al. 2015, Zhang, Luk et al. 2019). However, the underlying mechanisms of autosis are still unclear, especially how excessive autophagy causes necrotic cell death. It has been reported that knockdown of some core autophagy proteins such as ATG5, ATG7, and Beclin1 can rescue Tat-vFLIP-α2 and Tat-Beclin1-induced autosis (Liu, Shoji-Kawata et al. 2013, Zhang, Luk et al. 2019). In addition, the process of autosis could be reserved by the inhibition or knockdown of $Na^+/K^+$-ATPase (Liu, Shoji-Kawata et al. 2013). The interaction between Beclin1 and $Na^+/K^+$-ATPase can be observed in mice under autophagy- and autosis-inducing stresses such as starvation, exercise, and ischemia (Fernández, Liu et al. 2020). Whether Beclin1 directly interacts with $Na^+/K^+$-ATPase to modulate autosis requires further studies. Our data demonstrate that Tat-SP4 is an autosis-inducing agent, and the exact mechanism of Tat-SP4-induced autosis-like cell death needs to be further investigated.

Another notable feature of Tat-SP4-induced autotic cell death is the involvement of mitochondria. Our results showed that Tat-SP4 cause mitochondrial dysfunction in living cells including by loss of membrane potential, decreased OXPHOS and increased ROS. These effects were

observed in HCC cells before autosis occurred. Further live cell studies confirmed that Tat-SP4 can induce mitochondrial swelling and the opening of the mitochondrial permeability transition pore (MPTP) prior to cell death. Compared to the electron microscopy data of other papers, they showed the morphological features of autosis showed an abnormal internal mitochondrial and ER structure in dying cells, which likely acts as a downstream event rather than cause of autosis (Liu, Shoji-Kawata et al. 2013). The mitochondria, as the powerhouse of the cell, plays a crucial role in server cell death programs such as apoptosis, necroptosis, ferroptosis (Bock and Tait 2020). Additionally, the opening of the mitochondrial outer membrane permeabilization (MOMP) is a defining event in apoptosis, leading to the release of mitochondrial intermembrane space proteins into the cytosol and activating caspases, ultimately resulting in apoptotic cell death (Tait and Green 2010). The mitochondrial permeability transition (MPT) can also lead to the release of pro-inflammatory molecules, such as mitochondrial DNA, and trrigger necrotic cell death (Berghe, Linkermann et al. 2014) (Galluzzi, Vitale et al. 2018). Our results showed that Tat-SP4 can induce multiple aspects of mitochondrial dysfunction and the opening of mitochondrial permeability transition pore (MPTP) in HCC cells. Those results provide new insights into the mechanism of autosis and its connection to mitochondrial

dysfunction. Although further studies are needed to uncover the molecular targets involved in such effects of Tat-SP4 on mitochondria, our findings suggest that mitochondrial dysfunction may be a trigger for autosis.

Besides mitochondrial dysfunctions, intracellular $Ca^{2+}$ homeostasis also plays an important role in Tat-SP4 induced autotic cell death. We observed that Tat-SP4 could induce prompt release of $Ca^{2+}$ concentrations in the ER and a raise in mitochondrial and cytosolic $Ca^{2+}$ concentrations after treatment for 1 min in absence of extracellular $Ca^{2+}$. This effect could be rescued by the use of digoxin. $Ca^{2+}$ ion, as one of the most critical physiological cations, are not only implicated in cell survival and cell proliferation, but also closely linked to different modes of cell death, such as apoptosis, necrosis, anoikis, and autophagic cell death (Zhivotovsky and Orrenius 2011, Giorgi, Danese et al. 2018). Studies have reported the $Ca^{2+}$ dynamics at the ER and mitochondria is the main modulator of apoptosis (Marchi, Patergnani et al. 2018). The release of $Ca^{2+}$ from ER can trigger an increase in mitochondrial calcium though the membrane connection sites of ER-mitochondria. A rapid overload of $Ca^{2+}$ in the mitochondrial matrix is the primary step in triggering apoptosis (Giorgi, Danese et al. 2018). Overloading of mitochondrial $Ca^{2+}$ is also a main step inducing MPTP (Zhou, Jing et al. 2022). However, the

relationship between intracellular $Ca^{2+}$ homeostasis and autosis is still unclear. Based on our data, we speculate that the interference of Tat-SP4 on intracellular $Ca^{2+}$ homeostasis contributes to Tat-SP4 induced mitochondrial dysfunctions and autosis. As mentioned earlier, digoxin is a type of autosis inhibitor. Our data showed that digoxin can block the effect of Tat-SP4 induced intracellular $Ca^{2+}$ changes and then rescue Tat-SP4 induced autotic death. In addition, after treatment with Tat-SP4, extracellular $Ca^{2+}$ could induce a significant uptake of mitochondrial and cytosolic $Ca^{2+}$. We also found that extracellular $Ca^{2+}$ also plays a protective role in Tat-SP4 induced cell death and mitochondrial dysfunctions. The Tat-sequence is a positively charged short peptide that serves as a protein transduction domain. To be transported across the plasma membrane in a non-invasive manner, the Tat-sequence can interact with negatively charged compounds in the membrane (Berks, Palmer et al. 2003). Previous studies have reported that the Tat-sequence can decrease membrane potential when it is transported from the outside into cytosol (Trofimenko, Grasso et al. 2021). We supposed that our Tat-SP4 may impact plasma membrane function, leading to the entrance of extracellular compounds into the cytosol and disrupting $Ca^{2+}$ homeostasis. Although further studies are still needed to investigate the molecular

targets involved in the effect of Tat-SP4 on intracellular $Ca^{2+}$ homeostasis, our data provide new insights into the mechanism of autosis.

To improve the effect of Tat-SP4, future studies will aim to address the molecular mechanism of its transport across the cell membrane and determine its subcellular locations. Tat-sequence is a type of cell-penetrating peptide (CPPs) including nine positive charges. Our stapled peptides as a cargo linked with the Tat-sequence. However, the mechanism for cellular uptake of Tat-SP4 is currently unknown, as non-fluorescent peptide is difficult to detect. To overcome this challenge, we have tried labeling the peptide with rhodamine and FITC. But the results showed the rhodamine-labeled stapled peptide on cancer cell proliferation is different from the Tat-labeled stapled peptides. We also add different fluorophores such as FITC at the N-terminal of SPs (FITC-SP4) or at the C-terminal of the entire Tat-SP4 (Tat-SP4-FITC), which also shows different effects with Tat-SP4 induced HCC cell death and even inability to enter cells. The replacement of the Tat-sequence and additional fluorophores may influence the functions of the SP segment. We will try transmission electron microscopy (TEM) to investigate the uptake manner and subcellular distribution of Tat-SP4. To carry out this assay, we would require a specifically targeting antibody against either the Tat-sequence, the SP segment, or the entire Tat-SP4. In addition, we also plan

to determine the route of Tat-SP4 entry cells. The mechanism of CPPs delivery is broadly divided into direct penetration and endocytosis (Pescina, Ostacolo et al. 2018). Direct penetration is an energy-independent manner and endocytosis is an energy-dependent process for CPPs penetration. The delivery efficiency of Tat-SP4 could be examined in cells after treatment with different inhibitors of compounds of plasma membrane. Heparin can inhibit heparan sulphate in a competitive manner. If heparin treatment inhibits the transport efficiency of Tat-SP4, that would suggest the process of delivery Tat-SP4 into cells requires glycosaminoglycans, a main compound of plasma membrane (Lim, Kim et al. 2015). Other inhibitors of endocytosis such as chlorpromazine (clathrin-mediated endocytosis inhibitor), methyl-beta cyclodextrin (lipid raft-mediated endocytosis inhibitor), and amiloride (micropinocytosis inhibitor) would be used to detect whether those inhibitors impact the delivery efficiency of Tat-SP4 (Lim, Kim et al. 2015). Such information will be helpful to understand the mechanism of Tat-SP4 transportation.

To improve the potential of Tat-SP4 as a treatment for HCC tumors, we will also investigate its interaction with therapeutic immune responses. Our data showed Tat-SP4 can induce autosis in HCC cells, inhibit tumor growth in the PDXT mouse models without significant toxicity. Immunogenic cell death (ICD) is a type of cell death that not only trigger

inflammation but also an adaptive immune response (Kroemer, Galassi et al. 2022). In the case of malignant cells, certain chemotherapeutics can elicit ICD by releasing specific signals, which enhances the efficacy of treatment (Wu and Waxman 2018). ICD is primarily characterized by the secretion of a series of damage-associated molecular patterns (DAMPs) such as calreticulin, which serves as a “eat me” signal located on ER (Obeid, Tesniere et al. 2007), ATP a “find me” signal (Michaud, Martins et al. 2011), and the DNA of dead cancer cells (Garg, Vandenberk et al. 2017). Additionally, heat-shock proteins (HSPs), which translocate in response to stress, high-mobility group box 1 (HMGB1), which is necessary for stimulation of dendritic cells, are also considered as DAMPs (Apetoh, Ghiringhelli et al. 2007). Given that Tat-SP4 has been shown to induce autosis, leading to the rupture of both the cell and nuclear membranes, potentially resulting in the release of cancer cell DNA and the above-mentioned DAMPs. This process may be considered ICD, we plan to determine if this is the case by analyzing the leakage of intracellular ATP and nuclear protein HMGB1 after treatment with Tat-SP4. If confirmed, this would enhance the potential of Tat-SP4 as a novel treatment for hepatocellular carcinoma (HCC). Additionally, we will investigate the anti-tumor growth effect of Tat-SP4 in an

immunocompetent mouse model to further understand the relationship between Tat-SP4-induced cell death and the immune response.

Finally, we will assess the safety of our peptides through in vitro and in vivo studies. In vitro, we will use normal liver cell lines to evaluate the cytotoxicity of Tat-SP4. For in vivo studies, we will conduct chronic and acute toxicity assessments in mouse models. We will collect data such as histopathology of vital organs and biochemical analysis of serum to evaluate the cytotoxicity, and also determine the metabolism of Tat-SP4 in vital organs for potential use as a drug for HCC treatment.

# Reference


Abou-Alfa, G. K., T. Meyer, A.-L. Cheng, A. B. El-Khoueiry, L. Rimassa, B.-Y. Ryoo, I. Cicin, P. Merle, Y. Chen and J.-W. J. N. E. J. o. M. Park (2018). "Cabozantinib in patients with advanced and progressing hepatocellular carcinoma." **379**(1): 54-63.

Aguilar, F., C. Harris, T. Sun, M. Hollstein and P. J. S. Cerutti (1994). "Geographic variation of p53 mutational profile in nonmalignant human liver." **264**(5163): 1317-1319.

Aita, V. M., X. H. Liang, V. Murty, D. L. Pincus, W. Yu, E. Cayanis, S. Kalachikov, T. C. Gilliam and B. J. G. Levine (1999). "Cloning and genomic organization of beclin 1, a candidate tumor suppressor gene on chromosome 17q21." **59**(1): 59-65.

Aittomäki, S., M. J. B. Pesu, c. pharmacology and toxicology (2014). "Therapeutic targeting of the Jak/STAT pathway." **114**(1): 18-23.

Alqahtani, A., Z. Khan, A. Alloghbi, T. S. Said Ahmed, M. Ashraf and D. M. Hammouda (2019). "Hepatocellular Carcinoma: Molecular Mechanisms and Targeted Therapies." Medicina (Kaunas) **55**(9).

Alves, I. D., N. Goasdoué, I. Correia, S. Aubry, C. Galanth, S. Sagan, S. Lavielle and G. J. B. e. B. A.-G. S. Chassaing (2008). "Membrane interaction and perturbation mechanisms induced by two cationic cell penetrating peptides with distinct charge distribution." **1780**(7-8): 948-959.

Apetoh, L., F. Ghiringhelli, A. Tesniere, M. Obeid, C. Ortiz, A. Criollo, G. Mignot, M. C. Maiuri, E. Ullrich and P. J. N. m. Saulnier (2007). "Toll-like receptor 4–dependent contribution of the immune system to anticancer chemotherapy and radiotherapy." **13**(9): 1050-1059.

Apte, U., M. D. Thompson, S. Cui, B. Liu, B. Cieply and S. P. J. H. Monga (2008). "Wnt/β-catenin signaling mediates oval cell response in rodents." **47**(1): 288-295.

Aravalli, R. N., C. J. Steer and E. N. Cressman (2008). "Molecular mechanisms of hepatocellular carcinoma." Hepatology **48**(6): 2047-2063.

Asoh, S., I. Ohsawa, T. Mori, K.-i. Katsura, T. Hiraide, Y. Katayama, M. Kimura, D. Ozaki, K. Yamagata and S. J. P. o. t. N. A. o. S. Ohta (2002). "Protection against ischemic brain injury by protein therapeutics." **99**(26): 17107-17112.

Balmanno, K. and S. J. Cook (2009). "Tumour cell survival signalling by the ERK1/2 pathway." Cell Death Differ **16**(3): 368-377.

Balogh, J., D. Victor III, E. H. Asham, S. G. Burroughs, M. Boktour, A. Saharia, X. Li, R. M. Ghobrial and H. P. J. J. o. h. c. Monsour Jr (2016). "Hepatocellular carcinoma: a review." **3**: 41.

Bechara, C. and S. J. F. l. Sagan (2013). "Cell-penetrating peptides: 20 years later, where do we stand?" **587**(12): 1693-1702.

Berasain, C., M. U. Latasa, R. Urtasun, S. Goñi, M. Elizalde, O. Garcia-Irigoyen, M. Azcona, J. Prieto and M. A. J. C. Ávila (2011). "Epidermal growth factor receptor (EGFR) crosstalks in liver cancer." **3**(2): 2444-2461.

Berghe, T. V., A. Linkermann, S. Jouan-Lanhouet, H. Walczak and P. J. N. r. M. c. b. Vandenabeele (2014). "Regulated necrosis: the expanding network of non-apoptotic cell death pathways." **15**(2): 135-147.

Berks, B. C., T. Palmer and F. Sargent (2003). "The Tat protein translocation pathway and its role in microbial physiology." Adv Microb Physiol **47**: 187-254.

Birchmeier, C., W. Birchmeier, E. Gherardi and G. F. Vande Woude (2003). "Met, metastasis, motility and more." Nat Rev Mol Cell Biol **4**(12): 915-925.

Bock, F. J. and S. W. J. N. r. M. c. b. Tait (2020). "Mitochondria as multifaceted regulators of cell death." **21**(2): 85-100.

Boisguerin, P., C. Redt-Clouet, A. Franck-Miclo, S. Licheheb, J. Nargeot, S. Barrère-Lemaire and B. J. J. o. c. r. Lebleu (2011). "Systemic delivery of BH4 anti-apoptotic peptide using CPPs prevents cardiac ischemia–reperfusion injuries in vivo." **156**(2): 146-153.

Boix, L., J. L. Rosa, F. Ventura, A. Castells, J. Bruix, J. Rodes and R. Bartrons (1994). "c-met mRNA overexpression in human hepatocellular carcinoma." Hepatology **19**(1): 88-91.

Borsello, T., P. G. Clarke, L. Hirt, A. Vercelli, M. Repici, D. F. Schorderet, J. Bogousslavsky and C. J. N. m. Bonny (2003). "A peptide inhibitor of c-Jun N-terminal kinase protects against excitotoxicity and cerebral ischemia." **9**(9): 1180-1186.

Bright, R., A. P. Raval, J. M. Dembner, M. A. Pérez-Pinzón, G. K. Steinberg, M. A. Yenari and D. J. J. o. N. Mochly-Rosen (2004). "Protein kinase C δ mediates cerebral reperfusion injury in vivo." **24**(31): 6880-6888.

Bruix, J., S. Qin, P. Merle, A. Granito, Y.-H. Huang, G. Bodoky, M. Pracht, O. Yokosuka, O. Rosmorduc and V. J. T. L. Breder (2017). "Regorafenib for patients

with hepatocellular carcinoma who progressed on sorafenib treatment (RESORCE): a randomised, double-blind, placebo-controlled, phase 3 trial." **389**(10064): 56-66.

Burrel, M., M. Reig, A. Forner, M. Barrufet, C. R. de Lope, S. Tremosini, C. Ayuso, J. M. Llovet, M. I. Real and J. J. J. o. h. Bruix (2012). "Survival of patients with hepatocellular carcinoma treated by transarterial chemoembolisation (TACE) using Drug Eluting Beads. Implications for clinical practice and trial design." **56**(6): 1330-1335.

Cao, G., W. Pei, H. Ge, Q. Liang, Y. Luo, F. R. Sharp, A. Lu, R. Ran, S. H. Graham and J. J. J. o. N. Chen (2002). "In vivo delivery of a Bcl-xL fusion protein containing the TAT protein transduction domain protects against ischemic brain injury and neuronal apoptosis." **22**(13): 5423-5431.

Cao, Y., Y. Wang, W. F. Abi Saab, F. Yang, J. E. Pessin and J. M. J. B. J. Backer (2014). "NRBF2 regulates macroautophagy as a component of Vps34 Complex I." **461**(2): 315-322.

Capozzi, M., C. De Divitiis, A. Ottaiano, C. von Arx, S. Scala, F. Tatangelo, P. Delrio and S. Tafuto (2019). "Lenvatinib, a molecule with versatile application: from preclinical evidence to future development in anti-cancer treatment." Cancer Manag Res **11**: 3847-3860.

Caruso, S., A.-L. Calatayud, J. Pilet, T. La Bella, S. Rekik, S. Imbeaud, E. Letouzé, L. Meunier, Q. Bayard, N. Rohr-Udilova, C. Péneau, B. Grasl-Kraupp, L. de Koning, B. Ouine, P. Bioulac-Sage, G. Couchy, J. Calderaro, J.-C. Nault, J. Zucman-Rossi and S. Rebouissou (2019). "Analysis of Liver Cancer Cell Lines Identifies Agents With Likely Efficacy Against Hepatocellular Carcinoma and Markers of Response." Gastroenterology **157**(3): 760-776.

Cervello, M., D. Bachvarov, N. Lampiasi, A. Cusimano, A. Azzolina, J. A. McCubrey and G. Montalto (2012). "Molecular mechanisms of sorafenib action in liver cancer cells." Cell Cycle **11**(15): 2843-2855.

Cha, C. and R. P. Dematteo (2005). "Molecular mechanisms in hepatocellular carcinoma development." Best Pract Res Clin Gastroenterol **19**(1): 25-37.

Chen, J., X. Zhang, S. Gao, N. Li, V. Keng and Y. Zhao (2022). "A Beclin 1-targeting stapled peptide synergizes with erlotinib to potently inhibit proliferation of non-small-cell lung cancer cells." Biochem Biophys Res Commun **636**(Pt 1): 125-131.

Cheng, A. L., Y. K. Kang, Z. Chen, C. J. Tsao, S. Qin, J. S. Kim, R. Luo, J. Feng, S. Ye, T. S. Yang, J. Xu, Y. Sun, H. Liang, J. Liu, J. Wang, W. Y. Tak, H. Pan, K. Burock, J. Zou, D. Voliotis and Z. Guan (2009). "Efficacy and safety of sorafenib in patients in

the Asia-Pacific region with advanced hepatocellular carcinoma: a phase III randomised, double-blind, placebo-controlled trial." Lancet Oncol **10**(1): 25-34.

Dai, J., Q. Huang, K. Niu, B. Wang, Y. Li, C. Dai, Z. Chen, K. Tao and J. Dai (2018). "Sestrin 2 confers primary resistance to sorafenib by simultaneously activating AKT and AMPK in hepatocellular carcinoma." Cancer Med **7**(11): 5691-5703.

De Coupade, C., A. Fittipaldi, V. Chagnas, M. Michel, S. Carlier, E. Tasciotti, A. Darmon, D. Ravel, J. Kearsey and M. J. B. J. Giacca (2005). "Novel human-derived cell-penetrating peptides for specific subcellular delivery of therapeutic biomolecules." **390**(2): 407-418.

Degenhardt, K., R. Mathew, B. Beaudoin, K. Bray, D. Anderson, G. Chen, C. Mukherjee, Y. Shi, C. Gélinas, Y. Fan, D. A. Nelson, S. Jin and E. White (2006). "Autophagy promotes tumor cell survival and restricts necrosis, inflammation, and tumorigenesis." Cancer Cell **10**(1): 51-64.

Derossi, D., A. H. Joliot, G. Chassaing and A. J. J. o. B. C. Prochiantz (1994). "The third helix of the Antennapedia homeodomain translocates through biological membranes." **269**(14): 10444-10450.

Dhanasekaran, R., S. Bandoh and L. R. J. F. Roberts (2016). "Molecular pathogenesis of hepatocellular carcinoma and impact of therapeutic advances." **5**.

Dimri, M. and A. Satyanarayana (2020). "Molecular Signaling Pathways and Therapeutic Targets in Hepatocellular Carcinoma." Cancers (Basel) **12**(2).

Ding, Z.-B., Y.-H. Shi, J. Zhou, S.-J. Qiu, Y. Xu, Z. Dai, G.-M. Shi, X.-Y. Wang, A.-W. Ke and B. J. C. r. Wu (2008). "Association of autophagy defect with a malignant phenotype and poor prognosis of hepatocellular carcinoma." **68**(22): 9167-9175.

Dupuy, A. J., L. M. Rogers, J. Kim, K. Nannapaneni, T. K. Starr, P. Liu, D. A. Largaespada, T. E. Scheetz, N. A. Jenkins and N. G. J. C. r. Copeland (2009). "A modified sleeping beauty transposon system that can be used to model a wide variety of human cancers in mice." **69**(20): 8150-8156.

Egan, D. F., D. B. Shackelford, M. M. Mihaylova, S. Gelino, R. A. Kohnz, W. Mair, D. S. Vasquez, A. Joshi, D. M. Gwinn and R. J. S. Taylor (2011). "Phosphorylation of ULK1 (hATG1) by AMP-activated protein kinase connects energy sensing to mitophagy." **331**(6016): 456-461.

Elmquist, A., M. Hansen and Ü. J. B. e. B. A.-B. Langel (2006). "Structure–activity relationship study of the cell-penetrating peptide pVEC." **1758**(6): 721-729.

Farazi, P. A. and R. A. J. N. R. C. DePinho (2006). "Hepatocellular carcinoma pathogenesis: from genes to environment." **6**(9): 674-687.

Ferlay, J., H. R. Shin, F. Bray, D. Forman, C. Mathers and D. M. Parkin (2010). "Estimates of worldwide burden of cancer in 2008: GLOBOCAN 2008." Int J Cancer **127**(12): 2893-2917.

Fernández, Á. F., Y. Liu, V. Ginet, M. Shi, J. Nah, Z. Zou, A. Zhou, B. A. Posner, G. Xiao and M. J. J. i. Tanguy (2020). "Interaction between the autophagy protein Beclin 1 and Na+, K+-ATPase during starvation, exercise, and ischemia." **5**(1).

Frazier, N. M., T. Brand, J. D. Gordan, J. Grandis and N. Jura (2019). "Overexpression-mediated activation of MET in the Golgi promotes HER3/ERBB3 phosphorylation." Oncogene **38**(11): 1936-1950.

Futaki, S., T. Suzuki, W. Ohashi, T. Yagami, S. Tanaka, K. Ueda and Y. J. J. o. B. C. Sugiura (2001). "Arginine-rich peptides: an abundant source of membrane-permeable peptides having potential as carriers for intracellular protein delivery." **276**(8): 5836-5840.

Galavotti, S., S. Bartesaghi, D. Faccenda, M. Shaked-Rabi, S. Sanzone, A. McEvoy, D. Dinsdale, F. Condorelli, S. Brandner and M. J. O. Campanella (2013). "The autophagy-associated factors DRAM1 and p62 regulate cell migration and invasion in glioblastoma stem cells." **32**(6): 699-712.

Galli, A., G. Svegliati-Baroni, E. Ceni, S. Milani, F. Ridolfi, R. Salzano, M. Tarocchi, C. Grappone, G. Pellegrini and A. J. H. Benedetti (2005). "Oxidative stress stimulates proliferation and invasiveness of hepatic stellate cells via a MMP2-mediated mechanism." **41**(5): 1074-1084.

Galluzzi, L., I. Vitale, S. A. Aaronson, J. M. Abrams, D. Adam, P. Agostinis, E. S. Alnemri, L. Altucci, I. Amelio, D. W. J. C. D. Andrews and Differentiation (2018). "Molecular mechanisms of cell death: recommendations of the Nomenclature Committee on Cell Death 2018." **25**(3): 486-541.

Gao, C., S. Mao, H. J. Ditzel, L. Farnaes, P. Wirsching, R. A. Lerner, K. D. J. B. Janda and m. chemistry (2002). "A cell-penetrating peptide from a novel pVII–pIX phage-displayed random peptide library." **10**(12): 4057-4065.

Garcia-Vilas, J. A. and M. A. Medina (2018). "Updates on the hepatocyte growth factor/c-Met axis in hepatocellular carcinoma and its therapeutic implications." World J Gastroenterol **24**(33): 3695-3708.

Garg, A. D., L. Vandenberk, S. Fang, T. Fasche, S. Van Eygen, J. Maes, M. Van Woensel, C. Koks, N. Vanthillo, N. J. C. D. Graf and Differentiation (2017). "Pathogen response-like recruitment and activation of neutrophils by sterile immunogenic dying cells drives neutrophil-mediated residual cell killing." **24**(5): 832-843.

Giles, R. H., J. H. Van Es and H. J. B. e. B. A.-R. o. C. Clevers (2003). "Caught up in a Wnt storm: Wnt signaling in cancer." **1653**(1): 1-24.

Giordano, S. and A. Columbano (2014). "Met as a therapeutic target in HCC: facts and hopes." J Hepatol **60**(2): 442-452.

Giorgi, C., A. Danese, S. Missiroli, S. Patergnani and P. Pinton (2018). "Calcium Dynamics as a Machine for Decoding Signals." Trends in Cell Biology **28**(4): 258-273.

Golabi, P., S. Fazel, M. Otgonsuren, M. Sayiner, C. T. Locklear and Z. M. Younossi (2017). "Mortality assessment of patients with hepatocellular carcinoma according to underlying disease and treatment modalities." Medicine (Baltimore) **96**(9): e5904.

Gong, C., C. Bauvy, G. Tonelli, W. Yue, C. Delomenie, V. Nicolas, Y. Zhu, V. Domergue, V. Marin-Esteban and H. J. O. Tharinger (2013). "Beclin 1 and autophagy are required for the tumorigenicity of breast cancer stem-like/progenitor cells." **32**(18): 2261-2272.

Guidotti, G., L. Brambilla and D. Rossi (2017). "Cell-Penetrating Peptides: From Basic Research to Clinics." Trends in Pharmacological Sciences **38**(4): 406-424.

Hamasaki, M. and T. J. F. l. Yoshimori (2010). "Where do they come from? Insights into autophagosome formation." **584**(7): 1296-1301.

Hao, C., G. Liu and G. J. T. a. i. r. d. Tian (2019). "Autophagy inhibition of cancer stem cells promotes the efficacy of cisplatin against non-small cell lung carcinoma." **13**: 1753466619866097.

Hao, F., Y. Li, J. Zhu, J. Sun, B. Marshall, R. J. Lee, L. Teng, Z. Yang and J. J. C. m. c. Xie (2019). "Polyethylenimine-based formulations for delivery of oligonucleotides." **26**(13): 2264-2284.

Harris, J., M. Hartman, C. Roche, S. G. Zeng, A. O'Shea, F. A. Sharp, E. M. Lambe, E. M. Creagh, D. T. Golenbock, J. Tschopp, H. Kornfeld, K. A. Fitzgerald and E. C. Lavelle (2011). "Autophagy controls IL-1beta secretion by targeting pro-IL-1beta for degradation." J Biol Chem **286**(11): 9587-9597.

He, C. and B. J. C. o. i. c. b. Levine (2010). "The beclin 1 interactome." **22**(2): 140-149.

He, S., Z. Zhao, Y. Yang, D. O'connell, X. Zhang, S. Oh, B. Ma, J.-H. Lee, T. Zhang and B. J. N. c. Varghese (2015). "Truncating mutation in the autophagy gene UVRAG confers oncogenic properties and chemosensitivity in colorectal cancers." **6**(1): 1-14.

Herce, H. D. and A. E. J. P. o. t. N. A. o. S. Garcia (2007). "Molecular dynamics simulations suggest a mechanism for translocation of the HIV-1 TAT peptide across lipid membranes." **104**(52): 20805-20810.

Hoek, J. B. and J. G. J. A. Pastorino (2002). "Ethanol, oxidative stress, and cytokine-induced liver cell injury." **27**(1): 63-68.

Horie, Y., A. Suzuki, E. Kataoka, T. Sasaki, K. Hamada, J. Sasaki, K. Mizuno, G. Hasegawa, H. Kishimoto and M. J. T. J. o. c. i. Iizuka (2004). "Hepatocyte-specific Pten deficiency results in steatohepatitis and hepatocellular carcinomas." **113**(12): 1774-1783.

Hsu, C. C., P. M. Hsieh, Y. S. Chen, G. H. Lo, H. Y. Lin, C. Y. Dai, J. F. Huang, W. L. Chuang, Y. L. Chen, M. L. Yu and C. W. Lin (2019). "Axl and autophagy LC3 expression in tumors is strongly associated with clinical prognosis of hepatocellular carcinoma patients after curative resection." Cancer Med **8**(7): 3453-3463.

Huang, D., T. Li, L. Wang, L. Zhang, R. Yan, K. Li, S. Xing, G. Wu, L. Hu, W. Jia, S. C. Lin, C. V. Dang, L. Song, P. Gao and H. Zhang (2016). "Hepatocellular carcinoma redirects to ketolysis for progression under nutrition deprivation stress." Cell Res **26**(10): 1112-1130.

Huang, D., T. Li, L. Wang, L. Zhang, R. Yan, K. Li, S. Xing, G. Wu, L. Hu and W. J. C. r. Jia (2016). "Hepatocellular carcinoma redirects to ketolysis for progression under nutrition deprivation stress." **26**(10): 1112-1130.

Huang, X., G. Gan, X. Wang, T. Xu and W. Xie (2019). "The HGF-MET axis coordinates liver cancer metabolism and autophagy for chemotherapeutic resistance." Autophagy **15**(7): 1258-1279.

Huh, C. G., V. M. Factor, A. Sanchez, K. Uchida, E. A. Conner and S. S. Thorgeirsson (2004). "Hepatocyte growth factor/c-met signaling pathway is required for efficient liver regeneration and repair." Proc Natl Acad Sci U S A **101**(13): 4477-4482.

Inagawa, S., M. Itabashi, S. Adachi, T. Kawamoto, M. Hori, J. Shimazaki, F. Yoshimi and K. Fukao (2002). "Expression and prognostic roles of beta-catenin in

hepatocellular carcinoma: correlation with tumor progression and postoperative survival." Clin Cancer Res **8**(2): 450-456.

Inoue, D., T. Suzuki, Y. Mitsuishi, Y. Miki, S. Suzuki, S. Sugawara, M. Watanabe, A. Sakurada, C. Endo, A. Uruno, H. Sasano, T. Nakagawa, K. Satoh, N. Tanaka, H. Kubo, H. Motohashi and M. Yamamoto (2012). "Accumulation of p62/SQSTM1 is associated with poor prognosis in patients with lung adenocarcinoma." Cancer Sci **103**(4): 760-766.

Ishizawa, T., K. Hasegawa, T. Aoki, M. Takahashi, Y. Inoue, K. Sano, H. Imamura, Y. Sugawara, N. Kokudo and M. J. G. Makuuchi (2008). "Neither multiple tumors nor portal hypertension are surgical contraindications for hepatocellular carcinoma." **134**(7): 1908-1916.

Itakura, E., C. Kishi, K. Inoue and N. J. M. b. o. t. c. Mizushima (2008). "Beclin 1 forms two distinct phosphatidylinositol 3-kinase complexes with mammalian Atg14 and UVRAG." **19**(12): 5360-5372.

Järver, P., I. Mäger and Ü. J. T. i. p. s. Langel (2010). "In vivo biodistribution and efficacy of peptide mediated delivery." **31**(11): 528-535.

Jin, S. and E. J. A. White (2007). "Role of autophagy in cancer: management of metabolic stress." **3**(1): 28-31.

Johansson, H. J., S. El-Andaloussi, T. Holm, M. Mäe, J. Jänes, T. Maimets and Ü. J. M. T. Langel (2008). "Characterization of a novel cytotoxic cell-penetrating peptide derived from p14ARF protein." **16**(1): 115-123.

Joliot, A., C. Pernelle, H. Deagostini-Bazin and A. J. P. o. t. N. A. o. S. Prochiantz (1991). "Antennapedia homeobox peptide regulates neural morphogenesis." **88**(5): 1864-1868.

Kang, C., Y. Sun, J. Zhu, W. Li, A. Zhang, T. Kuang, J. Xie and Z. J. C. D. M. Yang (2016). "Delivery of nanoparticles for treatment of brain tumor." **17**(8): 745-754.

Kang, M. R., M. S. Kim, J. E. Oh, Y. R. Kim, S. Y. Song, S. S. Kim, C. H. Ahn, N. J. Yoo and S. H. Lee (2009). "Frameshift mutations of autophagy-related genes ATG2B, ATG5, ATG9B and ATG12 in gastric and colorectal cancers with microsatellite instability." J Pathol **217**(5): 702-706.

Kaposi-Novak, P., J. S. Lee, L. Gòmez-Quiroz, C. Coulouarn, V. M. Factor and S. S. Thorgeirsson (2006). "Met-regulated expression signature defines a subset of human hepatocellular carcinomas with poor prognosis and aggressive phenotype." J Clin Invest **116**(6): 1582-1595.

Kauffman, W. B., T. Fuselier, J. He and W. C. J. T. i. b. s. Wimley (2015). "Mechanism matters: a taxonomy of cell penetrating peptides." **40**(12): 749-764.

Keng, V. W., D. Sia, A. L. Sarver, B. R. Tschida, D. Fan, C. Alsinet, M. Sole, W. L. Lee, T. P. Kuka, B. S. Moriarity, A. Villanueva, A. J. Dupuy, J. D. Riordan, J. B. Bell, K. A. Silverstein, J. M. Llovet and D. A. Largaespada (2013). "Sex bias occurrence of hepatocellular carcinoma in Poly7 molecular subclass is associated with EGFR." Hepatology **57**(1): 120-130.

Keng, V. W., B. R. Tschida, J. B. Bell and D. A. Largaespada (2011). "Modeling hepatitis B virus X-induced hepatocellular carcinoma in mice with the Sleeping Beauty transposon system." Hepatology **53**(3): 781-790.

Keng, V. W., A. Villanueva, D. Y. Chiang, A. J. Dupuy, B. J. Ryan, I. Matise, K. A. Silverstein, A. Sarver, T. K. Starr, K. Akagi, L. Tessarollo, L. S. Collier, S. Powers, S. W. Lowe, N. A. Jenkins, N. G. Copeland, J. M. Llovet and D. A. Largaespada (2009). "A conditional transposon-based insertional mutagenesis screen for genes associated with mouse hepatocellular carcinoma." Nat Biotechnol **27**(3): 264-274.

Kew, M. C. J. L. i. (2003). "Synergistic interaction between aflatoxin B1 and hepatitis B virus in hepatocarcinogenesis." **23**(6): 405-409.

Kheloufi, M., C. M. Boulanger, P. Codogno and P. E. J. H. Rautou (2015). "Autosis occurs in the liver of patients with severe anorexia nervosa." **62**(2): 657-658.

Kihara, A., Y. Kabeya, Y. Ohsumi and T. J. E. r. Yoshimori (2001). "Beclin–phosphatidylinositol 3-kinase complex functions at the trans-Golgi network." **2**(4): 330-335.

Kim, J. H., S. K. Hong, P. K. Wu, A. L. Richards, W. T. Jackson and J. I. Park (2014). "Raf/MEK/ERK can regulate cellular levels of LC3B and SQSTM1/p62 at expression levels." Exp Cell Res **327**(2): 340-352.

Kim, M. S., E. G. Jeong, C. H. Ahn, S. S. Kim, S. H. Lee and N. J. J. H. p. Yoo (2008). "Frameshift mutation of UVRAG, an autophagy-related gene, in gastric carcinomas with microsatellite instability." **39**(7): 1059-1063.

Kiss, A., N. J. Wang, J. P. Xie and S. S. Thorgeirsson (1997). "Analysis of transforming growth factor (TGF)-alpha/epidermal growth factor receptor, hepatocyte growth Factor/c-met,TGF-beta receptor type II, and p53 expression in human hepatocellular carcinomas." Clin Cancer Res **3**(7): 1059-1066.

Kitamura, H., T. Torigoe, H. Asanuma, S. I. Hisasue, K. Suzuki, T. Tsukamoto, M. Satoh and N. Sato (2006). "Cytosolic overexpression of p62 sequestosome 1 in neoplastic prostate tissue." Histopathology **48**(2): 157-161.

Komatsu, M., S. Waguri, T. Ueno, J. Iwata, S. Murata, I. Tanida, J. Ezaki, N. Mizushima, Y. Ohsumi, Y. Uchiyama, E. Kominami, K. Tanaka and T. Chiba (2005). "Impairment of starvation-induced and constitutive autophagy in Atg7-deficient mice." J Cell Biol **169**(3): 425-434.

Komatsu, M., S. Waguri, T. Ueno, J. Iwata, S. Murata, I. Tanida, J. Ezaki, N. Mizushima, Y. Ohsumi and Y. J. T. J. o. c. b. Uchiyama (2005). "Impairment of starvation-induced and constitutive autophagy in Atg7-deficient mice." **169**(3): 425-434.

Kroemer, G., C. Galassi, L. Zitvogel and L. J. N. i. Galluzzi (2022). "Immunogenic cell stress and death." **23**(4): 487-500.

Kulik, L. and H. B. J. G. El-Serag (2019). "Epidemiology and management of hepatocellular carcinoma." **156**(2): 477-491. e471.

Kuma, A., M. Hatano, M. Matsui, A. Yamamoto, H. Nakaya, T. Yoshimori, Y. Ohsumi, T. Tokuhisa and N. J. N. Mizushima (2004). "The role of autophagy during the early neonatal starvation period." **432**(7020): 1032-1036.

Kuroyanagi, H., J. Yan, N. Seki, Y. Yamanouchi, Y.-i. Suzuki, T. Takano, M.-a. Muramatsu and T. J. G. Shirasawa (1998). "Human ULK1, a Novel Serine/Threonine Kinase Related to UNC-51 Kinase ofCaenorhabditis elegans: cDNA Cloning, Expression, and Chromosomal Assignment." **51**(1): 76-85.

Lane, J. D. and H. J. E. i. b. Nakatogawa (2013). "Two ubiquitin-like conjugation systems that mediate membrane formation during autophagy." **55**: 39-50.

Lee, E. F., M. A. Perugini, A. Pettikiriarachchi, M. Evangelista, D. W. Keizer, S. Yao and W. D. J. A. Fairlie (2016). "The BECN1 N-terminal domain is intrinsically disordered." **12**(3): 460-471.

Lengyel, E., D. Prechtel, J. H. Resau, K. Gauger, A. Welk, K. Lindemann, G. Salanti, T. Richter, B. Knudsen, G. F. Vande Woude and N. Harbeck (2005). "C-Met overexpression in node-positive breast cancer identifies patients with poor clinical outcome independent of Her2/neu." Int J Cancer **113**(4): 678-682.

Leung, C. O. N., M. Tong, K. P. S. Chung, L. Zhou, N. Che, K. H. Tang, J. Ding, E. Y. T. Lau, I. O. L. Ng, S. Ma and T. K. W. Lee (2020). "Overriding Adaptive Resistance

to Sorafenib Through Combination Therapy With Src Homology 2 Domain–Containing Phosphatase 2 Blockade in Hepatocellular Carcinoma." **72**(1): 155-168.

Levine, B. and G. Kroemer (2019). "Biological Functions of Autophagy Genes: A Disease Perspective." Cell **176**(1-2): 11-42.

Levine, B. and G. J. C. Kroemer (2019). "Biological functions of autophagy genes: a disease perspective." **176**(1-2): 11-42.

Levine, B., R. Liu, X. Dong and Q. Zhong (2015). "Beclin orthologs: integrative hubs of cell signaling, membrane trafficking, and physiology." Trends Cell Biol **25**(9): 533-544.

Levine, B., N. Mizushima and H. W. J. N. Virgin (2011). "Autophagy in immunity and inflammation." **469**(7330): 323-335.

Li, A., R. Zhang, Y. Zhang, X. Liu, R. Wang, J. Liu, X. Liu, Y. Xie, W. Cao, R. Xu, Y. Ma, W. Cai, B. Wu, S. Cai and X. Tang (2019). "BEZ235 increases sorafenib inhibition of hepatocellular carcinoma cells by suppressing the PI3K/AKT/mTOR pathway." Am J Transl Res **11**(9): 5573-5585.

Li, J., B. Yang, Q. Zhou, Y. Wu, D. Shang, Y. Guo, Z. Song, Q. Zheng and J. J. C. Xiong (2013). "Autophagy promotes hepatocellular carcinoma cell invasion through activation of epithelial–mesenchymal transition." **34**(6): 1343-1351.

Li, L., D. Pan, S. Zhang, D. Xie, X. Zheng and H. J. E. R. M. P. S. Chen (2018). "Autophagy regulates chemoresistance of gastric cancer stem cells via the Notch signaling pathway." **22**(11): 3402-3407.

Li, S. S., L. Z. Xu, W. Zhou, S. Yao, C. L. Wang, J. L. Xia, H. F. Wang, M. Kamran, X. Y. Xue, L. Dong, J. Wang, X. D. Ding, L. Bella, L. Bugeon, J. Xu, F. M. Zheng, M. J. Dallman, E. W. F. Lam and Q. Liu (2017). "p62/SQSTM1 interacts with vimentin to enhance breast cancer metastasis." Carcinogenesis **38**(11): 1092-1103.

Li, W., F. Yue, Y. Dai, B. Shi, G. Xu, X. Jiang, X. Zhou, G. P. Pfeifer and L. Liu (2019). "Suppressor of hepatocellular carcinoma RASSF1A activates autophagy initiation and maturation." Cell Death Differ **26**(8): 1379-1395.

Li, X., L. He, K. H. Che, S. F. Funderburk, L. Pan, N. Pan, M. Zhang, Z. Yue and Y. Zhao (2012). "Imperfect interface of Beclin1 coiled-coil domain regulates homodimer and heterodimer formation with Atg14L and UVRAG." Nat Commun **3**: 662.

Liang, C., W. Li, H. Ge, K. Zhang, G. Li, J. J. O. Wu and therapy (2018). "Role of Beclin1 expression in patients with hepatocellular carcinoma: a meta-analysis." **11**: 2387.

Liang, X. H., S. Jackson, M. Seaman, K. Brown, B. Kempkes, H. Hibshoosh and B. J. N. Levine (1999). "Induction of autophagy and inhibition of tumorigenesis by beclin 1." **402**(6762): 672-676.

Liang, X. H., L. K. Kleeman, H. H. Jiang, G. Gordon, J. E. Goldman, G. Berry, B. Herman and B. Levine (1998). "Protection against fatal Sindbis virus encephalitis by beclin, a novel Bcl-2-interacting protein." J Virol **72**(11): 8586-8596.

Lim, S., W.-J. Kim, Y.-H. Kim, S. Lee, J.-H. Koo, J.-A. Lee, H. Yoon, D.-H. Kim, H.-J. Park and H.-M. J. N. c. Kim (2015). "dNP2 is a blood–brain barrier-permeable peptide enabling ctCTLA-4 protein delivery to ameliorate experimental autoimmune encephalomyelitis." **6**(1): 8244.

Liu, C. Y., K. F. Chen and P. J. Chen (2015). "Treatment of Liver Cancer." Cold Spring Harb Perspect Med **5**(9): a021535.

Liu, Y., S. Shoji-Kawata, R. M. Sumpter Jr, Y. Wei, V. Ginet, L. Zhang, B. Posner, K. A. Tran, D. R. Green and R. J. J. P. o. t. N. A. o. S. Xavier (2013). "Autosis is a Na+, K+-ATPase–regulated form of cell death triggered by autophagy-inducing peptides, starvation, and hypoxia–ischemia." **110**(51): 20364-20371.

Liu, Y., S. Shoji-Kawata, R. M. Sumpter, Jr., Y. Wei, V. Ginet, L. Zhang, B. Posner, K. A. Tran, D. R. Green, R. J. Xavier, S. Y. Shaw, P. G. Clarke, J. Puyal and B. Levine (2013). "Autosis is a Na+,K+-ATPase-regulated form of cell death triggered by autophagy-inducing peptides, starvation, and hypoxia-ischemia." Proc Natl Acad Sci U S A **110**(51): 20364-20371.

Liu, Y., S. Shoji-Kawata, R. M. Sumpter, Y. Wei, V. Ginet, L. Zhang, B. Posner, K. A. Tran, D. R. Green, R. J. Xavier, S. Y. Shaw, P. G. H. Clarke, J. Puyal and B. Levine (2013). "Autosis is a Na<sup>+</sup>,K<sup>+</sup>-ATPase–regulated form of cell death triggered by autophagy-inducing peptides, starvation, and hypoxia–ischemia." **110**(51): 20364-20371.

Llovet, J. M., R. Montal, D. Sia and R. S. Finn (2018). "Molecular therapies and precision medicine for hepatocellular carcinoma." Nature Reviews Clinical Oncology **15**(10): 599-616.

Llovet, J. M., S. Ricci, V. Mazzaferro, P. Hilgard, E. Gane, J.-F. Blanc, A. C. de Oliveira, A. Santoro, J.-L. Raoul, A. Forner, M. Schwartz, C. Porta, S. Zeuzem, L. Bolondi, T. F. Greten, P. R. Galle, J.-F. Seitz, I. Borbath, D. Häussinger, T. Giannaris,

M. Shan, M. Moscovici, D. Voliotis and J. Bruix (2008). "Sorafenib in Advanced Hepatocellular Carcinoma." **359**(4): 378-390.

Llovet, J. M., S. Ricci, V. Mazzaferro, P. Hilgard, E. Gane, J. F. Blanc, A. C. de Oliveira, A. Santoro, J. L. Raoul, A. Forner, M. Schwartz, C. Porta, S. Zeuzem, L. Bolondi, T. F. Greten, P. R. Galle, J. F. Seitz, I. Borbath, D. Häussinger, T. Giannaris, M. Shan, M. Moscovici, D. Voliotis and J. Bruix (2008). "Sorafenib in advanced hepatocellular carcinoma." N Engl J Med **359**(4): 378-390.

Llovet, J. M., A. Villanueva, J. A. Marrero, M. Schwartz, T. Meyer, P. R. Galle, R. Lencioni, T. F. Greten, M. Kudo and S. J. J. H. Mandrekar (2021). "Trial design and endpoints in hepatocellular carcinoma: AASLD consensus conference." **73**: 158-191.

Lo, S. L. and S. J. B. Wang (2008). "An endosomolytic Tat peptide produced by incorporation of histidine and cysteine residues as a nonviral vector for DNA transfection." **29**(15): 2408-2414.

Lock, R., C. M. Kenific, A. M. Leidal, E. Salas and J. J. C. d. Debnath (2014). "Autophagy-Dependent Production of Secreted Factors Facilitates Oncogenic RAS-Driven InvasionAutophagy-Dependent Secretion and Invasion." **4**(4): 466-479.

Lorin, S., A. Hamaï, M. Mehrpour and P. Codogno (2013). Autophagy regulation and its role in cancer. Seminars in cancer biology, Elsevier.

Lundberg, P., S. El-Andaloussi, T. Sütlü, H. Johansson and Ü. J. T. F. J. Langel (2007). "Delivery of short interfering RNA using endosomolytic cell-penetrating peptides." **21**(11): 2664-2671.

Ma, M. K. F., E. Y. T. Lau, D. H. W. Leung, J. Lo, N. P. Y. Ho, L. K. W. Cheng, S. Ma, C. H. Lin, J. A. Copland, J. Ding, R. C. L. Lo, I. O. L. Ng and T. K. W. Lee (2017). "Stearoyl-CoA desaturase regulates sorafenib resistance via modulation of ER stress-induced differentiation." Journal of Hepatology **67**(5): 979-990.

Ma, M. K. F., E. Y. T. Lau, D. H. W. Leung, J. Lo, N. P. Y. Ho, L. K. W. Cheng, S. Ma, C. H. Lin, J. A. Copland and J. J. J. o. h. Ding (2017). "Stearoyl-CoA desaturase regulates sorafenib resistance via modulation of ER stress-induced differentiation." **67**(5): 979-990.

Macdonald, A., K. Crowder, A. Street, C. McCormick, K. Saksela and M. J. J. o. B. C. Harris (2003). "The Hepatitis C Virus Non-structural NS5A Protein Inhibits Activating Protein–1 Function by Perturbing Ras-ERK Pathway Signaling." **278**(20): 17775-17784.

MacDonald, B. T., K. Tamai and X. He (2009). "Wnt/beta-catenin signaling: components, mechanisms, and diseases." Dev Cell **17**(1): 9-26.

Macintosh, R. L., P. Timpson, J. Thorburn, K. I. Anderson, A. Thorburn and K. M. J. C. C. Ryan (2012). "Inhibition of autophagy impairs tumor cell invasion in an organotypic model." **11**(10): 2022-2029.

Magzoub, M., S. Sandgren, P. Lundberg, K. Oglęcka, J. Lilja, A. Wittrup, L. G. Eriksson, Ü. Langel, M. Belting, A. J. B. Gräslund and b. r. communications (2006). "N-terminal peptides from unprocessed prion proteins enter cells by macropinocytosis." **348**(2): 379-385.

Majumder, M., A. K. Ghosh, R. Steele, R. Ray and R. B. J. J. o. v. Ray (2001). "Hepatitis C virus NS5A physically associates with p53 and regulates p21/waf1 gene expression in a p53-dependent manner." **75**(3): 1401-1407.

Marchi, S., S. Patergnani, S. Missiroli, G. Morciano, A. Rimessi, M. R. Wieckowski, C. Giorgi and P. J. C. c. Pinton (2018). "Mitochondrial and endoplasmic reticulum calcium homeostasis and cell death." **69**: 62-72.

Marrogi, A. J., M. A. Khan, H. E. van Gijssel, J. A. Welsh, H. Rahim, A. J. Demetris, K. V. Kowdley, S. P. Hussain, J. Nair and H. J. J. o. t. N. C. I. Bartsch (2001). "Oxidative stress and p53 mutations in the carcinogenesis of iron overload-associated hepatocellular carcinoma." **93**(21): 1652-1655.

Martorana, F., L. Brambilla, C. F. Valori, C. Bergamaschi, C. Roncoroni, E. Aronica, A. Volterra, P. Bezzi and D. J. H. M. G. Rossi (2012). "The BH4 domain of Bcl-XL rescues astrocyte degeneration in amyotrophic lateral sclerosis by modulating intracellular calcium signals." **21**(4): 826-840.

Mates, L., M. K. Chuah, E. Belay, B. Jerchow, N. Manoj, A. Acosta-Sanchez, D. P. Grzela, A. Schmitt, K. Becker, J. Matrai, L. Ma, E. Samara-Kuko, C. Gysemans, D. Pryputniewicz, C. Miskey, B. Fletcher, T. VandenDriessche, Z. Ivics and Z. Izsvak (2009). "Molecular evolution of a novel hyperactive Sleeping Beauty transposase enables robust stable gene transfer in vertebrates." Nat Genet **41**(6): 753-761.

Mathew, R., C. M. Karp, B. Beaudoin, N. Vuong, G. Chen, H.-Y. Chen, K. Bray, A. Reddy, G. Bhanot and C. J. C. Gelinas (2009). "Autophagy suppresses tumorigenesis through elimination of p62." **137**(6): 1062-1075.

Mathew, R., C. M. Karp, B. Beaudoin, N. Vuong, G. Chen, H. Y. Chen, K. Bray, A. Reddy, G. Bhanot, C. Gelinas, R. S. Dipaola, V. Karantza-Wadsworth and E. White (2009). "Autophagy suppresses tumorigenesis through elimination of p62." Cell **137**(6): 1062-1075.

Matsunaga, K., T. Saitoh, K. Tabata, H. Omori, T. Satoh, N. Kurotori, I. Maejima, K. Shirahama-Noda, T. Ichimura and T. J. N. c. b. Isobe (2009). "Two Beclin 1-binding proteins, Atg14L and Rubicon, reciprocally regulate autophagy at different stages." **11**(4): 385-396.

Matsuura, A., M. Tsukada, Y. Wada and Y. J. G. Ohsumi (1997). "Apg1p, a novel protein kinase required for the autophagic process in Saccharomyces cerevisiae." **192**(2): 245-250.

Maycotte, P., K. L. Jones, M. L. Goodall, J. Thorburn and A. J. M. c. r. Thorburn (2015). "Autophagy Supports Breast Cancer Stem Cell Maintenance by Regulating IL6 SecretionAutophagy Regulates IL6 Secretion and Breast Cancer Stem Cells." **13**(4): 651-658.

Mazzoccoli, G., L. Miele, J. Oben, A. Grieco and M. Vinciguerra (2016). "Biology, Epidemiology, Clinical Aspects of Hepatocellular Carcinoma and the Role of Sorafenib." Curr Drug Targets **17**(7): 783-799.

McClain, C. J., D. B. Hill, Z. Song, I. Deaciuc and S. J. A. Barve (2002). "Monocyte activation in alcoholic liver disease." **27**(1): 53-61.

McKnight, N. C., Y. Zhong, M. S. Wold, S. Gong, G. R. Phillips, Z. Dou, Y. Zhao, N. Heintz, W.-X. Zong and Z. Yue (2014). "Beclin 1 Is Required for Neuron Viability and Regulates Endosome Pathways via the UVRAG-VPS34 Complex." PLOS Genetics **10**(10): e1004626.

McKnight, N. C., Y. Zhong, M. S. Wold, S. Gong, G. R. Phillips, Z. Dou, Y. Zhao, N. Heintz, W.-X. Zong and Z. J. P. g. Yue (2014). "Beclin 1 is required for neuron viability and regulates endosome pathways via the UVRAG-VPS34 complex." **10**(10): e1004626.

Meng, Y. C., X. L. Lou, L. Y. Yang, D. Li and Y. Q. Hou (2020). "Role of the autophagy-related marker LC3 expression in hepatocellular carcinoma: a meta-analysis." J Cancer Res Clin Oncol **146**(5): 1103-1113.

Merle, P. and C. J. V. Trepo (2009). "Molecular mechanisms underlying hepatocellular carcinoma." **1**(3): 852-872.

Michaud, M., I. Martins, A. Q. Sukkurwala, S. Adjemian, Y. Ma, P. Pellegatti, S. Shen, O. Kepp, M. Scoazec and G. J. S. Mignot (2011). "Autophagy-dependent anticancer immune responses induced by chemotherapeutic agents in mice." **334**(6062): 1573-1577.

Milletti, F. J. D. d. t. (2012). "Cell-penetrating peptides: classes, origin, and current landscape." **17**(15-16): 850-860.

Mizushima, N. and M. J. C. Komatsu (2011). "Autophagy: renovation of cells and tissues." **147**(4): 728-741.

Mizushima, N. and B. Levine (2020). "Autophagy in Human Diseases." **383**(16): 1564-1576.

Mizushima, N., H. Sugita, T. Yoshimori and Y. J. J. o. B. C. Ohsumi (1998). "A new protein conjugation system in human: the counterpart of the yeast Apg12p conjugation system essential for autophagy." **273**(51): 33889-33892.

Mizushima, N., T. Yoshimori and B. J. C. Levine (2010). "Methods in mammalian autophagy research." **140**(3): 313-326.

Moriya, K., K. Nakagawa, T. Santa, Y. Shintani, H. Fujie, H. Miyoshi, T. Tsutsumi, T. Miyazawa, K. Ishibashi and T. J. C. r. Horie (2001). "Oxidative stress in the absence of inflammation in a mouse model for hepatitis C virus-associated hepatocarcinogenesis." **61**(11): 4365-4370.

Morris, M. C., S. Deshayes, F. Heitz and G. J. B. o. t. C. Divita (2008). "Cell-penetrating peptides: from molecular mechanisms to therapeutics." **100**(4): 201-217.

Nakamura, T., S. Mizuno, K. Matsumoto, Y. Sawa, H. Matsuda and T. Nakamura (2000). "Myocardial protection from ischemia/reperfusion injury by endogenous and exogenous HGF." J Clin Invest **106**(12): 1511-1519.

Nelson, W. J. and R. J. S. Nusse (2004). "Convergence of Wnt, ß-catenin, and cadherin pathways." **303**(5663): 1483-1487.

Obeid, M., A. Tesniere, F. Ghiringhelli, G. M. Fimia, L. Apetoh, J.-L. Perfettini, M. Castedo, G. Mignot, T. Panaretakis and N. J. N. m. Casares (2007). "Calreticulin exposure dictates the immunogenicity of cancer cell death." **13**(1): 54-61.

Oehlke, J., E. Krause, B. Wiesner, M. Beyermann and M. J. F. l. Bienert (1997). "Extensive cellular uptake into endothelial cells of an amphipathic β-sheet forming peptide." **415**(2): 196-199.

Oehlke, J., A. Scheller, B. Wiesner, E. Krause, M. Beyermann, E. Klauschenz, M. Melzig and M. J. B. e. B. A.-B. Bienert (1998). "Cellular uptake of an α-helical amphipathic model peptide with the potential to deliver polar compounds into the cell interior non-endocytically." **1414**(1-2): 127-139.

Osna, N. A., D. L. Clemens and T. M. J. H. Donohue Jr (2005). "Ethanol metabolism alters interferon gamma signaling in recombinant HepG2 cells." **42**(5): 1109-1117.

Pankiv, S., T. H. Clausen, T. Lamark, A. Brech, J. A. Bruun, H. Outzen, A. Øvervatn, G. Bjørkøy and T. Johansen (2007). "p62/SQSTM1 binds directly to Atg8/LC3 to facilitate degradation of ubiquitinated protein aggregates by autophagy." J Biol Chem **282**(33): 24131-24145.

Park, J., J. Ryu, K.-A. Kim, H. J. Lee, J. H. Bahn, K. Han, E. Y. Choi, K. S. Lee, H. Y. Kwon and S. Y. J. J. o. G. V. Choi (2002). "Mutational analysis of a human immunodeficiency virus type 1 Tat protein transduction domain which is required for delivery of an exogenous protein into mammalian cells." **83**(5): 1173-1181.

Peng, H., T. W. Li, H. Yang, M. P. Moyer, J. M. Mato and S. C. Lu (2015). "Methionine adenosyltransferase 2B-GIT1 complex serves as a scaffold to regulate Ras/Raf/MEK1/2 activity in human liver and colon cancer cells." Am J Pathol **185**(4): 1135-1144.

Peng, Q., J. Qin, Y. Zhang, X. Cheng, X. Wang, W. Lu, X. Xie, S. J. J. o. E. Zhang and C. C. Research (2017). "Autophagy maintains the stemness of ovarian cancer stem cells by FOXA2." **36**(1): 1-12.

Peng, Y.-F., Y.-H. Shi, Z.-B. Ding, A.-W. Ke, C.-Y. Gu, B. Hui, J. Zhou, S.-J. Qiu, Z. Dai and J. J. A. Fan (2013). "Autophagy inhibition suppresses pulmonary metastasis of HCC in mice via impairing anoikis resistance and colonization of HCC cells." **9**(12): 2056-2068.

Pescina, S., C. Ostacolo, I. Gomez-Monterrey, M. Sala, A. Bertamino, F. Sonvico, C. Padula, P. Santi, A. Bianchera and S. J. J. o. C. R. Nicoli (2018). "Cell penetrating peptides in ocular drug delivery: State of the art." **284**: 84-102.

Petherick, K. J., A. C. Williams, J. D. Lane, P. Ordóñez-Morán, J. Huelsken, T. J. Collard, H. J. Smartt, J. Batson, K. Malik, C. Paraskeva and A. Greenhough (2013). "Autolysosomal β-catenin degradation regulates Wnt-autophagy-p62 crosstalk." Embo j **32**(13): 1903-1916.

Petrick, J. L., A. A. Florio, A. Znaor, D. Ruggieri, M. Laversanne, C. S. Alvarez, J. Ferlay, P. C. Valery, F. Bray and K. A. J. I. j. o. c. McGlynn (2020). "International trends in hepatocellular carcinoma incidence, 1978–2012." **147**(2): 317-330.

Pouny, Y., D. Rapaport, A. Mor, P. Nicolas and Y. J. B. Shai (1992). "Interaction of antimicrobial dermaseptin and its fluorescently labeled analogs with phospholipid membranes." **31**(49): 12416-12423.

Qiu, D. M., G. L. Wang, L. Chen, Y. Y. Xu, S. He, X. L. Cao, J. Qin, J. M. Zhou, Y. X. Zhang and Q. E (2014). "The expression of beclin-1, an autophagic gene, in hepatocellular carcinoma associated with clinical pathological and prognostic significance." BMC Cancer **14**: 327.

Qu, X., J. Yu, G. Bhagat, N. Furuya, H. Hibshoosh, A. Troxel, J. Rosen, E. L. Eskelinen, N. Mizushima, Y. Ohsumi, G. Cattoretti and B. Levine (2003). "Promotion of tumorigenesis by heterozygous disruption of the beclin 1 autophagy gene." J Clin Invest **112**(12): 1809-1820.

Rawlings, J. S., K. M. Rosler and D. A. J. J. o. c. s. Harrison (2004). "The JAK/STAT signaling pathway." **117**(8): 1281-1283.

Rehermann, B. and M. J. N. R. I. Nascimbeni (2005). "Immunology of hepatitis B virus and hepatitis C virus infection." **5**(3): 215-229.

Rhee, M. and P. J. J. o. B. C. Davis (2006). "Mechanism of uptake of C105Y, a novel cell-penetrating peptide." **281**(2): 1233-1240.

Riley, J., H. G. Mandel, S. Sinha, D. J. Judah and G. E. J. C. Neal (1997). "In vitro activation of the human Harvey-ras proto-oncogene by aflatoxin B1." **18**(5): 905-910.

Roayaie, S., G. Jibara, P. Tabrizian, J. W. Park, J. Yang, L. Yan, M. Schwartz, G. Han, F. Izzo and M. J. H. Chen (2015). "The role of hepatic resection in the treatment of hepatocellular cancer." **62**(2): 440-451.

Sadler, K., K. D. Eom, J.-L. Yang, Y. Dimitrova and J. P. J. B. Tam (2002). "Translocating proline-rich peptides from the antimicrobial peptide bactenecin 7." **41**(48): 14150-14157.

Sahin, F., R. Kannangai, O. Adegbola, J. Wang, G. Su and M. Torbenson (2004). "mTOR and P70 S6 kinase expression in primary liver neoplasms." Clin Cancer Res **10**(24): 8421-8425.

Saito, T., Y. Ichimura, K. Taguchi, T. Suzuki, T. Mizushima, K. Takagi, Y. Hirose, M. Nagahashi, T. Iso, T. Fukutomi, M. Ohishi, K. Endo, T. Uemura, Y. Nishito, S. Okuda, M. Obata, T. Kouno, R. Imamura, Y. Tada, R. Obata, D. Yasuda, K. Takahashi, T. Fujimura, J. Pi, M. S. Lee, T. Ueno, T. Ohe, T. Mashino, T. Wakai, H. Kojima, T. Okabe, T. Nagano, H. Motohashi, S. Waguri, T. Soga, M. Yamamoto, K. Tanaka and M. Komatsu (2016). "p62/Sqstm1 promotes malignancy of HCV-positive hepatocellular carcinoma through Nrf2-dependent metabolic reprogramming." Nat Commun **7**: 12030.

Saitoh, T., N. Fujita, M. H. Jang, S. Uematsu, B.-G. Yang, T. Satoh, H. Omori, T. Noda, N. Yamamoto and M. J. N. Komatsu (2008). "Loss of the autophagy protein Atg16L1 enhances endotoxin-induced IL-1β production." **456**(7219): 264-268.

Saitoh, T., N. Fujita, M. H. Jang, S. Uematsu, B. G. Yang, T. Satoh, H. Omori, T. Noda, N. Yamamoto, M. Komatsu, K. Tanaka, T. Kawai, T. Tsujimura, O. Takeuchi, T. Yoshimori and S. Akira (2008). "Loss of the autophagy protein Atg16L1 enhances endotoxin-induced IL-1beta production." Nature **456**(7219): 264-268.

Samatar, A. A. and P. I. Poulikakos (2014). "Targeting RAS-ERK signalling in cancer: promises and challenges." Nat Rev Drug Discov **13**(12): 928-942.

Santoro, A., L. Rimassa, I. Borbath, B. Daniele, S. Salvagni, J. L. Van Laethem, H. Van Vlierberghe, J. Trojan, F. T. Kolligs and A. J. T. l. o. Weiss (2013). "Tivantinib for second-line treatment of advanced hepatocellular carcinoma: a randomised, placebo-controlled phase 2 study." **14**(1): 55-63.

Sanyal, A. J., S. K. Yoon and R. J. T. o. Lencioni (2010). "The etiology of hepatocellular carcinoma and consequences for treatment." **15**(S4): 14-22.

Schirripa, M., F. Bergamo, C. Cremolini, M. Casagrande, S. Lonardi, G. Aprile, D. Yang, F. Marmorino, G. Pasquini, E. Sensi, C. Lupi, G. De Maglio, N. Borrelli, S. Pizzolitto, G. Fasola, R. Bertorelle, M. Rugge, G. Fontanini, V. Zagonel, F. Loupakis and A. Falcone (2015). "BRAF and RAS mutations as prognostic factors in metastatic colorectal cancer patients undergoing liver resection." Br J Cancer **112**(12): 1921-1928.

Sclip, A., A. Tozzi, A. Abaza, D. Cardinetti, I. Colombo, P. Calabresi, M. Salmona, E. Welker, T. J. C. d. Borsello and disease (2014). "c-Jun N-terminal kinase has a key role in Alzheimer disease synaptic dysfunction in vivo." **5**(1): e1019-e1019.

Seif, F., M. Khoshmirsafa, H. Aazami, M. Mohsenzadegan, G. Sedighi, M. J. C. c. Bahar and signaling (2017). "The role of JAK-STAT signaling pathway and its regulators in the fate of T helper cells." **15**(1): 1-13.

Shanbhogue, A. K., S. R. Prasad, N. Takahashi, R. Vikram and D. V. Sahani (2011). "Recent advances in cytogenetics and molecular biology of adult hepatocellular tumors: implications for imaging and management." Radiology **258**(3): 673-693.

Shi, J., Y. Ma, J. Zhu, Y. Chen, Y. Sun, Y. Yao, Z. Yang and J. J. M. Xie (2018). "A review on electroporation-based intracellular delivery." **23**(11): 3044.

Shi, Y. H., Z. B. Ding, J. Zhou, B. Hui, G. M. Shi, A. W. Ke, X. Y. Wang, Z. Dai, Y. F. Peng, C. Y. Gu, S. J. Qiu and J. Fan (2011). "Targeting autophagy enhances sorafenib

lethality for hepatocellular carcinoma via ER stress-related apoptosis." Autophagy **7**(10): 1159-1172.

Shi, Y. H., Z. B. Ding, J. Zhou, S. J. Qiu and J. Fan (2009). "Prognostic significance of Beclin 1-dependent apoptotic activity in hepatocellular carcinoma." Autophagy **5**(3): 380-382.

Shimizu, S., T. Takehara, H. Hikita, T. Kodama, H. Tsunematsu, T. Miyagi, A. Hosui, H. Ishida, T. Tatsumi, T. Kanto, N. Hiramatsu, N. Fujita, T. Yoshimori and N. Hayashi (2012). "Inhibition of autophagy potentiates the antitumor effect of the multikinase inhibitor sorafenib in hepatocellular carcinoma." **131**(3): 548-557.

Shimizu, S., T. Takehara, H. Hikita, T. Kodama, H. Tsunematsu, T. Miyagi, A. Hosui, H. Ishida, T. Tatsumi, T. Kanto, N. Hiramatsu, N. Fujita, T. Yoshimori and N. Hayashi (2012). "Inhibition of autophagy potentiates the antitumor effect of the multikinase inhibitor sorafenib in hepatocellular carcinoma." Int J Cancer **131**(3): 548-557.

Shimoda, R., M. Nagashima, M. Sakamoto, N. Yamaguchi, S. Hirohashi, J. Yokota and H. J. C. r. Kasai (1994). "Increased formation of oxidative DNA damage, 8-hydroxydeoxyguanosine, in human livers with chronic hepatitis." **54**(12): 3171-3172.

Singal, A. G., P. Lampertico and P. Nahon (2020). "Epidemiology and surveillance for hepatocellular carcinoma: New trends." J Hepatol **72**(2): 250-261.

Sirsi, S. R., R. C. Schray, X. Guan, N. M. Lykens, J. H. Williams, M. L. Erney and G. J. J. H. g. t. Lutz (2008). "Functionalized PEG–PEI copolymers complexed to exon-skipping oligonucleotides improve dystrophin expression in mdx mice." **19**(8): 795-806.

Sivaprasad, U. and A. Basu (2008). "Inhibition of ERK attenuates autophagy and potentiates tumour necrosis factor-alpha-induced cell death in MCF-7 cells." J Cell Mol Med **12**(4): 1265-1271.

Snyder, E. L., B. R. Meade, C. C. Saenz and S. F. J. P. b. Dowdy (2004). "Treatment of terminal peritoneal carcinomatosis by a transducible p53-activating peptide." **2**(2): e36.

Song, J., X. Guo, X. Xie, X. Zhao, D. Li, W. Deng, Y. Song, F. Shen, M. Wu and L. J. J. o. c. b. Wei (2011). "Autophagy in hypoxia protects cancer cells against apoptosis induced by nutrient deprivation through a Beclin1-dependent way in hepatocellular carcinoma." **112**(11): 3406-3420.

Steelman, L. S., S. C. Pohnert, J. G. Shelton, R. A. Franklin, F. E. Bertrand and J. A. McCubrey (2004). "JAK/STAT, Raf/MEK/ERK, PI3K/Akt and BCR-ABL in cell cycle progression and leukemogenesis." Leukemia **18**(2): 189-218.

Su, N., P. Wang and Y. Li (2016). "Role of Wnt/β-catenin pathway in inducing autophagy and apoptosis in multiple myeloma cells." Oncol Lett **12**(6): 4623-4629.

Sugita, T., T. Yoshikawa, Y. Mukai, N. Yamanada, S. Imai, K. Nagano, Y. Yoshida, H. Shibata, Y. Yoshioka, S. J. B. Nakagawa and b. r. communications (2007). "Improved cytosolic translocation and tumor-killing activity of Tat-shepherdin conjugates mediated by co-treatment with Tat-fused endosome-disruptive HA2 peptide." **363**(4): 1027-1032.

Sui, Z., H. Xue, F. Jing and P. J. C. P. Leng (2001). "Sorafenib plus Capecitabine for Patients with Advanced Hepatocellular Carcinoma."

Sun, Q., W. Fan, K. Chen, X. Ding, S. Chen and Q. J. P. o. t. N. A. o. S. Zhong (2008). "Identification of Barkor as a mammalian autophagy-specific factor for Beclin 1 and class III phosphatidylinositol 3-kinase." **105**(49): 19211-19216.

Sun, Q., J. Zhang, W. Fan, K. N. Wong, X. Ding, S. Chen and Q. J. J. o. B. C. Zhong (2011). "The RUN domain of rubicon is important for hVps34 binding, lipid kinase inhibition, and autophagy suppression." **286**(1): 185-191.

Sung, H., J. Ferlay, R. L. Siegel, M. Laversanne, I. Soerjomataram, A. Jemal and F. Bray (2021). "Global Cancer Statistics 2020: GLOBOCAN Estimates of Incidence and Mortality Worldwide for 36 Cancers in 185 Countries." CA Cancer J Clin **71**(3): 209-249.

Tai, W. T., C. W. Shiau, H. L. Chen, C. Y. Liu, C. S. Lin, A. L. Cheng, P. J. Chen and K. F. Chen (2013). "Mcl-1-dependent activation of Beclin 1 mediates autophagic cell death induced by sorafenib and SC-59 in hepatocellular carcinoma cells." Cell Death Dis **4**(2): e485.

Tait, S. W. and D. R. J. N. r. M. c. b. Green (2010). "Mitochondria and cell death: outer membrane permeabilization and beyond." **11**(9): 621-632.

Takahashi, Y., D. Coppola, N. Matsushita, H. D. Cualing, M. Sun, Y. Sato, C. Liang, J. U. Jung, J. Q. Cheng and J. J. J. N. c. b. Mul (2007). "Bif-1 interacts with Beclin 1 through UVRAG and regulates autophagy and tumorigenesis." **9**(10): 1142-1151.

Tang, F., R. Gao, B. Jeevan-Raj, C. B. Wyss, R. K. R. Kalathur, S. Piscuoglio, C. K. Y. Ng, S. K. Hindupur, S. Nuciforo, E. Dazert, T. Bock, S. Song, D. Buechel, M. F. Morini, A. Hergovich, P. Matthias, D. S. Lim, L. M. Terracciano, M. H. Heim, M. N.

Hall and G. Christofori (2019). "LATS1 but not LATS2 represses autophagy by a kinase-independent scaffold function." Nat Commun **10**(1): 5755.

Thennarasu, S., A. Tan, R. Penumatchu, C. E. Shelburne, D. L. Heyl and A. J. B. j. Ramamoorthy (2010). "Antimicrobial and membrane disrupting activities of a peptide derived from the human cathelicidin antimicrobial peptide LL37." **98**(2): 248-257.

Tobin, J. F., A. Laban and D. F. J. P. o. t. N. A. o. S. Wirth (1991). "Homologous recombination in Leishmania enriettii." **88**(3): 864-868.

Tong, H., H. Yin, M. A. Hossain, Y. Wang, F. Wu, X. Dong, S. Gao, K. Zhan and W. J. J. o. c. b. He (2019). "Starvation-induced autophagy promotes the invasion and migration of human bladder cancer cells via TGF-β1/Smad3-mediated epithelial-mesenchymal transition activation." **120**(4): 5118-5127.

Tooze, S. A. (2010). The role of membrane proteins in mammalian autophagy. Seminars in cell & developmental biology, Elsevier.

Tran, S., W. D. Fairlie and E. F. Lee (2021). "BECLIN1: Protein Structure, Function and Regulation." Cells **10**(6).

Tripathi, P. P., H. Arami, I. Banga, J. Gupta and S. J. O. Gandhi (2018). "Cell penetrating peptides in preclinical and clinical cancer diagnosis and therapy." **9**(98): 37252.

Trofimenko, E., G. Grasso, M. Heulot, N. Chevalier, M. A. Deriu, G. Dubuis, Y. Arribat, M. Serulla, S. Michel, G. Vantomme, F. Ory, L. C. Dam, J. Puyal, F. Amati, A. Lüthi, A. Danani and C. Widmann (2021). "Genetic, cellular, and structural characterization of the membrane potential-dependent cell-penetrating peptide translocation pore." eLife **10**: e69832.

Trofimenko, E., G. Grasso, M. Heulot, N. Chevalier, M. A. Deriu, G. Dubuis, Y. Arribat, M. Serulla, S. Michel and G. J. E. Vantomme (2021). "Genetic, cellular, and structural characterization of the membrane potential-dependent cell-penetrating peptide translocation pore." **10**: e69832.

Tünnemann, G., G. Ter-Avetisyan, R. M. Martin, M. Stöckl, A. Herrmann and M. C. J. J. o. p. s. a. o. p. o. t. E. P. S. Cardoso (2008). "Live-cell analysis of cell penetration ability and toxicity of oligo-arginines." **14**(4): 469-476.

Turcios, L., E. Chacon, C. Garcia, P. Eman, V. Cornea, J. Jiang, B. Spear, C. Liu, D. S. Watt, F. Marti and R. Gedaly (2019). "Autophagic flux modulation by Wnt/β-catenin pathway inhibition in hepatocellular carcinoma." PLoS One **14**(2): e0212538.

Umemura, A., F. He, K. Taniguchi, H. Nakagawa, S. Yamachika, J. Font-Burgada, Z. Zhong, S. Subramaniam, S. Raghunandan, A. Duran, J. F. Linares, M. Reina-Campos, S. Umemura, M. A. Valasek, E. Seki, K. Yamaguchi, K. Koike, Y. Itoh, M. T. Diaz-Meco, J. Moscat and M. Karin (2016). "p62, Upregulated during Preneoplasia, Induces Hepatocellular Carcinogenesis by Maintaining Survival of Stressed HCC-Initiating Cells." Cancer Cell **29**(6): 935-948.

Vega-Rubín-de-Celis, S., L. Kinch and S. Peña-Llopis (2020). "Regulation of Beclin 1-Mediated Autophagy by Oncogenic Tyrosine Kinases." Int J Mol Sci **21**(23).

Venook, A. P., C. Papandreou, J. Furuse and L. L. de Guevara (2010). "The incidence and epidemiology of hepatocellular carcinoma: a global and regional perspective." Oncologist **15 Suppl 4**: 5-13.

Villanueva, A. (2019). "Hepatocellular Carcinoma." New England Journal of Medicine **380**(15): 1450-1462.

Villanueva, A., D. Y. Chiang, P. Newell, J. Peix, S. Thung, C. Alsinet, V. Tovar, S. Roayaie, B. Minguez, M. Sole, C. Battiston, S. Van Laarhoven, M. I. Fiel, A. Di Feo, Y. Hoshida, S. Yea, S. Toffanin, A. Ramos, J. A. Martignetti, V. Mazzaferro, J. Bruix, S. Waxman, M. Schwartz, M. Meyerson, S. L. Friedman and J. M. Llovet (2008). "Pivotal role of mTOR signaling in hepatocellular carcinoma." Gastroenterology **135**(6): 1972-1983, 1983.e1971-1911.

Vives, E., P. Brodin and B. J. J. o. B. C. Lebleu (1997). "A truncated HIV-1 Tat protein basic domain rapidly translocates through the plasma membrane and accumulates in the cell nucleus." **272**(25): 16010-16017.

Vousden, K. H. and X. J. N. R. C. Lu (2002). "Live or let die: the cell's response to p53." **2**(8): 594-604.

Wadia, J. S., R. V. Stan and S. F. J. N. m. Dowdy (2004). "Transducible TAT-HA fusogenic peptide enhances escape of TAT-fusion proteins after lipid raft macropinocytosis." **10**(3): 310-315.

Walensky, L. D. and G. H. Bird (2014). "Hydrocarbon-Stapled Peptides: Principles, Practice, and Progress." Journal of Medicinal Chemistry **57**(15): 6275-6288.

Walensky, L. D. and G. H. Bird (2014). "Hydrocarbon-stapled peptides: principles, practice, and progress." J Med Chem **57**(15): 6275-6288.

Waly Raphael, S., Z. Yangde and C. Yuxiang (2012). "Hepatocellular carcinoma: focus on different aspects of management." ISRN Oncol **2012**: 421673.

Wang, H., M. Naghavi, C. Allen, R. M. Barber, Z. A. Bhutta, A. Carter, D. C. Casey, F. J. Charlson, A. Z. Chen and M. M. J. T. l. Coates (2016). "Global, regional, and national life expectancy, all-cause mortality, and cause-specific mortality for 249 causes of death, 1980–2015: a systematic analysis for the Global Burden of Disease Study 2015." **388**(10053): 1459-1544.

Wang, J., P. Sun, Y. Chen, H. Yao and S. Wang (2018). "Novel 2-phenyloxypyrimidine derivative induces apoptosis and autophagy via inhibiting PI3K pathway and activating MAPK/ERK signaling in hepatocellular carcinoma cells." Sci Rep **8**(1): 10923.

Wang, R. C., Y. Wei, Z. An, Z. Zou, G. Xiao, G. Bhagat, M. White, J. Reichelt and B. J. S. Levine (2012). "Akt-mediated regulation of autophagy and tumorigenesis through Beclin 1 phosphorylation." **338**(6109): 956-959.

Wang, S., M. Zhu, Q. Wang, Y. Hou, L. Li, H. Weng, Y. Zhao, D. Chen, H. Ding, J. Guo and M. Li (2018). "Alpha-fetoprotein inhibits autophagy to promote malignant behaviour in hepatocellular carcinoma cells by activating PI3K/AKT/mTOR signalling." Cell Death Dis **9**(10): 1027.

Wang, W., R. Smits, H. Hao and C. J. C. He (2019). "Wnt/β-catenin signaling in liver cancers." **11**(7): 926.

Wender, P. A., D. J. Mitchell, K. Pattabiraman, E. T. Pelkey, L. Steinman and J. B. J. P. o. t. N. A. o. S. Rothbard (2000). "The design, synthesis, and evaluation of molecules that enable or enhance cellular uptake: peptoid molecular transporters." **97**(24): 13003-13008.

White, E., C. Karp, A. M. Strohecker, Y. Guo and R. Mathew (2010). "Role of autophagy in suppression of inflammation and cancer." Curr Opin Cell Biol **22**(2): 212-217.

Whittaker, S., R. Marais and A. J. O. Zhu (2010). "The role of signaling pathways in the development and treatment of hepatocellular carcinoma." **29**(36): 4989-5005.

Whittaker, S., R. Marais and A. X. Zhu (2010). "The role of signaling pathways in the development and treatment of hepatocellular carcinoma." Oncogene **29**(36): 4989-5005.

Wilhelm, S. M., C. Carter, L. Tang, D. Wilkie, A. McNabola, H. Rong, C. Chen, X. Zhang, P. Vincent, M. McHugh, Y. Cao, J. Shujath, S. Gawlak, D. Eveleigh, B. Rowley, L. Liu, L. Adnane, M. Lynch, D. Auclair, I. Taylor, R. Gedrich, A. Voznesensky, B. Riedl, L. E. Post, G. Bollag and P. A. Trail (2004). "BAY 43-9006 Exhibits Broad Spectrum Oral Antitumor Activity and Targets the RAF/MEK/ERK

Pathway and Receptor Tyrosine Kinases Involved in Tumor Progression and Angiogenesis." Cancer Research **64**(19): 7099-7109.

Wu, D. H., T. T. Wang, D. Y. Ruan, X. Li, Z. H. Chen, J. Y. Wen, Q. Lin, X. K. Ma, X. Y. Wu and C. C. Jia (2018). "Combination of ULK1 and LC3B improve prognosis assessment of hepatocellular carcinoma." Biomed Pharmacother **97**: 195-202.

Wu, J. and D. J. J. C. l. Waxman (2018). "Immunogenic chemotherapy: dose and schedule dependence and combination with immunotherapy." **419**: 210-221.

Wu, S., Y. He, X. Qiu, W. Yang, W. Liu, X. Li, Y. Li, H.-M. Shen, R. Wang, Z. Yue and Y. Zhao (2018). "Targeting the potent Beclin 1–UVRAG coiled-coil interaction with designed peptides enhances autophagy and endolysosomal trafficking." **115**(25): E5669-E5678.

Wu, S., Y. He, X. Qiu, W. Yang, W. Liu, X. Li, Y. Li, H. M. Shen, R. Wang, Z. Yue and Y. Zhao (2018). "Targeting the potent Beclin 1-UVRAG coiled-coil interaction with designed peptides enhances autophagy and endolysosomal trafficking." Proc Natl Acad Sci U S A **115**(25): E5669-e5678.

Xie, Q., Y. Su, K. Dykema, J. Johnson, J. Koeman, V. De Giorgi, A. Huang, R. Schlegel, C. Essenburg, L. Kang, K. Iwaya, S. Seki, S. K. Khoo, B. Zhang, F. Buonaguro, F. M. Marincola, K. Furge, G. F. Vande Woude and N. Shinomiya (2013). "Overexpression of HGF Promotes HBV-Induced Hepatocellular Carcinoma Progression and Is an Effective Indicator for Met-Targeting Therapy." Genes Cancer **4**(7-8): 247-260.

Xu, J., A. R. Khan, M. Fu, R. Wang, J. Ji and G. J. J. o. C. R. Zhai (2019). "Cell-penetrating peptide: a means of breaking through the physiological barriers of different tissues and organs." **309**: 106-124.

Xue, S. T., K. Li, Y. Gao, L. Y. Zhao, Y. Gao, H. Yi, J. D. Jiang and Z. R. Li (2020). "The role of the key autophagy kinase ULK1 in hepatocellular carcinoma and its validation as a treatment target." Autophagy **16**(10): 1823-1837.

Yakes, F. M., J. Chen, J. Tan, K. Yamaguchi, Y. Shi, P. Yu, F. Qian, F. Chu, F. Bentzien and B. J. M. c. t. Cancilla (2011). "Cabozantinib (XL184), a novel MET and VEGFR2 inhibitor, simultaneously suppresses metastasis, angiogenesis, and tumor growth." **10**(12): 2298-2308.

Yang, J., Y. Luo, M. A. Shibu, I. Toth and M. J. C. d. d. Skwarczynskia (2019). "Cell-penetrating peptides: efficient vectors for vaccine delivery." **16**(5): 430-443.

Yang, Q., X. Qiu, X. Zhang, Y. Yu, N. Li, X. Wei, G. Feng, Y. Li, Y. Zhao and R. Wang (2021). "Optimization of Beclin 1-Targeting Stapled Peptides by Staple Scanning Leads to Enhanced Antiproliferative Potency in Cancer Cells." J Med Chem **64**(18): 13475-13486.

Yang, Q., X. Qiu, X. Zhang, Y. Yu, N. Li, X. Wei, G. Feng, Y. Li, Y. Zhao and R. J. J. o. M. C. Wang (2021). "Optimization of Beclin 1-Targeting Stapled Peptides by Staple Scanning Leads to Enhanced Antiproliferative Potency in Cancer Cells." **64**(18): 13475-13486.

Yang, Z. and D. J. Klionsky (2010). "Mammalian autophagy: core molecular machinery and signaling regulation." Curr Opin Cell Biol **22**(2): 124-131.

Yang, Z. and D. J. J. C. o. i. c. b. Klionsky (2010). "Mammalian autophagy: core molecular machinery and signaling regulation." **22**(2): 124-131.

Yang, Z., J. Shi, J. Xie, Y. Wang, J. Sun, T. Liu, Y. Zhao, X. Zhao, X. Wang and Y. J. N. b. e. Ma (2020). "Large-scale generation of functional mRNA-encapsulating exosomes via cellular nanoporation." **4**(1): 69-83.

Yao, S., E. F. Lee, A. Pettikiriarachchi, M. Evangelista, D. W. Keizer, W. D. J. B. e. B. A.-P. Fairlie and Proteomics (2016). "Characterisation of the conformational preference and dynamics of the intrinsically disordered N-terminal region of Beclin 1 by NMR spectroscopy." **1864**(9): 1128-1137.

Yim, W. W.-Y. and N. Mizushima (2020). "Lysosome biology in autophagy." Cell Discovery **6**(1): 6.

Yuan, H., A. J. Li, S. L. Ma, L. J. Cui, B. Wu, L. Yin and M. C. Wu (2014). "Inhibition of autophagy significantly enhances combination therapy with sorafenib and HDAC inhibitors for human hepatoma cells." World J Gastroenterol **20**(17): 4953-4962.

Yue, C., X. Yang, J. Li, X. Chen, X. Zhao, Y. Chen, Y. J. B. Wen and B. R. Communications (2017). "Trimethylamine N-oxide prime NLRP3 inflammasome via inhibiting ATG16L1-induced autophagy in colonic epithelial cells." **490**(2): 541-551.

Yue, Z., S. Jin, C. Yang, A. J. Levine and N. Heintz (2003). "Beclin 1, an autophagy gene essential for early embryonic development, is a haploinsufficient tumor suppressor." Proc Natl Acad Sci U S A **100**(25): 15077-15082.

Zachari, M. and I. G. J. E. i. b. Ganley (2017). "The mammalian ULK1 complex and autophagy initiation." **61**(6): 585-596.

Zhang, G., B. T. Luk, X. Wei, G. R. Campbell, R. H. Fang, L. Zhang, S. A. J. C. d. Spector and disease (2019). "Selective cell death of latently HIV-infected CD4+ T cells mediated by autosis inducing nanopeptides." **10**(6): 1-14.

Zhang, Z., T. Liu, M. Yu, K. Li and W. Li (2018). "The plant alkaloid tetrandrine inhibits metastasis via autophagy-dependent Wnt/β-catenin and metastatic tumor antigen 1 signaling in human liver cancer cells." J Exp Clin Cancer Res **37**(1): 7.

Zhao, X.-L., B.-C. Chen, J.-C. Han, L. Wei and X.-B. J. S. R. Pan (2015). "Delivery of cell-penetrating peptide-peptide nucleic acid conjugates by assembly on an oligonucleotide scaffold." **5**(1): 1-11.

Zhivotovsky, B. and S. J. C. c. Orrenius (2011). "Calcium and cell death mechanisms: a perspective from the cell death community." **50**(3): 211-221.

Zhong, Y., Q. J. Wang, X. Li, Y. Yan, J. M. Backer, B. T. Chait, N. Heintz and Z. J. N. c. b. Yue (2009). "Distinct regulation of autophagic activity by Atg14L and Rubicon associated with Beclin 1–phosphatidylinositol-3-kinase complex." **11**(4): 468-476.

Zhou, B., Q. Lu, J. Liu, L. Fan, Y. Wang, W. Wei, H. Wang and G. Sun (2019). "Melatonin Increases the Sensitivity of Hepatocellular Carcinoma to Sorafenib through the PERK-ATF4-Beclin1 Pathway." Int J Biol Sci **15**(9): 1905-1920.

Zhou, Q., V. W. Lui and W. Yeo (2011). "Targeting the PI3K/Akt/mTOR pathway in hepatocellular carcinoma." Future Oncol **7**(10): 1149-1167.

Zhou, Y., S. Jing, S. Liu, X. Shen, L. Cai, C. Zhu, Y. Zhao and M. J. J. o. n. Pang (2022). "Double-activation of mitochondrial permeability transition pore opening via calcium overload and reactive oxygen species for cancer therapy." **20**(1): 1-14.

Zhu, A. X., J. O. Park, B.-Y. Ryoo, C.-J. Yen, R. Poon, D. Pastorelli, J.-F. Blanc, H. C. Chung, A. D. Baron and T. E. F. J. T. L. O. Pfiffer (2015). "Ramucirumab versus placebo as second-line treatment in patients with advanced hepatocellular carcinoma following first-line therapy with sorafenib (REACH): a randomised, double-blind, multicentre, phase 3 trial." **16**(7): 859-870.

Zhu, H., D. Wang, L. Zhang, X. Xie, Y. Wu, Y. Liu, G. Shao and Z. J. O. r. Su (2014). "Upregulation of autophagy by hypoxia-inducible factor-1α promotes EMT and metastatic ability of CD133+ pancreatic cancer stem-like cells during intermittent hypoxia." **32**(3): 935-942.